Modelling Biogeochemical Controls on Planetary Habitability

Andrew J. Rushby

August 2015

A thesis submitted to the School of Environmental Sciences of the University of East Anglia in partial fulfilment of the requirements for the degree of Doctor of Philosophy

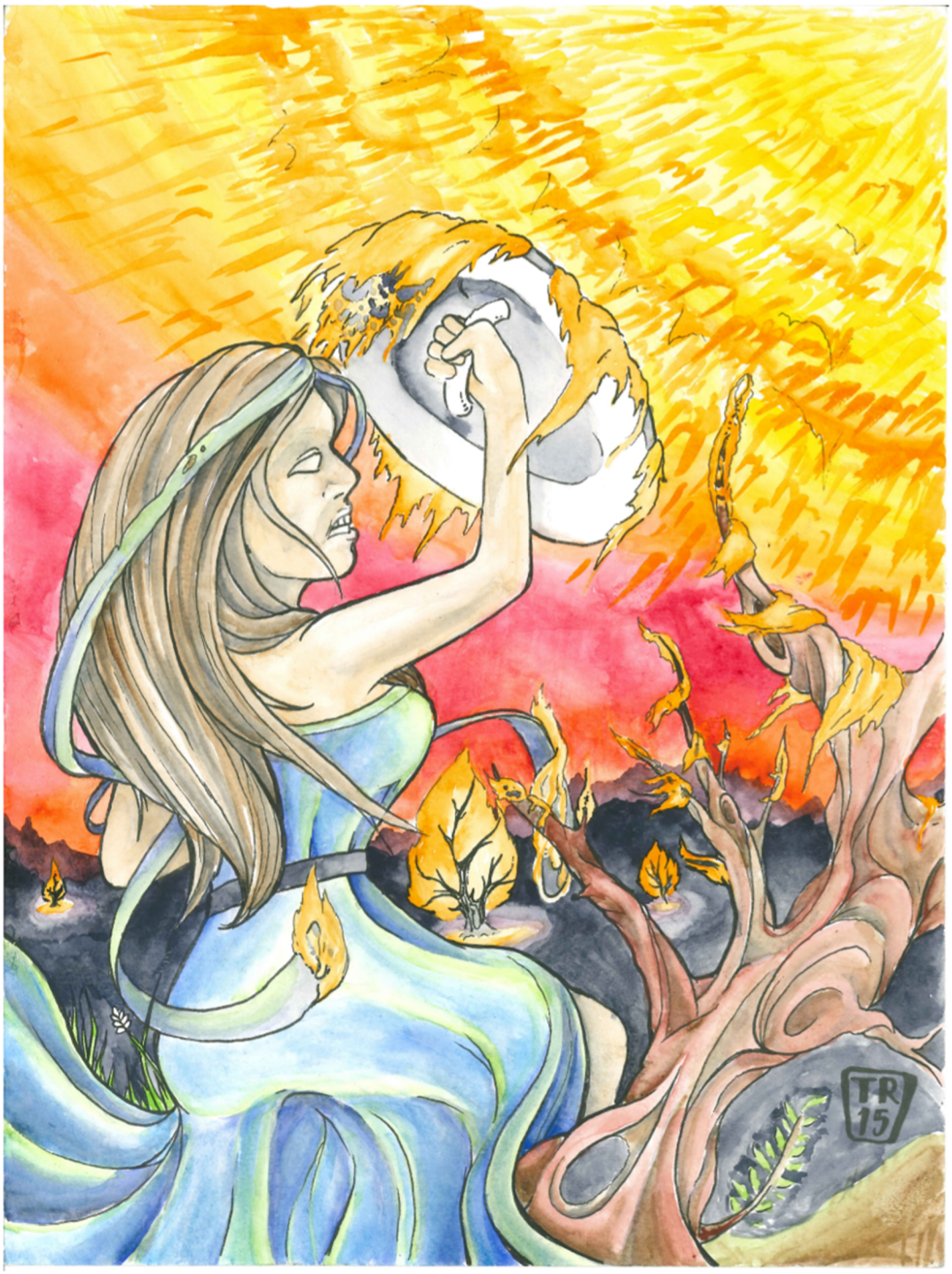

The Last Stand of Gaia, original artwork by Thom Reynolds (2015).

Abstract

The length of a planet's 'habitable period' is an important controlling factor on the evolution of life and of intelligent observers. This can be defined as the amount of time the surface temperature on the planet remains within defined 'habitable' limits. Complex states of habitability derived from complex interactions between multiple factors may arise over the course of the evolution of an individual terrestrial planet with implications for long-term habitability and biosignature detection. The duration of these habitable conditions are controlled by multiple factors, including the orbital distance of the planet, its mass, the evolution of the host star, and the operation of any (bio)geochemical cycles that may serve to regulate planetary climate. A stellar evolution model was developed to investigate the control of increasing main-sequence stellar luminosity on the boundaries of the radiative habitable zone, which was then coupled with a zero-D biogeochemical carbon cycle model to investigate the operation of the carbonate-silicate cycle under conditions of varying incident stellar flux and planet size.

The Earth will remain within habitable temperature limits for 6.34 Gyr (1.8 Gyr from present), but photosynthetic primary producers will experience carbon-starvation due to greatly increased terrestrial weathering from ∼5.38 Gyr (0.84 Gyr from present) onwards, with significant implications for planetary habitability. Planet mass was discovered to have a significant control on the length of the habitable period of Earth-like planets, but more data on the bulk density and atmospheric composition of newly-discovered exoplanets is required before definitive estimates of their long-term habitability can be made. Exoplanet case studies reveal habitable periods significantly longer than that of the Earth, possibly up to ∼80 Gyr in the case of planets in the orbit of M-dwarfs. Contemporary measures of habitability that rely strongly on surface temperatures are becoming obsolete, and a move towards the inclusion of integrated biogeochemical cycle models and the development of multiparameter habitability indices will strengthen contemporary understanding of the distribution and evolution of potentially habitable terrestrial worlds.

Acknowledgements

> We are all here on Earth to help
> others; what on Earth the
> others are here for I don't know.
>
> **John Foster Hall**
> *The Parson Addresses His Flock*
> (1923)

I'd like to extend my thanks to my original supervisors, Andrew Watson and Mark Claire, but especially to my adoptive supervisor Martin Johnson, for nearly 4 years of guidance and encouragement. As far as supervisory teams go, I could not have hoped for a more supportive and knowledgeable group. Thanks also to Ben Mills for help with MATLAB, for general advice and direction in navigating the murky quagmire of postgraduate research, and for enjoyable evenings of music and mirth. Thanks go to my colleagues and friends at the UEA for good times and lively conversation. Clare Ostle deserves a special mention for her encouragement and contagious positivity. To my non-scientist friends, Thom Reynolds and the Kitchen, Rosie Ruttley-Dornan, Johnny Shirley, as well as all the members of Scallywag's Cove; I thank you all for your continued and valued friendship and welcome distraction from academia.

I'd also like to the thank the 'abnormally large' renal calculus that lodged itself in my left kidney just as I began pulling my thesis together towards the end of 2014. In the throes of the debilitating six weeks of agony that followed, my desire to finish my research and get into better physical shape was a catalyst for wider perspective and productivity.

Finally, the greatest thanks of all goes to my family - my mother Lynda and sister Allison - for the sacrifices they made, large and small, that allowed me to be able to be in the position to carry out this work, especially towards the end.

Andrew Rushby, August 2015.
University of East Anglia, Norwich.

Dedicated to the memory of my father, William Sydney Rushby (1936 - 2012).
A navigator of seas, a rescuer of men, and a paragon of humility.

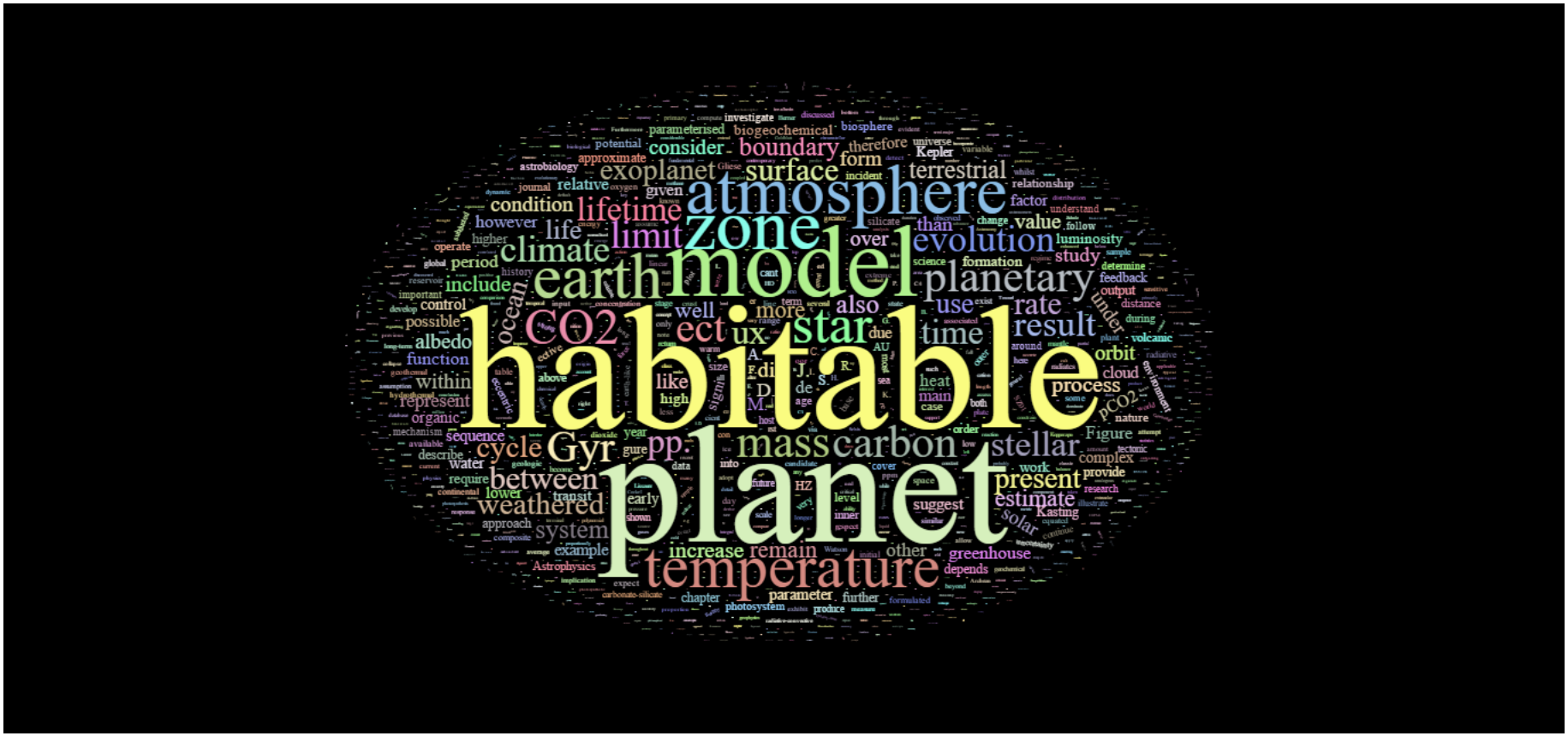

What to expect: word cloud generated from thesis contents (http://timdream.org/wordcloud/)

Contents

1 Introduction

> If we crave some cosmic purpose, then let us find ourselves a worthy goal.
>
> **Carl Sagan**
> *Pale Blue Dot: A Vision of the Human Future in Space* (1994)

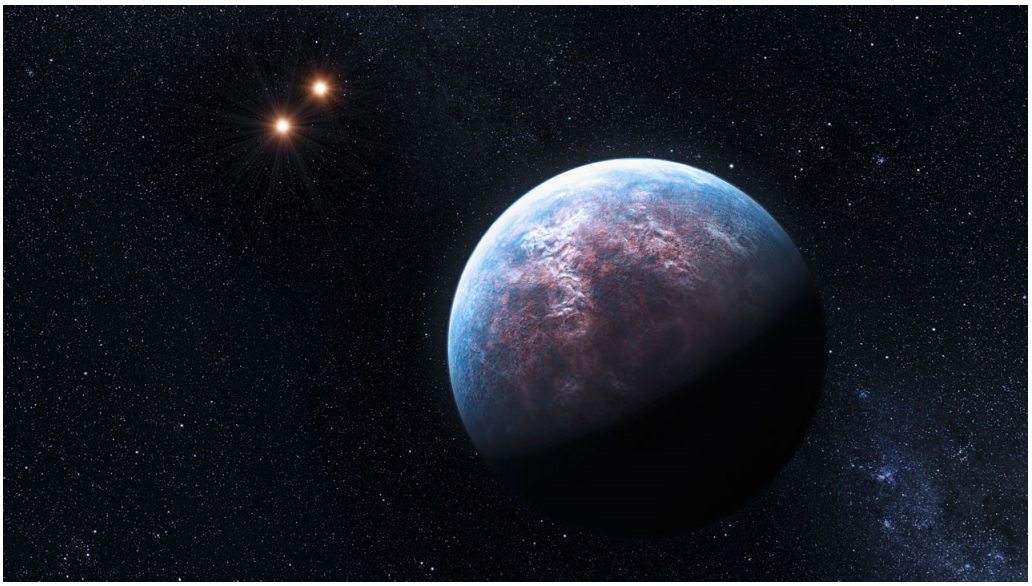

Placing humanity in some universal context, both temporally and spatially, is arguably one of the primary philosophical drivers behind the scientific revolution and enlightenment movement. Questions such as 'are we alone?' have pervaded scientific and popular thought for centuries, but definitive answers remain difficult to obtain. In terms of planetary science, the relative commonality of the Sun, the Earth and the Solar System remains a key research topic, and evidence that our physical place in the Universe is in some way unique or privileged (the 'Rare Earth' hypothesis) would provide some perspective on these larger issues. However, with limited evidence this hypothesis remains scientifically and philosophically problematic, with researchers pointing to an inherent 'anthropic bias' from which we, by virtue of being intelligent observers, remain inextricably

bound. The relatively recent discovery of planets that orbit stars other than the Sun is casting some light on these questions, particularly on the relative normalcy of our planet relative to those in neighbouring star systems. However, these surveys have also revealed shortcomings in our understanding of the term 'habitability' in the context of alien worlds. This concept has been previously framed in terms of the 'circumstellar habitable zone' theory, in which surface temperatures able to sustain liquid water are computed based on distance from the star under a model atmosphere strongly resembling that of the Earth. However, as more exoplanets are discovered within this zone, it is becoming apparent that considerations of unique characteristics and planetary evolution need to be taken into account in order to make a robust assessment of their potential habitability. In particular, the operation of stabilising feedback mechanisms on planetary climate should form a key component of future

studies. Furthermore, given the limited data available for exoplanets and the limitations of our current observational technologies, modelling studies making use of this restricted dataset will prove particularly important in identifying key planets of interest based on improvements in our understanding of the factors that control planetary habitability, as well as how signs of life (biosignatures) could be detected and quantified to make the most of contemporary and near-future imaging capabilities.

1.1 Planetary Habitability

1.1.1 Star and Planet Formation

Theories of planet formation have been built from observations of planets and small bodies in our Solar System, exoplanet systems and young stars in vast 'stellar nurseries' — molecular interstellar dust clouds associated with high rates of stellar formation; the Orion nebula for example (Seager & Lissauer, 2010). Dynamical models of the evolution of the solar system, such as the NICE and NICE2 models, are also used to explain the formation, configuration and potential migration of planets (Tsiganis *et al.*, 2005; Levison *et al.*, 2011). The gravitational collapse of matter at the

centre of one of these primitive solar nebulae, comprised mainly of molecular hydrogen, helium, heavier organic material, volatiles and dust with various combinations of carbon, hydrogen, nitrogen and oxygen (including: carbon monoxide, cyanide, caesium, silicon monoxide, hydroxide radicals, water vapour, hydrogen cyanide, sulphur dioxide and hydrogen sulphate), leads to the formation of a star (de Pater & Lissauer, 2007; Montmerle *et al.*., 2006). Molecular clouds are generally intrinsically stable as the internal pressure of the cloud is more than sufficient to balance the inward forces of gravity (de Pater & Lissauer, 2007). However, a number of factors can trigger gravitational collapse, including the compressive effects of transit though the spiral arm of a galaxy and distant supernova explosions (de Pater & Lissauer, 2007). Collapse may trigger fragmentation of the solar nebula, especially if rotation is rapid, which can lead to the development of a number of 'sub-clouds' each of which may collapse to form a star and result in a binary or multiple star system (de Pater & Lissauer, 2007).

At the centre of the vast molecular cloud, material governed by the conservation of angular momentum exhibits significant increases in velocity, which in turn increases the probability and energy of atomic collisions (Montmerle *et al.*., 2006; Zeilik & Gregory, 1998). The collisions release heat from the conversion of gravitational energy to kinetic energy which in turn raises pressure at the centre of nebula to that of hydrostatic equilibrium (de Pater & Lissauer, 2007; Montmerle *et al.*., 2006). At approximately 10^6 K nuclear reactions that result from the conversion of deuterium (^{2}H) to helium begin and restrict further contraction of the star, until which point the supply of deuterium becomes exhausted (de Pater & Lissauer, 2007). At this point the star shrinks in size, increasing in temperature to 10^7 K and initiating hydrogen fusion, and evolution along the 'main sequence' (Montmerle *et al.*., 2006; Zeilik & Gregory, 1998). Stellar classification and the influence of different properties of stars on their host planets will be further discussed in Chapter 2.

The remaining matter forms a dense, circumstellar disk that rotates around the young star, within which small grains of material collide, coalesce and accrete at random to form planets, moons and other small bodies such as

asteroids and minor planets (Montmerle *et al.*., 2006; Raymond *et al.*., 2007). Whilst the considerable majority of the mass of the initial system is contained in the star, up to 98% of the angular momentum lies in the disk (de Pater & Lissauer, 2007)

Depending on the orbital distance from the star, planetesimals can form terrestrial (rocky) planets, icy planets with rocky cores as well as the cores of gas giants at considerable distances exceeding the snow or frost line where it is cool enough for hydrogen compounds like water, methane and ammonia to condense into solid ice particles and form a thick atmosphere around the solid core (Lissauer & Stevenson 2007; Kokubo & Ida, 2002; Lineweaver, 2001). The temperature of condensation varies by compound and the partial pressure of vapour in the circumstellar disk. Physical models used to compute the 'frost line' for H_2O for example use varying values for these factors, returning distances and temperatures between 2.7 and 3.2 AU, and 143 and 170 K, respectively (Hiyashi, 1981; Podolak & Zucker, 2010; Martin & Livio, 2012).

Giant planets are thought to start their growth in the same manner as terrestrial planets, but then go on to accrete massive amounts of gas prior to the exhaustion of the circumstellar disk (Seager & Lissauer, 2010). The strong gravitational force exerted by ice and gas giants can perturb the orbits of terrestrial planets as well as asteroids and minor planets in the inner star-system; this explanation remains the most likely cause of the Late Heavy Bombardment of the inner Solar System ∼4.1 billion years ago (Ga) (Gomes *et al.*., 2005; Morbidelli *et al.*., 2005). Based on computer simulations, the rate of planetary accretion within the circumstellar disk is hypothesised to be relatively rapid; for example, it is thought that planetary formation within the Solar System was essentially complete in ∼100 million years, before the Sun entered the main sequence (Gomes *et al.*., 2005; Kleine *et al.*., 2002; Montmerle *et al.*., 2006; Raymond *et al.*., 2007; Wadhwa *et al.*., 2006).

1.1.2 Planet Formation and Geological Evolution

The Earth is the planet that has been studied in the most depth and detail by humanity. It is from this world, and from observations of other planets in our Solar System, that we have developed our understanding of the formation and possible evolution of planets. The Earth was formed from the circumstellar disk of the young Sun approximately 4.54 Gyr ago (Newman, 2007). Accretionary models, supported by empirical evidence from Hafnium-Tungsten (Hf-W) isotopic analyses of meteorites suggest that the planet was assembled, and differentiated into an iron core and silicate mantle and crust, within ∼30 million years (Myr) of initial accretion (Kleine *et al.*., 2002).

The Earth experienced a severely reducing magma-ocean stage very early in its history due to the excess energy resulting from planetary accretion, and a cataclysmic Moon-forming impact with a Mars-sized body (known as Theia), 30 — 50 million years after formation (Nutman, 2006; Zahnle *et al.*., 2007). The longevity of this phase is uncertain but likely geologically rapid (Nutman, 2006; Shaw, 2008; Wood *et al.*., 2006). Zahnle *et al.*. (2007) suggest that the magma-ocean persisted for as little as 2 million years, its cooling rate dependent on the level of atmospheric insulation, and tidal heating from the newly formed Moon. Continuous degassing accompanied the magma-ocean phase, and also facilitated the separation of metals from silicates, eventually leading to the formation of the Earth's core by chemical-gravitational differentiation 30 to 60 million years after accretion (Kleine *et al.*., 2002; Ernst, 2007).

Due to a lack of preservation, erosion, weathering, subduction and metamorphic alteration, the abundance of extant rocks declines exponentially with age (Garrels & Mackenzie, 1969). Only the most physically and chemically robust minerals tend to be suitable for analysis when considering Hadean eon (older than 4 Gyr) rocks. Recent studies suggest that zircons can be used for this purpose because of their extreme durability and ability to preserve the original chemistry and isotopic composition from the time of their crystallisation, and because they are the only known extant minerals from the Hadean eon (Trail *et al.*., 2011).

Zirconium silicate ($ZrSiO_4$), occurring naturally as zircon, is a silicate mineral found widely throughout the Earth's crust in igneous and metamorphic rocks, and as detrital grains in sedimentary rocks (Anthony *et al.*., 2001). Zircon has extensive application in radiometric dating as it incorporates uranium (U) and thorium (Th) into its crystal structure, but rejects lead (Pb) (Anthony *et al.*., 2001). Therefore, the empirically-derived decay rate of U to Pb can be measured by modern analytical techniques, as it is assumed that the entire Pb inventory of the zircon is radiogenic in source (Schoene, 2014).

Zircons returned from the Jack Hills area of western Australia are currently the oldest known minerals on Earth after being dated using their U/Pb ratio to 4.404±8 billion years (Wilde *et al.*., 2001). The oxygen isotope ratios of these samples ($\delta^{18}O$ from 7.4 to 5.0 ‰) suggests that they evolved from a magmatic source and that they had some interaction with a liquid hydrosphere during their formation (Wilde *et al.*., 2001). This evidence alludes to the existence of continental crust and oceans at this date in the early history of the Earth (Mojzsis *et al.*., 2001; Wilde *et al.*., 2001).

In accordance with the admittedly sparse geological evidence from early Earth history, it seems very likely that there were substantial oceans and continental crust present in the Hadean (Nutman, 2006; Shaw, 2008). Sedimentary rocks, igneous amphibolites and tonalites (formed from the partial melting of hydrated basaltic crust) and evidence of hydrothermal activity suggest that by 4 Gyr ago the Archean geological regime was dominated by plate tectonics, characterised by clear division between oceans and continents, extending back to perhaps as early as 4.4 Ga (Mojzsis *et al.*., 2001; Wilde *et al.*., 2001; Nutman, 2006; Trail *et al.*., 2011). Morphologically, the land masses of the late Hadean are hypothesised as several island-arc belts of newly emerging continental crust undergoing extreme volcanism and subduction. The formation of these early proto-continents was also accompanied by high rates of ocean crust production driven by orders-of-magnitude higher rates of convection than at present (Shaw, 2008).

Impacts associated with the Late Heavy Bombardment (LHB) of the inner

Solar System are no longer thought to have been the dominant geological process affecting the formation of the crust, but the dissipation of impact energy would most likely have disrupted the primitive internally-driven plate-tectonic mechanism of the time (Nutman, 2006; Shaw, 2008). It is not yet known whether the processes that shaped the Earth during its formation and early history are typical of those that operate on small, rocky planets elsewhere, but the study of planets around other stars in the galaxy (exoplanets, extrasolar planets) may provide answers to these issues in the future.

1.1.3 Exoplanets: Detection Techniques

Over 99% of all known planets orbit stars other than our Sun, and the study of these exoplanetary systems have provided limits on the mode and action of planet formation models, as described above. (Schneider *et al.*., 2011; Seager & Lissauer, 2010). As of the time of writing (August 2015), 1948 exoplanets had been discovered and catalogued in the online exoplanet.eu database, maintained by researchers at the Paris Observatory, but it should be noted that this is one of a series of exoplanet databases available online, and these rarely agree in their raw planet counts due to differing detection and confirmation criteria of the researchers responsible for their administration. For example *NASA's Exoplanet Archive* lists 1887 planets, whilst the *Habitable Exoplanet Catalog* contains 1942 planets.

Over half of these newly discovered planets ($n = 1030$, as of August 2015) were detected by NASA's *Kepler* space observatory, launched in 2009 (Lissauer *et al.*., 2014). *Kepler* detects exoplanets using a transit photometry method: as a planet passes in front of its star, seen edge on relative to the instrument, a small yet consistent amount of radiation from the star is obscured, resulting in a verifiable signal that can be used to determine planetary characteristics, such as radius and distance from the star (Koch *et al.*., 2010). Partial eclipses by rocky, Earth-analogue planets may only obscure 80 parts per million (ppm) of the stellar flux, compared to 1% (10000 ppm) for Jupiter-sized planets, so *Kepler* boasts a photometric precision of 30 ppm in order to detect these smaller worlds (Lissauer *et al.*.,

2014). Whilst not only detecting the smallest and most 'Earth-like' planets to orbit Sun-like stars, *Kepler* has also provided an improved understanding of the most common architecture of planetary systems, illustrating that the Sol-family planets may not be typical or particularly representative of most planetary configurations (Lissauer *et al.*., 2014; Scharf, 2014). For example, it appears from the *Kepler* data that 'Super-Earth'-sized terrestrial planets (with masses greater than 10 Earth masses ($M_\oplus$), but less than $\sim$17 $M_\oplus$) are common, yet the solar system does not have a representative of this particular mass class (NASA, 2014). This insight is significant, both scientifically and philosophically, as it continues the trend of demotion of the Earth, from centre stage in the cosmos to suburban outlier that began in earnest with Copernicus in 1543, but may also simultaneously reveal unique characteristics of the solar system that could make life here more, or less, likely than might be expected on average (Scharf, 2014).

Other missions, such as the High Accuracy Radial Velocity Planet Searcher (*HARPS*) based at ESO's La Silla Observatory in Chile or the *HIRES* spectrometer at the Keck telescopes, use a method known as radial velocity to determine the gravitational effects of orbiting planets on the host stars. Given the high accuracy of these instruments ($\sim$1 m/s), it is possible to measure planet mass and orbital distance by measuring the change in velocity of the star, relative to Earth, caused by the gravitational 'tug' of orbiting planets (Mayor *et al.*., 2003). This technique is responsible for the discovery of 574 planets to date, according to the *exoplanet.eu* database.

1.1.4 Theoretical Exoplanetary Geophysics

Beyond descriptive information regarding size, mass and orbital distance, relatively little information regarding planetary dynamics (atmospheric circulation, plate tectonics etc.) is available for most exoplanets, and is especially lacking for small, rocky planets of interest to astrobiologists. For example, Earth is the only planet so far confirmed to exhibit thermal convection in the form of plate tectonics. Despite this, planetary volcanism is expected to be a widespread characteristic of rocky planets resulting from partial melting of their silicate mantle (Kite *et al.*., 2009). There is some

disagreement as to whether plate tectonics would operate on massive planets, and to what alternative form their tectonic regimes may conform (Keltenegger *et al.*., 2010; Kite *et al.*., 2009). A dynamic tectonic regime in the form of plate tectonics and volcanism are important factors in determining the atmospheric composition of planets, the strength of their magnetic field as well as for maintaining fundamental biogeochemical cycling processes (e.g. the carbonate-silicate cycle on Earth) (Kasting & Catling, 2003). Therefore, many astrobiologists consider volcanism and plate tectonics to be a necessarily prerequisite for long-term planetary habitability (Korenaga, 2012; Kasting & Catling, 2003).

The atmosphere of a planet is the dynamic product of: gases that have accreted from the stellar nebula, those degassed during planet formation and subsequent impact accretion as well as those gasses released from volcanic sources due to subsequent geological activity (Kite *et al.*., 2009; Papuc & Davies, 2008). Atmospheric escape and (bio)geochemical cycling will alter the composition over time (Korenaga, 2012; Kasting & Catling, 2003). Using near-future observational techniques and equipment (the James Webb Space Telescope for example), it is considered theoretically feasible to detect eruptive volcanism and products of volcanic outgassing on extrasolar planets by spectroscopically analysing atmospheric signature gases, especially sulphur dioxide (SO_2) (Keltenegger *et al.*. 2010; Valencia *et al.*., 2007).

Some contention exists within the scientific literature regarding plate tectonics on massive exoplanets (Kite *et al.*., 2009). Some studies suggest the greater shear stresses and thinner plates thought to be associated with planets of higher masses will favour subduction by decreasing the overall resistance to plate motion (Valencia *et al.*., 2007). Others maintain that a stagnant lid or episodic tectonic regime may be a more realistic assumption because of a modelled reduction in the ratio of driving to resistive forces and increased fault strength under high gravity (O'Niell & Lenardic, 2007). Further modelling and eventual observation of exoplanet atmospheres and/or interiors will settle the debate with time. As well as controlling the evolution of the atmosphere through volcanic degassing and maintaining planetary-scale biogeochemical feedback mechanisms, plate tectonics also

points to the existence of a planetary magnetic field, which is considered vital protection against atmospheric erosion from charged solar particles (Korenaga, 2012; Kasting & Catling, 2003).

Whilst the temperature of Earth's mantle has exhibited a trend of secular cooling since the planet's formation, the rate of convection has been increasing, contrary to theoretical expectations (Korenaga, 2012). Mantle viscosity is inversely proportional to temperature: lower temperatures should be associated with higher viscosity and proportionally reduced rates of subduction and volcanism (Korenaga, 2012). Recent research suggests that water may be important for the initiation of plate tectonics by hydrating the initially dry mantle, thereby increasing its fluidity (i.e. decreasing viscosity) and reducing plate yield strength and friction at faults, compensating for the trend of secular cooling (Korenaga, 2012; Keltenegger *et al.*., 2010; Valencia *et al.*., 2007). As well as its rate, water content may exhibit a strong control on the mode of volcanism: water-deficient planets with dry, viscous lithospheres may have less explosive volcanic activity, which has implications for their potential detection and spectroscopic analysis as explosive events are thought to liberate volcanic species into the stratosphere enabling easier remote detection (Keltenegger *et al.*., 2010).

The rate of mantle convection on planets smaller than Earth (Mars, for example) would decrease rapidly following formation and the planet would cool more quickly, inhibiting plate tectonics. This has important implications for planetary habitability, as the carbonate-silicate cycle that regulates the planetary climate over geological timescales requires active plate tectonics and volcanism to facilitate the subduction of organic carbon as well as the volcanic release of CO_2 (Kasting & Catling, 2003).

As well as size, the age of a planet also exhibits a control on volcanicity. A newly-formed planet will have greater residual accretion energy and a large inventory of both long lived (^{40}K, ^{232}Th, ^{235}U and ^{238}U) and short lived (^{26}Al) radionuclides which form major components of the internal heat flux and drive increased tectonic activity and subduction rates (Keltenegger *et al.*., 2010). However, recent work by Frank *et al.*. (2014) suggests that young (<1 Gyr), hot rocky planets are more likely to be geologically active,

as the later a planet forms in galactic history the smaller its radiogenic inventory of thorium (^{232}Th) and potassium (^{40}K) is likely to be. They note that long-lived radionuclides such as (^{232}Th) will dominate the radiogenic heating regime of ancient planets, whilst (^{40}K) will most likely dominate on younger planets, and could affect long-term planetary habitability.

1.1.5 Biogeochemical Feedbacks

This work is conducted under the assumption that on planets with a similar ocean/continental configuration and composition (with a crust comprised primarily of silicate minerals as on the Earth) an analogous carbonate-silicate weathering feedback on atmospheric CO_2 and planetary climate will be in operation, and that this process would have a significant effect on long term habitability. On Earth, the terrestrial cycle of silicate weathering and volcanic outgassing buffers atmospheric CO_2 and global climate over geological time, but the potential for this feedback to be operating on newly discovered Earth-like exoplanets has not been explored in detail. In fact, previous studies concerned with quantifying habitability (i.e. Kasting *et al.*., 1993; Rushby *et al.*., 2013; Kopparapu *et al.*., 2014) have neglected this process completely by necessity, focussing instead on the dynamics of a model atmosphere with no dynamic carbon cycle operating to stabilise the climate over the long term. Previous studies focussing on Mars (e.g. Haberle *et al.*, 1994) do identify and account for alternative mechanisms of active carbon partitioning controlled by polar cap formation. As our understanding of the operation of these processes on the Earth evolves, it seems appropriate to begin to apply biogeochemical modelling techniques to studies of exoplanetary habitability in order to better understand the effect of these processes on planets of different sizes, at different orbital distances, and with different continent/ocean coverage.

1.1.6 Defining Boundaries of Habitability

Habitability is a notoriously difficult concept to define with a single parameter - temperature for example (see discussion in chapter 2). The

term, a 'non-natural kind' in the parlance of analytical philosophy, is not reducible to simple objectively measurable physical constants (Cleland & Chyba, 2002). Furthermore, the entirety of the concept hinges on the ability to identify habitats in which an organism can live. The limitations revealed in this statement are obvious: for what organism are we making our assessments? What does it mean to 'live' in this definition? What constitutes a habitat, and how does this definition vary in space and time?

Following Cockell *et al.*. (2015) — this study itself a concatenation and summary of years of astrobiological and ecological research — a habitat can be defined as: "an environment capable of supporting the activity of at least one known organism", where 'activity' is considered analogous to metabolic activity that results in the long-term survival and growth of that organism. Including the requirements for survival and growth via the implicit assumption of metabolic activity eliminates uncertainty when considering dormant or 'resting' microbial states — of organisms that have been ejected into space within bolides from an impact for example, or the unintentional delivery to other planetary environments of microorganisms by spacecraft with poor planetary protection mechanisms (Cockell *et al.*., 2015). Furthermore, considering the physical space which the organism occupies (its 'habitat') as well as the set of conditions and resources that allow the continued metabolic activity of the organism (its 'niche'), is also important in understanding the spatiotemporal evolution of habitable conditions (Cockell *et al.*., 2015). This definition however does allude to the conservative nature of the concept of habitability; limited in its scope by the contemporary state of the field of biology.

Another approach that seeks to neutralise some of this inherent terrabiological bias is to consider the amount of available free energy for redox reactions, again assuming that other life in the universe uses Gibbs free energy in analogous reactions (Hoehler, 2007). It remains impossible at this stage to know whether the diversity of terrestrial life forms are representative of the universal morphology of life, or whether the environmental conditions that allow life to emerge (whatever they may be) are numerous or limited, but avoiding other speculative energy sources and limiting habitability to known life allows astrobiologists to investigate the

term whilst avoiding the intellectual quagmire of attempting to define life (Cleland & Chyba, 2002).

1.1.7 Habitable for Whom?

The physical and chemical environments that are created and maintained by the proximity of a given planet to a star of a given class, as well as the magnetic, radiative and atmospheric variability that results from this association, represent the most fundamental controls on the ability of life to evolve and flourish. However, our understanding of the prerequisites, subsequent requirements and limits of both 'simple' and advanced life has been shaped by the study of organisms on Earth. Therefore, our knowledge of the limitations on the ability of organisms to evolve is a product of the terrestrial environment in which, at present, all life has been found. In recent times our understanding of the physical and chemical boundaries for life, here on Earth and in the Solar System and beyond, have been radically revolutionised by the discovery of several species of 'extremophile'; defined as organisms that can tolerate "...conditions that disrupt the integrity or function of aqueous solutions of organic compounds..." (pg. 114, Rothschild, 2007). This definition illustrates the importance of water as a solvent, and organic carbon as the basis of life on Earth. Extremophilic species can be found in the Archaea, Eubacteria and Eukarya taxa (Rothschild, 2007).

1.1.8 Habitability in Space and Time

The fundamental interplay and feedbacks between life and the environment will inexorably result in the alteration of the planetary environment, which may change the habitable space for other organisms. Consider, for example, the emergence of oxygenic photosynthesisers and the subsequent oxygenation of the atmosphere during the Proterozoic eon on Earth: to the established anaerobic biosphere that predated the oxygenic photosynthesisers, this atmospheric revolution represented a toxic transition which significantly limited the surface habitability of the planet for these

organisms. Therefore, the habitability of the planet, as measured by habitat/niche availability for example, decreased considerably for anaerobic metabolisms whilst expanding significantly for oxygenic photosynthesisers and aerobic respirators, despite limited changes to the surface temperature (excluding the possibility of Snowball Earth events triggered by this oxic transition) — a more limited definition of habitability.

To further muddy the conceptual waters of habitability research, Cockell *et al.*. (2012) explores the concept of uninhabited habitable environments, as well as vacant niches within a habitat (Cockell, 2011). It is possible to consider a physical space, possibly planetary in scale, which contains no life whilst providing the necessary resources and conditions required to support life. This line of enquiry can be expanded to consider what extent of a planet would need to be within habitable limits for the planet to be considered as habitable at any given time. For example, the very great majority (>99%) of the Earth in terms of its volume remains uninhabited, yet this planet is considered the *prima facie* best example of a habitable planet we are currently aware of (Jones & Lineweaver, 2010). Alternatively, habitable conditions on Mars have been reported, but these may be vestigial remnants of habitable refugia that have become isolated and degraded in their ability to host and support life as the conditions on the planet change over geological time (Grotzinger *et al.*., 2014; Haberle *et al.*, 1994). The expectation that a biosphere will emerge when a suitable habitat and available niches are extant to support it is unnecessarily anthropocentric, and the likelihood of life emerging when conditions are suitable is currently unknown, but the probability is non-zero; if abiogenesis is to occur, it holds that it must do so in a habitable environment. Consider the probabilistic model of Watson (2008) in the context of geological evidence from the Earth that suggests that life was likely established on the Earth by 3.8 Ga, and exhibiting cell division by 3.2 Ga (Knoll & Barghoorn, 1977; Ohmoto *et al.*., 2014). Given the duration of habitable conditions on the planet mitosis represents a significant evolutionary step, which had a less than 0.01% probability of occurring within that timescale (Watson, 2008).

This raises the further consideration, which this work will seek to emphasise: the change in habitability over time. For how long should a

planet be able to support an organism to be considered a habitable planet? Continuous versus instantaneous planetary habitability describes a spatiotemporal spectrum between localised (in space and time) conditions that meet the biochemical requirements of an organism, and planetary-scale (interior and exterior) habitable environments over the course of geological timescales. This latter concept is the focus of this study; the planet as a habitable entity, the evolution of which is quantified over the course of the planet's existence. It follows therefore, that a 'list' of requirements for life can be complied, and these investigated as metrics for general habitability on a given planet. Cockell *et al.*. (2015) identify the following as candidates:

- Liquid water: H_2O is the only solvent known to be used by life, although it remains theoretically possible for others to exist, including organic solvents.
- Temperature: strong evidence of metabolic activity has been reported in microbes at temperatures of ∼-13 °C (Wells & Deming, 2006). The upper extreme is more complex as water can remain in a liquid phase, under high pressure, up to 300 °C. Microbial growth has been reported by Takai *et al.*. (2008) at 122 °C (395 K). Cowan (2004) estimates that the point at which the amount of harnessable energy is less than the energy required for cell repair due to the rate of chemical reaction (proportional to temperature), is ∼140 °C. 'Normal' biomolecules such as chlorophyll degrade above ∼70°C (Rothschild, 2007). This 70 °C limit will form the upper boundary of the temperature-dependent habitable zone in the remainder of this work due to the relative importance of chlorophyll in primary production, and the coupling of the temperature and 'photosystem limit' of habitability, which will be discussed later in this chapter.
- Physiochemical conditions: other environmental factors, such as a high radiation flux, extremes of pH, toxicity, salinity and desiccation may further prevent the establishment and proliferation of life. The effect of multiple states of environmentally-induced physiological stress is also unknown.

- Energy: On Earth, most energy is acquired via redox reactions that involve the transfer of an electron from a donor molecule to an acceptor molecule. This process can be driven by a chemical gradient (chemotrophy or chemoautotrophy/chemolithotrophy), or via sunlight (phototrophy). A habitable environment would therefore have an acceptable source of electron donors and acceptors for life to exploit to generate sufficient energy for growth. It remains very difficult to determine the amount of energy (in the form of Gibbs free energy) available to a given organism in a given environment, as there are a multitude of unknowns in both the supply and consumption of energy (i.e. for continued survival when dealing with several environmental stressors).
- Elements: On Earth, carbon, hydrogen, nitrogen, oxygen, phosphorus and sulphur are considered crucial for the construction of the macromolecules vital for life. Depending on planetary conditions (temperature, redox balance of the surface) these six elements may occur in several forms and in various abundances that would likely vary from planet to planet. Furthermore, other elements (iron, cobalt, copper, magnesium) may be required by specific organisms in lesser amounts.

It is becoming increasingly evident that a multifaceted approach for quantifying habitability for the purposes of its study, taking into consideration the philosophical baggage that accompanies the term, is required in which several parameters are considered simultaneously to produce an index or metric for planetary habitability (e.g. Schulze-Makuch *et al.*., 2011). This work will, however, suggest that surface temperature must remain a primary measure of habitability at this stage in the evolution of the field despite its limitations, as the parameters required to calculate it (star size, planet semi-major axis, planet size) are more readily available to astronomers and exoplanet scientists and it therefore has the advantage of a degree of 'observability'.

As a primary filter, this measure remains a very effective means of readily dismissing planets with extremes of temperature from habitability surveys.

Furthermore, many of the other factors discussed above can be estimated, very roughly at least, with knowledge of the surface temperature of the planet due to the inherent interconnectedness of this fundamental parameter with other aspects of the planetary system: water availability, available energy, possible electron donors etc. However, complications arise when considering the composition of the interior of the planet (a possible subsurface habitable environment may exist several astronomical units outside of the 'traditional' circumstellar habitable zone), as well as that of the atmosphere of the planet of interest; at this stage, humanity does not have the technological capabilities to resolve the atmospheres of small, possibly terrestrial planets, and therefore simplifying assumptions have to be made. These assumptions will alter the habitability prognosis of any survey, as the atmosphere is a key component of the planetary system: contributing a greenhouse or possibly an anti-greenhouse effect, as on Titan for example, and allowing for the (bio)geochemical cycling of carbon and other potentially biologically-important elements through the planet system (McKay *et al.*, 1991). Given these reservations, surface temperature remains a key component of any habitability study, but other metrics should be considered alongside in order to develop a more coherent approach to habitability.

Given the potential output of the model herein described, the planet in question will be considered 'habitable' to first order when the global average temperature (GAT) falls between 273 K and 343 K. This upper limit (70 °C) was chosen as beyond this temperature chlorophyll biomolecules critical for photosynthesis degrade (Rothschild, 2007). Given the evidence laid out above, this range may still appear too conservative. However, excluding the survival of extremophiles, this 'liquid water temperature limit' encapsulates the habitats of most life on the planet. Setting an arbitrary 'habitable' limit when global average temperatures are 273 K may also be too limiting in terms of the stability of the climate, as a strong positive ice-albedo feedback will most likely result in an entirely glaciated planet up to a GAT of 278 K (Pierrehumbert, 2010). However, with no latitudinal dimension, options for including the ice-albedo feedback into this formulation effectively are fairly limited (Pierrehumbert, 2010).

Furthermore, extremophile organisms on Earth have been reported to endure temperatures extremes ranging between ∼-20 °C (253 K) and 122 °C (395 K) (Junge *et al.*., 2004; Takai *et al.*., 2008).

As mentioned above, surface temperature is not the only metric available to astrobiologists when assessing habitability and should not be taken in isolation when considering the complexities of the planetary system. However, caution is required when in applying metrics formulated around an 'Earth-similarity' framework as this approach seems unnecessarily terracentric, and neglects the possibility of planets with different habitable regimes (ocean-covered planets, subsurface habitability etc.), or those that are possibly 'more habitable' than the Earth itself; so-called 'superhabitable worlds' (Heller & Armstrong, 2014). This supplants the binary division of habitable and uninhabitable, but illustrates the point that a comparison between the habitability of any two planets can only take place relative to an agreed metric, for example surface temperature, the carrying capacity of the planet, or biological diversity.

1.1.9 Photosystem Limits to Habitability

Further to temperature, the ability of a planet to support a biosphere depends on its ability to host primary producers at the base of the planetary trophic pyramid. Photosynthetic primary producers on Earth require atmospheric carbon dioxide to bind with water to produce organic compounds to fuel respiration, producing oxygen as a by-product of this process, and low levels of atmospheric CO_2 will inhibit these organisms' metabolic function, and by implication, also effect levels of atmospheric oxygen crucial to the metabolism of eukaryotic organisms (including humans). Three biochemical pathways are used in photosynthetic carbon fixation: C4, C3, and crassulacean acid metabolism (CAM) photosynthesis. C3 carbon fixation is comparatively more ancient than both the C4 and CAM pathways, originating during the Paleozioc era. It is also more common, representing the primary carbon fixation mechanism of ∼95% of Earth's plant biomass. It seems likely that CAM photosynthesis also evolved in early vascular plants, and today is found in xerophytic organisms

under high temperatures and extreme water stress - as it is more efficient at conserving water - as well as some species of aquatic macrophytes (Keeley & Rundel, 2003). C4 photosynthesis is a relatively more recently evolved process, arising sometime during the Oligocene (25 - 32 million years ago; the specific timing is contentious), but becoming well established only 4 - 7 million years ago (Keeley & Rundel, 2003; Osborne & Beerling, 2006). C4 photosynthesis has a competitive advantage in conditions of water limitation, high temperatures and CO_2 and nitrogen deficits, and is characterised by an efficient CO_2 concentrating mechanism, which results in proportionally greater photosynthetic efficiency in these conditions (Osborne & Beerling, 2006). This pathway is restricted to flowering plants, including human food crops such as maize, millet and sugar cane, and is found in approximately 3% of photosynthesising plant species (Keeley & Rundel, 2003). However, these organisms dominate in contemporary tropical savannah environments, and are therefore estimated to represent $\sim$30% of terrestrial carbon fixation (Osborne & Beerling, 2006).

The effect of terrestrial and aquatic photosynthetic organisms on the biogeochemical history of this planet cannot be overstated. They are primary producers, representing the base of the global trophic web, and their existence has undeniably and fundamentally altered the composition of the atmosphere; for example, the evolution of oxygenic photosynthesis in cyanobacteria drove the 'great oxidation event' that occurred approximately 2.3 billion years ago, allowing for the emergence of the more energy efficient oxygen respiration mechanism that drives more complex organisms (Holland, 2006). Furthermore, biotic enhancement of weathering after the colonisation of the land surface during the Ordovician had significant implications for global carbon cycling.

It remains difficult, and would be unnecessarily speculative, to consider at this stage the existence of hypothetical extra-terrestrial metabolisms or sources of energy (gravitational, magnetic, electromagnetic, kinetic, radioactive, tectonic etc.) that preclude the need for photosynthesising primary producers, and therefore consider these organisms to be a fundamental feature of any potentially habitable planet: their co-evolution with the planet system driving and shaping processes on the planet surface

and atmosphere as they have done on Earth (Schulze-Makuch & Irwin, 2004). A further 'habitability limit' can therefore be defined, based the minimum level of atmospheric CO_2 required to drive C3 photosynthesis - approximately 150 ppm of CO_2 - and labelled as the 'photosystem limit' (Lovelock & Whitfield, 1982; Caldeira & Kasting, 1992; O'Malley-James *et al.*., 2013; O'Malley-James *et al.*., 2014). While this limit is ∼10 ppm for C4 plants, and as low as 1 ppm CO_2 for cyanobacterial carbon concentrating mechanisms, a conservative C3 limit is applied in most of the results to follow as this represents the large majority of plant species (>95%), but it should be noted that C4 carbon fixation accounts for ∼30% of global terrestrial productivity due to the dominance of C4 plant species in tropical and warm-temperate grasslands (Caldeira & Kasting, 1992; O'Malley-James *et al.*., 2013; Urban *et al.*, 2010).

A planet with similar geochemical process to those on Earth (i.e. a process analogous to a carbonate/silicate cycle) may therefore enter a complex, CO_2 depleted regime as atmospheric carbon dioxide is stripped from the air by increased drawdown due to the high solar influx and enhanced weathering associated with the end of a planet's life. A CO_2 crisis may then occur as temperatures are still within traditionally 'habitable' limits, but without primary producers undergoing (oxygenic) photosynthesis, the planet's ecological support systems will collapse: chemical cycling of many biologically important species would slow or stop and atmospheric oxygen would decline as oxygenic photosynthesis became increasingly inefficient under conditions of extreme CO_2 stress.

Theoretically, nominal C5/C6... photosystems able to sustain photosynthesis at much lower levels of atmospheric CO_2 than the 150 ppm C3- or 10 ppm C4-limit discussed here could exist. Furthermore, CO_2 dissolved in seawater may allow marine photosynthesisers to maintain biological productivity for longer than terrestrial organisms, resulting in a further spatiotemporal differentiation of habitable zones on the planet itself. Quantification of this limit remains beyond the scope of this work as it would require a more detailed parameterisation of aqueous/gas phase marine chemistry than possible in this model, but would be a potentially fruitful area for future study.

1.2 Habitability Criteria Used in this Work

The definition of 'habitability' used throughout this work will focus on temperature and carbon availability, the latter defined above as the photosystem limit. Future discussion of the term will, where relevant, be considered as a combination of both these factors and clearly stated as such. However, Chapter 2 was written and published in the peer-reviewed literature in 2013 at a stage when the photosystem limited had not yet been considered. Therefore, mentions of 'habitability' in Chapter 2 are purely temperature dependent. The 70 °C limit is chosen as beyond this temperature chlorophyll begins to degrade (Rothschild, 2007). Given the coupling of carbon availability and temperature in the combined consideration of habitability, this limit is a reasonable choice. Furthermore, results presented in Chapter 3 and 4 illustrate that due to the rapid runaway-greenhouse effect occurring at the end of a planet's habitable period, the difference in timing between average surface temperatures exceeding 70 °C and exceeding 100 °C, for example, is negligible.

1.3 Thesis Structure & Hypotheses

The first data chapter of this study will contain a more comprehensive overview of the concept of the stellar habitable zone and stellar evolution models, as well as providing a brief outline and critique of our current understanding of habitability. The second and third data chapters will go into more detail on the mechanics of planetary biogeochemical cycling, explored by describing the structure of a carbon cycle model adapted for this purpose, as well as the potential impact of these processes on long-term habitability.

Hypotheses

- The length of a planet's 'habitable period' is an important controlling factor on the evolution of intelligent observers.
- Planets discovered in orbit around other stars in the galaxy will have

habitable periods of different lengths relative to the Earth, and the duration of these habitable conditions can be estimated based on the orbital distance and from the evolution of their host stars.

- The operation of (bio)geochemical cycles on these exoplanets will affect the length of their habitable period.
  - The mass of the planet itself will control the length of habitable conditions.

2 Habitable Zone Lifetimes of Exoplanets around Main Sequence Stars

> We are like butterflies who flutter for a day and think it's forever.
>
> **Carl Sagan**
> *Cosmos* (1980)

The work presented in this chapter has been published in the peer-reviewed literature as:

Rushby, A.J., Claire, M.W., Osborn, H., Watson, A.J. (2013). Habitable Zone Lifetimes of Exoplanets around Main Sequence Stars. *Astrobiology* **13**(9) pp. 883 - 849

2.1 Abstract

The potential habitability [1] of newly discovered exoplanets is initially assessed by determining whether their orbits fall within the circumstellar habitable zone of their star. However, the habitable zone is not static in time or space, and its boundaries migrate outwards at a rate proportional to the increase in luminosity of a star undergoing stellar evolution, possibly including or excluding planets over the course of the star's main sequence lifetime. We describe the time that a planet spends within the habitable zone as its 'habitable zone lifetime.' The habitable zone lifetime of a planet has strong astrobiological implications and is especially important when considering the evolution of complex life, which is likely to require a longer residence time within the habitable zone. Here, we present results from a simple model built to investigate the evolution of the habitable zone over

[1] As this chapter was published several years before the finalisation of my thesis, the definition of 'habitability' used in this section is based purely on temperature.

time, while also providing estimates for the evolution of stellar luminosity over time in order to develop a 'hybrid' HZ model. These models return estimates for the habitable zone lifetimes of Earth and seven confirmed habitable zone-exoplanets and twenty-eight unconfirmed Kepler candidates. The habitable zone lifetime for Earth ranges between 6.29 and 7.79 $\times$ 10^9 years (Gyr). The seven exoplanets fall in a range between $\sim$1 and 54.72 Gyr, while the twenty-eight Kepler candidate planets' habitable zone lifetimes range between 0.43 and 18.8 Gyr. Our results show that exoplanet HD 85512b is no longer within the habitable zone, assuming it has an Earth analogue atmosphere. The habitable zone lifetime should be considered in future models of planetary habitability as setting an upper limit on the lifetime of any potential exoplanetary biosphere, and also for identifying planets of high astrobiological potential for continued observational or modeling campaigns.

2.2 Introduction

2.2.1 The Habitable Zone

Understanding the nature and distribution of planets and moons throughout the Galaxy that are able to sustain life is a major research theme identified by the NASA *Astrobiology Roadmap 2008* (Des Marais *et al.*, 2008). The study of planetary habitability encompasses research and methodological approaches from a wide variety of disciplines within the physical and environmental sciences. Reflecting this trend, a number of multi-parameter habitability indices, most closely analogous to those employed for ecological surveys, have been recently developed (e.g., Planetary Habitability Laboratory, 2012; Schulze-Makuch *et al.*, 2011) in an attempt to provide a quantitative framework for the assessment of the habitability of the ever-growing catalogue of extrasolar planets. Habitability metrics are useful diagnostic and comparative tools for investigating the potential for extrasolar planets to host life, and they allow for classification and comparison between exoplanets and Earth. Crucially, they are also valuable for prioritizing interesting planetary candidates for

future or continued observational campaigns. However, most indices described to date neglect the evolving nature of planetary habitability over astronomical and geological time.

The location of a planet within the circumstellar habitable zone is a measure that has been adopted to determine planetary habitability to first order (Kasting *et al.*, 1993; Selsis *et al.*, 2007). The habitable zone forms a fundamental component of many contemporary habitability metrics, and our understanding of the distribution and formation of habitable planetary environments strongly depends on the criteria used to set the boundaries of the habitable zone. Despite the integral role of planetary habitability in astrobiological research, the habitable zone remains a relatively rigid quantification of an inherently complex, multi-faceted problem.

The habitable zone (HZ) describes the circumstellar distance at which surface temperatures allow liquid water to be present on the planet surface, assuming variable $H_2O/CO_2/CH_4$ greenhouse forcings. The circumstellar HZ concept is based on Earth-analog terrestrial planets that exhibit dynamic lithospheric tectonic activity with magnetospheres, high ($\sim$80%) humidity, and 1 bar atmospheres of N_2, H_2O and CO_2 (Kasting *et al.*, 1993; Raymond *et al.*, 2007). The HZ has a minimum and maximum extent, forming inner (closer to the star) and outer boundaries that are set in part by biogeochemical climate feedback mechanisms and stellar luminosity (see figures 2.1 and 2.2).

The minimum extent, or inner boundary, is set by the water-vapour feedback mechanism, and the maximum, outer boundary is controlled by the operation of the carbon-silicate cycle (Kasting *et al.*, 1993). The water-vapour feedback describes a positive ('runaway') feedback mechanism that operates on a planet with liquid water at its surface, experiencing high rates of evaporation and increasing humidity. The resulting increase in temperature serves to further accelerate evaporation, eventually resulting in the irreversible evaporation of the ocean into the atmosphere (Kasting, 1988; Goldblatt & Watson, 2012). The outer boundary is set at the temperature at which CO_2 clouds first start to form in the atmosphere of a planet with a fixed 273 K surface temperature in the 'conservative' model

used by Kasting *et al.* 1993. The radiative effects of these clouds are complex and likely wavelength-dependent, and their effect on climate has not yet been well constrained (Colaprete & Toon, 2003; Goldblatt & Zahnle, 2011; Joshi & Haberle, 2012; Kitzmann *et al.*, 2010; Zsom *et al.*, 2012). Selsis *et al.* (2007) attempted to reconcile this effect by considering these clouds as purely reflective, albedo features. However, it is also possible that CO_2 clouds may have the additional effect of reflecting outgoing thermal radiation back to the surface of the planet, contributing to a net warming effect (von Bloh *et al.*, 2007). More sophisticated climate modelling approaches are required to fully constrain the complex effect that clouds, in atmospheres of varying compositions, will have on planetary climate under different stellar environments.

The carbon-silicate cycle is fundamental in determining the CO_2 mixing ratio of the atmosphere, and active plate tectonics and volcanism are necessary for this biogeochemical cycle to operate (Sleep & Zahnle, 2001). However, it is possible that more massive 'super-Earths' may exhibit an entirely different mode of thermal evolution due to the fact that they are likely to have internal pressures tens of times higher than those found in Earth's interior, large viscosities, and higher melting temperatures (Kite *et al.*, 2009; Stamenkovi *et al.*, 2012). Some studies suggest that the greater shear stresses and thinner plates thought to be associated with planets of higher masses will favour subduction by decreasing the overall resistance to plate motion (Valencia et al., 2007). Others maintain that a 'stagnant lid' or episodic tectonic regime may be a more realistic assumption because of a modelled reduction in the ratio of driving to resistive forces and increased fault strength under high gravity (ONiell & Lenardic, 2007). Further modelling and eventual observation of exoplanet atmospheres and/or interiors will settle this debate with time.

The existence of surficial liquid water is thought to be a fundamental prerequisite for the emergence and continued survival of life because of its important role as a solvent for biochemical reactions. In addition, water is available in appreciable amounts across the Galaxy and in interstellar clouds (Lammer *et al.*, 2009). Water is also present in significant quantities in comets and protoplanetary bodies; delivery of the water reservoir of

Earth is thought to have been via impact with similar, water-rich objects during the early, violent stages of planetary accretion (Lammer *et al.*, 2009; Raymond *et al.*, 2007). The existence of liquid water also requires planetary temperatures to be within the range expected to be optimal for life.

2.2.2 On the Definition of the 'Habitable Zone'

Throughout this paper, we use the seminal HZ study of Kasting *et al.* (1993) and the Selsis *et al.* (2007) extension of this work, but it should be recognized that this definition is one of many and is applicable only under the assumptions of 'Earth-like' planetary mass and composition, tectonics, and atmospheric pressure and composition. The planets in our sample are unlikely to conform to all these conditions, and these restrictions should be considered when interpreting our results. To date, a true Earth analogue planet has not been detected.

The concept of a 'habitable zone' is continuously evolving, from the original form to subsurface and tidal habitable zones (Barnes *et al.*, 2012; Heller *et al.*, 2011), dry planet habitable zones (Abe *et al.*, 2011), and even possible galactic habitable zones (Lineweaver *et al.*, 2004). Pierrehumbert & Gaidos (2011) provided an alternative definition of the HZ that extends to larger distances than the Earth-analog HZ of Kasting *et al.* (1993) for exoplanets with primordial hydrogen-rich atmospheres, and the possibility of ejected 'rogue' planets in interstellar space has also been considered (Abbot & Switzer, 2011). A detailed summary of the factors affecting exoplanetary habitability can be found in Seagar (2013).

Kopparapu *et al.* (2013) made further revisions to the Kasting *et al.* (1993) model, using a 1-D radiative-convective model, and results suggest an inner boundary of the habitable zone further from the star. We expect that many more habitable zone models of varying complexity will be developed in the future as understanding of this area advances; our aim is to provide a model framework that can be applied to any radiative habitable zone model by coupling luminosity evolution with HZ boundary transition rates to return a habitable zone lifetime estimate. Additionally, we focus on stellar-based

habitable zone estimations because they can provide a certain degree of observability that other parameterizations cannot; direct measurements of stellar luminosity can be made and theories regarding stellar evolution and effective temperature are well developed in the astronomical literature.

While the definition of the HZ boundary will continue to be refined with further research, these uncertainties are not the focus of this study. Regardless of the definition used to identify their particular position in space, the boundaries of a radiative habitable zone are unequivocally not temporally static, but rather they vary over astronomical time as a function of the secular increase in luminosity of a star undergoing stellar evolution (Claire *et al.*, 2012; Kasting *et al.*, 1993). As a star evolves through the main sequence, its luminosity increases and the boundaries of the habitable zone 'migrate' outwards at a rate proportional to this increase. The effect that this well-known and uncontroversial process has on the evolution of the habitable zone has not been well quantified, and the accelerating discovery of habitable planets necessitates its estimation. As planets move out of, or into, the habitable zone over the course of a star's main sequence lifetime, the time that any particular planet spends within the HZ can then be defined as its habitable period or 'habitable zone lifetime.' The habitable zone lifetime of a planet is especially important when considering the potential for the evolution of complex life, which is likely to require a longer residence time within the habitable zone (Watson, 2008).

Towards the end of a planet's habitable zone lifetime, steadily increasing stellar luminosity is likely to result in a runaway greenhouse event, which would represent a catastrophic and terminal extinction event for any surface biosphere present on the planet (Goldblatt & Watson, 2012; Pierrehumbert, 2010). The end of a planet's habitable zone lifetime and the end of its host star's main sequence lifetime do not necessarily have to coincide. For example, the Sun is likely to become a red giant several billion years after the likely cessation of habitable conditions on Earth. Estimations for the termination of Earth's biosphere have been calculated by other workers who used models optimized for this planet; we attempt a more general, flexible, and stellar-centred approach that can be applied to both Earth and to extrasolar Earth-analogues (Caldeira & Kasting, 1992; Franck *et al.*, 2000;

Goldblatt & Watson, 2012; O'Malley-James *et al.*, 2013).

2.3 Methods

2.3.1 Stellar Evolution Models

The basis of this habitable zone lifetime model is derived from an estimated 'transition rate' of the dynamic habitable zone boundaries over the course of stellar evolution, from the Zero Age Main Sequence (ZAMS) (Figure 2.1) to the Termination of the Main Sequence (TMS) (Figure 2.2) configurations. Main sequence lifetime is denoted as τ in the following sections, and stellar mass normalized to the Sun, where $1\mathrm{M}_{\odot} = 1$ solar mass.

2.3.2 Luminosity Evolution

The rates of transition of the habitable zone's boundaries are proportional to the change in stellar luminosity over the star's lifetime. In the first iteration of this model, this secular increase in stellar luminosity over time (ZAMS to TMS) was assumed to be linear to first order. While a relatively justifiable assumption for a model of this complexity, we felt that more realistic tracks of luminosity over time were required to better capture the non-linear nature of early and late stellar evolution. Therefore, we used a multi-dimensional (3 by 5) polynomial fit to determine luminosity (L) as a function of both mass (M) and time (τ). Luminosity is measured in solar units, where $L = 1$ is equivalent to the current luminosity of the Sun, given as 3.846×10^{26} W.

Baraffe *et al.* (1998) created stellar evolutionary models across the 0.075 to 1.0 $\mathrm{M}_{\odot}$ and an age range spanning 0 to 12.6 Gyr. These models produced values for effective temperature (T_{eff}), surface gravity (log g), and absolute bolometric magnitude (M_{bol}). Although the authors varied metallicity ([M/H]) and helium mass fraction (Y), we held [M/H] constant at solar values (0.0) and Y at 0.275.

Luminosity was calculated by using both the log g and bolometric

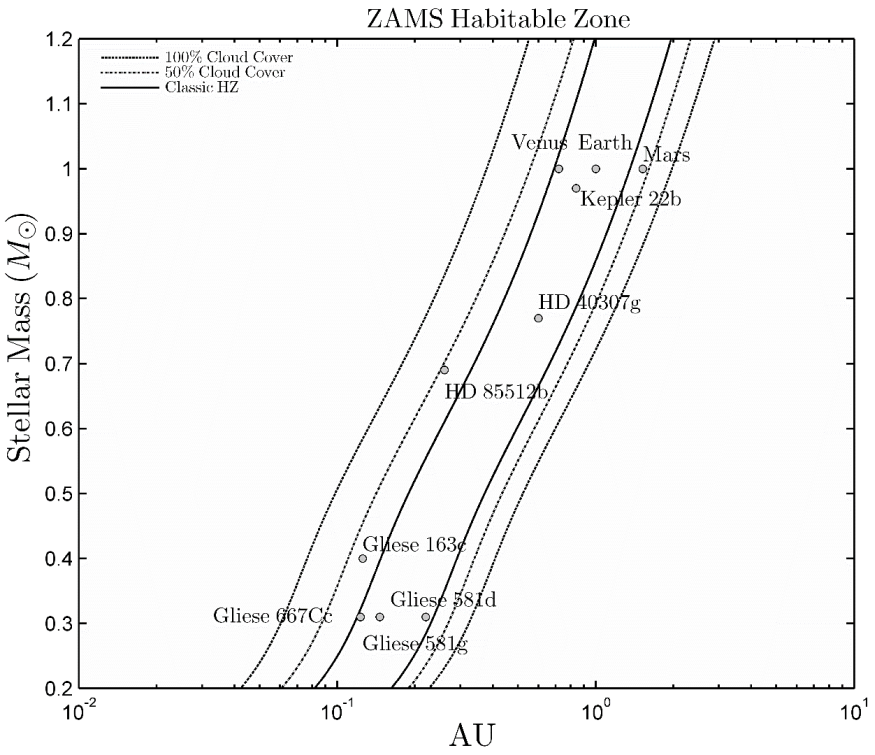

Figure 2.1: The position of the habitable zone (HZ) at the zero-age main sequence (ZAMS) stage of stellar evolution as a function of stellar mass. Earth and seven confirmed habitable zone exoplanets are also plotted, along with Mars and Venus as proxies for distance in the solar system. The outer dashed lines represent a 100% cloud cover scenario, the dotted lines 50% and the solid lines the 'classic' HZ.

magnitude values:

$$L_{M_{Bol}} = 10 \left(\frac{4.75 - M_{bol}}{2.5} \right) \tag{2.1}$$

$$L_{log_g} = 4\pi \left(\frac{GM}{10^{logg}} \right) \sigma T^4 \tag{2.2}$$

These values agreed to within 2%, and a mean luminosity was calculated by taking an average to provide L_{mean}.

The Baraffe model begins pre-main sequence where the continued collapse

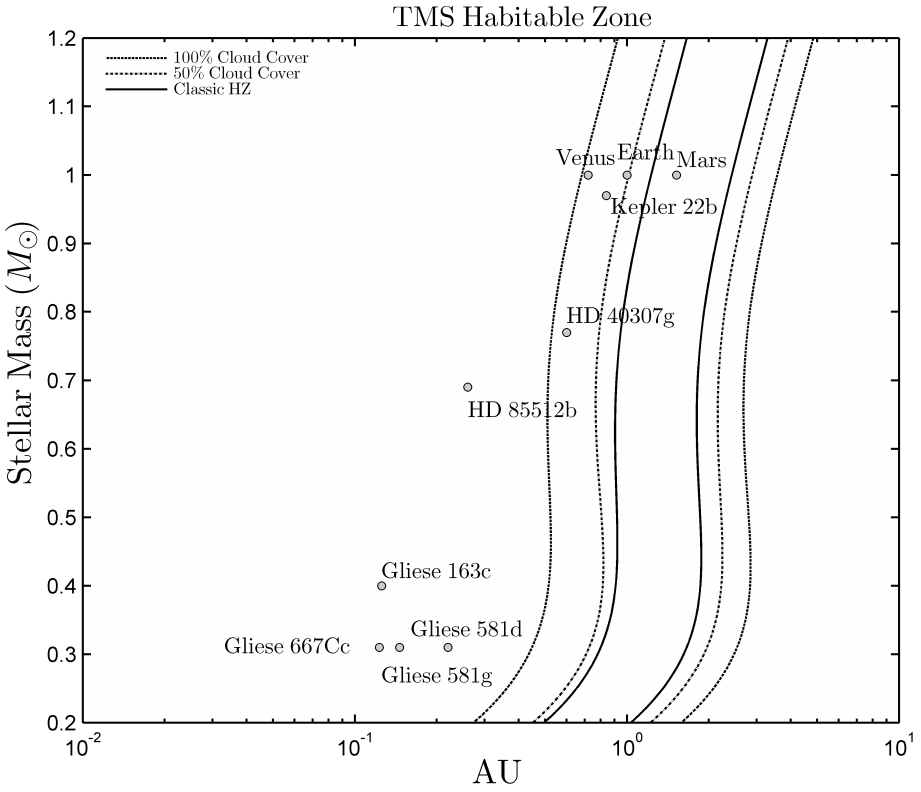

Figure 2.2: The position of the habitable zone (HZ) at the termination of the main sequence (TMS) stage of stellar evolution as a function of stellar mass

as set out by the Henyey and Hayshi tracks cause a decrease in luminosity. This is especially prominent in low-mass stars, which do not settle onto the main sequence for up to 1 Gyr. By estimating the point at which the star's luminosity became stable, we removed this initial decrease in order to fit curves to the main sequence regions.

We plotted polynomials to the data, but initial results represented the low-mass regions of the data poorly, and so the data was split by mass at 0.45 $M_\odot$:

$$L(M,\tau) = p_{00} + p_{10}\tau + p_{01}M + p_{20}\tau^2 + p_{11}\tau M + p_{02}M^2 + p_{21}\tau^2 M + p_{12}\tau M^2$$

$$+ \ p_{22}\tau^2 M^2 \ + \ p_{13}\tau M^2 \ + \ p_{04}M^4 \quad (2.3)$$

p_{00}	p_{10}	p_{01}	p_{20}	p_{11}	p_{02}
-0.0009502	0.0001695	-0.001583	-4.403 $\times 10^{-6}$	-0.003114	0.2553
p_{21}	p_{12}	p_{03}	p_{22}	p_{13}	p_{04}
6.739 $\times 10^{-5}$	0.01549	-0.6876	-0.0002243	-0.01762	0.9136

Table 2.1: Elements of the fitting matrices for 0.08 $\geq$ Mass ($M_\odot$) $<$ 0.45 and $0 > \tau$ (Gyr) $<$ 12.6

p_{00}	p_{10}	p_{01}	p_{20}	p_{11}	p_{02}	p_{21}	p_{12}
-2.245	0.7376	16.03	-0.02348	-4.596	-44.2	0.1212	10.5
p_{03}	p_{22}	p_{13}	p_{04}	p_{23}	p_{14}	p_{05}	
59.23	-0.2047	-10.43	-38.59	0.1132	0.9136	3.82	10.46

Table 2.2: Elements of the fitting matrices for 0.45 $\geq$ Mass ($M_\odot$) $<$ 1 and $0 > \tau$ (Gyr) $<$ 12.6

$$L(M,\tau) = p_{00} + p_{10}\tau + p_{20}\tau^2 + p_{11}\tau M + p_{02}M^2 + p_{21}\tau^2 M + p_{12}\tau M^2$$

$$+ \ p_{22}\tau^2 M^2 + p_{13}\tau M^2 + p_{04}M^4 + p_{14}\tau M^4 + p_{05}M^5 \quad (2.4)$$

The fits were corrected by to conform to 1 $M_\odot$ = 1 $L_\odot$ at τ = 4.54 Gyr, and were linearly extended to L_{TMS} with figures from Guo *et al.* (2009), as shown in Figure 2.3 and Table 2.3.

To approximate main sequence lifetime (τ) in Gyr as a function of stellar mass, we used the 2012 online update to the Dartmouth Stellar Evolution Database to obtain isochrones for low mass stars (using solar parameters) at 4.56, 10, and 15 Gyr (modelled) (Dotter *et al*, 2008). As expected for the lower mass stars with minimal luminosity evolution, the mass-luminosity relations for each isochrone were nearly identical and are fitted by:

$$L(M) = 0.1155\left(\frac{M}{M_\odot}\right)^{1.9513} \quad (>0.08<0.42M_\odot) \quad (2.5)$$

$$L(M) = 0.9455\left(\frac{M}{M_\odot}\right)^{4.7772} \quad (>0.42<0.8M_\odot) \quad (2.6)$$

Where we have used the 10 Gyr isochrones to make the fits. The fits for

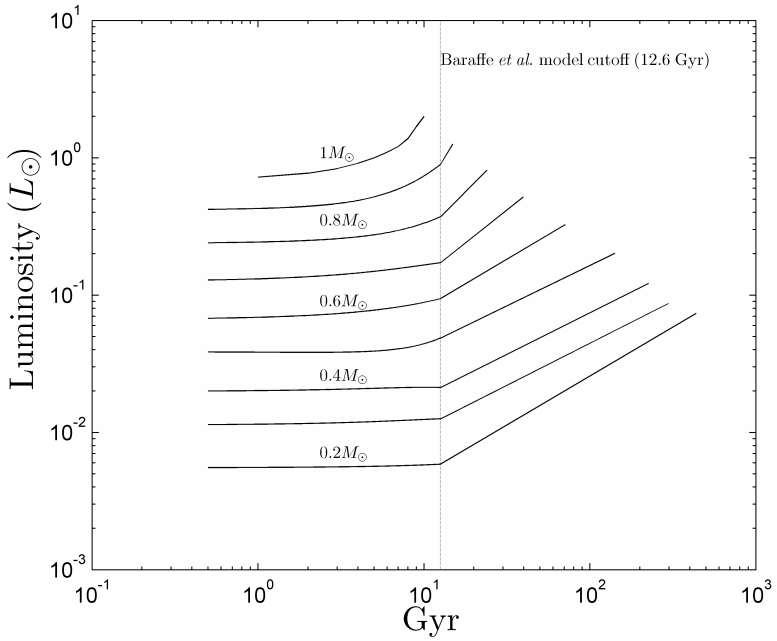

Figure 2.3: Main sequence luminosity as a function of stellar mass (at 0.1 $M_\odot$ intervals) and time. From 1 to ∼12.6 Gyr, luminosity evolution was modelled by using equations 2.3 and 2.4 (above), and extended linearly to L_{TMS} at τ

K-class stars (0.42 to 0.8 $M_\odot$) provided here are the result of the normalization of the multiplicative factors after the initial fitting to ensure that the parameterizations remain continuous at the overlaps between the mass classes. For higher mass stars (0.8 to 1.2 $M_\odot$), we have adopted a simple scaling (Nebojsa, 2004):

$$L(M) = \left(\frac{M}{M_\odot}\right)^4 \ (>0.8<1.2M_\odot) \tag{2.7}$$

We can then compute main sequence lifetimes in the zeroth order manner:

$$L(M) = 10.9 \times \left(\frac{M}{L}\right) \tag{2.8}$$

Where τ is in Gyr, 10.9 is the solar main sequence lifetime and L(M) are in the age ranges above (Sackmann, 1993).

These estimates of main sequence lifetimes are shown in Table 2.3 and Figure 2.4. For the lowest mass stars (0.08 to 0.25 $M_{\odot}$), this procedure results in main sequence lifetimes from 350 to 1000 Gyr and returns comparable values to those of Laughlin (1997), within an order of magnitude. Our results are likely to be less robust as they are not direct computations from observational data, but we used our fitted main sequence lifetimes for consistency as there are no comparable calculations of main sequence lifetimes for stars between 0.25 and 0.5 $M_{\odot}$.

Table 2.3 provides values of luminosity at 12 Gyr (L_{12Gyr}), which represents the final data from the Baraffe et al. (1998) stellar evolution model, luminosity at the end of the main sequence (L_{TMS}) from Guo *et al.* (2009), and main sequence lifetime (τ), computed as shown above.

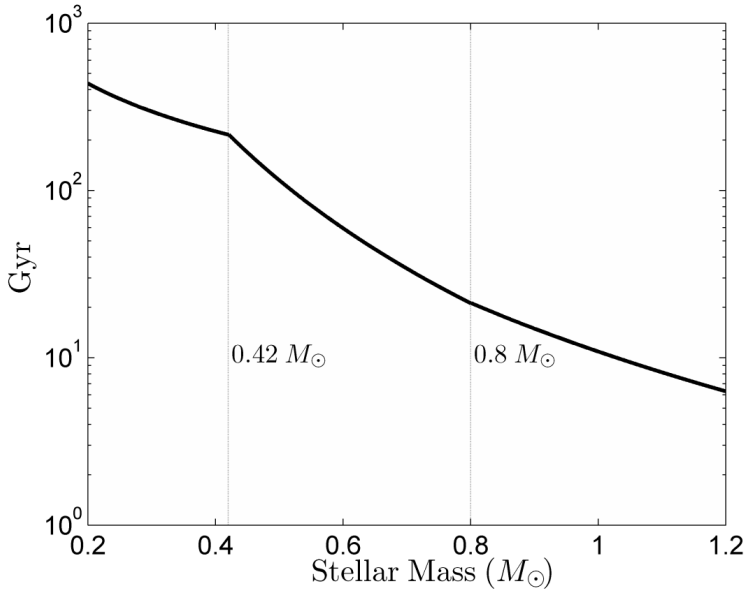

Figure 2.4: Main Sequence Age as a function of stellar mass for stars between 0.2 and 1.2 $M_{\odot}$. Between 0.08 and 0.42 $M_{\odot}$, see equation 2.5. Between 0.42 and 0.8 $M_{\odot}$ equation 2.6 is used, and equation 2.7 governs the relationship between the mass range 0.8 and 1.2 $M_{\odot}$.

Between 0.2 and 0.9 $M_{\odot}$,the Baraffe dataset allows for polynomial fits of L(, M) between ∼0.5 and 12 Gyr. Solar mass (1 $M_{\odot}$) fits extend to 8 Gyr. However, many low mass stars have main sequence lifetimes an order of magnitude greater than this upper limit. Accordingly, we used the initial

Mass ($M_\odot$)	$L_{12Gyr}(L_\odot)^a$	$L_{TMS}(L_\odot)^b$	τ(Gyr)
0.2	0.0051099	0.073602	436.3
0.25	0.0081265	0.081851	352.8
0.3	0.011746	0.086928	296.7
0.35	0.015975	0.098572	256.2
0.4	0.020817	0.12201	225.6
0.45	0.025177	0.15688	210.4
0.5	0.038696	0.20191	141.3
0.6	0.070764	0.3262	71
0.7	0.13689	0.51758	39.6
0.8	0.3292	0.813	23.9
0.9	0.8181	1.2576	14.9
1	—	2.28	10.9
1.1	—	3.1	8.2
1.2	—	4.25	6.3

[a]Baraffe *et al.* (1998), [b]Guo *et al.* (2009)

Table 2.3: Luminosity at 12 Gyr (L_{12Gyr}), luminosity at the end of the main sequence (L_{TMS}) and main sequence lifetime (τ) for stars between 0.2 and 1.2 $M_\odot$

polynomial fits between $0.5 > \tau < 12$ ($0.5 > \tau < 8$ Gyr for 1 $M_\odot$), and assumed a linear progression to the final L_{TMS} stage to produce a 'hybrid' track of L, where L_{TMS} is given by Guo et al. (2009), and τ_{TMS} is given by equations 2.5 to 2.8, normalised to $\tau_{Sun} = 10.9$ Gyr.

2.3.3 Determining the Habitable Zone

The inner and outer boundaries of the radiative habitable zone are set by the limit of the water-vapor feedback mechanism and the CO_2 condensation limit, respectively. These boundaries are computed from fits to 1-D radiative-convective climate models applied to an 'Earth-like' atmosphere of $CO_2/H_20/N_2$ (Kasting *et al.*, 1993). Whilst these early estimates are developed with implicit knowledge of the stabilising mechanism of the carbonate-silicate cycle, an explicit carbon cycle is not included in these formulations; the focus of these investigations is atmospheric dynamics computing a water loss and CO_2 condensation based on absorption and scattering coefficients in a N_2 dominated, cloud-free, isothermal stratosphere, with 300 ppm CO_2 and no O_2 or O_3. The inner boundary of

the climatic HZ for a star with a given luminosity and effective stellar temperature, T_{eff} (in Kelvin), can be calculated by according to the work of Jones *et al.* (2006):

$$HZ_{inner} = \left(\frac{L}{S_{in}(T_{eff})} \right)^{0.5} \tag{2.9}$$

Where the critical stellar flux at the inner boundary of the HZ, $S_{in}(T_{eff})$, dependent on the T_{eff} of the star, is given as a second order polynomial:

$$S_{in}(T_{eff}) = (4.190 \times 10^{-8}\, T_{eff}^2) - (2.139 \times 10^{-4}\, T_{eff}) + 1.296 \tag{2.10}$$

Luminosity, stellar radius, and effective temperature are related according to the StefanBoltzmann law:

$$L = 4\pi R^2 \sigma T_{eff}^4 \tag{2.11}$$

Where σ is the Stefan-Boltzmann constant, given as 5.67×10^8 J s^{-1} m^{-2} K^{-4} and R is stellar radius.

Jones *et al.* (2006) went on to define the outer limit of the HZ as:

$$HZ_{outer} = \left(\frac{L}{S_{out}(T_{eff})} \right)^{0.5} \tag{2.12}$$

The critical stellar flux at the outer boundary of the HZ, $S_{out}(T_{eff})$, is given by:

$$S_{in}(T_{eff}) = (6.190 \times 10^{-9}\, T_{eff}^2) - (1.139 \times 10^{-5}\, T_{eff}) + 0.2341 \tag{2.13}$$

To ascertain the luminosity of a given star at ZAMS and TMS, it is necessary to invoke a number of formulae and fitting coefficients, taken from table 1 of Guo *et al.*,(2009).

Due to the relative uncertainties regarding the mechanisms that control the actual extent of the habitable zone, especially the ambiguous hot zone/inner boundary transition, we have also used the HZ boundary estimations outlined by Selsis *et al.* (2007) to consider the effect of 50 and 100% cloud cover regimes, given by:

$$HZ_{inner} = (HZ_{inner\odot} - \alpha_{in}T_*^2 - b_{in}T_*^2)\left(\frac{L}{L_\odot}\right)^{0.5} \tag{2.14}$$

$$HZ_{outer} = (HZ_{outer\odot} - \alpha_{out}T_*^2 - b_{out}T_*^2)\left(\frac{L}{L_\odot}\right)^{0.5} \tag{2.15}$$

Here, $\alpha_{in} = 2.7619 \times 10^{-5}$, $b_{in} = 3.8095 \times 10^{-9}$, $\alpha_{out} = 1.3786 \times 10^{-4}$, $b_{out} = 1.4286 \times 10^{-9}$, and $T_* = (T_{eff} — 5700\ K)$. Fifty percent cloud cover boundaries are set by the authors as $HZ_{inner\odot}$= 0.68 to 0.76 AU (mean: 0.72 AU) and $HZ_{outer\odot}$= 1.67 AU. The boundary for a 100% cloud cover HZ is $HZ_{inner\odot}$= 0.46 to 0.51 AU (mean = 0.49 AU) and $HZ_{inner\odot}$= 2.4 AU. Equations 2.14 and 2.15 provide a similar result to 2.9 and 2.12 under a ∼30% cloud cover scenario, but for the purposes of this study and for consistency, we maintain the classical HZ as defined by 9 and 12, and utilize 8 and 9 for testing varying cloud cover regimes only (Selsis *et al.*,2007). We note, however, that the 'cloud cover' included in this model is justifiably parameterized as an albedo (i.e., reflective) feature, and not the result of modeling the multi-parameter effect of water vapour or CO_2 clouds on climate over long timescales. We adopt the nomenclature of Lammer *et al.* (2009) and designate planets within these near-inner or outer boundary zones of the habitable zone as Class II habitable planets. Class I planets are those that fall within the classical HZ, as given in 2.9 and 2.12.

2.3.4 Habitable Zone Boundary Transition Rates

As discussed in the previous section, two estimations of the change in L over time can be used to model the change in the habitable zone over time: one hybrid fit (polynomial fit for $L(M,\tau)$ to L_{12Gyr} coupled with a linear

extrapolation to L_{TMS}) and the other purely linear (simply L_{TMS} - L_{ZAMS}/τ).

It is then possible to attain a 'transition rate' of the inner and outer boundaries (denoted by μ_{inner} and μ_{outer} respectively) of the habitable zone for main sequence stars between 0.2 and 1.2 Solar Masses (M_{odot}) by using a simple linear relationship:

$$\mu_{inner} = \frac{\left(HZ_{inner}^{TMS} - HZ_{inner}^{ZAMS}\right)}{\tau} \tag{2.16}$$

$$\mu_{outer} = \frac{\left(HZ_{outer}^{TMS} - HZ_{outer}^{ZAMS}\right)}{\tau} \tag{2.17}$$

Our results are presented in AU Gyr^{-1} in Figure 2.6. The terms HZ_{inner}^{TMS} and HZ_{inner}^{ZAMS} describe the distance (in AU) of the position of the inner boundary of the HZ at the Termination of the Main Sequence (TMS) and the Zero Age Main Sequence (ZAMS) stages of stellar evolution, and are related to the values for L_{ZAMS} and L_{TMS} given in the work of Guo *et al.* (2009) by equations 2.9 and 2.12. The corresponding terms in 2.17 relate to the outer boundary. Stars with masses less than 0.2 $M_{\odot}$ have been excluded as it is unlikely that the mass and metallicity of their circumstellar disks will be high enough to support the formation of planets above the habitable planet mass limit of 0.3 Earth masses ($M_{\oplus}$) (Raymond *et al.*, 2007).

The approach outlined above can then be used to provide an approximation of the gradual evolution of the habitable zone distance. The habitable zone transition rate can be used to estimate the habitable zone lifetime of a planet, which we consider to terminate at the stage at which the inner boundary of the HZ and the semi-major axis of the planet's orbit become identical, signalling its entry into the hot zone of the star:

$$\tau_h = \left(\frac{\alpha_{planet} - HZ_{inner}^{ZAMS}}{\mu_{inner}}\right) \tag{2.18}$$

Where α_{planet} denotes the semi-major axis. Substituting the outer transition

rate (μ_{outer}) and HZ_{outer}^{ZAMS} into 2.18 this technique can be used to estimate the transitional period, or pre-habitable phase, of a Class II habitable planet within the outer boundary zone, thereby effectively approximating its entry into the HZ area and initiating its habitable zone lifetime.

The more complex approach to this problem is to derive estimates for the change in the HZ boundaries over time by using the hybrid polynomial/linear relationship between luminosity, mass, and time (eqs. 3 and 4). This method produces well constrained ($r^2 > 0.99$) second-order polynomial fits between HZ distance and at 0.1 $M_{\odot}$ intervals. As before, attaining a value for the habitable zone lifetime (τ_h) can then be done by determining the value of τ when the HZ distance is identical to the semi-major axis of the planet of interest (α_{planet}).

Based on the predictions of other studies, the polynomial fits probably overestimate τ_h, while the linear fits are likely too conservative (Caldeira & Kasting, 1992; Goldblatt & Watson, 2012). The difference in the habitable zone lifetime that results are due to variations in the slope of the L(t) distribution and the behaviour of L in the early and late stages of the star's lifetime. This, however, translates into a significant dissimilarity in the rate of the habitable zone boundary transition rate and consequently the habitable zone. We have included results from both schemes where possible to act as upper and lower bounds of the habitable zone lifetime, and also to illustrate the errors and uncertainties associated with these calculations, originating from the strong control of the shape of the L(t) slope on the output. More research and better constraints of main sequence lifetime, as well as the change in luminosity over this period, are required to further reduce these uncertainties.

The model is calibrated for Earth, and therefore we assume 'Earth-like' conditions on the planets included in the test sample. These include Mars (or rather, an Earth-like planet at Mars' orbital distance) as well as seven exoplanets confirmed to be within the habitable zone of their stars by the online *Habitable Exoplanets Catalog* (HEC) maintained by the Planetary Habitability Laboratory at the University of Puerto Rico, Arecibo (PHL, 2012) as of 11 December 2012. These are: Kepler 22b, HD 85512b, HD

40307g, Gliese 163c, Gliese 667Cc, Gliese 581d, and Gliese 581g. We note that Gliese 581g and HD 40307g are considered 'planet candidates', and more data are required to definitively classify them as planets. Twenty-eight unconfirmed Kepler candidates, also identified to be orbiting in their stars' HZ by the HEC (figure 2.5), were also included in the results. We also note that the HEC utilizes the HZ model of Selsis *et al.* (2007), which includes the effect of reflective clouds mentioned previously.

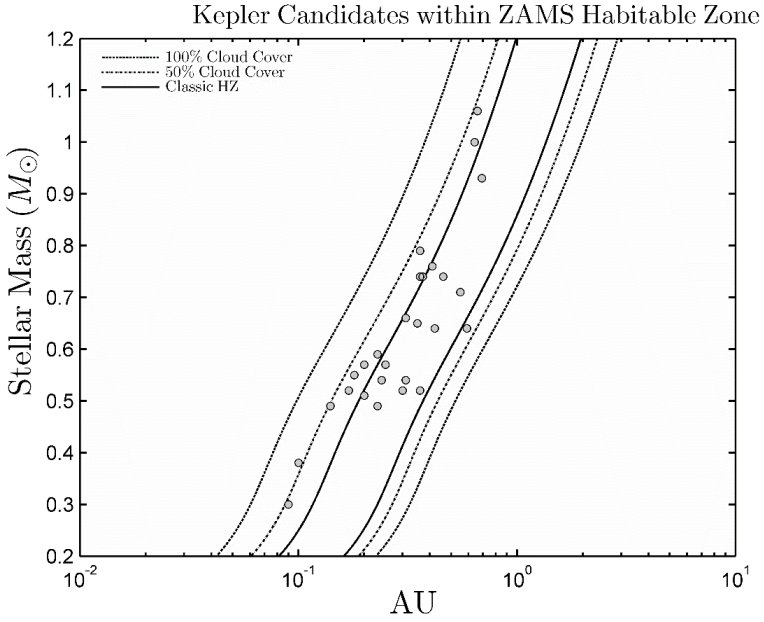

Figure 2.5: Position of 28 Kepler candidates within the ZAMS habitable zone. The outer dashed lines represent a 100% cloud cover scenario, the dotted lines 50% and the solid lines the 'classic' HZ.

2.4 Results

2.4.1 The Temporally Dynamic Habitable Zone

Equations 2.14 and 2.15 for the linear transition rate of the inner and outer habitable zone boundaries for stars between 0.2 and 1.2 $M_\odot$ over their entire main sequence lifetime are displayed in black in Figure 2.6. Inner boundary habitable zone transition rates (μ_{inner}) fall in a range between 9.5 $\times$ 10^{-4} to 1.06 $\times$ 10^{-1} AU Gyr $^{-1}$; outer transition rates (μ_{outer}) lie

between 2×10^{-3} and 2.1×10^{-1} AU Gyr^{-1}, depending on stellar mass. M- and K-type stars (>0.08 to 0.8 $M_{\odot}$) have lower rates of because of their long hydrogen-burning lifetimes relative to the G-class Sun, which experiences rates of μ_{inner} of approximately 5×10^{-3} AU Gyr^{-1} and μ_{outer} of 0.1×10^{-1} AU Gyr^{-1}. The outer HZ boundary exhibits a slightly more rapid rate of outwards migration under all mass classes relative to the inner boundary due to the proportionality between planetary effective temperature and distance from the star approximated by the inverse-square law. As stellar main sequence age has a strong control on μ, equations 2.5, 2.6, and 2.7 result in three distinct trends between mass classes: lower mass (0.2 - 0.43 $M_{\odot}$), mid-range (0.43 to 0.8 $M_{\odot}$), and higher mass (0.8 to 1.2 $M_{\odot}$) linear transition rates can be calculated with the second-order polynomials provided in table 2.4.

The grey lines shown in Figure 2.6 represent habitable zone transition rates when using the hybrid stellar evolution model described above, and also shown in Figure 2.3, for stars between 0.2 and 1 $M_{\odot}$ (at 0.1 $M_{\odot}$ intervals) between 0.5 and 12.6 Gyr of stellar evolution, as set by the Baraffe *et al.* (1998) model. This model does not take the full main sequence luminosity evolution of stars older than 12.6 Gyr into account, and therefore the results are less well constrained. Lower mass stars exhibit an order of magnitude slower transition rates under this scheme, with the effect becoming less pronounced with increasing mass.

$M_{\odot}$	μ_{inner}	μ_{outer}
0.2 - 0.43	-0.0108$M_{\odot}^2$ + 0.0189$M_{\odot}$ - 0.025	-0.0262$M_{\odot}^2$ + 0.0413$M_{\odot}$ - 0.053
0.43 - 0.8	0.0716$M_{\odot}^2$ - 0.0324$M_{\odot}$ + 0.0046	0.142$M_{\odot}^2$ - 0.0642$M_{\odot}$ + 0.0094
0.8 - 1.2	0.4022$M_{\odot}^2$ - 0.6084$M_{\odot}$ + 0.2554	0.7877$M_{\odot}^2$ - 1.1894$M_{\odot}$ + 0.4995
All fits: $r^2 > 0.999$		

Table 2.4: Fitting equations for linear habitable zone transition rates (AU Gyr^{-1}) as a function of star mass.

Substituting these values into equation 2.18, it is possible to estimate the approximate habitable zone lifetime of a planet, where its semi-major axis (a) is known. The results are shown in figure 2.7. The two lines, denoted the 'Typical Habitable Zone lifetime', running through this figure are normalization factors produced by calculating the habitable zone lifetime of

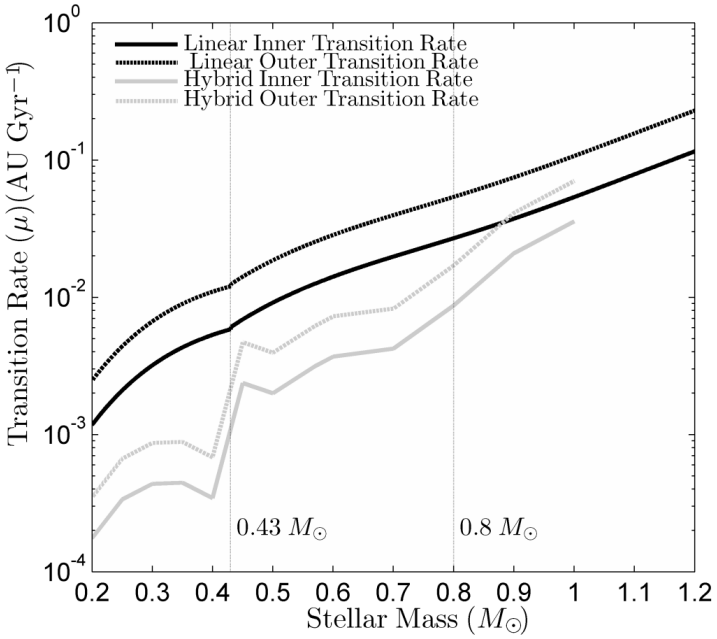

Figure 2.6: Radiative habitable zone boundary transition rates as a function of stellar mass in astronomical units (AU) per Gyr (10^9 years) when using the linear migration model (black lines) shown in equations 2.16 and 2.17, as well as the hybrid luminosity evolution model (grey lines) for the first 12.6 Gyr of stellar evolution.

a hypothetical planet formed directly in the center of the habitable zone at the ZAMS stage under each mass class considered, and under both the linear and hybrid version of the habitable zone lifetime model. They are included to illustrate the trend that planets orbiting smaller mass stars tend to have longer habitable zone lifetimes, when accounting for their relative location within the habitable zone. Note that the typical habitable zone lifetime for the linear L(t) relationship is significantly less than that of the typical habitable zone lifetime returned when using the hybrid L(t) fits due to lower rates of boundary transition shown in Figure 2.6. We have linearly extended the hybrid fit from 1 to 1.2 $M_{\odot}$. Individual deviations from this line illustrate a departure from the theoretical 'typical habitable zone lifetime' of the star system in time but also in space, as planets that form nearer the inner edge will have relatively shorter habitable zone lifetimes, irrespective of the lifespan of their star. Therefore, planets nearer the outer edge will plot above this line, while those nearer the inner edge

and hot zone will plot below. The exception to this is Mars, while not in the habitable zone at present, its future habitable zone lifetime (assuming Earth-like conditions) will be constrained by the main sequence lifetime of the Sun. The habitable zone lifetime of planets included in this plot follow the linear (more conservative) version of the model.

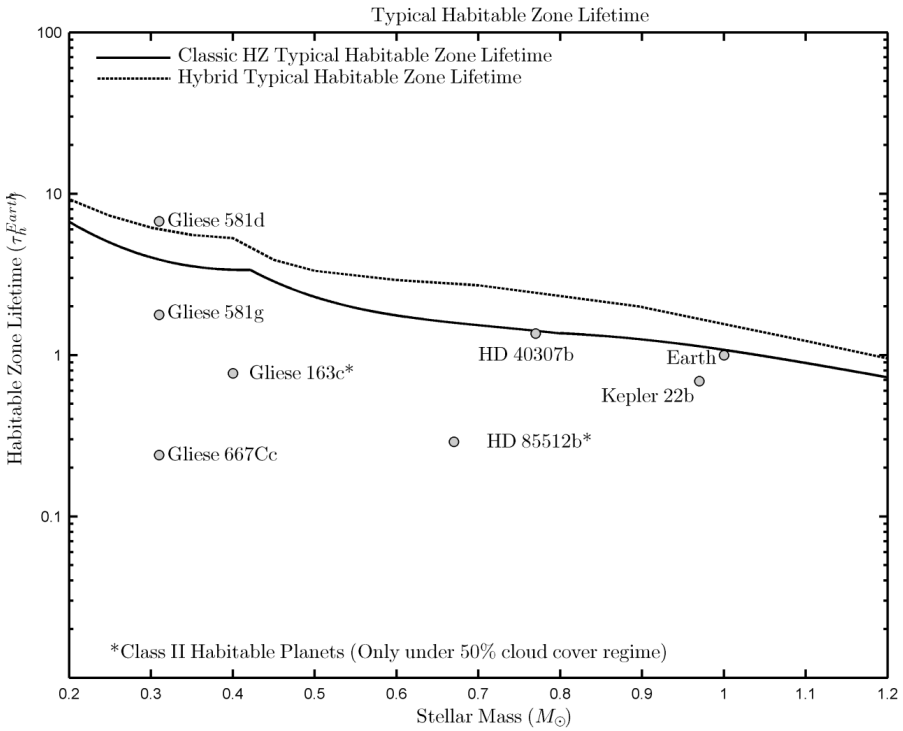

Figure 2.7: Habitable zone lifetime (τ_h) as a function of stellar mass, where τ_h is normalized to τ_h^{Earth} (6.29 Gyr). The 'typical habitable zone lifetime' lines running through the plot represent the habitable zone lifetime of a hypothetical planet that formed in the very center of the classical HZ at the ZAMS stage of stellar evolution under different stellar luminosity evolution models. Also plotted are Earth and seven habitable zone exoplanets. All planetary τ_h are based on the classical habitable zone and linear luminosity evolution, with the exception of HD85512 b and Gliese 163c which are both Class II habitable planets that can only be considered within the habitable zone under a 50% cloud cover regime

Unless stated, the figures provided for the planets and planetary candidates discussed below (and in figure 2.7) refer to the departure of a Class I habitable planet from the classical habitable zone (Lammer *et al.*, 2009). Where necessary, it is also possible to estimate the timing and duration of

the transition from the classical habitable zone to the uncertain inner boundary/hot zone, where planets require 50% or greater cloud cover to maintain habitable surface temperatures. The results of the following section are summarized in figure 2.9.

The linear L model predicts a total habitable zone lifetime for Earth (τ_h^{Earth}) of 6.29 Gyr, corresponding to a habitable-to-inhabitable transition occurring approximately 1.75 Gyr from present, taking the age of the planet as 4.54 Gyr. The hybrid L fit returns a τ_h^{Earth} of approximately 7.79 Gyr, the habitable zone lifetime terminating in 3.25 Gyr. The 1.5 Gyr difference between these estimates provides an upper and lower limit on the habitable period of the Earth. Similarly, Venus' habitable zone lifetime was on the order of 1.3 Gyr from ZAMS.

It should be noted that our approach in this case is primarily stellar, in that we focus on the evolution of main sequence stars rather than the biogeochemical processes that take place on a given planet in its orbit, which allows for application of this model to Earth-analog planets with otherwise unknown properties as a first-order assessment of their habitability through time. Therefore, we consider only the position of these planets in space and do not take into account other planetary characteristics that are certain to have bearing on their overall habitability, including planet mass, composition, tectonic and magnetic activity, or atmospheric and climatic conditions beyond those parameterized in the habitable zone model. These assumptions should be considered when interpreting the model results, which are intended to be presented along with other metrics to produce a more robust habitability index. Estimates provided by other workers (e.g., Caldeira & Kasting, 1992; Goldblatt & Watson, 2012) are on the order of 2 to 2.5 Gyr from present, due to the use of radiative transfer models of differing complexity and structure optimized for Earth's atmosphere. The results from a novel approach based on modelling the likely evolution of global biological community structure in response to increasing L adopted by O'Malley-James *et al.* (2013) suggest that unicellular life could persist in refugia on Earth 2.8 Gyr from present. Authors using a geodynamical approach have predicted the collapse of habitable conditions on Earth 1.4 Gyr from present (Franck et al., 2000).

However, under a regime of increasing solar luminosity, which is estimated to be 118% of the present-day value at 1.75 Gyr, we consider an irreversible runaway greenhouse scenario to be more likely (Goldblatt & Watson, 2012; Kasting, 1988).

Adopting the outer boundary transition rate of the solar habitable zone (μ_{outer}) as 0.1 AU Gyr^{-1}, the habitable zone for Earth-like planets will extend beyond the orbit of Mars approximately 1.57 (polynomial fit) and 1.66 (linear model) Gyr from present, and remain beyond 1.5 AU until the end of Sol's main sequence lifetime (τ_{Sol} = 10.9 Gyr), approximately 4.7 Gyr later (Nebojsa, 2004). Despite its residence in the habitable zone at this late stage in Sol's main sequence lifetime, it is unlikely that Mars will be 'habitable' as it has extremely low atmospheric pressure and limited geodynamics to power global geochemical cycling processes. We ignore the effect that Mars' complex orbital evolution, driven by its secularly increasing orbital eccentricity, may have on its future semi-major axis (Laskar *et al.*, 2004).

Super-Earth exoplanet Kepler 22-b has a slightly shorter τ_h of 4.31 Gyr ($\tau_h/\tau_h^{Earth} = 0.69$), or 6.11 Gyr ($\tau_h/\tau_h^{Earth} = 0.79$) when using the hybrid τ_h version, due to its analogous orbital (a = 0.84 AU) and parent star ($M_\odot$ = 0.97) characteristics. HD 40307 g, a Super-Earth or possibly Neptunian-sized exoplanet orbiting a K-class star with a mass of 0.77 $M_\odot$, has a relatively extensive habitable zone lifetime, estimated to be on the order of 8.6 Gyr ($\tau_h/\tau_h^{Earth} = 1.36$) to 14.2 Gyr ($\tau_h/\tau_h^{Earth} = 2.25$) (Barnes et al., 2009).

Orbital neighbors Gliese 581d and Gliese 581g exhibit markedly differing values of τ_h despite their shared red dwarf parent star ($M_\odot$ = 0.31) because of their disparate orbits. The existence of Gliese 581g remains unsettled to date, and more observations are required to definitively confirm the presence of the planet (Vogt *et al.*, 2012; Forveille *et al.*, 2011; Gregory, 2011; Tuomi, 2011). We have included it here as an interesting candidate with which to test the model; the results we present here make no attempt to confirm or validate the existence of the planet itself. While both planets in this system are in the ZAMS habitable zone, which extends from 0.119

to 0.23 AU, the innermost super-Earth planet Gliese 581 g ($a = 0.14$ AU), potentially the most habitable exoplanet found to date if confirmed, has a τ_h of 11.2 Gyr, approximately 5 Gyr longer than that of Earth ($\tau_h^{Earth} = 1.78$) (HEC, 2012). The polynomial $L(\tau)$ fit results in a substantially longer habitable zone lifetime of approximately 22.7 Gyr ($\tau_h^{Earth} = 2.94$). Because of its position nearer the outer edge of the classical HZ and the long main sequence lifetime of its star, Gliese 581 d ($a = 0.22$ AU) will remain in the HZ for 42.4 Gyr ($\tau_h^{Earth} = 6.74$) under the linear model and 54.7 Gyr ($\tau_h^{Earth} = 7.08$) when using the hybid fit, the longest τ_h of any exoplanet discovered to date.

Gliese 667Cc, also orbiting a 0.31 $M_\odot$ red dwarf, has a habitable zone lifetime of 1.5 Gyr ($\tau_h^{Earth} = 0.24$), due to its proximate orbit ($a = 0.123$), straddling the inner boundary of the habitable zone ($HZ_{inner}^{ZAMS} = 0.119$ AU). The polynomial L trend predicts a wider habitable zone for this star (HZ_{inner} at 0.5 Gyr = 0.109 AU), resulting in a longer habitable zone lifetime, on the order of 15.9 Gyr. The order-of-magnitude discrepancy between the linear and fitted habitable zone lifetimes for this planet remains difficult to reconcile; our initial conclusion is that the polynomial model performs poorly when considering very small distances between the semi-major axis of the planet and the inner boundary of the habitable zone, coupled with a different estimation of the initial HZ distance to that of the linear model.

HD 85512b ($a = 0.26$ AU, $M_\odot = 0.67$) and Gliese 163c ($a = 0.125$ AU, $M_\odot = 0.4$) represent complex cases and illustrate some of the uncertainty and weaknesses in our understanding of the complexities of the habitable zone. Orbiting near the highly ambiguous inner boundary/hot zone transition at ZAMS, these planets can only considered to be within the HZ under a 50% cloud cover scenario (see equation 2.8 and 2.9), and accordingly we would argue that their residence time within the HZ is uncertain (Keltenegger *et al.*, 2011). Following the work of Lammer *et al.* (2009), we designate HD 85512b and Gliese 163 c as Class II habitable planets (within the inner or outer edge of the habitable zone). Nevertheless, under the assumption of reflective cloud cover of at least 50%, the effective planetary temperature on HD 85512b and Gliese 163c may be within the bounds of habitability for 1.8

Gyr ($\tau_h^{Earth} = 0.29$) and 4.8 Gyr ($\tau_h^{Earth} = 0.77$) from ZAMS, respectively. These planets remain out of bounds of the hybrid polynomial L model, and HD 85512b will be subject to further discussion in the following section. We also chose to include 28 Kepler candidates in our sample to illustrate the ability for the model to compute habitable zone lifetimes for larger datasets and use candidates that display a broad range of host star masses (0.3 to 1.06 $M_\odot$) and orbital distances. We differentiated between Class I candidates ($n = 15$) in the more robust 'classical' HZ (i.e., 50% cloud cover) and Class II planets only considered to be habitable under a 50% and 100% cloud cover regime (Lammer *et al.*, 2009). Figure 2.5 illustrates the distribution of candidate planets throughout the habitable zone, twelve of which fall within the uncertain hot zone/inner boundary transition zone. The theoretically habitable zone lifetimes of these candidate planets fall within 0.47 and 23.2 Gyr, as shown in figure 2.8.

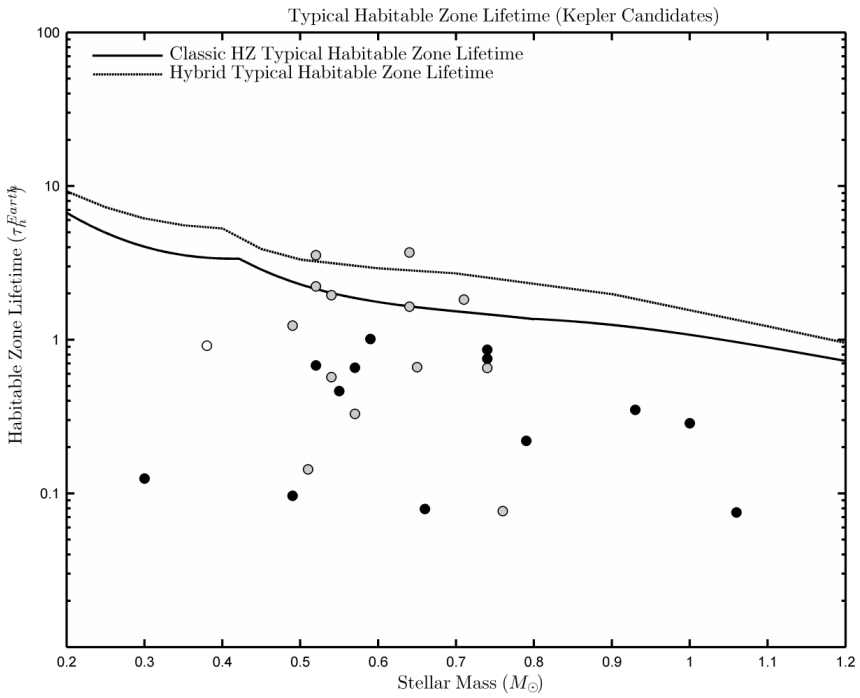

Figure 2.8: Habitable zone lifetime (τ_h) as a function of stellar mass, where τ_h is normalized to τ_h^{Earth} (6.29 Gyr), for 28 Kepler candidates detected within the habitable zone of their stars. We have differentiated between Class I planets (grey markers - within the classical HZ)($n = 15$), Class II planets (solid black markers - within the uncertain inner boundary/hot zone)($n = 11$) habitable only under a 50% cloud cover regime, and Class II planets (white marker) habitable only conditions of 100% cloud cover ($n = 1$) (see discussion for further commentary).

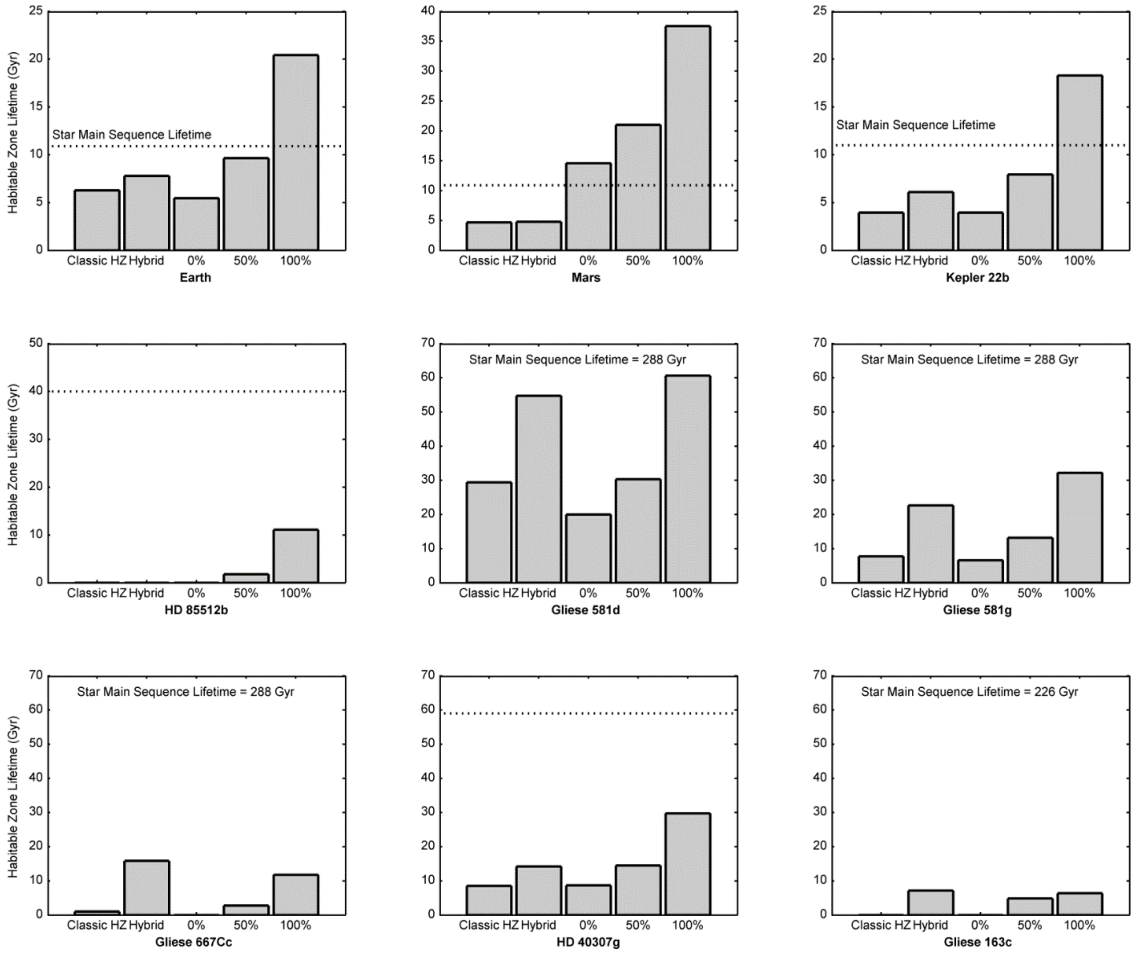

Figure 2.9: Habitable Zone Lifetimes for Earth, Mars and seven habitable zone exoplanets using differing habitable zone models. 'Classic HZ' refers to the radiative habitable zone advanced by Kasting *et al.* 1993 (equations 2.9 and 2.12), 'Hybrid' to the relationship outline in the previous section detailing the use of polynomial fits for $L(M_{\odot},\tau)$to 12.6 Gyr. 0%, 50% and 100% refer to the 0, 50 and 100% cloud cover regimes proposed by Selsis *et al.*,(2007) respectively.

2.4.2 Are These Planets Still in the Habitable Zone?

Arguably, the most useful practical application of this model is for ascertaining the absolute remaining habitable zone lifetime of an individual exoplanet when the age of their host star has been determined. For many of the planets contained in our sample, however, the ages of their stars are not well known. For example, the age of star Kepler 22 remains unknown to date, Gliese 667C has an age >2 Gyr, and the age of Gliese 163 remains very poorly constrained (HEC, 2012).

The age of Gliese 581 is estimated as 8 ± 1 Gyr, suggesting that both planet candidates remain with the HZ even under the more conservative classic HZ conditions (Selsis *et al.*, 2007). Similarly, star HD 40307 has an estimated age of ∼4.5 Gyr, suggesting that the planet HD 40307g is still within the habitable zone of its host star and will remain there for a further 4.1 Gyr under the classic HZ scenario (Tuomi *et al.*, 2013). Having orbited within the HZ of its host star (0.77 $M_{\odot}$) for a comparable time to that of the Earth, we suggest that this planet candidate makes for a very interesting subject for further study.

The age of HD 85512 is given as 5.61 ± 0.61 Gyr; however, some uncertainty also exists between the spectroscopic and isochrone data for this star resulting in a mass estimate of 0.69 ± 0.08 $M_{\odot}$ (Pepe *et al.*, 2011). Other workers also initially assessed the habitability of the planet HD 85512b, using the Selsis *et al.* (2007) model and returned a similar result to that presented above, placing the planet in the 50% cloud cover zone (Keltenegger *et al.*, 2011). However, it does not appear that they have considered the evolution of the luminosity of this star over its main sequence lifetime to date. Even given the mass and age range, and assuming an Earth-analogue atmosphere, our results suggest that HD 85512b is no longer in the habitable zone (except under 100% cloud cover) and has not been for several billion years. While the estimated semi-major axis of HD 85512b is 0.26 AU, the inner boundary of the habitable zone for a 0.65 $M_{\odot}$ star (lower estimate) with an age range between 5 and 6.22 Gyr is ∼0.36 and ∼0.38 AU respectively under the classic HZ scenario and 0.28 to 0.30 AU under 50% cloud cover regime. For the upper mass limit (0.73

$M_\odot$), the classical habitable zone inner limit is ∼0.47 AU at 5 Gyr and ∼0.48 AU at 6.22 Gyr, while the 50% cloud cover scenario returns limits of ∼0.32 and ∼0.33 AU, respectively.

The current measured luminosity of HD 85512 is 0.126 ± 0.008 $L_\odot$ (Pepe *et al.*, 2011). This value agrees well with our modelled luminosity ($L_\odot$ = 0.1256) for a star of this age (5.61 Gyr) if its mass is ∼0.67 $M_\odot$. With these parameters, the habitable zone inner limit is 0.385 AU when using the classic model, and 0.30 AU under the 50% cloud cover scenario. The classic and 50% cloud cover habitable zone lifetimes are 0 Gyr and 1.8 Gyr, respectively. Accordingly, we would suggest that HD 85512b should no longer be considered a viable habitable planet candidate.

2.4.3 Continuously Habitable Zones

The linear model also allows for the production of plots of 'continuously habitable zones' (CHZ) (Figure 2.10). These describe an area around a star that would remain within the radiative habitable zone for a given time, first hypothesized by Hart (1979) and developed further by Kasting *et al.* (1993) who defined it as a region around a star that remains within the habitable zone for the entirety of the star's main sequence lifetime - in our solar system between 0.95 — 1.15 AU. For example, figure 2.10 illustrates the continuously habitable zones for 1 Gyr, 5 Gyr, 10 Gyr, and 50 Gyr. Our 5 Gyr CHZ is comparable to that of Kasting *et al.* (1993), extends across all mass classes considered, and is especially pronounced around solar mass stars (0.94 — 1.45 AU) and above. The 10 Gyr CHZ is also fairly encompassing across the stellar mass range considered, but stars above 1.03 $M_\odot$ are unlikely to have main sequence lifetimes in excess of 10 Gyr. Solar mass stars have a 10 Gyr CHZ extending from approximately 1.18 to 1.45 AU, excluding both Earth and Mars, as expected. Only low mass stars (between 0.2 and roughly 0.31 $M_\odot$) have main sequence lifetimes that are able to support a CHZ of 50 Gyr, as shown in the bottom right plot of figure 2.10. We suggest that Earth-analog exoplanets or exomoons found to be orbiting within these areas should be identified as particularly interesting candidates for continued observation and study, especially if

coupled with a good estimate for the relative age of their star, as they may have spent an extensive zone lifetime of time within the habitable zone.

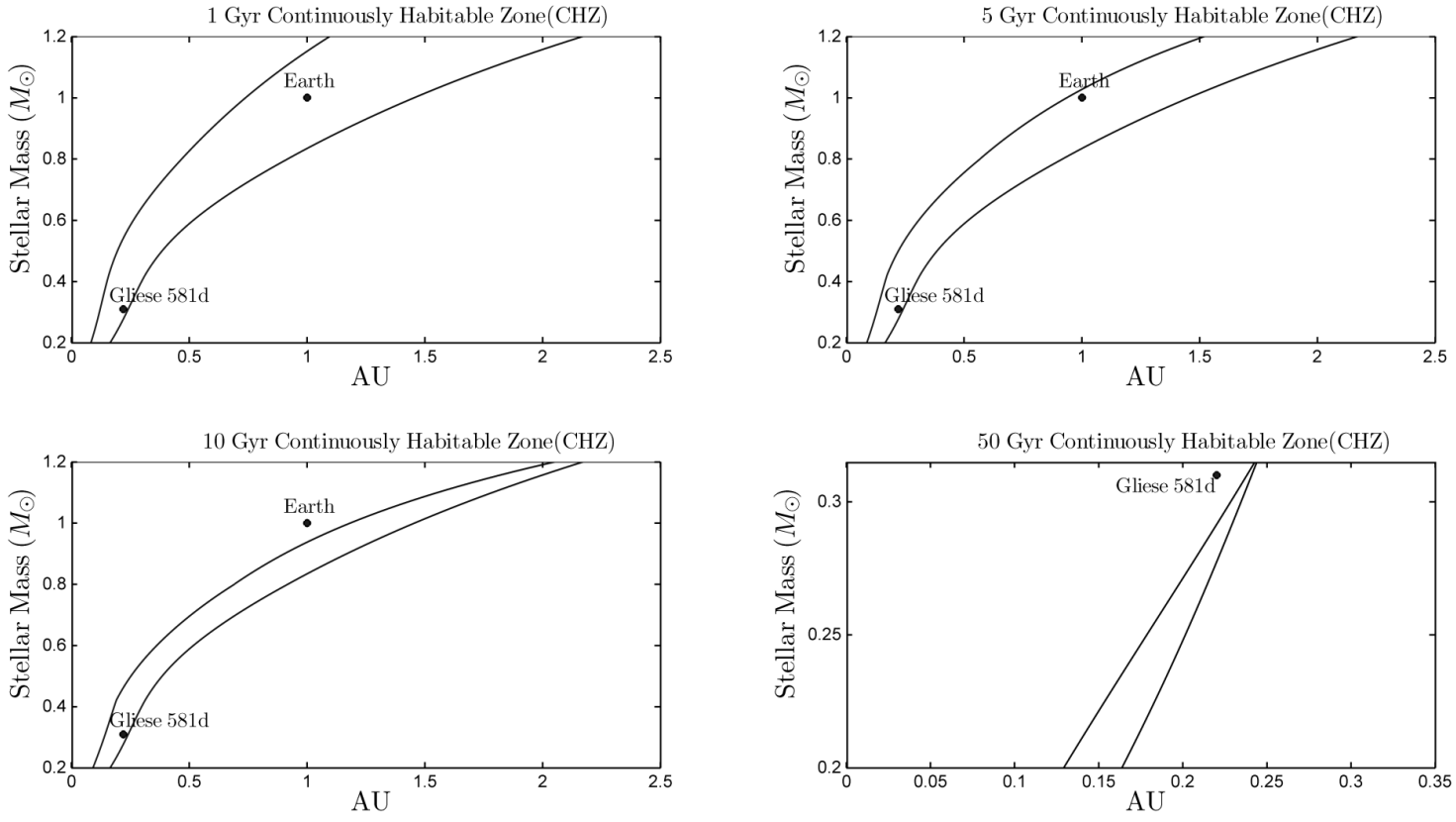

Figure 2.10: 1, 4.5, 10 and 50 Gyr Continuously Habitable Zones (CHZs), using the linear model as described above. Earth and Gliese 581d are included for reference. Note the change of scale of both axes in the 50 Gyr CHZ plot, bottom right.

Applying the linear habitable zone liftime (τ_h) model and modeled main sequence lifetime(τ), it is possible to devise a simple ratio between these relationships, shown in figure 2.11 and table 2.5. Lower mass stars, while exhibiting extremely long main sequence lifetimes, have proportionally lower τ_h/τ ratios than higher mass stars. For example, despite main sequence lifetime of 436 Gyr and typical habitable zone lifetime of 42 Gyr, a 0.2 $M_\odot$ star has a τ_h/τ ratio of 0.09, compared to a solar mass star with a τ value of 10.9 Gyr and a τ_h of 6.77 Gyr a τ_h/τ ratio of 0.62. Therefore, a planet that forms in the center of a solar mass star's habitable zone will be in the habitable zone for 62% of the duration of its host star's main sequence lifetime, compared to only 9-10% for a planet in the orbit of a 0.2 $M_\odot$ star. This relationship is both a result of the lower rates of stellar luminosity evolution resulting in proportionally lower rates of habitable zone boundary transition rates, and the fact that the difference (in space) between the inner and outer positions of the habitable zone at ZAMS and TMS is relatively greater around lower mass stars; the habitable zone 'migrates' proportionally further, covering a greater area.

$M_\odot$	**Main Sequence Lifetime (Gyr)(τ)**	**Typical Habitable Zone Lifetime (Gyr) (τ_h)**	τ_h/τ
0.2	436.3	42.16	0.097
0.3	296.6	25.34	0.085
0.4	225.6	21.24	0.094
0.5	115.1	14.42	0.125
0.6	59.5	11.07	0.186
0.7	34.2	9.63	0.282
0.8	21.2	8.56	0.404
0.9	14.9	7.86	0.526
1	10.9	6.77	0.621
1.1	8.2	5.62	0.686
1.2	6.3	4.57	0.725

Table 2.5: Typical Habitable Zone Lifetime and the ratio of the typical habitable zone lifetime (τ_h) to that of τ as a function of stellar mass.

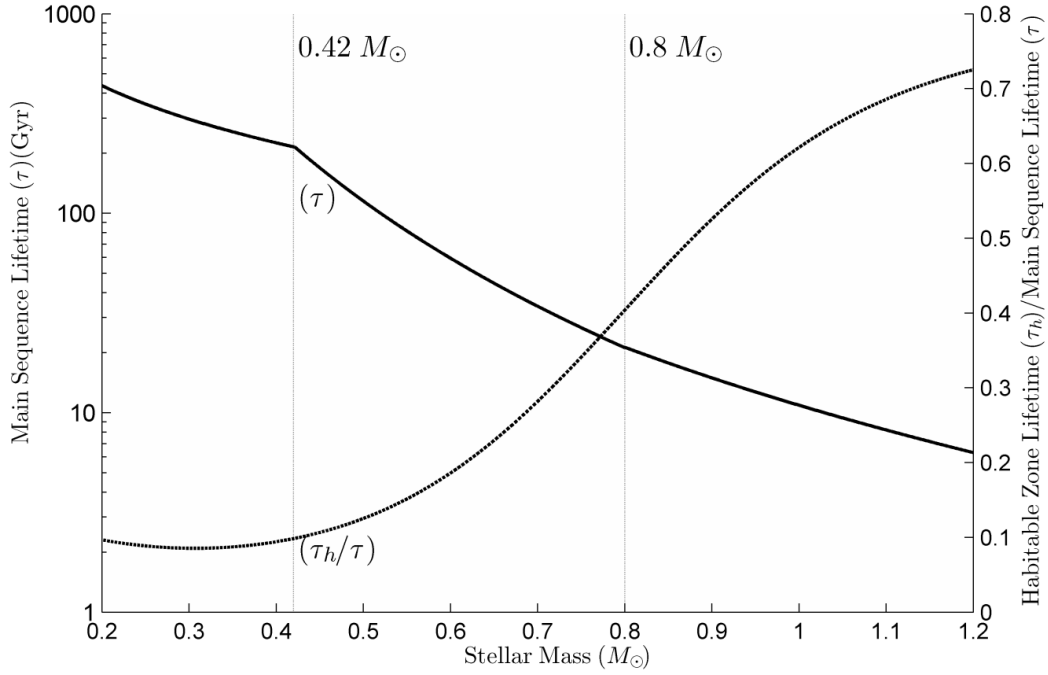

Figure 2.11: Main Sequence Age as a function of stellar mass for stars between 0.2 and 1.2 $M_\odot$ as well as the ratio of the typical habitable zone lifetime (τ_h) to that of τ

2.5 Discussion

We have presented a simple model, synthesizing current research in the area of radiative habitable zones around main sequence stars to produce some tentative estimates for the theoretically habitable zone lifetimes of exoplanets within these zones. We suggest that the habitable zone lifetime metric should be incorporated into a broader habitability index for exoplanets.

Our model provides an estimate for the total habitable zone lifetime (τ_h) for Earth of between 6.29 and 7.79 Gyr , ending between 1.75 and 3.25 Gyr from present. The implication is that we are roughly 70% of the way through the habitable zone lifetime of our planet – the period that the Earth will spend within the habitable zone of the Sun. We can begin to contrast and compare this value with that of other planets, if the age of

their star is known, but also use it as a means for quantifying the evolutionary history of Earth. A reliable estimate of the age of a planet's host star is integral to our understanding of its habitability. Planets Gliese 581d and g, as well as HD 40307g all provide interesting candidates for further observation because estimates of their habitable zone lifetimes can be used in conjunction with relatively well known star ages to produce a 'snapshot' of their habitable zone configuration at this point in time. Further to this, exoplanets like HD 85512b can be effectively excluded from further habitable exoplanet studies as knowledge of the age of its host star, coupled with an estimate of the transition rates of the habitable zone, reveal a planet now well outside the habitable zone.

The estimates returned by the model suggest that planets that have formed near the outer edge of the habitable zone would be in a more conducive orbital configuration for long residence times within the HZ. Planets nearer the inner hot zone boundary will spend less time in the habitable zone and may therefore be less suitable for the long-term evolution of complex life. However, the environmental conditions of planets near the cold outer boundaries and hot inner boundaries of their stars' habitable zones may present further limiting factors for life beyond those considered here. The boundaries of the habitable zone, integral to this and many other measures of habitability, are not well constrained. Initial research by Kasting *et al.* (1993) set boundary conditions that remain in use today. Development of the concept by Selsis *et al.* (2007) attempted to quantify the effect of clouds in terms of planetary habitability, but their parameterization as albedo features should have some bearing on the interpretation of the results of this model. Habitable zone lifetime estimations for some planets under 100% cloud cover regimes are an order of magnitude greater than the age of the universe (>100 Gyr). We agree with the conclusions of Goldblatt & Zahnle (2011), and consider the case under which exoplanets remain habitable only under these conditions to be stretching the interpretation of habitability and the habitable zone beyond realistically resolvable boundaries. We therefore urge caution in adopting this approach for identifying potentially habitable exoplanets in the future without first addressing this uncertainty by designating them as Class II habitable

planets. The planetary processes that control long term habitability on this scale are not well understood, and it remains beyond the scope of this project to speculate on the temporal dynamics of these cycles.

Parameterizations of complex climate processes will be required to resolve their effects on habitability metrics, and these are not the focus of the present study. From recent climate studies, other workers confirmed a small heating effect from CO_2 clouds on Earth-like exoplanets (Wordsworth *et al.*, 2010; Hu & Ding, 2010; Zsom *et al.*, 2012). When considering vertical atmospheric stratification, Kitzmann *et al.* (2010) reported a maximum 15% decrease in the HZ distance due the albedo effect of low altitude water clouds, coupled with a 35% increase in distance attributed to high-level ice clouds.

Habitable environments may exist on planets and moons beyond the habitable zone (Heller & Barnes, 2012). For example, the ice-covered ocean of Jupiter's moon Europa may harbour the highest astrobiological potential in the Solar System, despite falling 3.85 AU outside the Sun's habitable zone in the cold depths of the outer solar system (Pappalardo, 2010). It should be noted that the classical radiative habitable zone was initially established as an 'astronomical observable' HZ and represented a great advance in our understanding of the processes that control planetary climate. However, the rigidity of its definition — requiring liquid water on the surface of a planet — limits the possibility of including otherwise 'habitable' subterranean extraterrestrial environments on moons and planets in the cold zone of stars.

As more radiation is absorbed by greenhouse gases and Rayleigh scattering is more efficient when the host star radiates at shorter wavelengths, spectral type also has some control over the boundaries of the habitable zone (Pierrehumbert, 2010). For example, the habitable zones of low-mass M-dwarfs have been hypothesized to extend further due to a dampening of the ice-albedo feedback mechanism around these stars (Joshi & Haberle, 2012). Observations from the red dwarfs Gliese 436 and GJ 1214 show that they emit much of their radiation in the red and near-infrared portion of the electromagnetic spectrum, at wavelengths greater than 0.7 μm, and

significantly more in the 3 to 10 μm region than would be expected from a 'black-body' hypothesized M-type of a similar temperature. The albedo of ice and snow begins to decrease at wavelengths greater than 1 μm, and therefore the albedo of snow and ice covered surfaces on planets in the orbit of red dwarfs would be proportionally lower than that of the same surface on Earth (or any other planet in orbit around a G- or K-type star). This results in a weakening of the ice-albedo feedback mechanism and an extension of the habitable zone of between 10 and 30% (Joshi & Haberle, 2012).

Interpreting the results that have been returned by this simple model should be done with caution. While we have sought to estimate a theoretically habitable zone lifetime, we do not claim that the time that a planet spends within the habitable zone is the only control over habitability. Several fundamental biogeochemical feedback loops, essentially disconnected from the stellar habitable zone, operate on present Earth that boosts its habitability for multicellular aerobic organisms. The most notable of these is the secular oxygenation of the atmosphere that began with the Great Oxidation Event, approximately 2.4 Gyr ago, that facilitated the evolution of complex eukaryotic organisms (including humans) that exploit energy-efficient aerobic respiration (Catling *et al.*, 2005; Holland, 2006). The actual habitable zone lifetime of any given planet is unlikely to be controlled solely by planetary surface temperatures, and individual worlds may experience a variety of divergent (bio)geochemical evolutionary histories, possibly resulting in markedly different planetary environments to that of Earth. Habitability through time is likely to be as complex and multifaceted as habitability in space.

2.5.1 The Implications for the 'Anthropic Model'

Attempting to quantify the relative timing of biogenesis and the likely duration of the biosphere of habitable planets – from simple life to intelligent observers — has been a key area of research in astrobiology, extending back to the Drake Equation first devised in 1961, and the concept remains extremely pertinent to SETI campaigns.

The probabilistic anthropic model of Watson (2008), which draws on the theory of critical evolutionary transitions advanced by Szathmry & Maynard-Smith (1995) and the 'critical steps' model of Carter (1983), proposes that complex biology becomes increasingly probable with longer habitable zone lifetimes. A small (n <10) number of very difficult evolutionary transitions are needed to be overcome in order for intelligence of space-faring calibre to emerge. On Earth, for example, this step-wise progression began with the origin of life, continued through the transition from replicating molecules to RNA and then DNA, from prokaryotes to eukaryotes and cell differentiation, and concluded with the final step from primate to human societies. This hypothesis may at first appear to suggest an inference of determinism towards intelligence; a pinnacle towards which all evolution aspires. This tendency to view evolution as a progression towards increasing biological complexity and intelligence likely stems from an anthropocentric bias. However, it remains unnecessary to invoke any form of directionality in evolution; the area of focus of SETI campaigns is that of intelligence, which by its very nature is necessarily complex. Similarly, an organism able to alter its planetary environment to the extent at which biosignatures could be detected across interstellar space will undoubtedly require some level of complexity beyond that of simple replicating molecules. The critical steps model is an instrument used to estimate the probability of unlikely evolutionary events, and its applicability is not necessarily limited to considering the emergence of intelligence.

Our results seem to broadly support the conclusions of Watson (2008). Providing an upper limit for the potential lifespan of the biosphere, we note that critical evolutionary transitions appear to be few in number and approximately evenly spaced throughout the habitable zone lifetime of Earth. We would cautiously propose that, assuming that evolution by natural selection is a universal process for biological speciation, the duration of a planet's habitable zone lifetime may be an important factor limiting the possible complexity that life can evolve on its surface.

Following this approach, planets with a τ_h^{Earth} ratio less than 0.7 or 0.8 would be less likely to harbour complex life, but the possibility of prokaryote-like organisms should perhaps not be dismissed even on planets

with values as low as 0.2. Following the formation of Earth, it is thought that prokaryote life needed less than a billion years to establish, which appears to be more rapid than expected given the probabilities of the initial critical steps (Altermann & Kazmierczak, 2003; Speigel & Turner, 2012; Watson, 2008). Lineweaver & Davis (2002) quantified the probability of biogenesis on terrestrial habitable planets older than 1 Gyr ($\tau_h^{Earth} \leq 0.15$) as $< 13\%$ at the 95% confidence level, drawing on the perceived rapidity of biogenesis on Earth as key, and inferred from this that life is common in the Universe. However, until we have the opportunity to expand our dataset of inhabited planets, and refine the probabilities involved in these calculations, these first estimations remain extremely tentative. Table 2.6 below outlines some of the critical evolutionary transitions that have taken place on Earth and their corresponding τ_h value (based on the linear version of the HZ boundary transition).

τ_h^{Earth}	**Years since formation of Earth (Gyr)**	**Evolutionary Transitions**[1]
$\leq$0.15	$\sim$1Gyr	Replicating molecules; RNA to DNA
$>$ 0.25 $\leq$0.40	$\sim$1.5 - 2.5Gyr	Prokaryotes to Eukaryotes; Asexual clones
$>$0.55 $\leq$0.65	$\sim$3.5 - 4Gyr	Cell differentiation
$\geq$0.72(14)	4.54 Gyr	Primate to Human Societies (Homo Sapiens)[2]
0.72(15)	4.54 Gyr	Current habitable fraction index for Earth
1	6.29 Gyr	The Earth becomes uninhabitable
+0.28	+1.75 Gyr	Remaining lifespan of biosphere

[1]Szathmry & Maynard-Smith (1995), [2]McDougall *et al.*, (2005)

Table 2.6: Critical evolutionary transitions throughout Earth history, and their corresponding τ_h values (Watson, 2008)

Planets with very low τ_h ratios, Gliese 667Cc (0.24) for example, would under this classification remain targets of lower astrobiological potential, despite their residence within the HZ. Better constraints on star age would provide further information regarding the relative timing of habitable zone lifetimes, which could be used in conjunction with their absolute duration, and would avoid the inclusion of planets that are no longer in the habitable zone, such as HD 85512b. High value targets for SETI campaigns would be those planets that have been within the HZ for an equivalent amount of time as Earth, or longer; HD 40307g for example.

If the habitable zone lifetime is the only factor that controls the emergence of life and evolution of complexity required for intelligence, it follows that planets orbiting low mass stars with long habitable zone lifetimes are much more likely to host life and intelligent observers than planets orbiting higher mass stars. Our results show that low mass stars have CHZs possibly extending up to 50 Gyr, suggesting that any planets orbiting these stars are ∼5 times 'more habitable' than planets orbiting more massive stars with lower habitable zone lifetimes. Previous workers have attempted to build on the original models and quantify this anthropic selection effect for exoplanets, using probabilistic methods. While our estimates for the duration of the habitable zone lifetimes of M-dwarf exoplanets are an order of magnitude less than those discussed by Waltham (2011), we agree with the author's conclusion that the apparent habitability of these planets must be considerably reduced by other environmental factors.

2.6 Conclusions

It remains too early to know whether Earth's habitable zone lifetime is typical of inhabited planets, but from the limited sample provided above it is obvious that planets within the habitable zone exhibit a large range of habitable zone lifetimes, from significantly less than that of Earth to over five times Earth's habitable zone lifetime. Highlighting the example of HD 85512b, it is imperative that the transitory nature of the boundaries of the habitable zone are taken into account when considering the habitability of extrasolar planets. These first estimations, which we hope will be refined in the future as our understanding of the evolution of planetary habitability over time improves, provide an interesting first look at yet another fascinating component of planetary habitability.

2.7 Addendum

Following the publication of this chapter as Rushby *et al.* (2013) in the journal *Astrobiology* in September 2013, several improvements to the model were proposed in response to peer review and critiques from the wider

scientific community. The paper attracted unexpected media interest, both nationally and internationally, and as of late-2014, still ranks as the paper with the highest *Altmetric* score in *Astrobiology*, scoring higher in this measure than the other 328 articles with *Altmetric* scores in the journal. An incomplete but fairly comprehensive list of media coverage of the paper can be found here: http://bit.ly/Rushby2013Coverage. The paper ranks in the 99 percentile of all articles of a similar age, and remains in the top 5% of all articles tracked by *Altmetric*. More information about citation metrics for this paper can be found here: http://bit.ly/Rushby2013Altmetric.

The extensive media coverage helped to publicise the paper and hopefully instigate a conversation about this concept in the scientific community and the general public, but also revealed some weaknesses in our formulation of this issue, primarily that we neglected the evolution of the planetary system and the ability of the carbonate-silicate cycle to buffer the climate against increasing solar luminosity over the long-term. This was a valid critique: we assumed a constant atmospheric fraction of CO_2, and made no allowances for the operation of planetary biogeochemical cycling and the effect that these processes would have on the habitable zone lifetime of a terrestrial planet. For a model of relative simplicity and broad-spectrum applicability, this simplicity and normalisation could also be seen as a strength.

However, in response to these criticisms, it was decided that the field is generally lacking in intermediate-complexity geochemical models that adopt a 'systems-science' approach to the issue of planetary chemical evolution. Excellent work on exoplanetary atmospheric dynamics has been done by other researchers in the field exploiting recent advances in our understanding of high-complexity 3-D global circulation models (GCMs) from climate science, but this approach also has inherent weaknesses in its inability to model the geochemistry of terrestrial planets dynamically i.e. atmospheric carbon dioxide is introduced to the system and its effect on planetary habitability is investigated, but its concentration is not balanced by the action of continental weathering and carbon-fixation. In order to address this potential shortfall, a proposed model scheme built on the framework of previous work investigating the carbon-cycle on Earth was developed, and this forms the next chapter of this study.

3 The Carbonate-Silicate Cycle on Earth-like Planets: Implications for Long-Term Habitability

> How baffling it is that we
> imagined cities incinerated by
> alien bombs and death rays
> when all they really needed was
> Mother Nature and time.
>
> **Rick Yancey**
> *The Infinite Sea* (2014)

3.1 Abstract

The terrestrial cycle of silicate weathering and volcanic outgassing buffers atmospheric CO_2 and global climate over geological time on Earth. To first order, the operation of this cycle is assumed to occur on Earth-like exoplanets that exhibit similar continent/ocean configurations and has important implications for studies of planetary habitability. We present results from a simple biogeochemical model originally developed to describe carbon cycling during the Hadean era, which has subsequently been modified to investigate the possible operation of the carbonate-silicate cycle under conditions of differing planet mass and position within the radiative habitable zone. Our findings suggest that the carbonate-silicate cycle strongly buffers planetary climate, with marked effects on the length of a planet's habitable period, and that the weathering feedback on lower mass planets (<1 $M_\oplus$) appears less sensitive to atmospheric CO_2 than on planets larger than 1 $M_\oplus$, requiring proportionately higher levels of pCO_2 to remain within habitable temperature bounds.

3.2 Introduction

As the catalogue of known exoplanets continues to grow, the potential habitability of planets discovered around other stars in our galaxy remains of key interest to astrobiologists and planetary scientists. To first order, the initial 'habitability' of a newly discovered exoplanet is often assessed by determining whether or not its orbit falls within the circumstellar 'habitable zone' of its star (Kopparapu *et al.*, 2013). Ideally, detailed direct imaging of a given Earth-like exoplanet would be obtained to determine its ability to host and support life, but contemporary observational techniques are not sensitive enough to return the data required to make these assessments. Atmospheric spectroscopy can be used to obtain spectra from massive Jovian planets in close orbits around their stars to determine atmospheric composition and circulation, as well as disequilibrium effects, but this technique is not yet possible for smaller, Earth-sized planets of interest to astrobiologists (Swain *et al.*, 2008). Geophysical or geochemical modelling of exoplanetary systems is in its relative infancy as a discipline, but this approach is currently one of a very limited number of contemporary options for learning more about these enigmatic worlds. Previous studies investigating the potential long-term habitability of exoplanets have focussed on stellar evolution and its effect on the habitable zone whilst neglecting planetary evolution by necessity (Rushby *et al.*, 2013). However, the application of biogeochemical modelling to the Earth system is an approach that has been successfully exploited for many decades to investigate unanswered questions pertaining to the geochemical and climatological evolution of this planet, including the Faint Young Sun paradox and the operation of the carbon and oxygen cycles over geological time (Hayes & Waldbauer, 2006; Sleep & Zahnle, 2001). The 'Earth-systems' modelling approach seems well poised to be adapted to Earth-like planets outside of our solar system

3.2.1 Earth Systems Models

Building on the pioneering work of James Lovelock, the originator of the Gaia hypothesis in the latter part of the last century, the purpose of the Earth Systems modelling approach is to consider the planet as an interconnected and potentially self-regulating system comprised of the physical, chemical and biological domains. A seminal paper by Lovelock & Watson (1983), in which a simple biosphere (two competing species of daisy in this case) can act as a regulatory mechanism on the climate of the planet by altering the reflectivity of the planet surface (albedo), serves to illustrate regulation, or homeostasis, on the planetary-scale, and subsequent work developed the idea further in response to criticisms, primarily from the standpoint of evolutionary biology (Lenton, 1998). Influence of the earth systems modelling paradigm can be seen in contemporary climate models such as the UK Meteorological Office's HadGEM2 model, the US National Oceanographic and Atmospheric Administration's (NOAA) ESM2M model, and the NASA Goddard's GISS GCM packages, all of which attempt to incorporate elements of biology (ocean & land) and chemistry (ocean, geological, atmospheric) in addition to physical processes (Collins *et al.*, 2008; Dunne *et al.*, 2013; Schmidt *et al.*, 2006).

Recent developments in the field of exoplanet science and astrobiology are making the application of systems modelling approaches to issues of planetary habitability, exoplanet geochemistry and atmospheric chemistry more possible, and the potential for models of this variety to improve our understanding of these new frontiers in planetary science is now becoming apparent.

3.2.2 Defining Boundaries of Habitability

The reader is encouraged to refamiliarise themselves with the lengthy discussion of planetary habitability laid out in the introduction to this work (Chapter 1.1), as well as in Chapter 2, to avoid further repetition here.

In summary, habitable temperature boundaries are set at 273 and 343 K (0

— 70 °C) and the limit for photosystem habitability (i.e. the limit at which the ability of a photosynthesising biosphere to fix carbon from the atmosphere is significantly reduced) is 150 ppm pCO_2, roughly corresponding to the limit for C3 plants on Earth.

3.3 Methods

3.3.1 Biogeochemical Carbon Cycle Model

The model framework of Sleep & Zahnle (2001), henceforth 'SZ01', was adapted for this work, and was originally developed as a zero-dimensional, four-box biogeochemical model to investigate carbon cycling from the Hadean eon to present day on Earth. The early Earth could arguably be viewed as a hypothetical 'exoplanet' due to its extreme dissimilarity to present conditions: an anoxic and hazy planet on which different chemical and physical processes were dominant (Robinson *et al.*, 2011; Zerkle *et al.*, 2012). This paradigm is observed by adapting the model presented in SZ01 to investigate the operation of the long-term carbon cycle under hypothetical conditions possible on Earth-like planets at differing orbital distances.

This model was itself based on the earlier work of Walker *et al.*, (1981) and Berner *et al.*, (1983) (as well as Berner (1991, 1994) and Berner & Kothavala (2001)), who developed the 'WHAK' and 'BLAG'/'GEOCARB' models respectively. Early work on ocean carbon chemistry and the global carbon cycle using pioneering methods of chemical and radiocarbon tracers by Wallace Broecker proved crucial in understanding the partitioning and cycling of carbon throughout the planet system (Broecker *et al.*, 1979; Broecker & Peng 1982). The seminal work of Walker *et al.*, (1981) first quantified the effect of the carbonate-silicate cycle as a negative feedback mechanism for regulating the long-term climate of the Earth. Berner *et al.*, (1983) attempted to extend the scope of this work by investigating the effect of detailed geochemistry in the action of the carbonate-silicate cycle, including ocean chemistry, biological carbon fixation, seawater/rock kinetics and metamorphic decarbonation due to subduction at plate boundaries.

The GEOCARB model attempted to further simulate these processes, and included the detailed evolution of atmospheric CO_2 and O_2 over the Phanerozoic, incorporating biological weathering enhancement factors and an integrated sulphur cycle (Berner, 1991; 1994; Berner & Kothavala, 2001).

The model used here is constructed of four carbon reservoirs: Ocean/Atmosphere (R_{OA}), Oceanic Crust (R_{OC}), Continental Sediment (R_{CS}), and the Mantle (R_{MAN}) (see figure 3.1). Here 'continental sediment' indicates both the continental crust and shelf, which are not distinguished because the shelf is covered by terrigenous sediment. Carbon is cycled through the system by a series of fluxes solved for steady state and constrained by the assumption of steady state at the present day. Several approximations for surface temperature are explored, including a number of $CO_2/CH_4/H_2O$ greenhouse parameterisations, as well as an integrated 1-D radiative-convective climate model, and effective temperature is forced by a steadily increasing solar input (for stars of 0.2 to 1.2 solar masses) from the stellar evolution model described in the previous chapter as well as (Rushby *et al.*, 2013). The temporal resolution of the model is low and timesteps are on the order of 10^6 years. Mass balance calculations computed after running the model at timesteps between 10^4 years and 10^6 years showed negligible difference, and therefore 10^6 years was chosen for computational efficiency. Table 3.1 outlines the default values of the steady-state fluxes included in the model framework (i.e. the processes that transfer carbon between reservoirs) for reference, each of which will be described in detail in this chapter.

Flux	**Description**	**Present day value (10^{12} mols C yr^{-1})**
f_{hydro}	Hydrothermal carbonitization	1.65
f_{ridge}	Ridge degassing	2.55
f_{pel}	Pelagic deposition	13
f_{dep}	Shelf sea deposition	11
f_{sub}	Subduction	3.6
f_{subman}	Proportion of subducted carbon to mantle	2.7
f_{subarc}	Proportion of subducted carbon degassed by arc volcanism	0.9
f_{wedge}	Accretionary wedges	11
$f_{CO_{3_W}}$	Carbonate weathering	18
$f_{SiO_{3_W}}$	Silicate Weathering	6.5
f_{meta}	Metamorphism	4.5

Table 3.1: Model fluxes and present day values

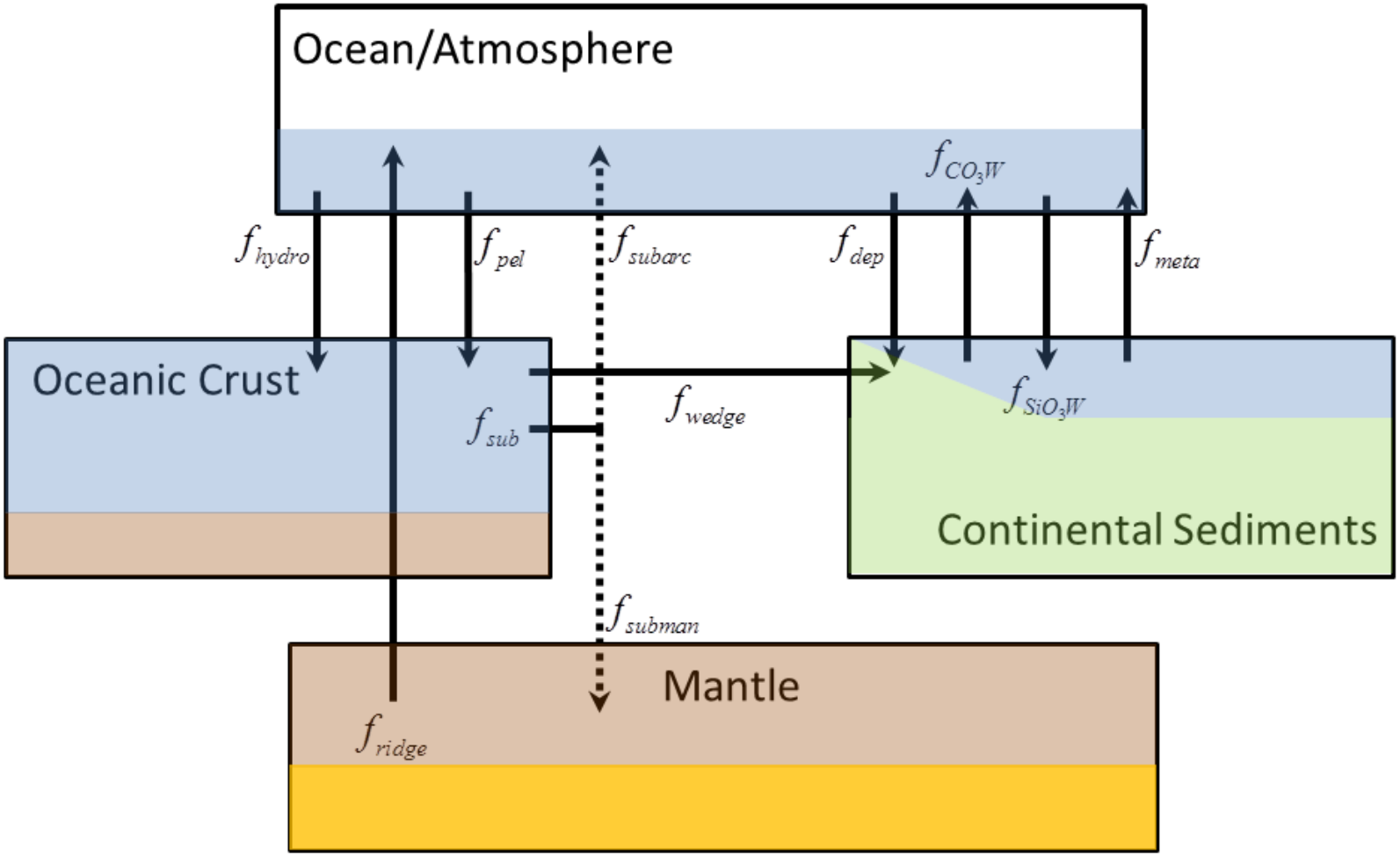

Figure 3.1: Schematic of the carbon cycle model

CO_2 fluxes between the ocean and the atmosphere are assumed to be in equilibrium, given the timescales considered, and the change in the total amount of carbon in ocean/atmosphere reservoir is given by:

$$\frac{dR_{OA}}{dt} = f_{meta} + f_{ridge} + f_{subarc} + f_{CO_3W} - f_{dep} - f_{pel} - f_{SiO_3W} - f_{hydro} \quad (3.1)$$

Where f_{meta}, f_{ridge}, f_{subarc}, f_{CO_3W}, f_{dep}, f_{pel}, f_{SiO^3W} and f_{hydro} are carbon fluxes from metamorphism, ridge volcanism, the proportion of subducted carbon emitted via arc volcanism, carbonate weathering, shelf deposition, pelagic deposition, silicate weathering and hydrothermal carbonitisation, respectively, in the units of teramoles (10^{12} mols) of C per year (yr^{-1}). Carbon inputs and outputs to the ocean crust are given by:

$$\frac{dR_{OC}}{dt} = f_{pel} + f_{hydro} - f_{sub} - f_{wedge} \quad (3.2)$$

Where f_{wedge} and f_{sub} are fluxes originating from accretionary wedges and subduction respectively. The continental crust reservoir is balanced in the form:

$$\frac{dR_{CS}}{dt} = f_{wedge} + f_{SiO^3W} + f_{dep} - f_{CO_3W} - f_{meta} \quad (3.3)$$

The mantle reservoir is calculated as:

$$\frac{dR_{MAN}}{dt} = f_{subman} - f_{ridge} \quad (3.4)$$

Where f_{subman} is the proportion of f_{sub} returned to the mantle.

The model is driven by increasing stellar luminosity derived from improvements made to the stellar evolution model presented in Rushby *et al.*, (2013), as well as geothermal heat flow (Q) which varies as a function of time. Whilst there is considerable uncertainty regarding the rate of geothermal heat loss during the Archean, we adopt the approach of SZ01

(as well as Lowell & Keller, 2003; Hayes & Waldbauer, 2006; Franck & Bounama, 1997) in assuming a simple, time-dependent decay function in the form:

$$Q = 1 + \left[\frac{t}{t_0}\right]^{-\mu} \tag{3.5}$$

Where μ is a scaling parameter representing the radiogenic heating regime; $\mu = 0.7$ for 'high heat flow' and $\mu = 0.2$ for 'low heat flow' (SZ01). t_0 is 4.54 Gyr. This dependence is explored in the sensitivity analysis in the later part of this chapter; from that exercise we adopt the latter form of this parameterisation, which predicts heat loss rates from the early Earth between ~4.5 and 3 times present day, which is also in keeping with other workers (Lowell & Keller, 2003; SZ01). In geodynamic models, the seafloor spreading rate is found to closely approximate Q^2 (Franck *et al.*, 1999), and has a strong control over the rate of subduction of oceanic crust into the mantle, and by implication the amount of carbon returned to the ocean/atmosphere system via arc volcanoes as well as via ridge degassing (f_{ridge}), metamorphism (f_{meta}), and the rate of seafloor hydrothermal carbonatization (f_{hydro}). The rate of subduction is therefore given as:

$$f_{sub} = f_{sub_0} \,.\, Q(t)^2 \,.\, \left(\frac{R_{OC}}{R_{OC_0}}\right) \tag{3.6}$$

Where f_{sub_0} represents the steady state solution at present day (3.6×10^{12} mols C year^{-1}), and it follows that the amount of subducted carbon is a function of the size of the oceanic crust reservoir driven into the mantle at subduction zones. Island arcs and ridge axes play a fundamental role in the global carbon cycle, the former representing a relatively rapid return flux of subducted carbon to the atmosphere. The lowered melting temperature and extreme pressures associated with the subduction of the near-saturated oceanic slab into the mantle results in formation of magma at depth underneath the overriding plate, which subsequently ascends to form an arc system parallel to the subduction fault (Iwamori, 1998). SZ01 estimate that approximately 25% of the subducted oceanic carbonate is returned to the

atmosphere/ocean system via island arc volcanoes, and therefore farc scales as $0.25 \times (f_{sub})$. The remainder of the subduction flux is delivered to the mantle, forming f_{subman} and closing the cycle. We also include accretionary wedges (f_{wedge}) as a transfer flux between the oceanic (subducting) and continental plates. Accretionary wedges are formed from sediments accreted onto the non-subducting plate at a convergent plate boundary and primarily consist of carbonitized basaltic rock and deposited pelagic sediments. In this formulation, the accretionary wedge 'flux' is proportional to the size of the ocean crust reservoir, and scales with the seafloor spreading rate.

Mid-ocean ridges represent a source of carbonate to the oceanic crust: pillow basalts are formed as magma erupts from spreading ridges, cooling and degassing rapidly. The depth at which the basalt is sourced from in the mantle has a control on the carbon abundance in the erupted basalts, and is parameterised as DS, where this 'source depth' parameter is equal to 56 km (SZ01). The amount of carbon expelled from ridge volcanic systems is also assumed to be primarily driven by the spreading rate, as well as the size of the mantle carbon reservoir cycled through the source depth zone. We simplify SZ01's parameterisation of ridge degassing (normalising for density by scaling with the relative size of the mantle carbon reservoir as opposed to its volume), in the form:

$$f_{ridge} = f_{ridge_0} \,.\, Q(t)^2 \,.\, \left(\frac{R_{MAN}}{R_{MAN_0}}\right) \,.\, D_s \tag{3.7}$$

Here the present day solution (f_{ridge_0}) is 2.55×10^{12} mols C year^{-1} (SZ01). Metamorphic degassing follows a similar formulation: proportional to the square of heat flow and the size of the continental sediment reservoir from which metamorphosed carbon would be drawn:

$$f_{meta} = f_{meta_0} \,.\, Q(t)^2 \,.\, \left(\frac{R_{CS}}{R_{CS_0}}\right) \tag{3.8}$$

The present day solution (f_{meta_0}) is given as 4.5×10^{12} mols C year^{-1} (SZ01).

The low-temperature alteration of seafloor basaltic rocks by hydrothermal vent systems was likely an important sink of carbon in the Archean, being independent of surface temperatures and temperature-dependent continental weathering fluxes, whilst also acting to close the Archean carbon cycle (Coogan & Gillis, 2013). Basic extrusive rocks, such as seafloor basalts, undergo carbonatization under the action of hydrothermal solutions rich in carbon dioxide emanating from depth.

$$Ca^{2+} + 2\,HCO_3^- \longrightarrow CaCO_3 + 2\,CO_2 + H_2O \tag{3.9}$$

Warm waters upwelling from hydrothermal vent systems result in kinetically enhanced rates of carbonate formation, and this sink would have been especially enhanced during the Archean geophysical regime which was associated with more vigorous mantle overturning, greater ocean ridge length and more rapid seafloor spreading rates (SZ01; Lowell & Keller, 2003):

$$f_{hydro} = f_{hydro_0} \,.\, Q(t)^2 \,.\, \left(\frac{R_{OA}}{R_{OA_0}}\right)^{\alpha} \tag{3.10}$$

Here, the exponent α represents the dependence of seafloor carbonitization on the concentration of CO_2 in the atmosphere (assumed, on the timescales associated with this model, to be in equilibrium with the carbon in the oceanic bottom water and correlated with temperature; discussed in more detail later in this chapter), where complete depletion of oceanic carbon dioxide corresponds to $\alpha = 1$. This is a simplification of the rock-water kinetics involved in the process of hydrothermal alteration, where the rate at which upwelled CO_2-rich waters delivered to the ocean crust via hydrothermal venting is the primary limiting factor in its uptake and the addition of calcium to basalt, assuming available cations (Ca_{2+}) are available. This assumption is subject to some uncertainty and it is not clear that the rate of reaction is linearly dependent on pCO_2, but rather acts as a complex function of cation availability, seafloor temperature and ocean crust K-feldspar uptake (Brady & Gslason, 1997; SZ01; Mills *et al.*, 2014). In our parameterisation of this process, we assume that hydrothermal

alteration is driven by spreading rate, $p\mathrm{CO}_2$ and tuned by α (we take our default value from SZ01 as 0.23, representing a weak dependence on $p\mathrm{CO}_2$), as shown in equation 3.10. We adopt the lower limit given in SZ01 and take f_{hydro_0} as equal to 1.65×10^{12} mols C year^{-1}.

3.3.2 Weathering Fluxes

The weathering of terrestrial silicate rocks is a crucial component of the long-term carbon cycle, and a key regulatory feedback mechanism between atmospheric carbon dioxide and global climate (Walker *et al.*, 1981). Silicate rocks are chemically weathered by a weak carbonic acid solution formed from the dissolution of atmospheric CO_2 in raindrops. This weathering process liberates bicarbonate and calcium ions to groundwater and rivers and eventually results in their delivery to the ocean where they are reprecipitated, primarily biogenically by the action of marine calcifying organisms, as calcium carbonate. If the calcium carbonate shells of these organisms fail to dissolve after their death, their carbonate-rich remains accumulate in oceanic benthic sediments. This 'pelagic deposition' flux is parameterised in our model as f_{pel}, and represents a loss of $\sim 13 \times 10^{12}$ mols C year^{-1} from the ocean/atmosphere reservoir to the oceanic crust reservoir in the present day (SZ01). Alternatively, the parameter f_{dep} attempts to account for the cases where marine organisms have fixed carbon for their shells, died and sunk to the bottom of shallow seas or continental shelf environments, constituting a flux of 11×10^{12} mols C yr^{-1} to the continental crust reservoir. Over geological time, the accumulated carbonate will eventually result in the formation of limestone, thereby immobilising an enormous reservoir of carbon until such time as it is exposed to weathering by tectonic uplift or subducted into the mantle to be eventually expelled volcanically. The general stoichiometry of the reaction, using the most common naturally occurring form of calcium silicate, wollastonite, is:

$$\mathrm{CaSiO_3} + \mathrm{CO_2} \longleftrightarrow \mathrm{CaCO_3} + \mathrm{SiO_2} \tag{3.11}$$

Known as the 'Ebelman-Urey reaction', this process is exclusively concerned with the weathering of Ca and Mg silicates as other forms of silicate mineral (Na and K for example) do not form common carbonates in sediments (Berner, 2004). If irreversible, this reaction would likely result in the depletion of atmospheric CO_2 within ~300,000 years. However, the opposite reaction in which the Ca silicate (in this case) is decarbonated via volcanic or metamorphic processes and the stored carbon returned to the atmosphere completes the carbonate-silicate cycle, as shown in figure 3.2

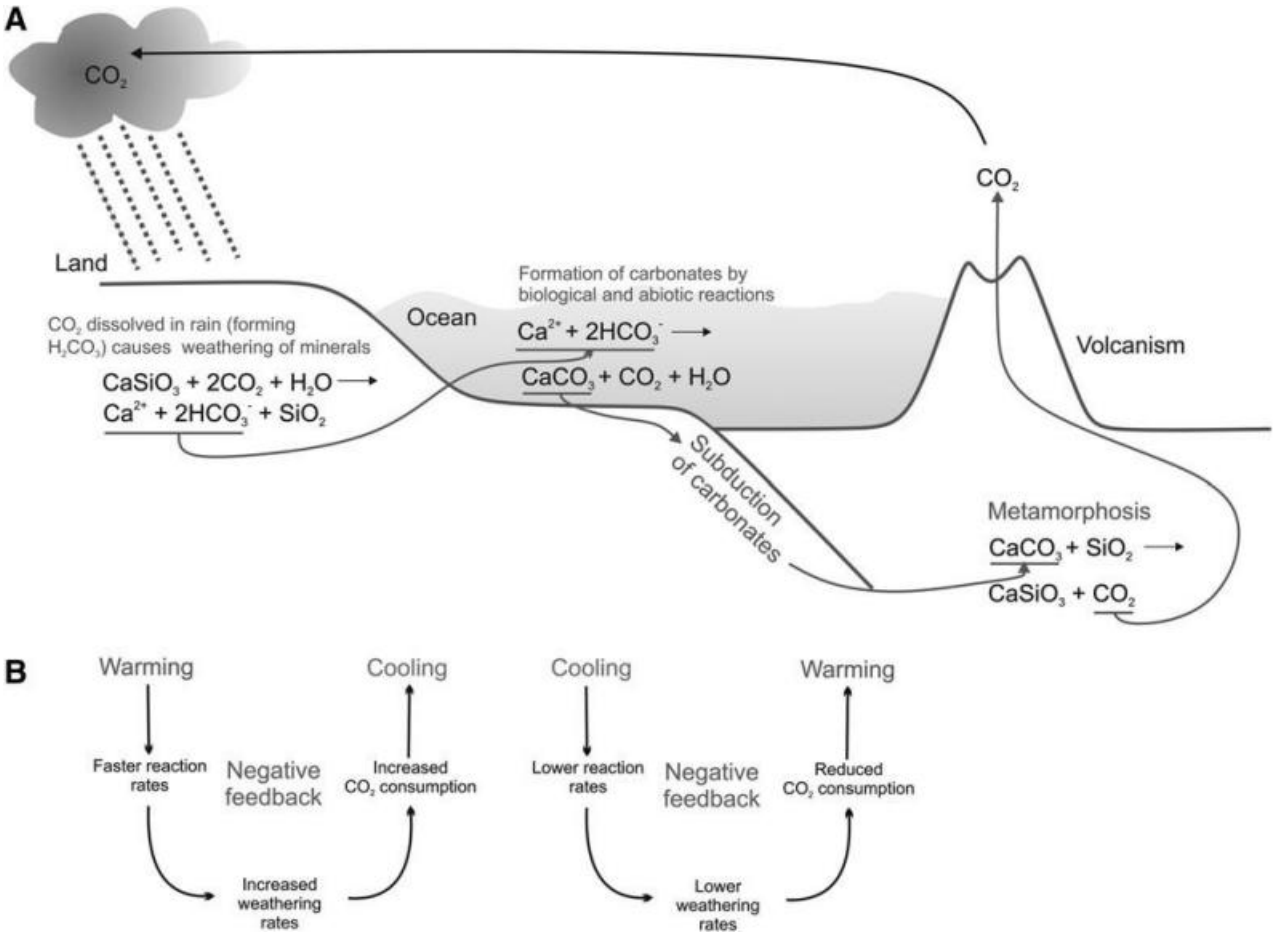

Figure 3.2: A) Generalised schematic of the carbonate-silicate cycle. B) Feedback loops associated with the carbonate-silicate cycle in response to perturbations in surface temperature. (Cockell *et al.*, 2016).

The general mechanisms of this reaction have been known for some time, but the importance of the cycle to global climatic regulation was initially advanced in a seminal paper by Walker *et al.*, (1981). A negative feedback

between the rate of weathering of silicate rocks, the surface temperature of the planet and the partial pressure of carbon dioxide in the atmosphere was theorised: as temperatures increase (due to steadily increasing solar output), rates of continental weathering increase thereby drawing down CO_2 and reducing the overall greenhouse forcing (Walker *et al.*, 1981). The rate of this mechanism is a strong function of temperature and a weak function of $p\mathrm{CO}_2$. Our formulation of this process, following SZ01, is:

$$f_{SiO_3W} = f_{SiO_3W_0} \,.\, CO_2^{\beta} \,.\, exp\left[\frac{T - T_0}{B}\right] \,.\, \kappa \tag{3.12}$$

Where β is an exponent that controls the sensitivity of the reaction to the partial pressure of atmospheric carbon dioxide and the rate of carbonic acid formation and B is a weathering calibration parameter suggested by Walker *et al.*, (1981) to account for runoff ($B = 13.7$). The additional parameter κ can be altered to simulate the effects of biotic enhancement of weathering, where organisms, via the action of their roots, metabolisms or exuded organic acids, increase the rate of weathering of silicate minerals beyond what would be expected in an abiotic environment (Berner, 1997; SZ01; Schwartzmann & Volk, 1989). The delivery of bicarbonate ions and silicate cations to the ocean via this mechanism is thought to be strongly limited by the ability of riverine systems to transport the weathered materials and this also acts as a limiting factor in the rate of drawdown of CO_2 (Mills *et al.*, 2011; West *et al.*, 2005). For steady state, $f_{SiO_3W_0}$ is given as 6.5×10^{12} mols C yr^{-1}.

Carbonate weathering, in which the inorganic carbon bound up in limestone is liberated from the continents, is a large flux of carbon into the Ocean/Atmosphere reservoir and is described by the reversible reaction:

$$H_2O + \underbrace{CO_2}_{\text{Remains in OA}} + \underbrace{CaCO_3}_{\text{CS} \longrightarrow \text{OA}} \longleftrightarrow Ca^{++} + 2HCO_3^- \tag{3.13}$$

This process represents the return of carbon stored in the continental sediments reservoir that was originally delivered by the pelagic and shelf sea depositional fluxes discussed above (f_{pel} and f_{dep}, respectively), to the

ocean/atmosphere reservoir. The present day rate is 18×10^{12} mols C yr^{-1} (SZ01), forming one of the largest fluxes in the model primarily due to the extensive size of the continental carbonate reservoir. Carbonate weathering is parameterised as a weak function of temperature, atmospheric carbon dioxide and the size of the continental reservoir available for weathering (SZ01):

$$f_{CO_3W} = f_{CO_3W_0} \,.\, CO_2^{\gamma} \,.\, exp\left[0.05(T - T_0)\right] \,.\, \left(\frac{R_{CS}}{R_{CS_0}}\right) \tag{3.14}$$

The exponent γ allows the dependence of the reaction to $p\mathrm{CO}_2$ to be calibrated, and is held at 0.3 in this work. f_{pel} and f_{dep} are approximately equivalent to the combined weathering flux ($f_{SiO_3W} + f_{CO_3W}$) over the long-term, balanced by ocean alkalinity (Berner & Kothavala, 2001).

3.3.3 Atmospheric CO_2

The ocean and atmosphere are considered to act as a single reservoir in the model, equilibrating over timescales shorter than the temporal resolution of the model and assumed to be in steady state. Division of carbon between the ocean and atmosphere is controlled by thermodynamic partitioning. In the ocean, carbon exists in the species CO_2(aq), the bicarbonate ion (HCO_3^-) and the carbonate ion ($\mathrm{CO}_3^=$); $p\mathrm{CO}_2$ can be determined by combining the equilibrium constants of the different CO_2 species, whilst accounting for alkalinity (Bergman *et al.*, 2004). Without a pH parameter or integrated calcium cycle however it is not possible however to ensure a close balance between alkalinity and the ratio of total aqueous CO_2, and we therefore assume an ocean saturated with respect to CaCO_3, with a constant calcium concentration and independent of ocean temperature. Here we diverge from SZ01 and, following Kump & Arthur (1999), determine that the paleoatmospheric CO_2 follows a simple scaling relationship, where the concentration of CO_2 in the atmosphere is relative to the square of changes in the ocean/atmosphere reservoir (total inorganic carbon) and present day values of $p\mathrm{CO}_2$(280 ppmv):

$$pCO_2(t) = \left(\frac{OA(t)}{OA_0}\right)^2 . pCO_2 + \left(\frac{pCO_2(t) \, . \, dT_{surf}}{K}\right) \qquad (3.15)$$

The original SZ01 formulation of this parameterisation ignored the effect that large changes in ocean temperature – for example those that would occur towards the end of the planet's habitable lifetime as solar output increases steadily – would have on the partitioning of carbon species between the ocean and the atmosphere. Recent modelling work from Omta *et al.* (2011) demonstrates an approximately exponential dependence between atmospheric CO_2 and average ocean temperature, and we have therefore also included an additional temperature-dependent scaling relationship that alters the partitioning of CO_2 between the ocean and the atmosphere as a function of temperature, where K is a composite chemical equilibrium constant equivalent to 27 $°C^{-1}$. This relationship results in an approximate 4% increase in atmospheric CO_2 per 1 K increase in ocean temperature, relative to present day ocean temperatures, as shown in figure 3.3 (Omta *et al.*, 2011).

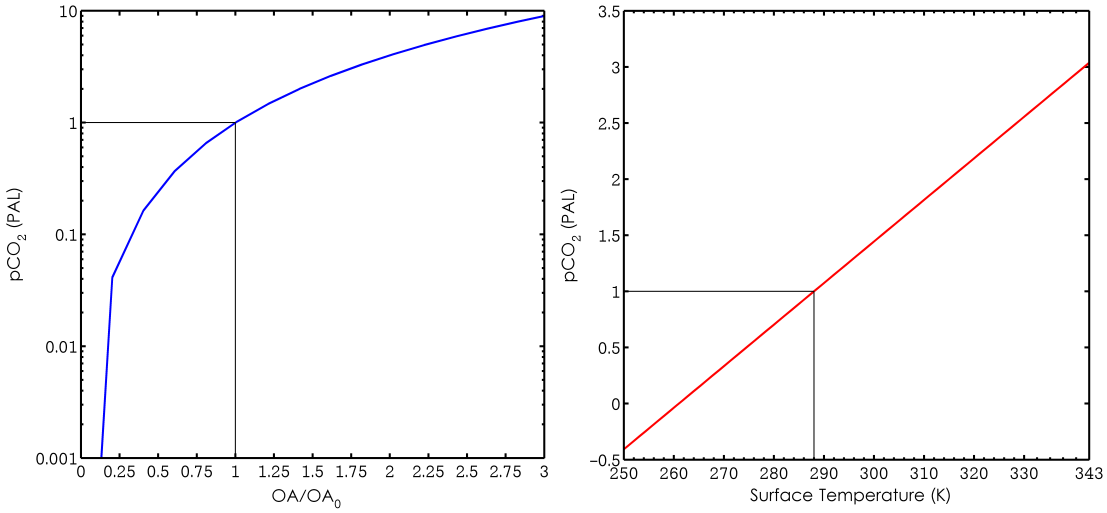

Figure 3.3: Graphical representation of equation 3.15. Left) Changes in pCO_2 as a function of the size of the ocean/atmosphere reservoir (OA/OA_0). Right) Changes in pCO_2 as a function of surface temperature.

3.3.4 Planetary Climate Parameterisations

Effective planetary temperature is computed as function of incoming stellar flux, derived from the stellar evolution model described in Rushby *et al.* (2013) and planetary albedo:

$$T_{eff} = \left(\frac{S(1-a)}{4\sigma} \right)^{0.25} \tag{3.16}$$

Where σ is the Stefan-Boltzmann constant, given as 5.67×10^{-8} J S^{-1} m^{-2} K^{-4}, and a is albedo. Astronomical constraints on effective temperature are described by:

$$S = \left(\frac{S_j(L_\odot)}{4\pi} \right) A^2(1-e^2)^{1/2} \tag{3.17}$$

S_j, the incident solar flux in W m^{-2}, is derived from a fit to results from the Dartmouth Stellar Evolution Database (see 'Methods' in chapter 2 for more details), $L_\odot$ denotes the current luminosity of the Sun, A is the semi-major axis of the planet (in AU) and e is the planet's eccentricity.

3.3.5 Albedo

Albedo is a non-dimensional, unitless quantification that describes the 'reflectivity' of a planetary surface; the fraction of incoming radiation (usually in the visible) that is reflected away. A black-body would have an albedo of 0, whereas a perfect reflector would represent an albedo of 1. The current 'bond albedo' of Earth which accounts for scattering and absorption at all wavelengths and phase angles is approximately 0.306 (Williams, 2014).[2]

The relationship between albedo and global ice cover represents a potentially powerful positive feedback, known as the ice-albedo feedback. As ice cover advances equator-ward from the poles, albedo increases as the

[2]An updated estimate of albedo of 0.29 from Stephens *et al.* (2015) will be used in future forms of this model.

reflectivity of the surface changes and this effect can 'run-away' as temperatures continue to fall, ice continues to form and planetary albedo continues to increase (von Paris *et al.*, 2013). Recent studies (e.g. Shields *et al.*, 2013) show that this effect is also wavelength-dependent. Stars of different mass-classes emit radiation at different wavelengths, and the reflective properties of surface ice changes significantly under different radiative environments. For example, this effect would be particularly important in the study of planets around smaller M stars, which emit a greater proportion of their radiation in the near-IR, where the snow and ice albedo is less than in the visible (Shields *et al.*, 2013).

The 'albedo-history' of the Earth is difficult to construct, as albedo leaves no explicit biogeochemical tracer or proxy that could be used to infer likely surface reflectivity. Given knowledge of the surface environment and temperature, estimations of planetary albedo could be constructed based on the likelihood of ice cover, photochemical haze etc. Some workers (e.g. Rosing *et al.*, 2010) have sought to explain the apparent 'Faint Young Sun' paradox by invoking lower albedo in the Archean (as low as $\sim$0.22), and therefore higher absorption of solar radiation, but their assumptions (significantly less continental area, fewer biologically-generated cloud condensation nuclei) are subject to scrutiny, and recent geochemical proxy evidence (see Zerkle *et al.*, 2012) seems to refute their claims regarding a lack of biogeochemical support for high levels of greenhouse gases.

Albedo is a difficult parameter to dynamically and self-consistently capture in a model of this complexity considering the seasonal and latitudinal variations in a planet's orbit, the 2-D nature of the ice-albedo relationship and the lack of accurate historical 'calibration'. Von Paris *et al.* (2013) also note that atmospheric properties (pressure, presence and concentrations of gases such as H_2O, CH_4, O_3) also have an effect on the reflectivity of the planetary surface by scattering incident stellar radiation at different wavelengths when compared to a 'clear-sky' case, an effect that is also beyond the scope of this work. Dependence on temperature may provide a first-order relationship of acceptable accuracy to represent ice-albedo feedback; SZ01 adopt a temperature-dependent fit from Caldeira & Kasting (1992) in the form:

$$a = 1.4891 - 0.0065979T + 8.567 \times 10^{-6}T^2 \tag{3.18}$$

Where T is surface temperature in K. It is likely that this fit underestimates albedo at very low temperatures, for example returning a value of a ∼0.4 at T = 240 K, but may provide a reasonable approximation at higher temperatures (see figure 3.4). Below ∼200 K and above 400 K this approximation collapses and cannot be used.

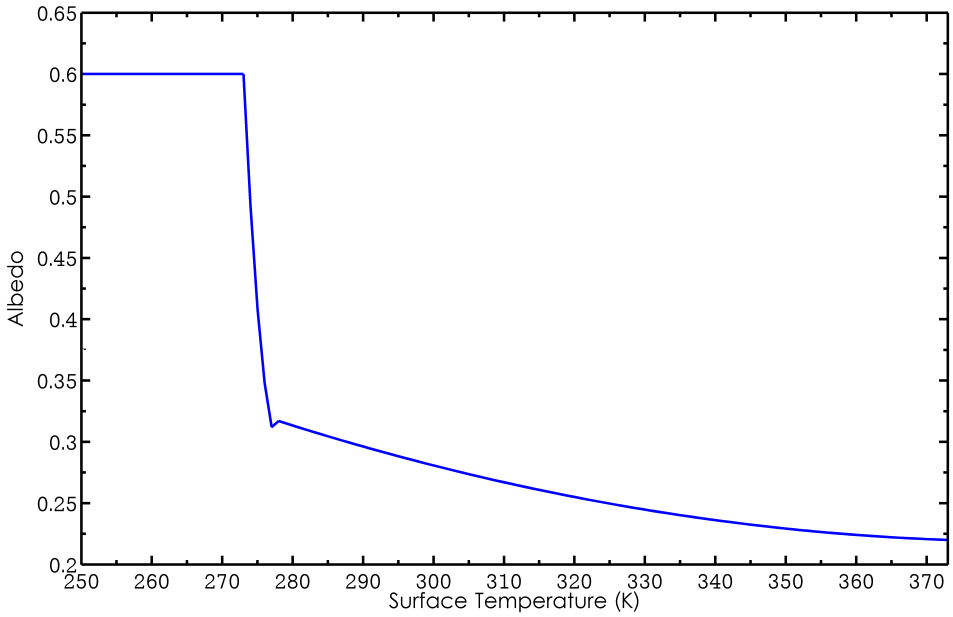

Figure 3.4: Dependence of surface albedo on temperature.

Therefore, in the formulation used in this work (when not using the 1-D radiative-convective model discussed in a later chapter) a conditional approach to albedo is adopted: albedo is fixed at 0.6 (a value that approximates bare sea ice) when the global average temperature is less than 273 K (T_i) to represent 'snowball Earth' conditions of pole-to-pole ice cover, and the temperature-dependent parameterisation (equation 3.18) is used when above 278 K (T_0). This temperature represents an unstable ice-albedo 'tipping point' in terms of latitudinal ice coverage, beyond which ice coverage will runaway and result in a fully glaciated planet

(Pierrehumbert, 2010). Between these temperatures, a gradual transition between global ice cover and ice-free conditions are parameterised in the form of a quadratic interpolation (Pierrehumbert, 2010):

$$a(T) = \begin{cases} a_i & \text{for } T \leq T_i \\ a_0 + (a_i - a_0)\frac{(T-T_0)^2}{(T_i-T_0)^2} & \text{for } T_i < T < T_0 \\ \text{eq. 3.18} & \text{for } T \geq T_0 \end{cases} \quad (3.19)$$

Equation 3.19 is plotted in figure 3.4. Standard model runs (with default starting conditions) utilising this temperature-dependent albedo parameterisation suggests a secular decline in albedo over the course of Earth history, as the planet warms over time.

3.3.6 Greenhouse Warming Factors for CO_2, CH_4 & H_2O

Greenhouse warming factors are included in the final temperature calculation. The initial formulation of this warming effect is taken from Caldeira & Kasting (1992), as it is used in SZ01, and was derived from a radiative-convective climate model taking the form of a second-order polynomial fit dependent on temperature and $p\mathrm{CO}_2$ in bars:

$$\Delta T_{CO_2} = 815.17 + (4.895 \times 10^7)T^{-2} - (3.9787 \times 10^5)T^{-1} - 6.7084(pCO_2^{-2})$$

$$+ 73.227(\mathrm{pCO}_2^{-1}) - 30882(T^{-1})(pCO_2^{-2}) \quad (3.20)$$

The function produces a peak warming factor of ~75 K at 8% $p\mathrm{CO}_2$ given present solar output (see figure 3.5). This fit suggests that in the Archean, proportionally higher levels of $p\mathrm{CO}_2$ would be required to produce an effective greenhouse effect (peak warming factor ~66 K at 12.7% $p\mathrm{CO}_2$). At $p\mathrm{CO}_2$ higher than these limits, increasing CO_2 cools the planet (analogous to CO_2 cloud formation) and the carbonate-silicate temperature regulation is therefore 'broken'. It should be noted that the author-defined limits of this fit are from 10^{-8} to 10^{-2} bars of CO_2.

Figure 3.5 can be expanded to investigate the climate response expected

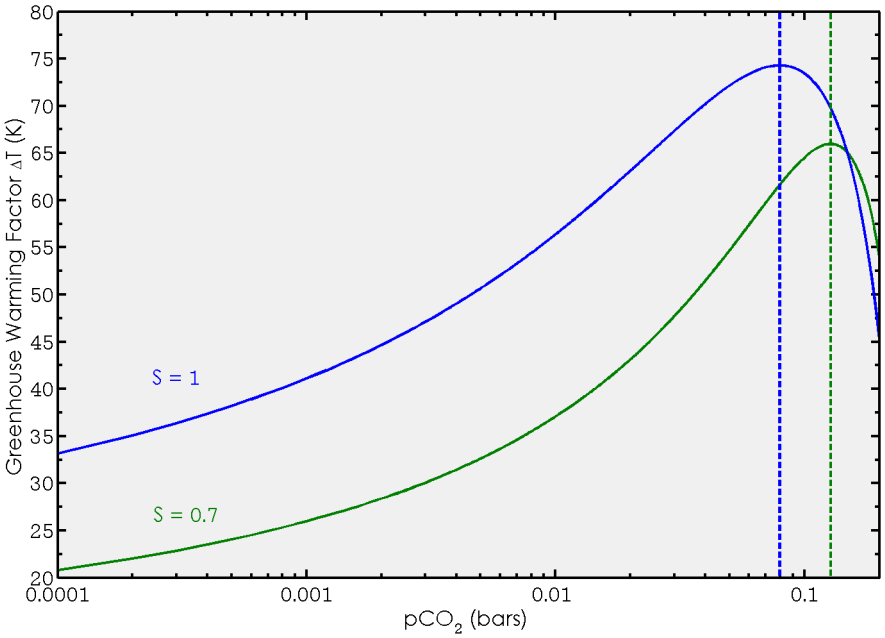

Figure 3.5: Greenhouse warming factor as a function of $p\mathrm{CO}_2$ under present day (S = 1) and Archean (S = 0.7) incident stellar flux from the climate parameterisation in Caldeira & Kasting (1992). The dashed lines represent the peak warming factor

under different stages of solar evolution (see figure 3.6 with warming factors under varying values of incident solar radiation, from 0.6 to 1.6 times present level). The parameterisation does not perform well under the higher levels of irradiation expected during the later stages of solar evolution; the greenhouse warming factor becomes inversely proportional to $p\mathrm{CO}_2$. This effect is unlikely to be representative of the atmospheric physics associated with climate under these conditions (i.e. CO_2 cloud condensation resulting in a cooling effect), but rather an artefact from pushing the fit outside of its intended limits. Therefore, we have chosen not to adopt this temperature parameterisation in our formulation of this model.

Other greenhouse warming parameterisations for gases in the Earth's atmosphere exist. The Fifth Assessment Report of the Intergovernmental Panel on Climate Change (IPCC) provides simplified expressions for radiative forcing of climate by CO_2, CH_4, nitrous oxide ($\mathrm{N}_2\mathrm{O}$) and various

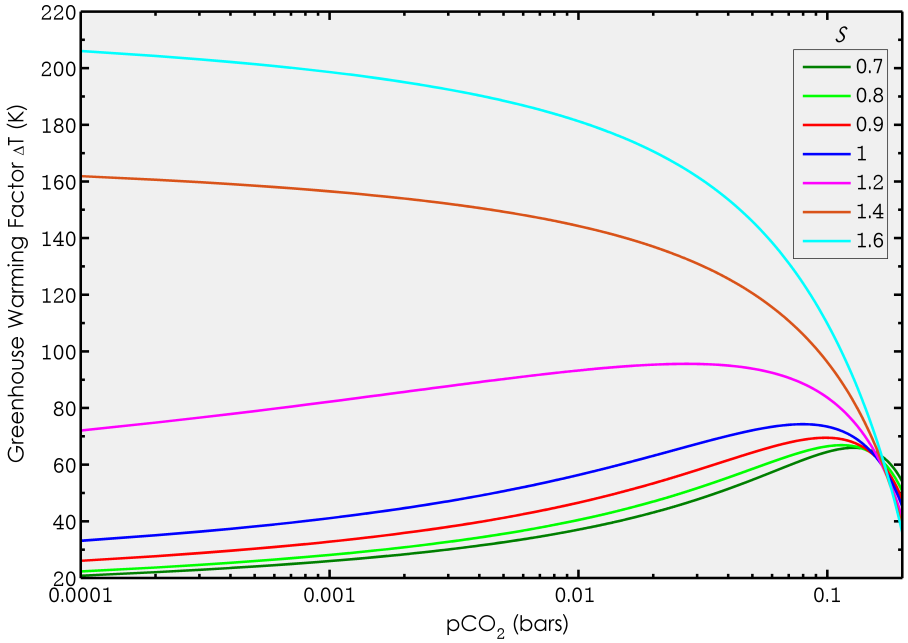

Figure 3.6: Greenhouse warming factors as a function of $p\mathrm{CO}_2$ under a range of stellar luminosity, from the climate parameterisation in Caldeira & Kasting (1992).

species of chlorofluorocarbons relevant to radiative forcing (Myhre *et al.*, 2013). Their formulation for carbon dioxide follows a logarithmic relationship between atmospheric concentrations (in ppm) and radiative forcing (ΔF) in W m^{-2}:

$$\Delta F_{CO_2} = \epsilon \ln \left(\frac{pCO_2}{pCO_{2_0}} \right) \tag{3.21}$$

Where the constant ϵ is 5.35 W m^{-2} and $p\mathrm{CO}_{2_0}$ represents pre-industrial concentrations (280 ppm). The constant in this formulation is derived from three-dimensional radiative transfer models of atmospheres containing well mixed greenhouse gases. (Myhre *et al.*, 1998). Previous editions of the report (i.e. 3rd report in 2001, 4th report in 2007) also include the additional expressions:

$$\Delta F_{CO_2} = \epsilon \ln \left(\frac{pCO_2}{pCO_{2_0}} \right) + \phi \left(\frac{\sqrt{pCO_2}}{\sqrt{pCO_{2_0}}} \right) \tag{3.22}$$

Here ϵ is 4.841 W m^{-2} and ϕ is 0.0906 W m^{-2}.

$$\Delta F_{CO_2} = \epsilon \left(\frac{g(pCO_2)}{g(pCO_{2_0})} \right) \tag{3.23}$$

In this case, ϵ is 3.35 W m^{-2} and $g(p\mathrm{CO}_2)$ is given as a third-order polynomial fit in the form:

$$g(pCO_2) = \ln(1 + 1.2(pCO_2) + 0.005(pCO_2)^2 + 1.4 \times 10^{-6}(pCO_2)^3) \tag{3.24}$$

In the above cases, the constants are derived with radiative transfer calculations using one-dimensional global average meteorological input data from Shi & Fan (1992) and Hansen *et al.* (1988). The respective Greenhouse Warming Factor (ΔT) can be found by equating the radiative forcing with a climate feedback or sensitivity parameter (λ):

$$\Delta T_{CO_2} = \lambda(\Delta F_{CO_2}) \tag{3.25}$$

This parameter (with units of K(W m^{-2})$^{-1}$) reconciles the global mean surface temperature response to the radiative forcing, and is nearly invariant, but its value is subject to debate and uncertainty. Estimates of λ are derived from the often addressed scenario in which carbon dioxide in the atmosphere doubles from its pre-industrial concentration; the IPCC derives a ΔF_{CO_2} of +3.7 W m^{-2} (under the assumption that without any other feedbacks, a doubling of CO_2 would result in a 1 K increase in surface temperatures) and a ΔT due to all well-mixed greenhouse gases of between 1.5 and 4.5 K, resulting in a λ of between 0.41 and 1.2 K(W m^{-2})$^{-1}$ respectively (Myhre *et al.*, 2013). We adopt a mean value for λ of 0.8 K(W m^{-2})$^{-1}$, which corresponds to a 3 K warming per doubling of CO_2, when

using this parameter to compute CO_2 greenhouse warming. A comparison of these IPCC formulations with that of Caldeira & Kasting (1992) can be seen in figure 3.7, with an additional inset figure illustrating the response of the these parameterisations over 'modern' concentrations of CO_2 (200 to 400 ppm).

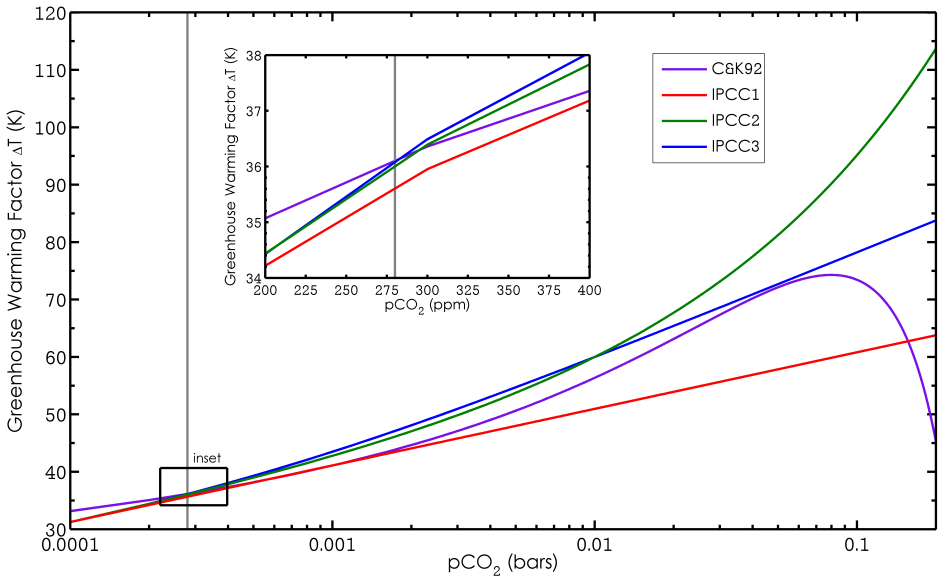

Figure 3.7: Greenhouse warming factors from a variety of climate parameterisations as a function of atmospheric CO_2. The inset figure displays the behaviour of these parameterisations under 'modern' values of pCO_2 (from 200 to 400 ppm on a linear axis, with default modern pCO_2 value of 280 ppm shown in grey) for comparison. (C&K92 = equation 3.20, IPCC1 = equation 3.21, IPCC2 = equation 3.22, IPCC3 = equation 3.23

)

This work adopts equation 3.22 ('IPCC2' in figure 3.7) in order to better capture the 'runaway' effect under high atmospheric CO_2. Whilst providing an interesting comparison these expressions have been developed to investigate the response of the climate system to increased anthropogenic carbon dioxide emissions over the relatively short term (tens to hundreds of years), as opposed to a generalised parameterisation that may hold throughout Earth's (or an Earth-like planet's) history (millions to billions of years). These approximations perform relatively well as climate parameterisations, but their insensitivity at low levels of pCO_2 does not

capture the climate 'collapse' seen when using the more parabolic curve from Caldeira & Kasting (1992), and predict 'habitable' conditions throughout the main-sequence lifetimes of the star (we make no allowance for the gradual expansion of the Sun and evolution to its red giant phase).

3.3.7 CO_2 Condensation & Cloud Formation

At some point, CO_2 in the atmosphere may reach such (very high) concentrations as to result in carbon dioxide cloud formation. It remains unclear as to whether these CO_2 clouds would be net absorbers or reflectors of short and/or long-wave radiation (Colaprete & Toon, 2003; Goldblatt & Zahnle, 2011; Joshi & Haberle, 2012; Kitzmann *et al.*, 2010; Zsom *et al.*, 2012). Their effect on albedo and the radiative balance of the planet will likely be affected by several complex factors (spectra of incident radiation, zenith angle, atmospheric lapse rate, pressure broadening etc.) beyond the scope of this simple model. However, it holds that if they are net reflectors of long wave radiation, and they have often been parameterised as albedo features (e.g. Selsis *et al.*, 2007), then there may be a limit at which very high $p\mathrm{CO}_2$ would prevent a breakout of an entirely glaciated planet (a 'snowball'), if that planet formed at a great distance from the star (near the outer edge of the HZ), because the carbonate-silicate weathering feedback would be essentially broken – higher levels of $p\mathrm{CO}_2$, emitted into the atmosphere from the mantle via arc volcanism for example, would result in greater cloud formation and planetary cooling. Furthermore, as terrestrial weathering would be negligible (given that the surface is covered by ice) and a spatial disconnect between the continents, the ocean and the atmosphere would exist, this configuration would resign the planet to a frozen waste. It would be impossible for the planet to 'breakout' of the snowball state, unless increasing stellar luminosity could end the stalemate between CO_2 condensation and cloud formation and albedo.

3.3.8 Estimating Greenhouse Warming & Albedo from a 1-D Radiative-Convective Climate Model

Further to the methods described above, fits can also be made to data from an updated 1-D radiative-convective climate model in order to improve the accuracy of the output. One such model is described by Kopparapu *et al.*, (2013), as a restructured version of that first presented in Haqq-Misra *et al.* (2008). 3-D interpolations of surface temperatures and albedo were made from output data from this model under a 1-bar, cloud- and ozone-free, N_2-dominated model atmosphere, which includes CO_2 and H_2O absorption coefficients from the HITRAN and HITEMP line-by-line databases (Kopparapu *et al.*, 2013). The plots shown in figures 3.8 and 3.9 (temperature, albedo) display the results of those interpolations, under normalised solar flux values from 0.7 to 1.7 (where $S = 1$ corresponds to present day solar values), and CO_2 mixing ratios between 0.0001 and 0.9.

It is worth noting that high solar insolation values (above 1.6 with low CO_2, and above 1.4 with high CO_2) results in both albedo and temperature interpolations displaying numerical instability as the physical limits of the model are reached. In these regions, the results of the model may be unrealistic, and convergence is difficult to achieve (Haqq-Misra, 2015, *personal correspondence*). However, the application of this model at high solar insolation is nearly always coupled with negligible levels of atmospheric CO_2, where the behaviour of the model is less unpredictable, as much of this atmosphere carbon reservoir has been depleted by the action of intense weathering.

This climate model has been used to produce updated estimates of the habitable zone (in Kopparapu *et al.* (2013)), superseding those first presented by Kasting *et al.* (1993), as well as for early Martian climate studies (Ramirez *et al.*, 2014a) and for investigating the possibility of inducing a runaway greenhouse catastrophe by increased atmospheric CO_2 (Ramirez *et al.*, 2014). Output from this model may underestimate albedo somewhat, as CO_2 is assumed to exhibit an inverse relationship with bond albedo in this formulation: at higher CO_2 levels Rayleigh scattering becomes significant reducing the overall reflectivity of the atmosphere.

Bond albedo under current conditions (shown as a blue star in both plots) is predicated to be ∼0.25, whereas other estimates place it closer to 0.30 (Williams, 2014). For internal consistency, when using this model (as opposed to the integrated temperature parameterisations discussed previously), the ice-albedo transition (equation 3.19) is disabled and albedo is computed at each timestep as a function of $p\mathrm{CO}_2$. Due to the inability of this fit to capture high albedo events (clouds, ice-albedo transitions etc.) albedo in these cases are likely underestimated.

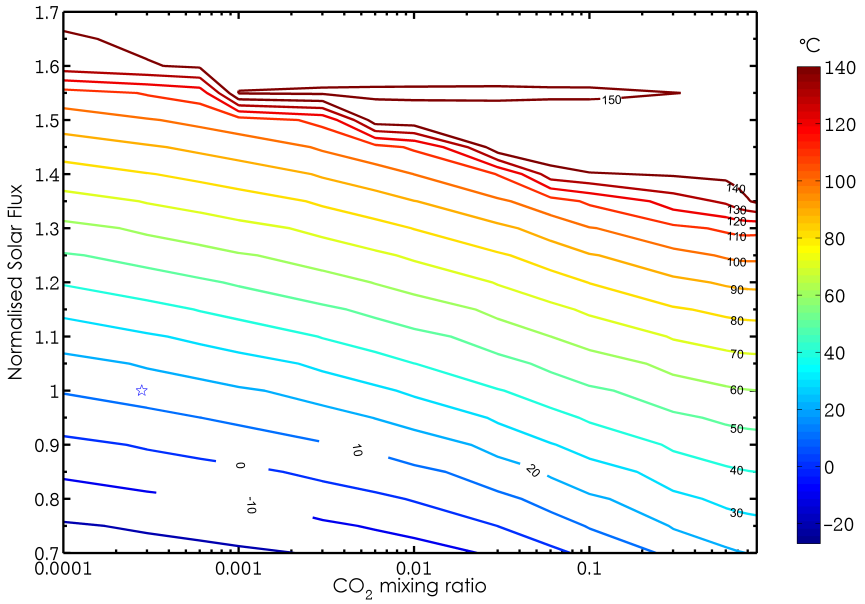

Figure 3.8: Greenhouse warming factor as a function of CO_2 and incident stellar flux, from the 1-D radiative convective model presented in Kopparapu *et al.* (2013).

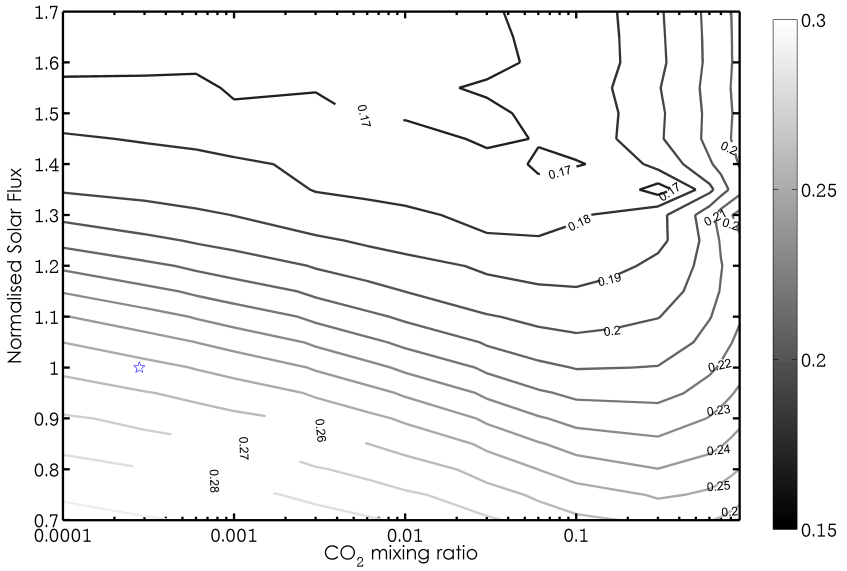

Figure 3.9: Planetary surface albedo as a function of CO_2 and incident stellar flux, from the 1-D radiative convective model presented in Kopparapu *et al.* (2013).

3.3.9 Methane Greenhouse

Methane concentrations in the early atmosphere of the Earth were probably much higher than today, resulting in the formation of an organic haze similar to that seen on the Saturnian moon Titan (Zerkle *et al.*, 2012). Methane is an effective greenhouse gas, and its increased abundance in the atmosphere of the early Earth has often been invoked as a solution to the 'Faint Young Sun' paradox (Haqq-Misra *et al.*, 2008). It remains very difficult to determine with sufficient accuracy the absolute mixing ratio of CH_4 in the Archean eon as little geological or geochemical proxy evidence remains. Biogeochemical modelling approaches suggest that methane concentrations could have reached ∼1000 ppm during the Archean, as opposed to the ∼2 ppm at present, thereby contributing significant warming to the climate of the Earth at the time (Haqq-Misra *et al.*, 2008). We adopt a similar greenhouse parameterisation for methane as described above for CO_2; taken from the IPCC 5th Report (Myhre *et al.*, 2013):

$$\Delta F_{CH_4} = 0.036(\sqrt{pCH_4} - \sqrt{pCH_{4_0}}) - (f(pCH_4, pN_2O) - f(pCH_{4_0}, pN_2O_0)) \tag{3.26}$$

Where $p\mathrm{CH}_4$ is atmospheric methane concentrations given in ppb (parts per billion by volume), $p\mathrm{CH}_{4_0}$ describes pre-industrial methane levels (∼700 ppb). Nitrous oxide ($\mathrm{N}_2\mathrm{O}$) is also included in this formulation, but is neglected for the purposes of this study ($\mathrm{N}_2\mathrm{O}$, $\mathrm{N}_{2_0}\mathrm{O} = 1$). The temperature forcing associated with the methane greenhouse can be calculated by equating the above radiative forcing estimation with a climate sensitivity parameter (λ).

$$\Delta T_{CH_4} = \lambda(\Delta F_{CH_4}) \tag{3.27}$$

Present day methane fluxes are on the order of 30×10^{12} mols C yr^{-1}, and atmospheric concentrations are approximately 1.8 ppm. See figure 3.10 below for a representation of the relationship between $p\mathrm{CH}_4$ and

greenhouse forcing. Claire *et al.*, (2006) estimates that pre-industrial flux of methane from methanogenesis would have been on the order of 400×10^{12} mols C yr^{-1}, which equates to approximately 22 ppm pCH_4, assuming it escaped into the atmosphere without oxidation in the benthic sediment.

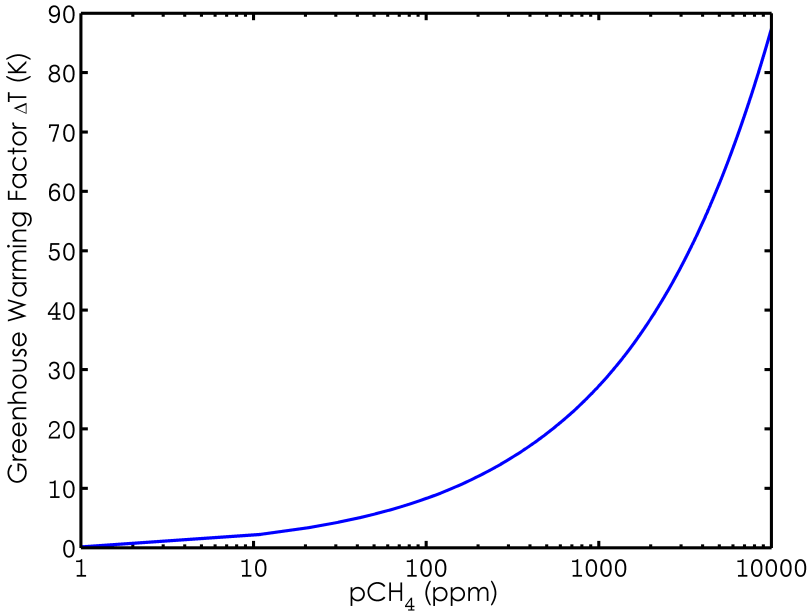

Figure 3.10: Greenhouse warming as function of pCH_4.

Sources of methane into the Archean atmosphere would have originated from volcanic sources, or from the decay or organic matter in anaerobic environments, and given the reducing nature of the atmosphere at the time would have persisted for longer and accumulated to higher concentrations than at present. Rates of methanogenesis in the Archean would almost certainly have been higher, due to lower rates of oxidation by methanotrophs in the anoxic ocean (Claire *et al.*, 2006). For this model, methane concentrations are held constant at 22 ppm throughout contributing a greenhouse forcing of approximately 3.5 K.

3.3.10 Water Vapour Greenhouse

Water vapour also acts as a powerful greenhouse gas on terrestrial planets with significant water on the surface, becoming optically thick at high

concentrations, and provides a strong positive feedback on climate. It is likely that the saturation of the Earth's atmosphere with water vapour will result in the termination of habitable conditions on the planet via a 'runaway greenhouse' event in the distant future; Goldblatt *et al.*, (2013) describe this limit as the point at which the absorbed solar flux at the planet exceeds the outgoing infrared flux, and modelling approaches suggest that 100 times the present atmospheric level of CO_2 may be sufficient to trigger a runaway climate catastrophe. It should be noted that the threshold limit for this scenario is not well defined however (Goldblatt *et al.*, 2013, Ramirez *et al.*, 2014). The amount of water vapour in the atmosphere depends exponentially on the surface pressure and logarithmically on the temperature, but as the physics of this process cannot be realistically captured with a model of this complexity, it is simplified here in the form:

$$\Delta T_{H_2O} = 29.7 + 0.5(T_S - 290) \tag{3.28}$$

The linear form of this function is due in part to the fact that whilst vapour pressure increases exponentially with temperature, greenhouse temperature increases logarithmically with vapour pressure resulting in a linear function overall (Walker *et al.*, 1981). This parameterisation is not included when calculating surface temperature from the climate model presented in Kopparapu *et al.* (2013).

The final formulation for surface temperature is therefore:

$$T_{Surf} = T_{eff} + T_{CO_2} + T_{CH_4} + T_{H_2O} \tag{3.29}$$

3.4 Sensitivity Analysis

3.4.1 Model Data Structure

For efficiency, data protection and backup, consideration was taken in designing a model structure that ensured visibility, effective graphical output, naming conventions and automatic storage and backup. The model structure can be illustrated diagrammatically:

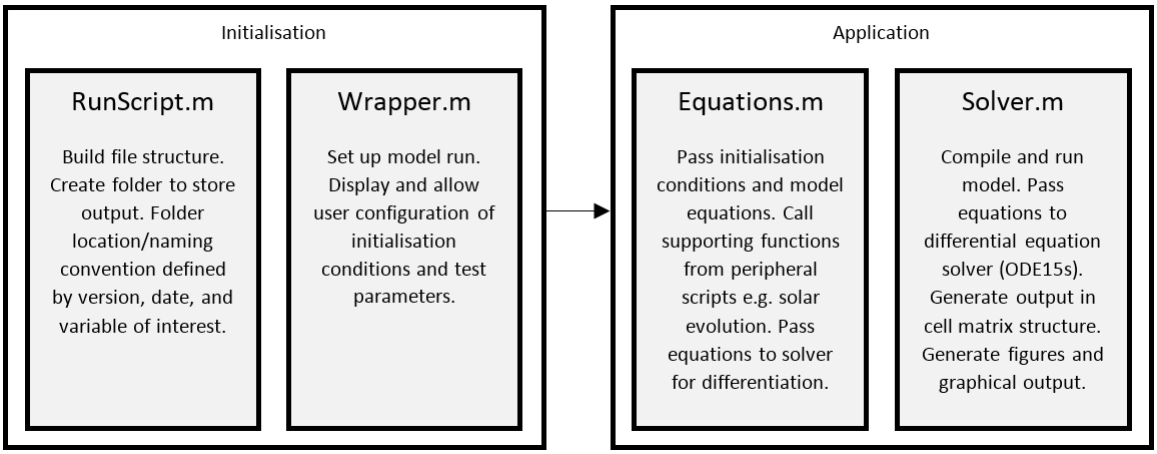

In order to determine the relative response of the model to the parameterisations and determine the likely uncertainties, limits and robustness of the system a sensitivity analysis was initially conducted using a One-at-a-time (OAT/OFAT) approach. This exercise is valuable in increasing understanding of the relationships between the input and output variables in the model, and in identifying the input(s) that cause significant uncertainty in the output. Model parameters with little effect on the output can also be identified and fixed and redundancies in the structure can be eliminated and the model as a whole simplified. Crucially, identifying the response of certain inputs in parameter space is integral to optimising the performance and predictability of the model i.e. the peak greenhouse heating factor under a given value of solar irradiation. The model was initialised using the temperature parameterisations (as opposed to the 1-D climate model fits) described above.

3.4.2 Effect of α on T and CO_2

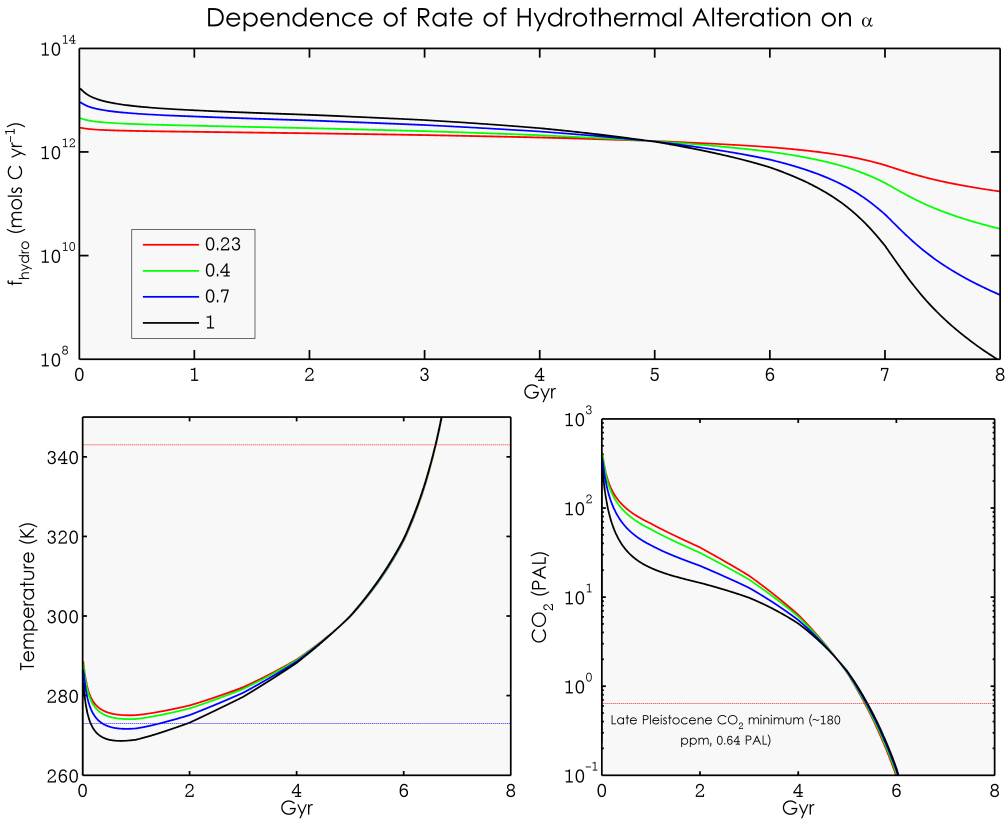

Figure 3.12: Model response to differing values of α (sensitivity of hydrothermal carbonitization to CO_2). Top: hydrothermal carbonitization flux. Bottom left: surface temperature. Bottom right: atmospheric CO_2.

Model output suggests that the dependence of the rate of seafloor hydrothermal alternation on the exponent α represents a strong control on the climate of the early Earth. α is a parameter that alters the dependence of seafloor carbonitization on the concentration of CO_2 in the atmosphere (assumed to be in equilibrium with that of the bottom waters), where complete depletion corresponds to $\alpha = 1$. In our formulation (see equation 3.10), hydrothermal carbonitization scales with the square of heat flow and therefore the proportionately much higher level of warm crust creation during the Archean would drive this process at a much more rapid rate than today. This process, spatially and geochemically independent of temperature-dependent terrestrial weathering processes, serves as a strong

sink for CO_2 during the early part of the Earth's geochemical history. Initially, it was thought that the relationship between ocean CO_2 and hydrothermal carbonitization of basaltic rocks would be a strong linear function (i.e. $f_{hydro} \propto RCO_2$) given fast reactions under a condition of a superabundance of cations (Ca^{2+}, Mg^{2+}, K^{+}, Na^{+}) (e.g. Franios & Walker, 1992), but subsequent laboratory experiments that attempted to empirically derive the dependence of the rock-water reactions involved in the process of hydrothermal alternation estimate the dependence to be much weaker in reality: Brady & Gslason (1997) conclude that $f_{hydro} \propto (RCO_2)^{0.23}$. This result is the only available empirical data constraining this important parameter. Mills *et al.* (2014) note that the shifting balance between terrestrial and seafloor carbon removal fluxes over the course of Earth history may be crucially important in determining not only the atmospheric CO_2 and climate, but also the amount of oxygen in the atmosphere by altering the chemical weathering flux and the rate of organic carbon burial.

Higher values of α result in lowering the predicted pCO_2 and global average temperature during the Archean due to the stronger negative feedback. Whilst representing a strong divergence during the early and very late stages of the model run, the dependence of f_{hydro} on α has little effect on the termination of habitable conditions. The climate of the early Earth is however very sensitive to the rate of f_{hydro} due to the higher level of crustal formation, spreading rates and proportionally greater levels hydrothermal alteration resulting in a stronger CO_2 sink.

A weaker dependence on CO_2 ($\alpha < \sim 0.5$) seems sufficient to ensure that global average temperatures remain above freezing during the Archean, with several hundred times the present atmospheric level (PAL) of CO_2 in the atmosphere. In reality, the water-rock kinetics involved in this reaction are likely to be dynamic and change over time as the availability of cations delivered from the continents varies.

It should be noted that contemporary modelling approaches, including the formulation described above, most likely do not capture to the mechanisms of seafloor weathering particularly accurately. Assuming that the temperature of bottom waters is a function solely of atmospheric CO_2

concentration is an oversimplification that would skew results when solar input is low and atmospheric CO_2 is high - in the Archean for example. Furthermore, localised water temperatures at sites of hydrothermal vents or spreading ridges are likely to be much higher than the mean temperature of oceanic bottom waters (or indeed the surface temperature), but as of present, no satisfactory parameterisation of seafloor weathering kinetics exists.

We adopt the lower limit given in SZ01 and take f_{hydro_0} as equal to 1.65×10^{12} mols C yr^{-1}, but note that estimates of f_{hydro_0} in the literature vary between 0.5 and 3×10^{12} mols C yr^{-1} (Mills *et al.*, 2014).

3.4.3 Effect of β on T and CO_2

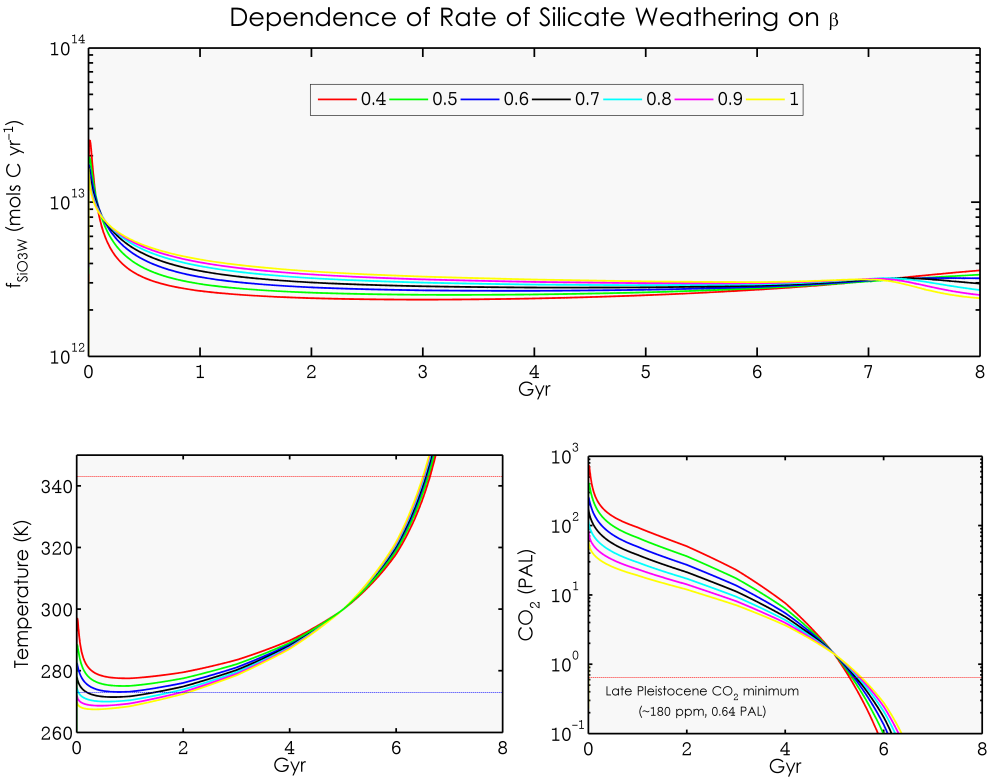

Figure 3.13: Model response to differing values of β (sensitivity of rate of terrestrial silicate weathering to CO_2). Top: silicate weathering flux. Bottom left: surface temperature. Bottom right: atmospheric CO_2.

Silicate weathering and its dependence on temperature and atmospheric CO_2 is an integral driver in controlling planetary climate. The dependence of the reactions involved in this process has been an area of study for several years due to the importance of this process as a feedback on global planetary climate (see discussion above). Equation 3.12 illustrates our parameterisation of silicate weathering, following SZ01, where the exponent β controls the sensitivity of the reaction to the partial pressure of atmospheric carbon dioxide and the rate of carbonic acid formation. Recall that the constant B (default value = 13.7) is derived from the parameterisation of temperature-dependent runoff kinetics, and attempts to capture the dissolution kinetics of silicate materials as a function of temperature (Berner & Kothavala, 2001; Walker *et al.*, 1981). Increasing the dependence of weathering on β results in lower global average temperatures and pCO_2 as the rate of weathering is proportionally higher for a given CO_2 concentration, thereby drawing down more CO_2 and reducing temperatures. SZ01 take β as equal to 0.3, which returns a present day weathering flux of 6.5×10^{12} mols C yr^{-1}, within the range of other workers in this area (e.g. Berner, 2006; Mills *et al.*, 2014), and given the uncertainties involved in the parameterisation of this process this figure is within expected estimates. The action of plant roots as a factor in accelerating terrestrial weathering has not been taken into account in these estimations, but will be addressed in a later section. Berner (1997) suggests calibration constants equivalent to taking $\beta = 0.5$ and B = 11.1. Given this form of Equation 3.12, present day $f_{SiO_{3_{W^0}}}$ is $\sim 6.7 \times 10^{12}$ mols C yr^{-1}.

3.4.4 Effect of μ on T and CO_2

The exponent μ controls the shape and magnitude of the exponential decay of geothermal heat flux (Q) over time (see equation 3.5). Estimates of μ range from 0.2 to 0.7, and the model was tested in this range under default conditions. Lower values of μ result in a shallower curve with a peak relative heat flow of between 3 and 4.5 present day, with more CO_2 in the atmosphere during the early part of the run, and higher temperatures. The higher values of this exponent seem to result in a crash of the system in

which nearly all the CO_2 is drawn down and the planet freezes. From figure 3.14 it seems that under conditions of more vigorous outgassing associated with higher values of μ the metamorphic flux drops reasonably sharply early on, and the excess carbon seems to be taken up by increased carbonisation on the seafloor.

Davies & Davies (2010) estimate the present day geothermal heat flux to be 0.0961 W m^{-2}, suggesting a heat flux of between 0.29 and 0.43 W m^{-2} in the very early stages of the planet's history under conservative estimates of μ, but much greater under higher values of μ. For example, assuming $\mu = 0.7$ as in SZ01, then the planetary geothermal heat flux peaked at 76 times present day, approximately 7 W m^{-2}, immediately following accretion. This flux is extremely high, similar to that of Jupiter's very tectonically-active satellite Io, which experiences high rates of geothermal heat flux from tidal flexing and gravitational interactions with Jupiter, Ganymede, and Europa resulting in a heat flux at the surface of between 2 and 13.5 W m^{-2} (Hagermann, 2005).

As shown the ensemble plot (figure 3.14), the effect of μ on the output of the model is significant, and especially pronounced in the control of the key carbon sinks, silicate weathering and seafloor carbonitization, during the early part of the simulation. Higher rates of geothermal heat flow result in an increase in silicate weathering of several orders of magnitude, and a 10-fold increase in hydrothermal carbonitization. However, these increases are not sufficient to buffer the high rates of outgassing, and pCO_2 remains much higher throughout high-μ simulations with a proportional response in the greenhouse forcing resulting in a significant increase in surface temperatures. We adopt the lower value of μ (0.2) in agreement with other workers in this area (Lowell & Keller, 2003; Franck *et al.*, 1999).

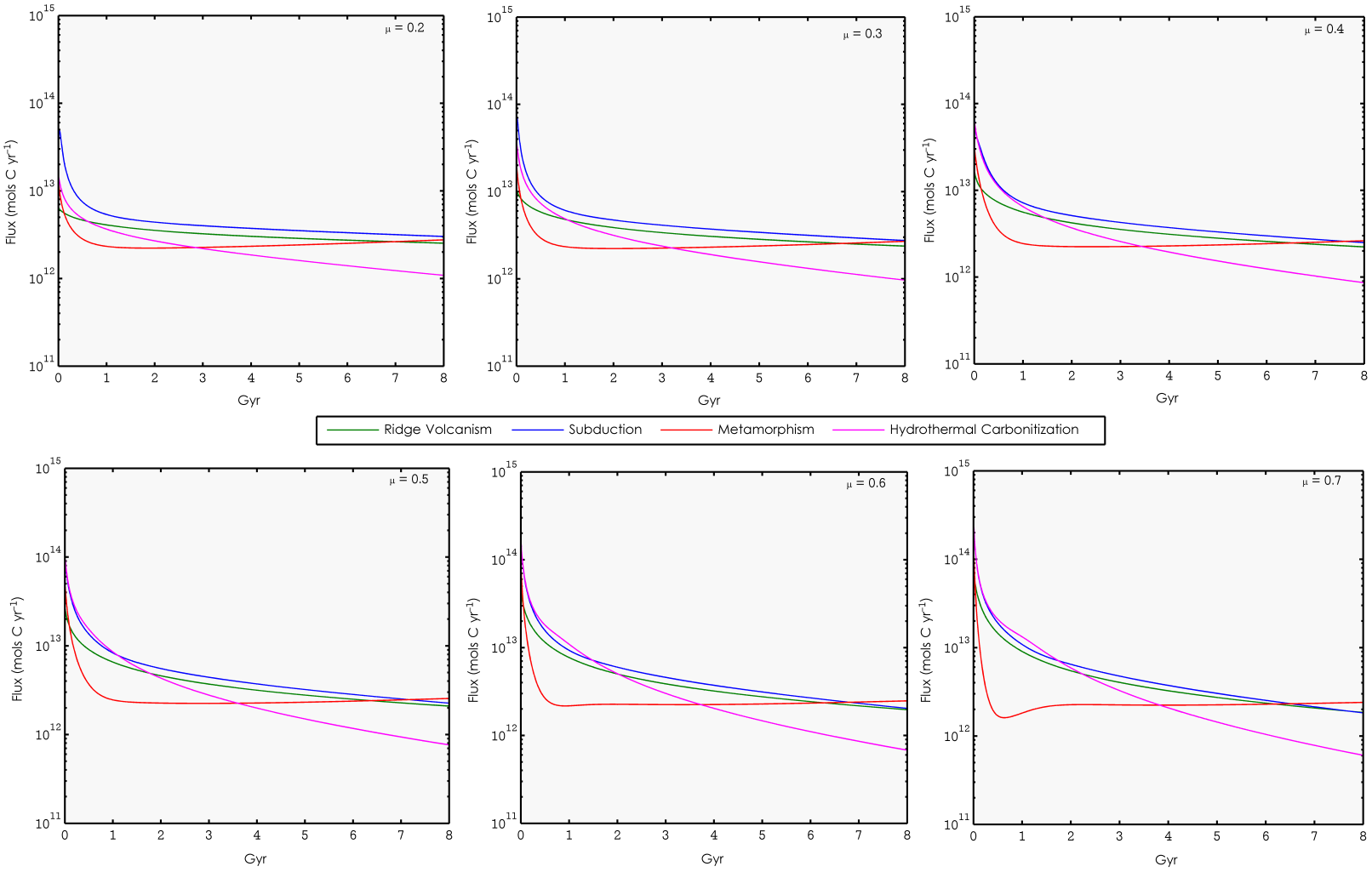

Figure 3.14: Response of fluxes dependent on geothermal heating to differing values of μ.

3.4.5 Effect of roots & biology on weathering rates

The emergence of land plants during the Devonian Period (400 - 360 million years ago) had a significant effect on the terrestrial carbon cycle. Mechanical erosion of strata by plant roots, and chemical dissolution by organic acids (oxalic, humic) secreted by symbiotic microorganisms and formed via leaf-litter decomposition, increases the rate of terrestrial weathering, which would in turn, increase the rate of CO_2 draw down from the atmosphere (Berner, 2005). Additionally, plants return a large proportion of carbon-rich organic matter for burial upon their deaths, and throughout their lifecycle represent a significant interface between the geosphere and biosphere. Plants also represent a key reservoir and recycling flux in the hydrological cycle via the process of evapotranspiration, whilst the action of their roots also serve to buffer against rainfall erosion. Contemporary workers estimate that the combined effect of these processes may accelerate silicate weathering rates by a factor of between 2 and 10 (Berner, 2005). Crucially, the biological enhancement factor (BEF, κ) that results in present-day weathering rates is not well constrained, and therefore this factor remains an area of uncertainty.

We adopt a conservative estimate for κ of 0.5, accepting that the action of roots and organic acids associated with plant life likely doubled the rate of terrestrial weathering. This is a time-dependent and/or optional parameter in the model framework, and can be negated to investigate the behaviour of an abiotic terrestrial environment, or 'turned on' at a given point during the evolution of the planet to attempt to replicate the colonisation of the land surface by plant life.

3.4.6 Comparisons between a radiative-convective climate model & temperature parameterisations

The parameterisations for albedo, as well as the CO_2, CH_4 and H_2O greenhouses that are described by Equations 3.20 – 3.28 and summarised by 3.29, provide a model framework for resolving the evolving planetary climate under a brightening sun and with an integrated carbon cycle to first

order. These are formulations taken from the wider literature fits to output from climate models of varying complexity that have been incorporated into the model to produce an approximation of the greenhouse warming contributed to the climate system by these important atmospheric gases. However, a 1-dimensional (vertically through the atmosphere) radiative-convective climate model using updated empirical data for updated CO_2 and H_2O absorption coefficients from the HITEMP and HITRAN line-by-line databases would most likely provide a better integrated and more self-consistent representation of the planetary climate system. This approach also produces output based on up-to-date empirical data, and exploits advances in our understanding of the climate system that have superseded those used in these earlier formulations For example, the temperature-dependent albedo and one CO_2 greenhouse parameterisation discussed above are from Caldeira & Kasting (1992), and the water vapour/temperature relationship was first presented in Walker *et al.* (1981) significant improvements in modelling and data assimilation have been made in the intervening three decades.

Comparisons between the output of the original formulation of the model (using multiple climate parameterisations) and that of the model when using a 3-D spline interpolation to data from the 1-D climate model discussed above, are shown in figure 3.15, where grey lines represent the former case. There is reasonable agreement between the two runs, with the 1-D climate case predicting lowered temperatures (with implications for the early history of the planet), lower albedo and higher levels of atmospheric CO_2 that persist for longer. A 'runaway greenhouse' event is also captured in this scenario, as surface temperatures increase significantly while albedo simultaneously drops markedly.

3.4.7 Comparison to the COPSE model

The COPSE (Carbon-Oxygen-Phosphorus-Sulphur-Evolution) biogeochemical model describes a scheme of similar complexity, but which operates within the particular environmental and biological framework of the Phanerozoic eon (3.9 Gyr to present) in Earth history, and has been

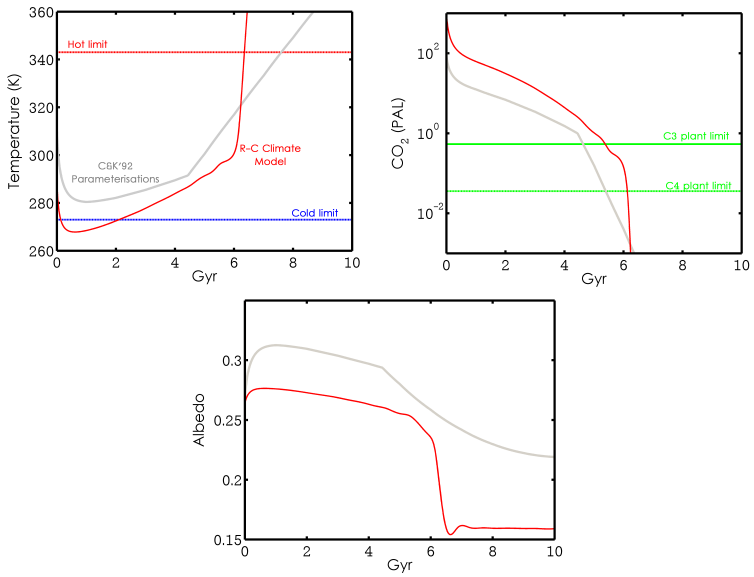

Figure 3.15: Comparisons between radiative-convective climate model (red) & temperature parameterisations (grey) from Caldeira & Kasting (1992). Note the rapid increase in temperatures and contemporaneous drop in albedo displayed by the radiative-convective climate model results, which is interpreted as a 'runaway greenhouse' event.

used to track fluxes of carbon and atmospheric oxygen over this time. First presented by Bergman *et al.* (2004), COPSE has a greater temporal resolution, and also includes a dynamic sulphur (S), phosphorus (P) and iron (Fe) cycle, important for accurately representing the global oxygen cycle, which produces more detailed, high resolution $p\mathrm{CO}_2$ predictions, as output is constrained by $\delta^{34}\mathrm{S}$ and $\delta^{13}\mathrm{C}$ isotope studies.

Our results demonstrate acceptable agreement with the output from the COPSE model during this period, but this model predicts stable temperatures over the Phanerozoic compared to COPSE, most likely due to the more detailed weathering and burial fluxes associated with the iron and sulphur cycle, both of which are absent in this work. As it is clear from this comparison that the model developed here lacks the ability to resolve highly temporally variable CO_2 and temperatures associated with the Phanerozoic, mean values of CO_2 and temperature from COPSE (split at the Permo-Carboniferous) have also been included for a more appropriate

comparison. COPSE predicts somewhat higher (>10 PAL) and generally more variable levels of pCO_2 throughout, with a marked decline in atmospheric carbon during the Permo-Carboniferous due to increased weathering rates from land plant evolution, and a shift of organic carbon burial from the ocean to the land.

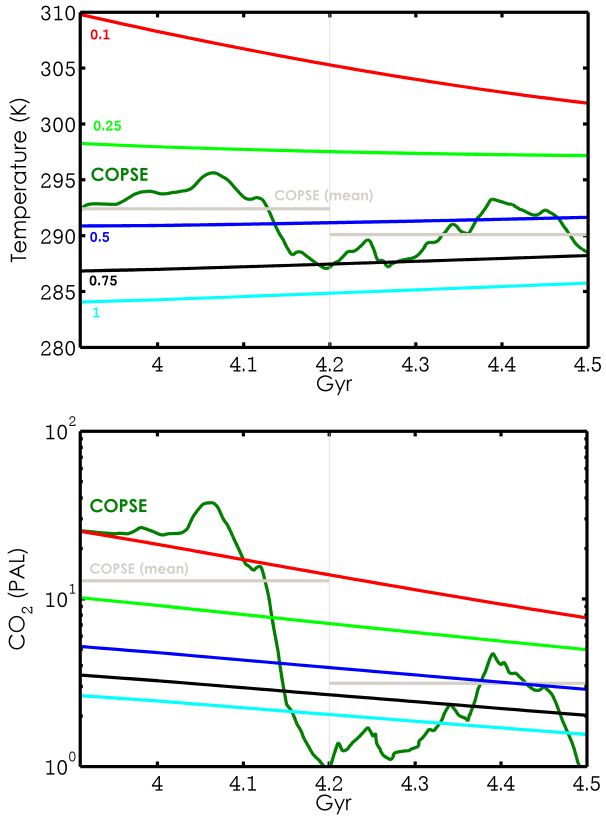

Figure 3.16: Model output under differing values of κ (biotic enhancement factor) compared to results from COPSE model (in dark green, with time-averaged values represented in grey)

In contrast, an ensemble of runs from the model developed here is also included on the above plot. These results are generated using differing values of κ, which is a 'biotic enhancement factor' for terrestrial weathering, as both models have an explicit formulation of this parameter. κ values range from 1 to 0.1, which in our model represents no enhancement to 10 times weathering enhancement by terrestrial plant life, respectively. All

runs suggests a secular decline in pCO_2 from 3.9 Gyr, unpunctuated by fluctuations associated with changing fluxes in the sulphur cycle seen in COPSE, but good correlation between the models occurs when using κ values between 0.25 and 0.75, with 0.5 resulting the best agreement. This suggests that plants approximately doubled the rate of terrestrial weathering following their colonisation of the continental surface. This is reflected further by the better agreement in both temperature and CO_2 between the models post-4.2 Gyr, when this factor is enabled in COPSE. pCO_2 levels in both models descend towards 1-3 PAL CO_2 at 4.5 Gyr, with 3 PAL representing the average pCO_2 value during the past ∼300 million years (SZ01).

Differences in the model can be explained by the fact that this model also includes a (static) CH_4 greenhouse effect, and utilises a different CO_2 greenhouse parameterisation to that of COPSE, whilst neglecting the effect of the oxygen cycle (and Fe, S and P cycles) on carbon burial and associated fluxes (Bergman *et al.*, 2004). The temporal resolution is also lower in our model, but is more suited to investigating the hypotheses presented here regarding long-term (geological/astronomical timescales) planetary habitability in the absence of an explicitly modelled oxygen cycle. COPSE remains the pre-eminent biogeochemical research tool for investigating paleo-atmospheric concentrations of oxygen and pCO_2 on the Earth during the Phanerozoic, and provides a good comparison for output from this model during that time.

3.4.8 Comparison to other pCO_2 proxies

Using the results published in a study by Fuelner (2012), a comparison between model output pCO_2 and empirical or geochemical proxy evidence from elsewhere can be made. Figure 3.16(a) displays pCO_2 as function of S/S_0 generated from default model conditions, as well as estimates of atmospheric carbon dioxide from other sources. This figure is modified slightly from Feulner (2012). Modelled pCO_2 from this work displays a reasonable agreement with estimates from these sources, falling within the error range of 4 of the 7 studies.

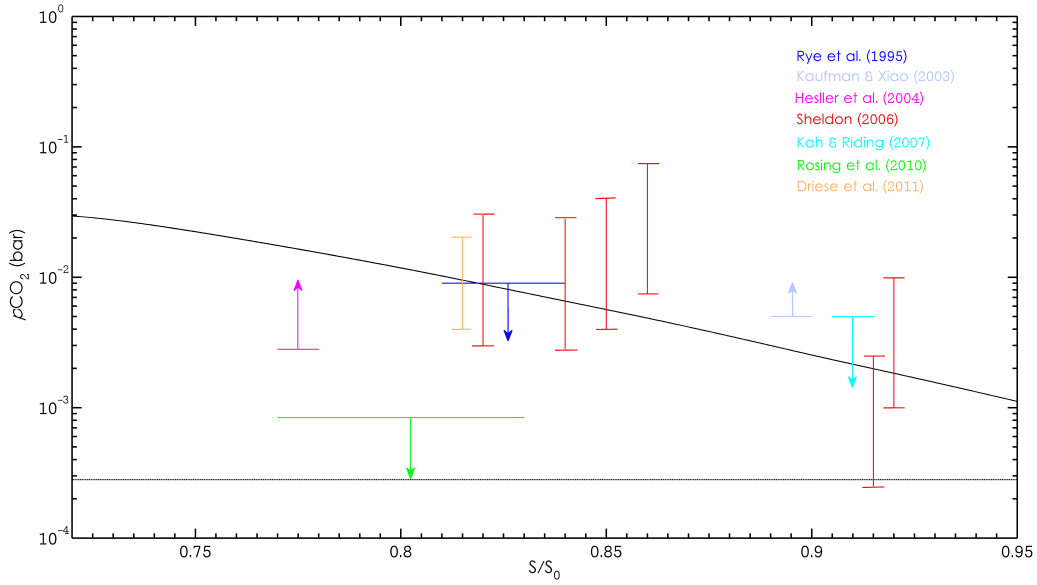

Figure 3.16(a): Modelled pCO_2 (in bars) (dark line) as a function of time/solar constant, and comparison with empirical estimates of atmospheric carbon dioxide. Figure modified from Feulner (2012). The dashed line indicates pre-industrial pCO_2 (0.000280 bar)

.

3.5 Results

3.5.1 Default Model Setup

Output from model will be used to assess the ability of the parameterisations to reproduce the biogeochemical history of Earth to first order, and therefore the model's predictive powers when applied to hypothetical cases. The 'default' state of the model is described by table 3.2, the contents of which have been compiled and summarised from the previous section on methodology.

Plots illustrating the output of the model initialised using these default conditions are show in figure 3.17. The model was run for a planet of 1 $M_\oplus$ for 10.9 billion years, determined by the stellar evolution model of Rushby *et al.*, (2013) as the likely main sequence lifetime of a 1 $M_\oplus$ star, and figure 3.17 displays, clockwise from top left, the global average temperature

Parameter	Definition	Value (Range)
α	Dependence of seafloor carbonitization on dissolved CO_2 in seawater	0.23 (0.23 - 1)
β	Dependence of terrestrial silicate weathering on CO_2	0.3 (0.3 - 1)
γ	Dependence of terrestrial carbonate weathering on CO_2	0.3 (0.3 - 1)
μ	Geothermal heat scaling parameter	0.2 (0.2 - 0.7)
κ	Biological enhancement factor for terrestrial weathering	0.5 (0.1 - 1)
a	Albedo	0.3 (0.1 - 0.6)
$M_\oplus$	Planet mass	1 (0.5 - 10)

Table 3.2: Default model parameters

(bounded by habitability limits in red (343 K) and blue (273 K)), atmospheric CO_2 concentrations (bounded by photosystem limits of 150 and 10 ppm for C3 and C4 plants respectively), outgoing longwave radiation, surface temperature as a function of incident stellar flux, the albedo, and the evolution of the geothermal heat flow from the planet interior to the surface. Global average temperature was computed from interpolated fits to the climate model described in section 3.3.8.

Geothermal heat flux from the planets interior drops off exponentially following accretion, peaking at 0.33 W m^{-2} or $\sim$3.4 times the present value (0.0961 W m^{-2}) soon after planet formation, before declining to less than 0.1 W m^{-2} within 3 Gyr. Given the strength of this forcing as a driver for many processes in the model, it is unfortunate to note that the shape of this decay function is fraught with significant uncertainty, but this relationship is in agreement with that of other modelling studies. Research in this area is limited by the difficulty in reconstructing radioisotopic

abundances in the crust of our planet, and also in observing comparative forms of geothermal heat flux on other planetary bodies.

Atmospheric CO_2 levels peak in the very early stages of the run at levels approximately 300 times the present atmospheric level (PAL) due to the high levels of geothermal heating and associated volcanic and tectonic fluxes, as well as the low temperatures and weathering removal fluxes, before a secular decrease through the first half of the planet's history, and culminating in a collapse as carbon dioxide is stripped from the atmosphere by enhanced terrestrial weathering due to higher temperatures. Atmospheric CO_2 drops below the C3 and C4 plant limit after 5.38 Gyr and 6.13 Gyr respectively, which would put increasing stress on primary producers dependent on oxygenic photosynthesis for energy production. The carbonate-silicate buffer begins to dismantle at this stage, as CO_2 is not returned to the atmosphere/ocean system at an equivalent rate as it is being removed due to the lower geothermal heat flux, ocean-floor spreading rates and tectonic outgassing. The planetary greenhouse becomes dominated by water vapour following this collapse, resulting in a strong positive feedback and producing a runaway greenhouse effect culminating in the termination of habitable conditions approximately 6.35 Gyr after planet formation. Methane concentrations, and their contribution to the planetary greenhouse, remain constant at 22 ppm and 3.5 K respectively throughout.

Surface temperatures are low at this early stage ($\sim$275 K), as incident solar flux is $\sim$30% less than present and albedo is $\sim$0.27, but are likely lower than temperatures would be in actuality as this model cannot capture the complexities of the immediate post-accretion surface and heat regime on a newly formed planet. The atmosphere of the new planet would be very different from that of the model atmosphere described above, and therefore the output for the first $\sim$1 Gyr immediately following planet formation is unlikely to be representative of the actual planetary conditions, and should therefore be interpreted as such for the purposes of this study. High impactor flux (analogous with the Late Heavy Bombardment for example) is also excluded.

Nevertheless, the model consistently underestimates surface temperature at

this early stage, and refinements to the radiative-convective model from which the fits for this work were drawn will have to be instigated to improve the performance of these parameterisations (Haqq-Misra *personal communication*. Furthermore, while it is unlikely that the planet would be covered by ice during this phase, albedo would likely be higher than the results presented below suggest, primarily due to the effect of a hazy methane greenhouse. The albedo of the planet ranges between 0.27 and 0.15 over the course of the the planet's history. This is also likely an underestimate that should be addressed in future updates to this climate model. Recent modelling work suggests a methane haze may have blanketed the planet during this period, further complicating the atmospheric chemistry, surface temperature and albedo history of the model planet (Zerkle *et al.*, 2012).

The amount of carbon stored in each of the four reservoirs (the mantle, continental sediments, oceanic crust and ocean/atmosphere), as well as the fluxes between these carbon pools, is shown in figure 3.18. Most notable is a sharp decline in the amount of carbon in the atmosphere and ocean over the first 5 Gyr as these are stripped by terrestrial weathering and hydrothermal carbonatization respectively at rates faster than they can be replenished. Most of this carbon is transferred to the continental sediments via the action of accretionary wedges, the run-off of carbon-rich weathered material fixed from the atmosphere on the terrestrial surface, as well as the deposition of carbonate-rich exoskeletons from marine organisms in shallow shelf-sea environments.

Due to the increasing size of the continental reservoir, metamorphism continues to act as a significant flux into atmosphere throughout the run despite the decline in heat flux from the planet interior, and especially so after the collapse of the oceanic/atmospheric reservoir. This process most likely takes the form of prograde metamorphism that acts at tectonic plate boundaries to release volatiles into the atmosphere under high temperature and pressure. The increase in the metamorphic flux post-1 Gyr is likely to due to the explicit dependence of this process on the size of the continental crust, which continues to accumulate carbon from the oceanic crust as well as the ocean/atmosphere reservoir.

During the early stages of the planet's history, the action of hydrothermal carbonatization of basaltic minerals at spreading ridges represents a significant carbon removal flux, dependent only on the amount of carbon dissolved in ocean waters, which remains relatively high at this stage. Critically, this process acts independently of temperature which would normally limit weathering and removal processes early in the planet's history when solar output and temperatures are low. However, the dominance of this process declines as atmospheric carbon dioxide concentrations drop and temperatures rise, giving way to terrestrial weathering as the dominant removal flux.

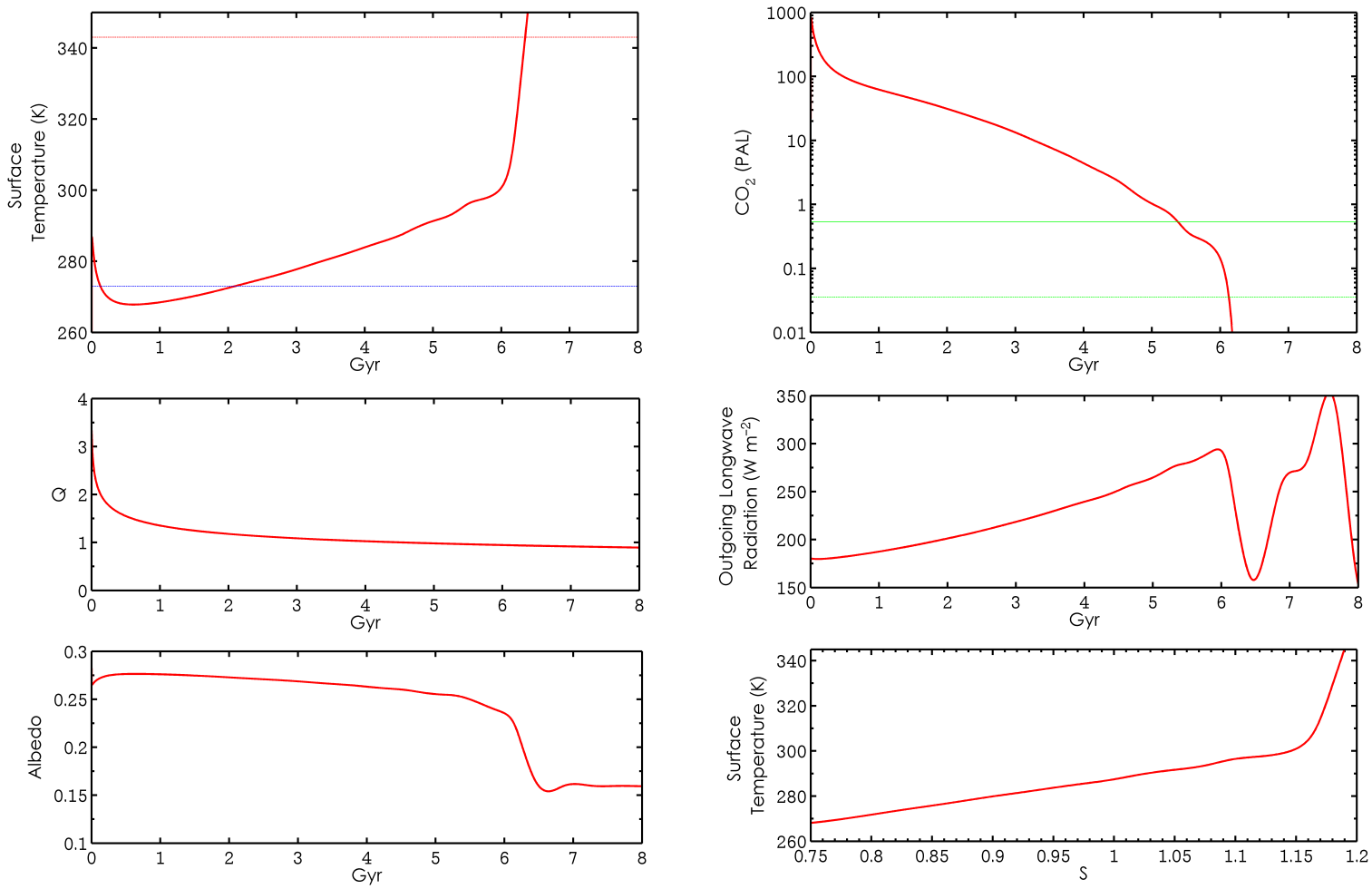

Figure 3.17: Model output using 1-D radiative-convective climate model. Top left: surface temperature. Top right: atmospheric CO_2. Middle left: Geothermal heat flow (Q). Middle right: Outgoing Longwave Radiation. Bottom left: Albedo (without snowball parameterisation). Bottom right: Surface temperature as function of incident stellar flux (S).

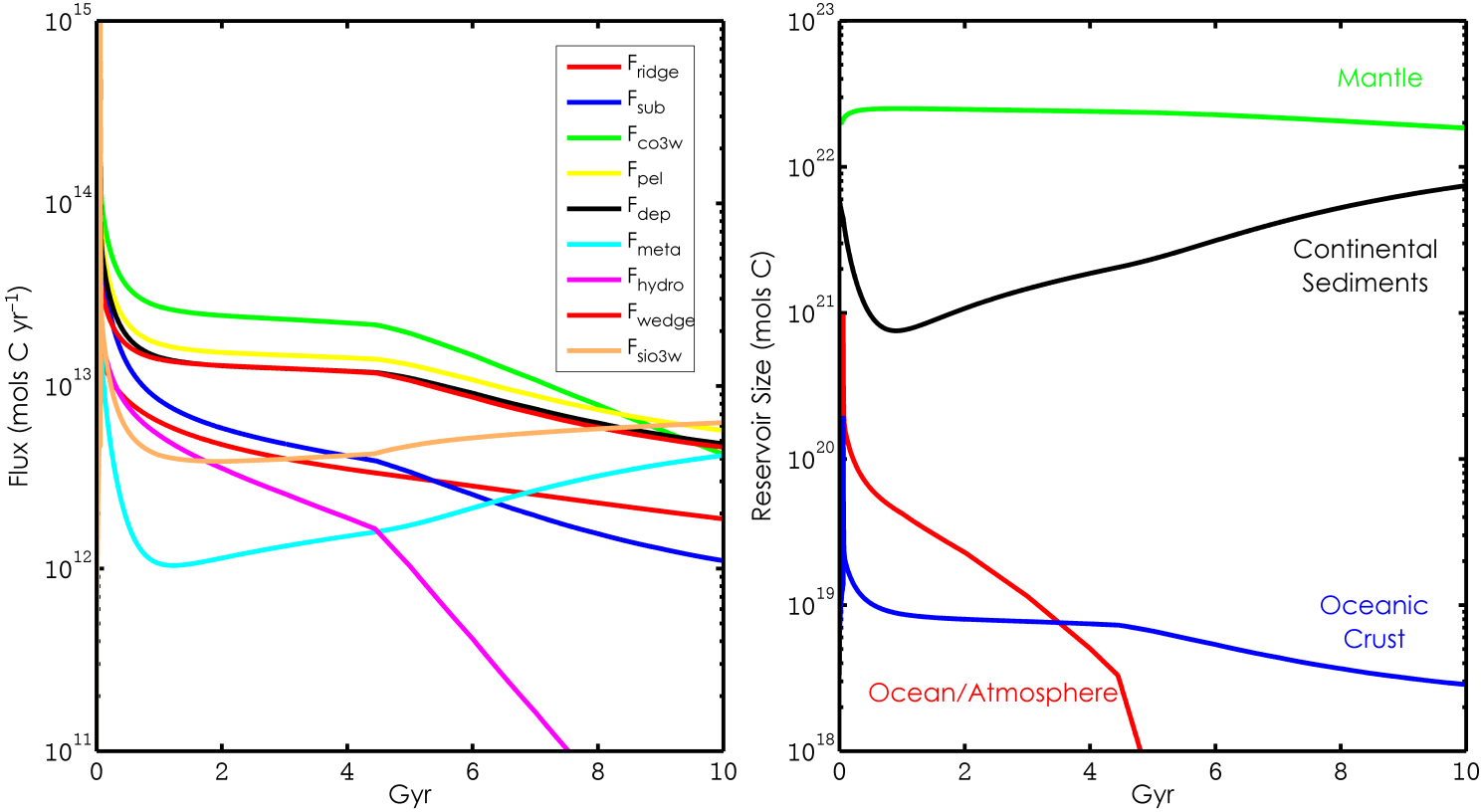

Figure 3.18: Left: Model carbon fluxes through time. Right: Model carbon reservoirs through time.

3.5.2 The Cold Start Climate Catastrophe

The primary reason that a variable/ice-transition albedo parameterisation is included is to investigate the behaviour of the model when considering a planet that initially forms in the 'cold zone' of its stars orbit (for example, Mars in our solar system). As stellar output increases over astronomical time, warming the planet to within habitable temperature limits, a transition between various degrees of habitability may take place: from ice-covered and barren to potentially warm and habitable. This is a concept that was initially presented in the preceding chapter and in Rushby *et al.*, (2013), but the physical, chemical and possibly biological processes associated with this 'cold-start' transition is more complex than that early analysis initially suggested.

Under conditions where the model planet forms at a distance from the star that would result in early conditions on the planet being cold (less than 273 K), the planet falls into a 'snowball' state which is further exacerbated by the ice-albedo effect: as the planetary surface is extremely reflective ($a = 0.6$), this acts to limit effective temperature on the planet to lower levels than would be expected had the planet formed at a similar distance from the star, but with less ice on its surface as shown in figure 3.19. This effect provides an example of a form of hysteresis in the behaviour of the model, where the temperature is not only dependent on the current input, but also history of the albedo of the surface. Due to the inefficiency of terrestrial weathering under the low temperatures, large amounts of CO_2 builds up in the atmosphere over geological time, primarily from volcanic sources - as the geothermal heat flux of the planet would still be relatively high after accretion but not to levels sufficient to break the planet out of the snowball state.

Once solar luminosity increases to a stage at which the combined effects of the high CO_2 atmosphere and stunted effective temperature manages to raise planetary temperatures to $\sim$278 K, the high-reflectivity surface morphology associated with the planetary snowball is dissipated extremely rapidly (within 200,000 years), resulting in a transient super-greenhouse catastrophe due to the lowered albedo and high solar flux, but still high

levels of CO_2 present in the atmosphere ($\sim$18 PAL), resulting in a rapid increase in temperature to $\sim$350 K. However, the increased weathering associated with newly exposed terrestrial surface, the higher temperatures and abundant atmospheric CO_2 hastily acts in tandem to pull the excess carbon out of the atmosphere, lowering the temperature to within habitable limits for a short time, until the buffering effect of the carbon cycle collapses under increasing solar radiation approximately 0.5 Gyr later.

The same steady increase in solar radiation that melted the snowball, also causes the planet's biogeochemical stabilisation mechanisms to eventually fail. Any potential biosphere that was able to survive, or emerge after, the extreme temperature swings associated with the melting of the snowball, would be subject to a terminal extinction event. Therefore, planets subject to an ice-covered 'cold start' may be considered to have a lower habitable period than would be expected relative to a planet that forms at a similar distance, but without extensive surface ice cover. Higher concentrations of greenhouse gases, or a low albedo haze scenario, could prevent the eventual 'cold start' climate collapse seen in the model following the dissipation of the planetary snowball.

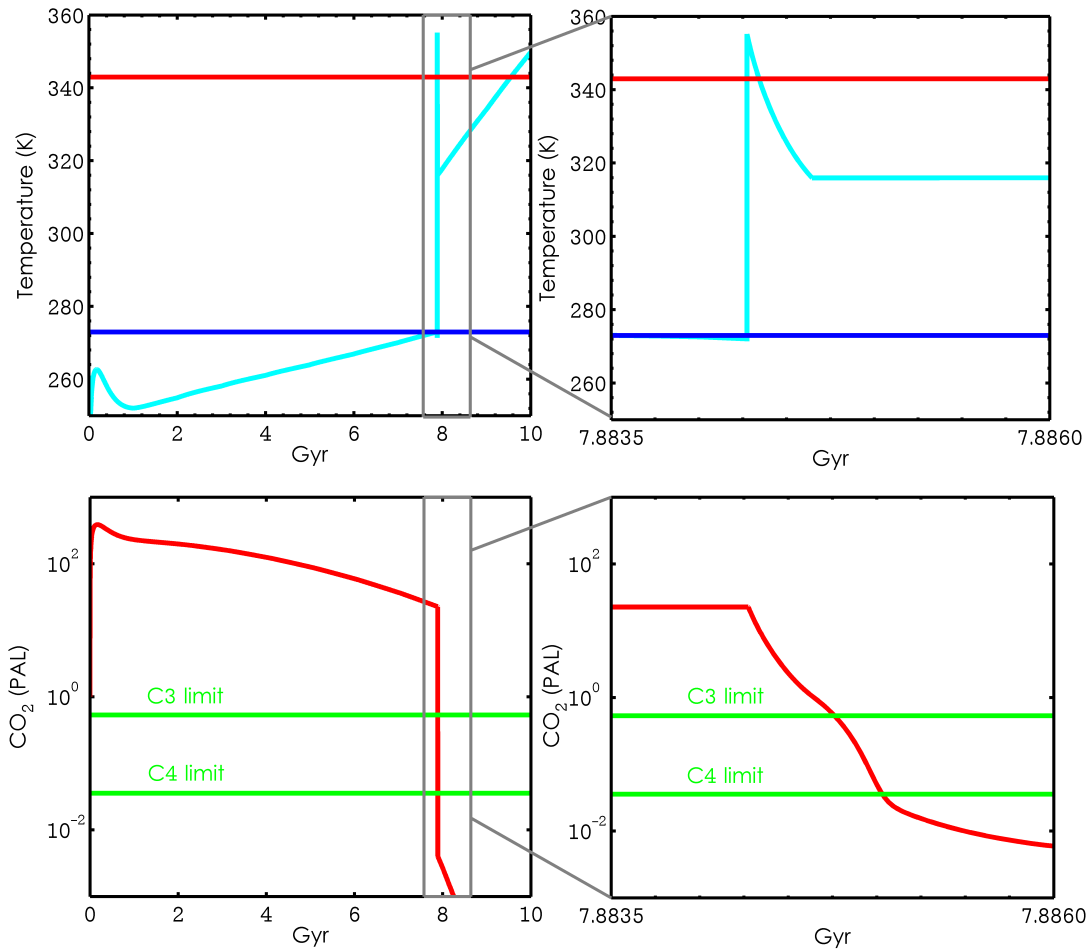

Figure 3.19: Model output when initialised with high albedo (a=0.6) to simulate formation of planet in 'cold zone' of star. Top right: surface temperatures. Top left: surface temperatures focussing on snowball breakout at ∼7.88 Gyr. Note change in x-axis. Bottom left: atmospheric CO_2. Bottom right: atmospheric CO_2 during dissipation of snowball event at ∼7.88 Gyr. Same x-axis as figure in top-right.

3.6 Discussion

The results presented above attempt to illustrate the difficulties encountered in modelling a system as complex as an Earth-like planet through the looking glass of planetary habitability. A simple biogeochemical model is presented that seeks to represent the dynamics of the biosphere-planet system over geological and astronomical time, with particular focus on the carbonate-silicate cycle due to its significant effect on the surface, interior and atmosphere of the planet. Using temperature and CO_2 concentrations as a first approximation of habitable conditions, it seems that the complex interplay between these components produces an uncertain conclusion: habitability is strongly variable in time, and falls along a spectrum as opposed to a clear binary distinction between 'uninhabitable' and 'habitable'. Conditions exist where, whilst average surface temperatures may fall within the traditional habitable boundaries, other factors act to reduce the overall habitability of the planet.

In the case of this model, another inhibiting factor is the low levels of CO_2 deemed necessary for primary producers, which results in a form of 'photosystem-limited habitability'. The planet enters this state towards the end of its habitable lifetime as surface temperatures increase under a brightening star, and the action of terrestrial weathering draws down CO_2 at a rate faster than it can be returned to the atmosphere by volcanic sources. Primary producers crucial for supporting the planet's biosphere would become CO_2-stressed, and this would eventually result in the collapse of the biosphere long before the planet becomes too warm. O'Malley-James *et al.* (2014) describe the changes likely to occur in the trophic hierarchy of the biosphere of a planet in a state of CO_2-stress: below $\sim$150 ppm CO_2, desiccation tolerant CAM and C4 plants would briefly dominate in spatially heterogeneous refugia (subterranean caves, high altitude environments), followed by a period of microbial anoxygenic photosynthesis when CO_2 falls below 10 ppm. Below 1 ppm CO_2, the end of all photosynthetic life is expected, and this juncture would represent a terminal extinction event for the biosphere, even if surface temperatures remained within habitable limits (O'Malley-James *et al.*, 2014). Figure 3.20

represents a synthesis of the finding of this chapter, where updated habitable zone boundaries, in the case of an Earth-like planet around a Sun-type star, for both the traditional temperature-only and photosystem-limited cases are presented as a function of time.

However, other factors (not modelled here) that would produce complex states of pseudo-habitability could also include the lack of atmospheric O_3 to act as a protective layer against UV radiation or very high (>30%) levels of O_2 which would present a significant fire hazard, for example.

It is becoming increasingly evident that current definitions of 'habitability' are obsolete. Considering the plethora of diverse worlds already discovered, and the new exoplanets that are being detected and added to databases at regular intervals, an updated conceptual understanding of the term, both in time and in space, needs to be developed. The model presented here, admittedly, does little to further the conceptualisation of habitability beyond introducing the possibility of multiple combinatorial states of temperature and carbon-limited environments that evolve temporally whilst being limited spatially i.e. a single environment whose degree of habitability changes over time. Furthermore, by the necessity of its formulation, this model is concerned only with planets that are able to sustain liquid water on their surfaces, whilst excluding the possibility of 'interior liquid water worlds', with analogues such as Europa and Enceladus in our solar system. These planets would, by many definitions of the term 'habitability', be considered environments able to sustain life, if perhaps not the multicellular photosynthetic life that forms the base of the biosphere on Earth, but this Terran chauvinism will only hamper efforts to more fully understand the true distribution of habitable environments in the universe.

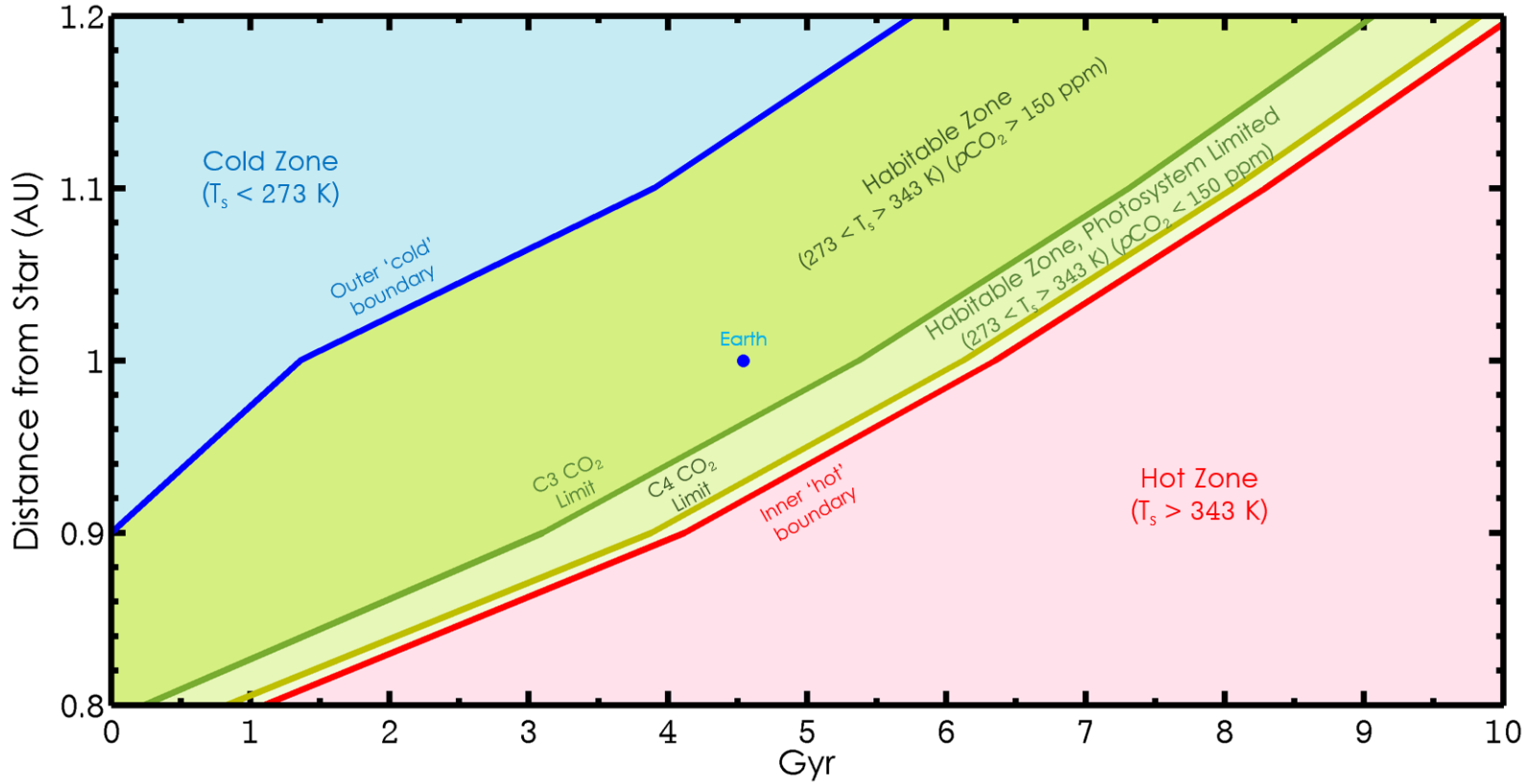

Figure 3.20: Updated habitable zone boundaries as a function of time for a solar mass star. Both low temperature (blue line) and high temperature (red line) boundaries are included, as well as the two 'photosystem limits' (green lines) that represents 150 ppm and 10 ppm of CO_2, the minimum pCO_2 required for C3 and C4 photosynthetic life, respectively. The location/timing of the cold boundary is likely overestimated (see 'results' section for discussion).

Results from this simple model illustrate the need to consider long-term planetary dynamics, in the form of biogeochemical cycling, geophysics, and atmospheric chemistry and physics in our consideration of this term. Surface temperature and atmospheric composition are now no longer robust benchmarks on which to base our understanding of habitability. Crucially, it remains difficult to separate 'life' from 'planet' when considering inhabited worlds such as our own, which begs the almost-paradoxical question: 'can a habitable planet emerge without the action of life?' Clearly, life itself can influence habitability, and the co-evolution of biology and the physical planetary system make for different worlds than those on which life cannot, or did not, emerge. The carbonate-silicate cycle is a prime example of this; driven or augmented by biology at nearly every step (weathering enhancement on the surface, carbon-fixation for exoskeletons and shells in the ocean), this system buffers the climate against ever-increasing radiation from the star, altering the composition of the atmosphere and surface temperatures, as well as affecting the environment for other forms of life.

It seems, from the results presented above, that the initial conditions following planet formation have a strong hysteretic control on the future biogeochemical trajectory of the planet. This is the stage at which the emergence of life is most likely, and whereby the action of this primitive biosphere would have the greatest effect on the planet itself. The initial conditions therefore have a strong control on the output, resulting in a nonlinear response.

The paradigm of planetary ecology which currently dominates discussions of habitability is necessarily Earth-centric. By seeking normalising factors throughout our investigations of alien worlds we can attempt to remove our inherent bias, but assumptions will always remain until we can expand our sample of inhabited planets. In this study I have chosen to focus on planetary temperature, and the abundance of CO_2 in the atmosphere - both as a greenhouse gas but also as a source of energy to power the metabolisms of photosynthesising primary producers.

3.7 Conclusions

Building on the stellar evolution and habitable zone model presented in the previous chapter, this study seeks to address the lack of planetary evolution evident in that work. Long term biogeochemical cycling of carbon will fundamentally alter the habitability of the planet by buffering the climate against increasing solar luminosity via the operation of the carbonate-silicate cycle over geological timescales. However, the mechanics of this process also introduces further complexity in terms of carbon availability of photosynthetic organisms that form the base of the planetary biosphere. By considering this dimension, various states of habitability can be identified based on either temperature constraints alone, or the requirement for sufficient $p\mathrm{CO}_2$ to allow for fixation by these organisms.

4 Biogeochemical Cycling on Earth-Like Exoplanets

> We are generalists. You can't draw neat lines around planet-wide problems. Planetology is a cut-and-fit science.
>
> **Frank Herbert**
> *Dune* (1965)

4.1 Abstract

Integrating the stellar habitable zone model with that of the Earth-systems model introduced in the previous chapter allows for a self-consistent, biogeochemical approach to planetary habitability, in which processes operating in the astrophysical and geophysical domains can be investigated. The results presented in the previous chapter illustrate the importance of considering planetary biogeochemical evolution on the regulation of long-term climate and atmospheric CO_2. In this chapter, sensitivity experiments are conducted to explore the effect of stellar mass, orbital distance and eccentricity, and planetary mass on the duration of habitable conditions on these analogue worlds. Latin hypercube analysis of the input variables of the model identify several statistically significant relationships between these parameters and the length of the habitable period. Planet mass (between 0.5 and 10 Earth masses ($M_\oplus$)) in particular is found to exert a strong control on the duration of habitable conditions.

4.2 Introduction

The previous two chapters introduced a model framework that attempts to assimilate processes important to habitability operating in both the

astrophysical and geophysical realms: a stellar evolution model coupled with a means of capturing the complexities of long-term planetary climate evolution. In this chapter, the effect of planet size, orbital distance and eccentricity will be explored using this model, and the effect on long term habitability considered.

4.3 Methods

4.3.1 Planet Scaling Relationships

Understanding the interiors of exoplanets remains problematic as investigations suffer from limited data for these newly-discovered planets. Radial velocity techniques allow for planet mass to be estimated based on the gravitational effect that the orbiting world has on its host star. Using transit photometry, the radius of an orbiting planet can be estimated based on the amount of light that the planet obscures, and its mass can be determined if the composition of the interior of the planet is known (Jenkins *et al.*, 2002). However, even if these radius and mass estimates were perfectly accurate, they alone are not sufficient to identify a planet's interior composition, with the possible exception being at the extremes in density – very low density planets are likely to be dominated by H and He, and very high density planets are likely composed primarily of Fe (Sotin *et al.*, 2010). Unfortunately, it is beyond the capability of contemporary instrumentation to determine the average bulk density of terrestrial exoplanets, and therefore scaling relationships based on simplifying assumptions can provide a first-order estimate of the mass of these worlds.

It remains fundamentally important to our understanding of planet formation, habitability and the search for similar terrestrial planets to understand the internal dynamics of these planets (circulation, convection, thermal evolution) but the occurrence or operation of Earth-analogue tectonic processes - primarily that of plate tectonics - remains a controversial and unanswered question in the field (Sotin *et al.*, 2010). Many astrobiologists consider volcanism and plate tectonics to be a necessarily prerequisite for long-term planetary habitability due to the

ability of volcanic outgassing to alter the composition of planetary atmospheres (Korenaga, 2012; Kasting & Catling, 2003). However, it remains too early to determine whether the tectonic regime observed on the Earth is typical of terrestrial planets of similar size, or indeed how these processes will change with planet size. Volcanism is expected to be a widespread characteristic of rocky planets resulting from partial melting of their silicate mantle under extremes of pressure, but contention exists over the form of thermal convection that would dominate on massive planets, and to what alternative form their tectonic regimes may conform (Keltenegger *et al.*, 2010; Kite *et al.*, 2009).

Scaling relationships between planet radius and mass can be used to constrain our understanding of geodynamical processes operating on exoplanets to first order, if a series simplifying assumptions are made regarding bulk composition, surface gravity, geothermal heat flux, as well as mantle and core radii (Sotin *et al.*, 2010; Seager *et al.*, 2007). As mass is a product of the volume of the planet and its density, it scales with the approximate cube of the radius, modified by the effect of the bulk composition of the interior. These relationships take a simple power-law form:

$$\frac{R}{R_{\oplus}} = a(\frac{M}{M_{\oplus}})^{b} \tag{4.1}$$

Where $R_{\oplus}$ is the radius of the Earth, and $M_{\oplus}$ its mass (Sotin *et al.*, 2010; Seager *et al.*, 2007). a and b are constants that control the slope of the curve, with b scaling inversely to planet size due to larger planetary mass resulting in greater compression and higher bulk density of the composition of the planet (Sotin *et al.*, 2010). Several workers have published values of these constants for different mass ranges, summarised in table 4.1 from Sotin *et al.* (2010).

'Oceanic' in this case, refers to planets comprised of >50% H_2O by mass, analogous to the large icy satellites of the outer solar system (Sotin *et al.*, 2010). It is important for this study to determine scaling relationships for planet sizes, as these will have a strong effect on the rate of geothermal

$M/M_{\oplus}$	Terrestrial		Oceanic		Murcurian
	a	b	a	b	
0.01-1[1]	1	0.306	1.258	0.302	
1-10[1]	1	0.274	1.262	0.275	
1-10[2]	1	0.267-0.272			$\sim$0.30
1-100[3]	1.01	0.252-0.285	1.253	0.239-0.272	

[1]Sotin *et al.*, (2007)
[2]Valencia *et al.*, (2006)
[3]Grasset *et al.* (2009)

Table 3.2: Planet mass/radius scaling relationships for Earth-like exoplanets

heating – a fundamental driver in the model. The radii of planets that contain 50% H_2O by mass are estimated to be $\sim$25% larger than Earth-like worlds, with implications for thermal convection and evolution, and geochemical cycling (Sotin *et al.*, 2007). Approximately 50% of planetary heat flux derives from cooling following accretion, the rate of which depends on the rate of mantle convection, whilst the remaining 50% is from the decay of long-lived radioactive elements such as ^{40}K, ^{235}U, ^{238}U and ^{232}Th (Sotin *et al.*, 2010). The implications of the timing of planet formation relative to galactic formation (and therefore the distribution and amount of radionuclides in star forming regions), as well as the initial metallicity of the protoplanetary disk is excluded — more detailed discussion of these implications can be found in Chapter 1 and 2. Assuming that the amount of radiogenic elements in the planet is proportional to mass, then the radiogenic heat flux varies as a function of planet mass, according to Sotin *et al.* (2010):

$$Q = Q_{\oplus}.(\frac{M}{M_{\oplus}})^{0.452} \tag{4.2}$$

Where $Q_{\oplus}$ is the geothermal heat flow evolution on the Earth, as described by equation 3.5 in the preceding chapter. This relationship has a significant control on the likely geochemical and climatic evolution of the planet in question, as planetary heat flow is parameterised as a major driver of several fluxes integral to planetary dynamics, including the rate of volcanic outgassing and the rate of ocean floor spreading. Figure 4.1 illustrates this

geothermal scaling relationship for planets up to 50 Earth masses, and also includes scalings for mantle thickness and bulk density laid out in Sotin *et al.* (2010). The geothermal heat flow relationship evolves over time as the planet ages, and therefore the relationship displayed below is calibrated relative to present day Earth ($Q = 1$ at 4.54 Gyr).

Sufficient heat flow and active tectonics are crucial for habitability (Lammer *et al.*, 2009). As well as generating volcanic outgassing and subduction, the existence of sufficient planetary heat flow also makes the assumption that the planet's core remains in a liquid state, thereby also contributing a magnetic dynamo that would serve to protect the atmosphere from being sputtered away by high-energy solar particles (Lammer *et al.*, 2009).

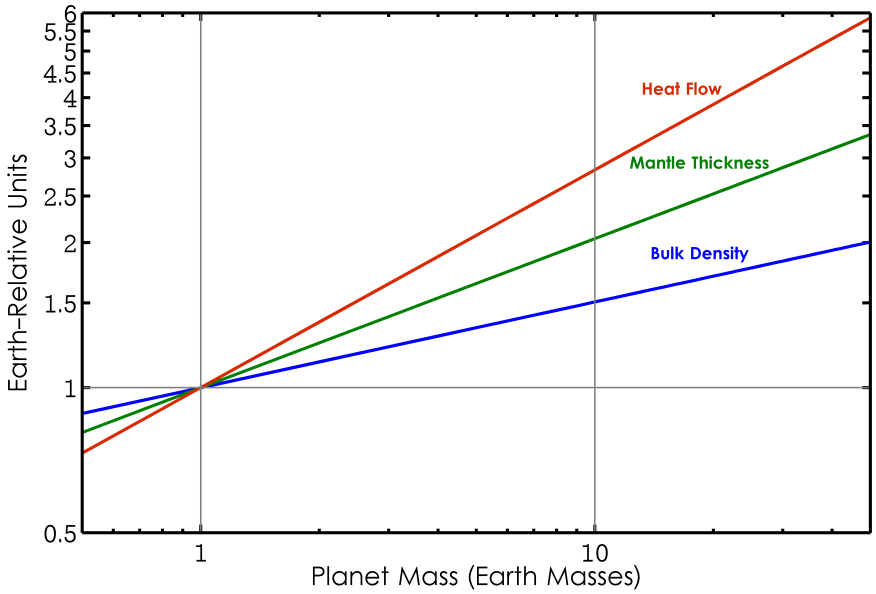

Figure 4.1: Scaling relationships for heat flow (Q), mantle thickness and bulk density for terrestrial exoplanets normalised to present day Earth values.

Inherent in the *a priori* assumptions of the approach of this work is the inferred universality of the carbonate-silicate cycle as a means of regulation of the climate of habitable planets. It is hypothetically possible for an ocean-covered planet with no vestiges of terrestrial weathering to remain habitable through mechanisms of planetary-scale regulatory feedback mechanisms, perhaps analogous to the CLAW hypothesis in which

biologically-produced organic compounds (dimethyl sulphide in the terrestrial case) form cloud condensation nuclei, which raise the albedo of the planet, lower temperature, reduce biological productivity, and by implication the emission of these compounds, forming a negative feedback loop (Charlson *et al.*, 1987). Contemporary research suggests that a possible unstable CO_2 feedback driven by the formation of high-pressure water ice may exist on volatile-rich ocean planets, but this process is not the focus of this study (Kitzmann *et al.*, 2015) Equally, a planet with little surface water may have a very different circumstellar habitable zone; contemporary modelling studies have shown that the lower atmospheric water vapour expected on these 'land planets' would buffer the climate of these worlds against increasing stellar output by the more efficient emission of longwave radiation in the tropics, and lower rates of hydrogen escape from the exobase (Abe *et al.*, 2011). The operation of a comparable terrestrial weathering/CO_2 homeostat on these dry worlds seems unlikely, as atmospheric water vapour is required to form a carbonic acid solution to facilitate chemical weathering via precipitation, and surface water is required for transport of erosional deposits to an oceanic environment for burial as sedimentary strata (Mills *et al.*, 2014). With insufficient data regarding the possible composition of the continents, their configuration, the atmospheric composition, as well as the distribution and variety of life on other habitable planets, it remains inherently difficult, and potentially runs counter to the scientific method, to postulate on possible hypothetical homeostatic regulation mechanisms. Therefore, we adopt the necessary assumption that the planets included as examples in this study share a similar continental/ocean fraction and an analogous means of climatic regulation as the Earth i.e. a carbonate-silicate cycle that provides a negative feedback on atmospheric CO_2.

4.3.2 The Effect of Ocean/Continental Fraction

The effect of the distribution and configuration of continents on the planet surface will have a significant effect on the energy balance of the planet and its climate, as terrestrial and oceanic environments have markedly different

albedos and thermal properties. The effect of continental configuration may be difficult to effectively capture in a box model lacking a spatial dimension, but this effect can be parameterised in the energy balance calculation. Without considering the spatial distribution of land, as well as the zenith angle of incoming stellar radiation, seasonal variations etc., it is possible to determine the effect of increasing ocean fraction on planetary albedo and climate to first order. For an Earth-mass planet around a Sun-like star, the albedo of the deep ocean is $\sim$0.1. The land, by contrast, has an albedo closer to $\sim$0.35, with an uncertainty of $\pm$0.05 depending on the level of soil moisture (Williams, 2014). Therefore, when considering the 'ocean fraction' of a planet, this effect can be illustrated by the contrast between these values and the average planetary albedo: as the 'ocean fraction' increases, the average planetary albedo decreases as the proportionally larger surface area covered by the dark ocean absorbs more incident radiation. As in previous sections of this work, the effect of clouds are neglected and these results should be considered as 'clear-sky' cases. Stephens *et al.* (2010) notes that the difference in TOA flux is likely much smaller between the ocean and the continent as there is proportionally more cloud cover over the ocean. Figure 4.2 illustrates this effect, where contours of downward top-of-the-atmosphere flux (in W m^{-2}) is displayed as a function of normalised stellar flux (where 1 represents the present day value of 342 W m^{-2} in this case) and ocean fraction (from 0.4 to 0.9). For a given incident flux, a greater proportion of this radiation is absorbed by the surface as the fraction of the planet covered ocean increases.

This effect can be extrapolated when considering long term planetary habitability: surface temperatures on oceanic planets will be proportionately warmer under a given incident flux, suggesting that these planets could be habitable earlier in their history when the luminosity of their host stars are lower, but may experience greenhouse catastrophes at an lower relative insolation than planets with a greater proportion of land surface. Contemporary exoplanet science does not have the capabilities to determine the land/ocean ratio of exoplanets, nor their particular spatial configuration. However, it remains important to consider the effect that continental and oceanic topographies will have on the level of uncertainty

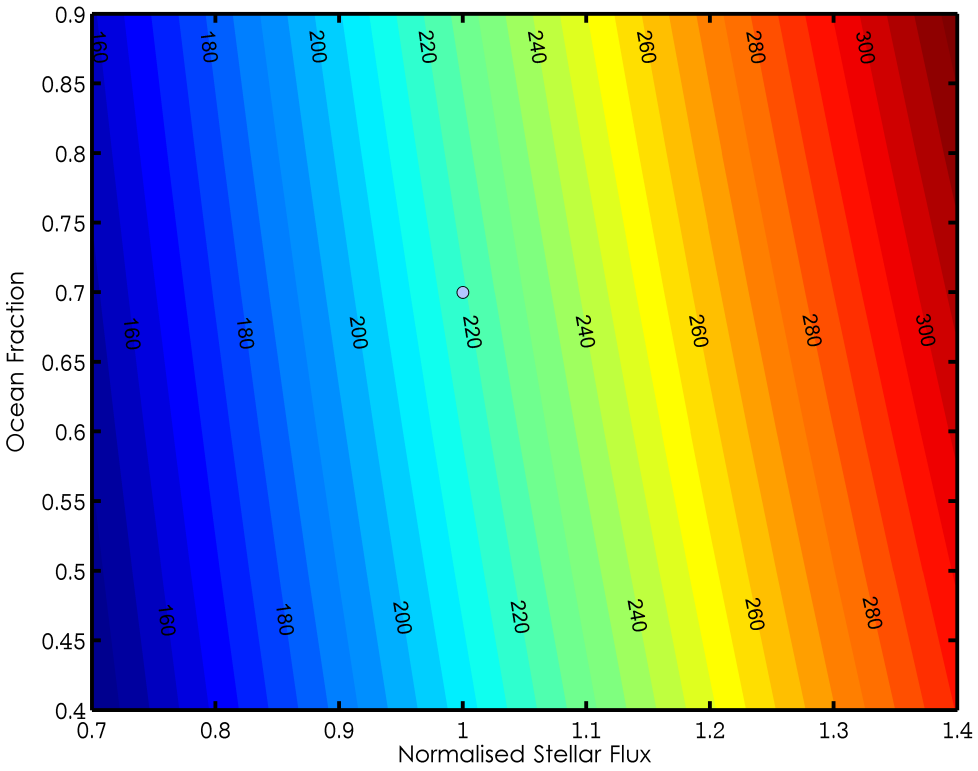

Figure 4.2: Downward top-of-the-atmosphere flux (in W m^{-2}) as a function of normalised stellar irradiation and planetary ocean fraction for a clear-sky (no clouds) scenario. The light blue marker represents the Earth.

in future studies of planetary habitability. For example, the limits of habitability of a given planet could be explored by applying the spectrum of possible land/ocean ratios, from near-complete land cover to oceanic, to determine the uncertainty that this variable would have on the end-member estimations of climate and long-term planetary habitability. For the remainder of this work, the ocean fraction will remain 'Earth-like' at 0.7.

4.3.3 Latin Hypercube Sampling (LHS)

Building on the sensitivity analysis carried out in the previous chapter, and given the multivariate nature of the model input, Latin hypercube sampling (LHS) was applied to seven key model parameters to generate a

pseudorandom orthogonal sample that effectively covered the parameter-space of these variables to assess their relative importance and control on the final model output, and to determine whether these correlations, should they exist, were statistically significant and worthy of further investigation. These variables are: albedo, α (controls sensitivity of seafloor carbonatization to oceanic carbon), β (controls silicate weathering rates), γ (controls carbonate weathering rates), κ (plant weathering amplification factor), μ (controls rate of heat flow from the interior of the planet) and planet mass in Earth masses ($M_{\oplus}$). The diagnostic output parameter is habitable period (in Gyr). Incident stellar flux on the planet surface in these simulations is taken as following the luminosity evolution track of a solar mass star, at an equivalent semi-major axis (1 AU). The default values of these parameters and their ranges are shown again in table 4.2.

In most cases, it was assumed that the range of uncertainty in these variables conformed approximately to a continuous uniform distribution, as the most likely value of each was known only from sparse empirical or modelling studies. Therefore, a pseudorandom non-normal sample ($n = 1800$) was extracted from each range and passed to the model. This approach has been shown to be computationally more efficient than Monte Carlo (MC) sampling, providing smooth, evenly-spaced input distributions without sampling artefacts, and with lower reported sampling errors and rates of convergence (McKay *et al.*, 1979).

Successful model runs (i.e. those that ran to completion and which exhibited habitable conditions at any point) were collated, and from that sample the habitable periods of these successful cases were computed based on the boundary conditions described earlier, specifically a 'photosystem habitable period' defined by the pCO_2 requirements of C3 plants ($\sim$150ppm) and a 'temperature habitable period' defined as exhibiting surface temperatures between 273 and 343 K.

In order to determine which of the input variables has the strongest control on the output of the model, a diagnostic output variable was chosen (in this case length of habitable period, both photosystem and temperature) and a

Parameter	Definition	Value (Range)
α	Dependence of seafloor carbonitization on dissolved CO_2 in seawater	0.23 (0.23 - 1)
β	Dependence of terrestrial silicate weathering on CO_2	0.3 (0.3 - 1)
γ	Dependence of terrestrial carbonate weathering on CO_2	0.3 (0.3 - 1)
μ	Geothermal heat scaling parameter	0.2 (0.2 - 0.7)
κ	Biological enhancement factor for terrestrial weathering	0.5 (0.1 - 1)
a	Albedo	0.3 (0.1 - 0.6)
$M_\oplus$	Planet mass	1 (0.5 - 10)

Table 4.2: Default values, and expected range, for input model parameters

partial rank correlation coefficient (PRCC) was computed for each input variable contained in the Latin hypercube matrix. Partial rank correlation returns a linear partial correlation between the pairs of input variables, whilst controlling for the remaining variables, and the built-in MATLAB PRCC function also returns p-values at the 95% confidence interval for determining statistical significance of these correlations. The covariance matrix of the variables x and z takes the form:

$$S = \begin{pmatrix} S_{xx} & S_{xz} \\ S_{xz}^T & S_{zz} \end{pmatrix} \tag{4.3}$$

Therefore the partial correlation matrix of the input variables (x), controlling for the diagnostic output variable (habitable period (z)) can be defined as a normalised version of the covariance matrix.

4.4 Results

By combining the stellar evolution and biogeochemical models presented in the previous chapters, a stellar-biogeochemical habitability assessment can be computed. The effect of planet mass on the duration of habitable conditions forms the primary focus of this chapter, but other characteristics of the planetary system can be investigated and accounted for, including revisiting the effect of star mass and orbital distance, and the effect of ocean/continent fraction and distribution and orbital eccentricity. The relative effects of particular components of the biogeochemical system — including albedo or the sensitivity of the weathering of terrestrial or oceanic crustal reservoirs to pCO_2 for example — can also be studied through the use of Latin hypercube sampling and statistical analysis. Identifying exisiting exoplanets from the *Kepler* database allows for the application of this method to a small sample of worlds to investigate their potential temporal habitability.

4.4.1 Potentially Habitable Planets from the HEC

The Planetary Habitability Laboratory at the University of Puerto Rico, Arecibo has compiled a list of 28 potentially habitable exoplanets from the catalogue of all known planets to date (January, 2015). These planets have been extracted from the larger exoplanet database based on available planetary characteristics: planet mass, incident stellar radiation, equilibrium temperature and their 'Earth-similarity Index' rating – a multi-parameter metric based on planet size, density, atmospheric escape velocity and potential surface temperature (Schulze-Makuch *et al.*, 2011). These candidates are shown in figure 4.3 below, which plots them in mass/stellar flux space. Errors bars denote upper and lower estimates of planetary mass from transit photometry studies where applicable. Because this method of exoplanet detection only returns estimates of planetary radius (proportional to the amount of light obscured), estimating mass when the average density of the composition of the planet is not known produces large uncertainties.

Further uncertainties exist when considering that the PHL database is fairly open in selecting planets from the sample of known worlds, and also includes currently unconfirmed 'planet candidates', the existence of which have not been validated by other detection techniques or via the observation of several orbits/occultations. Eight of these unconfirmed candidates populate the 28-planet table of most Earth-like planets, and should therefore be considered as subject to change based on future study. In chapter 1, it was suggested that the exoplanet Gliese 667C c should be subject to further investigation regarding its habitability as the age of its star is not well constrained. Our initial results suggested that the planet would be too warm at this stage to be included in the sample of habitable planets, but with little observational constraints on the age of Gliese 667C, the PHL remains open to its inclusion in the database.

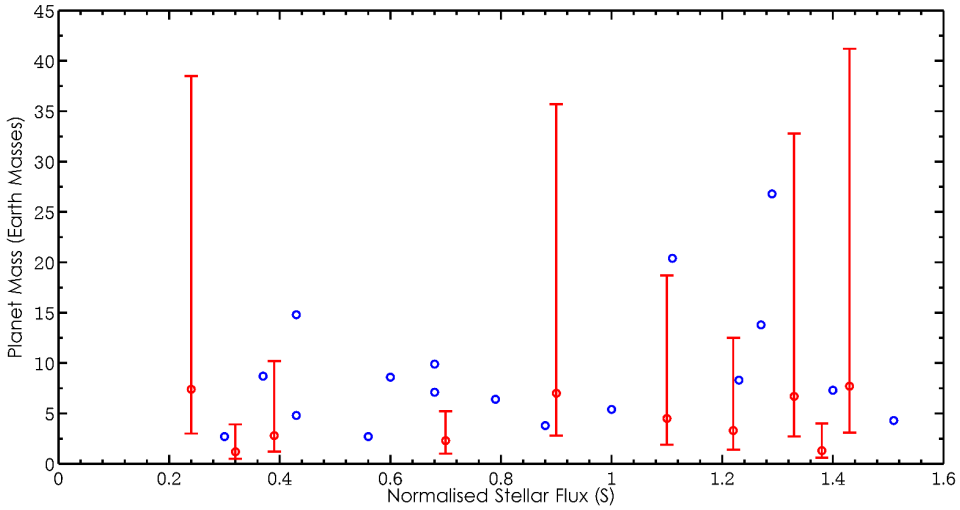

Figure 4.3: Habitable planet candidates from the PHL Habitable Exoplanets Catalogue (HEC) plotted as a function of incident stellar flux relative to the present day terrestrial value and planet mass, relative to the Earth. Errors (represented as red bars) stem from uncertainties in the bulk densities of candidate planets found via transit.

Figure 4.3 illustrates the 28 planets included in the PHL sample as function of their approximate normalised stellar flux (where S =1 is equivalent to the flux received by the present day Earth) and their mass in Earth masses ($M_{\oplus}$). The red error bars represent the upper and lower mass estimates of

the planets represented by red circles, as these candidates were detected using transit spectroscopy (via the Kepler space telescope), which produces a large uncertainty in terms of mass as only radius is known, as discussed above. The average mass of the planets in the database sample fall between $\sim$0.6 and $\sim$40 $M_{\oplus}$ (as a lower and upper mass estimate), and receive stellar flux between 0.24 and 1.51 the normalised solar value (S).

Whilst these uncertainties are a result of the lack of information regarding the bulk density of the planets in question, it is possible to address them by applying the scaling relationships described above under the assumption of terrestrial composition to the planet sample (i.e. following the 'terrestrial' isopycnal), as shown in figure 4.4. It seems that the planets included in the PHL database are modelled under the assumption of a higher bulk water content, which results in a slightly higher mass/radius scaling. Results presented herein will assume a terrestrial composition.

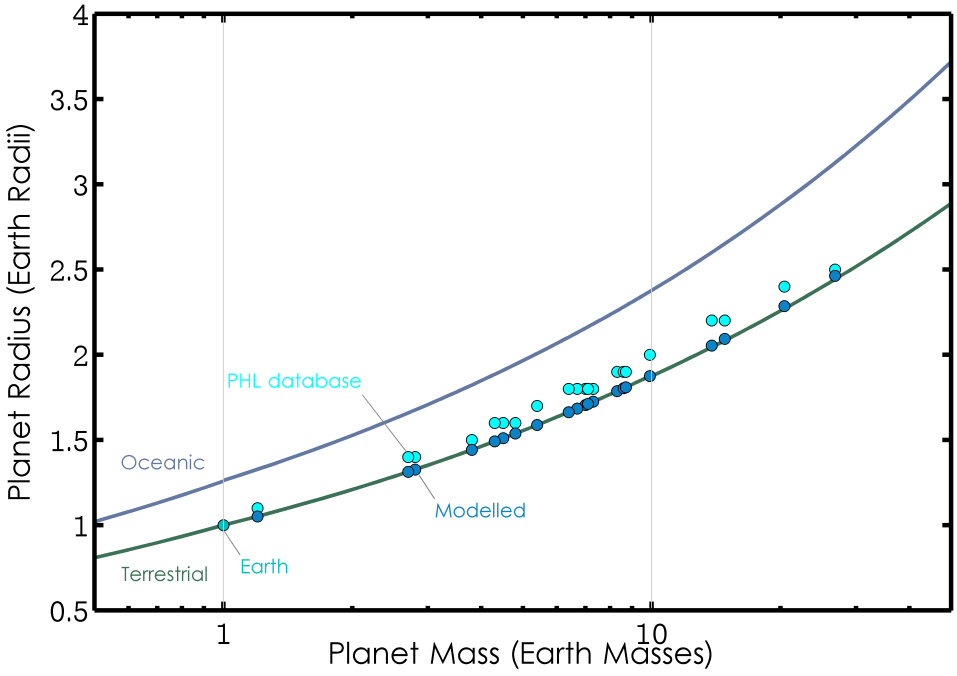

Figure 4.4: Modelled mass/radius scaling relationships for HEC candidate planets included in this study.

4.4.2 Planet Mass and the Habitable Zone

The model introduced in the previous chapter allows for the calculation of a circumstellar 'habitable zone' based on the stellar flux incident on the planet and the operation of geochemical cycling in response to this flux. The evolution of the planetary climate can be approximated over Sol-like astronomical timescales (∼10 Gyr), and several spatiotemporal states of habitability can be inferred from these results: a scenario in which temperatures are out of bounds of traditional habitability limits (0 – 70 °C), one in which temperatures remain within these limits and atmospheric carbon dioxide remains at levels that would allow for photosynthesis of the variety witnessed in primary producers on Earth (C3 and C4 photosystems), and a final scenario where the temperature requirements of habitability are met, but where the atmospheric CO_2 falls below the limit of terrestrial C4 organisms. The latter scenario occurs when the carbon-silicate cycle of the planet, perturbed by increasing stellar luminosity, extracts all available CO_2 from the atmosphere via the process of chemical weathering of carbonate minerals on the planet surface in an attempt to stabilise the climate against increasing stellar input. The terrestrial biosphere during this phase in the planet's 'habitable lifetime' would most probably be dominated by non-photolithoautotrophic organisms, such as chemolithoheterotrophs and chemoorganoheterotrophs (O'Malley-James *et al.*, 2013; O'Malley-James *et al.*, 2014).

This chapter will explore the effect that planet size has on the timing of these transitions. Other workers in the field (e.g. Kopparapu *et al.*, 2013a) have investigated the effect of planet mass on habitability, but this study differs in methodology in that a self-consistent dynamical carbon-cycle and carbonate-silicate feedback is included, as opposed to an explicit focus on the response of standard, non-dynamic model atmosphere. Admittedly, Kopparapu *et al.* (2013a) features a more detailed 1-D radiative-convective model, whereas this study utilises fits to the output of the same model. In this formulation, and in the context of planetary biogeochemical cycling, planetary heat flow, which scales according to planet size, is expected to be the primary driver of the variability in habitability due to its control on

volcanic outgassing and other tectonic processes vital for maintaining carbon cycling and climatic evolution late into the planets lifetime. Despite these differences in approach, our results broadly agree with those of Kopparapu *et al.* (2013a): larger planets have wider habitable zones. However, neglected in both Kopparapu *et al.* (2013a) and this work is the effect of varying atmospheric heat transport on larger planets. The study of terrestrial exoplanet atmospheres is in its infancy, and the effect of planetary size, rotation rate, gravity and other orbital factors on the rate and mode of atmospheric circulation and heat transport, as well as these processes effects on the boundaries of the habitable zone, is not yet well resolved (Showman *et al.*, 2010).

Figure 4.5 displays these habitable zone boundaries for terrestrial planets between 0.5 and 10 Earth masses ($M_\oplus$) as a function of incident stellar flux (normalised to the present day Earth), generated by the model using the default parameters and fits from the radiative-convective climate model for a 1-bar N_2-dominated atmosphere described by Haqq-Misra *et al.* (2008) and Kopparapu *et al.* (2013). CO_2 and H_2O clouds are neglected, as well as wavelength-dependent reflective variability (i.e. Joshi & Haberle, 2012) – the spectra of the incident stellar flux is approximated as solar. The blue line represents the lower temperature limit (273 K), the red line the higher temperature boundary (343 K), and the green lines the low CO_2 limits. Also included on the plot are Earth, and a sample ($n = 7$) of the PHL habitable planet database (with mass errors included) whose masses fell within the limits of the model (< 10 $M_\oplus$). The darker green line represents the CO_2 limit for C3 plants ($\sim$150 ppm), and the lighter green line the CO_2 limit for C4 plants ($\sim$10 ppm). The radiative-convective model however most likely underestimates temperature during the early history of the planet, predicting the initiation of habitable conditions at $S \sim 0.78$ for an Earth-mass planet for example, whereas geological evidence and climatological modelling of the conditions on the early Earth when values of S were lower than this limit suggests that temperatures were above 273 K. The processes controlling this cold boundary are notoriously complex, and this formulation excludes many of these factors but necessity, including latitudinal and wavelength-dependent ice-albedo feedbacks which would

alter the energy balance of the surface (Joshi & Haberle, 2012; Shields *et al.*, 2013), hazy atmospheres of different constituents, which would require resolving atmospheric photochemical processes and including a more substantive and integrated methane flux and redox balance, (Zerkle *et al.*, 2012) and the effect of atmospheric pressures greater than 1 bar (Kopparapu *et al.*, 2013a). These shortcomings are addressed in more detail in other sections of this work.

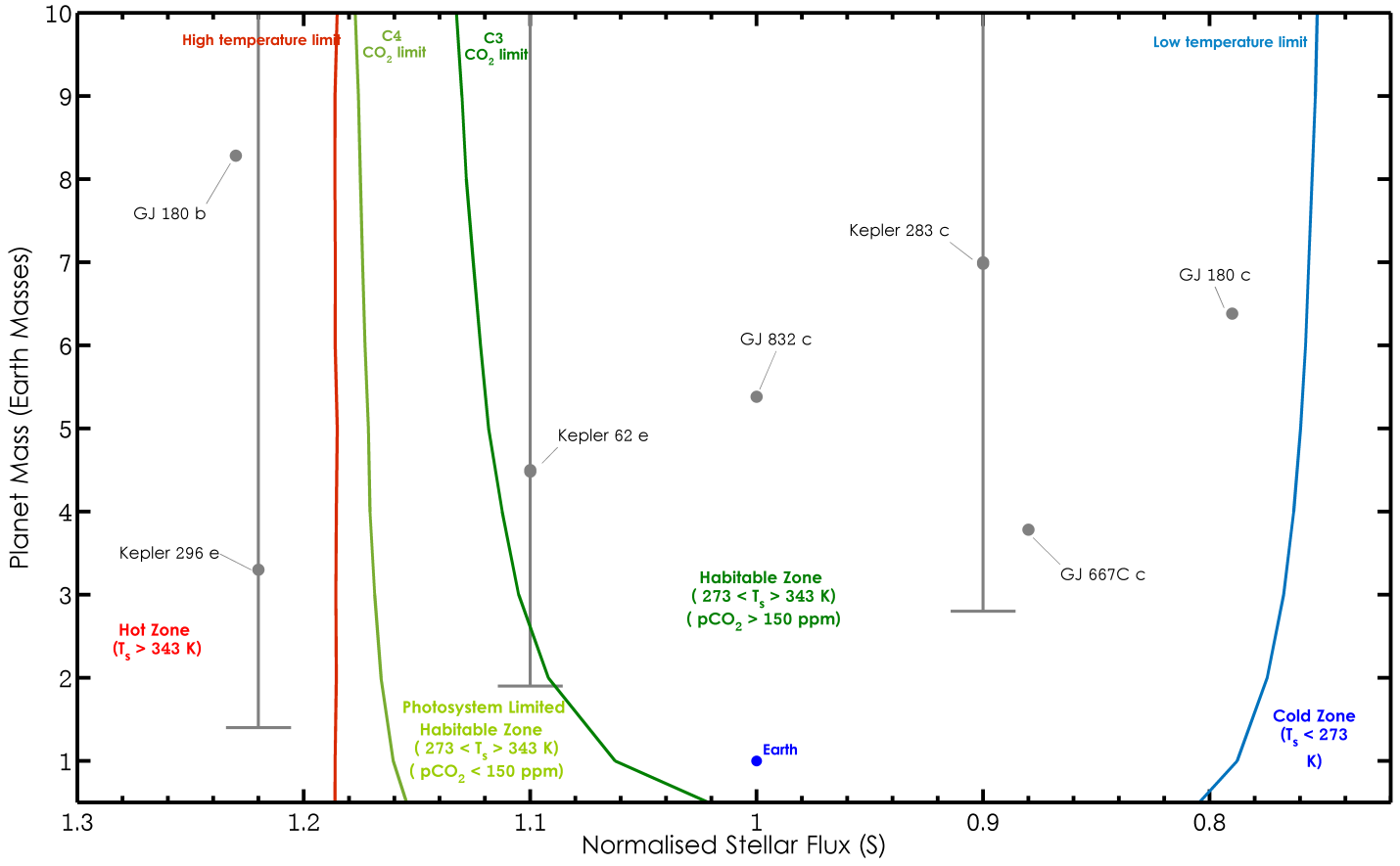

Figure 4.5: Temperature and photosystem habitable zone boundaries as a function of incident stellar flux and planet mass. HEC candidate planets (and mass errors) are included in grey, and Earth in blue.

Furthermore, this plot illustrates several effects that planet size has on these transitional boundaries. Smaller planets require proportionally greater incident stellar flux to initialise habitable conditions due to lower geothermal heat flow and rates of volcanic outgassing. This effect is further perpetuated at the CO_2 boundaries, where lower mass planets are less able to tolerate a high stellar flux before critical CO_2 drawdown takes place, due to the fact that volcanic outgassing (which serves to return CO_2 to the atmosphere) is lower, whilst the rate of carbonate-silicate weathering remains relatively independent of planetary mass. These combined effects decrease the overall habitable lifetime of smaller planets, but would serve to extend the duration of the low-CO_2, adequate temperature regime for proportionally longer than higher mass planets due to the very low atmospheric CO_2, limited geothermal heat flux and volcanic outgassing during this phase.

For example, a planet with a mass half that of the Earth would require an equivalent stellar flux of ∼0.8 to maintain temperatures above 273 K. Once S reached 1 (i.e. the present day flux on Earth) however, the rate of degassing (which is proportionately lower due to the lower heat flux) on this planet would be outstripped by terrestrial weathering (which is independent of heat flux, and therefore planet mass), lowering atmospheric CO_2 below C3 photosystem limits. The operation of this process on a $5M_\oplus$ planet however would buffer the climate against a stellar flux equivalent to $S \sim 1.1$, which corresponds to approximately ∼5.5 Gyr around a G dwarf with the mass of the Sun. However, planet mass has little effect on the termination of habitable conditions in terms of temperature; across all mass classes $S = 1.18$ appears to the be the runaway greenhouse limit. This is due to the fact that, regardless of variations in the timing of the collapse of the atmospheric CO_2 greenhouse, the end of the planet's habitable lifetime will be determined by incident stellar flux which remains independent of planet mass. The Earth itself will likely enter a CO_2-stressed regime at approximately $S = 1.06$, equivalent to 5.37 Gyr (0.83 Gyr from present), while temperatures would exceed 343 K at approximately $S = 1.18$ (6.35 Gyr, or 1.81 Gyr from present).

Of the exoplanets from the PHL database included on this plot, GJ 667 Cc,

GJ 180 c, Kepler 283 c, GJ 832 C and possibly Kepler 62 e (depending on its mass and which climate parameterisations are used) would fall within the habitable zone of their stars, and under the assumptions of the model would have surface temperatures and atmospheric CO_2 within habitable limits. This model predicts that GJ 180 b and Kepler 296 e receive an incident flux too great to maintain surface temperatures or CO_2 within habitable bounds, whilst other planets in the database HD 40307 g, Kepler 442 b and GJ 422 b (not shown on this plot as they receive an incident flux less than 0.7) likely do not receive sufficient irradiation, and are therefore relegated to the 'cold zone'. However, it should be reiterated at this juncture that the outer habitable zone boundary (the cold limit) is fraught with uncertainties and complexities likely beyond the scope of this work, and our estimates of the location of this boundary in stellar flux space is presented with less confidence. The primary interest and focus of this work remains the behaviour and interplay of temperature and CO_2 in terms of habitability, highlighted by the 'photosystem-limit' boundary. Both the radiative-convective model, as well as the parameterised climate scheme, suggest a planet-mass dependence on this transitional boundary, but the location of this limit changes depending on the model formulation used: the radiative-convective case providing a less conservative limit than that generated by the latter case.

4.4.3 Biogeochemical Processes Affecting Habitability

The ensemble of plots that comprise figure 4.6 provide detailed output from the model, including average surface temperature, pCO_2, albedo, silicate weathering flux from the land surface and hydrothermal carbonitization of the seafloor. These data were generated using the coupled carbon cycle and radiative convective model, and were initialised under default conditions. Planet sizes of 0.5, 1, 5 and 10 $M_\oplus$ are shown. Standard values of all other parameters (table 4.2) were used.

The effect of planet size is evident in the surface temperature and pCO_2 histories generated by the model. Smaller planets have, on average, higher surface temperatures but slightly lower levels of atmospheric carbon dioxide

during the early part of their habitable periods, with this trend reversing as the planet ages. This has implications for long term biological productivity on these worlds, and for the termination of habitable conditions.

Atmospheric CO_2 collapse and extreme stress on photosynthesisers will most likely mark the termination of habitable conditions and the biosphere on the planet before temperatures exceed 343 K, with a convergence towards a similar temperature trajectory in all of the cases considered here (as the stellar flux incident on the planet remains the same, independent of variation in planet size) following the decline of atmospheric carbon beyond the levels required for C3 photosynthesisers. Planet mass has a significant effect on the termination of the photosystem habitable zone, with smaller planets experiencing a pCO_2 collapse sooner than larger planets; a difference of $\sim$1.5 Gyr in the case of 0.5 versus 10 $M_\odot$ planets despite higher initial pCO_2 levels in the case of smaller planets (>100 PAL at 1 Gyr) and less vigorous silicate weathering. Rates of seafloor weathering also exhibit strong planet mass dependence as this parameter scales with heat flow (Q), which is strongly dependant on planet mass. Higher levels of hydrothermal carbonatization accounts for the lower pCO_2 levels on larger planets during their early history as this processes represents a significant removal flux for carbon until terrestrial silicate weathering becomes more effective under increasing temperatures. The effect of planet mass on the operation of both of these processes will be investigated statistically in Section 4.4.6

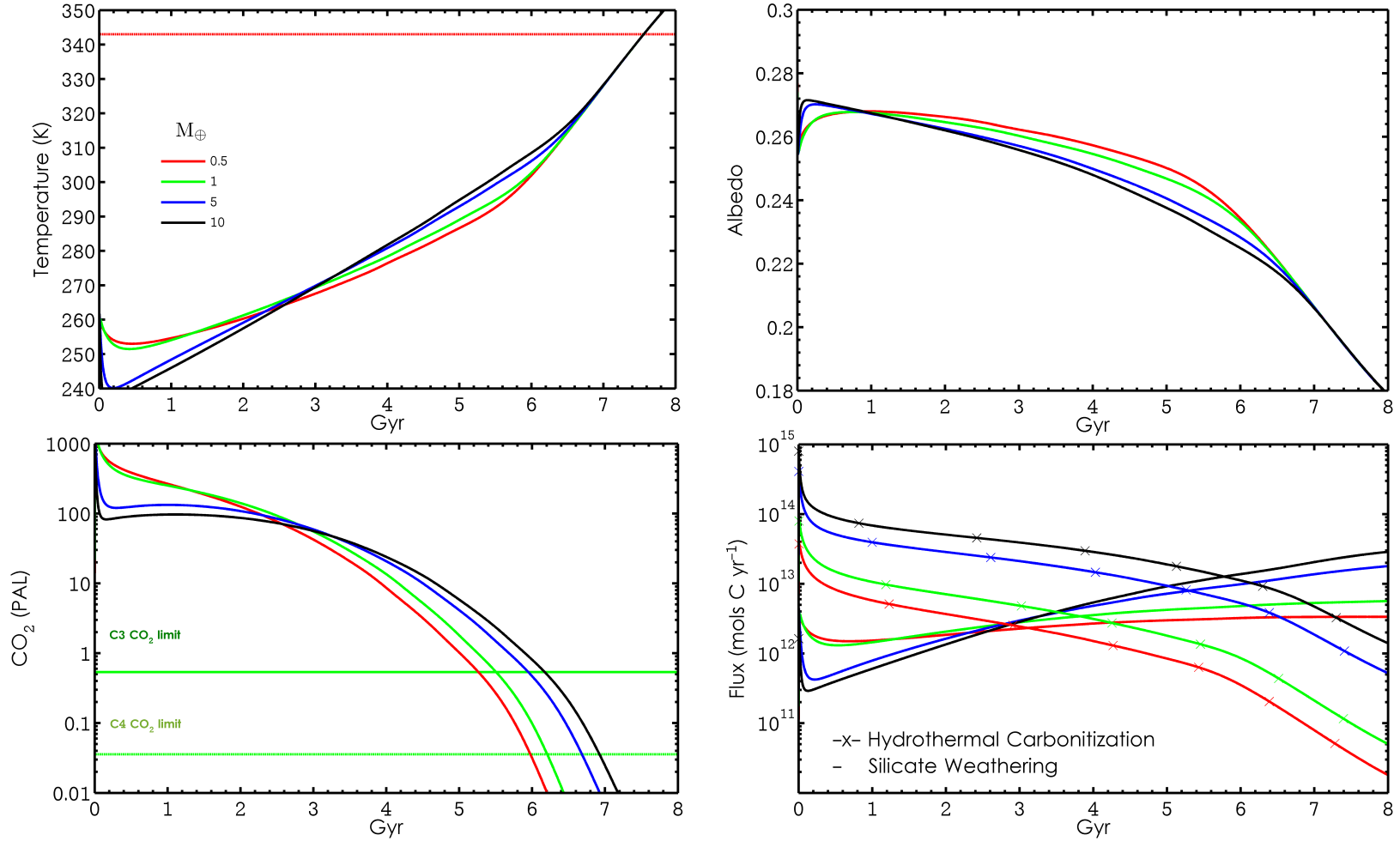

Figure 4.6: Ensemble plot representing model output as a function of planet mass. Top left: surface temperature. Top right: albedo. Bottom left: Atmospheric CO_2. Bottom right: Silicate and hydrothermal weathering fluxes.

4.4.4 Re-examining the Effect of Star Mass

It is expected that the size of the host star of a potentially habitable planet will have a significant effect on the duration of habitable conditions as the rate of the gradual increase in stellar output is directly proportional to the mass of the star, which in turn controls the boundaries of the habitable zone of that star (as introduced in Chapter 2 of this thesis, and Rushby *et al.*, 2013). Retesting this hypothesis using this model requires normalising for planet size, which for this subsection will be held at 1 $M_{\oplus}$, and distance from the star, which can be equated as an 'effective flux' parameter (F_E), where 1 F_E is equivalent to the amount of incident stellar flux at the top of the Earth's atmosphere, and scales according to the inverse-square law as $F_E \propto$ distance from star^{-2}.

The results displayed in the ensemble plot (figure 4.7) illustrates the control of stellar mass on the habitable zone lifetime of an Earth-mass planet at an equivalent distance from the host star. A polynomial fit was applied to the results from the model, as shown in the left-most figure. As expected, smaller stars with longer main sequence lifetimes and lower rates of habitable zone boundary migration host planets with longer habitable periods. Low-mass stars ($<0.7M_{\odot}$) may be able to support habitable conditions on Earth-sized planets with an equivalent present-day incident flux for >20 Gyr, or >3 times the predicated habitable lifetime of the Earth ($\tau_{h\oplus}$).

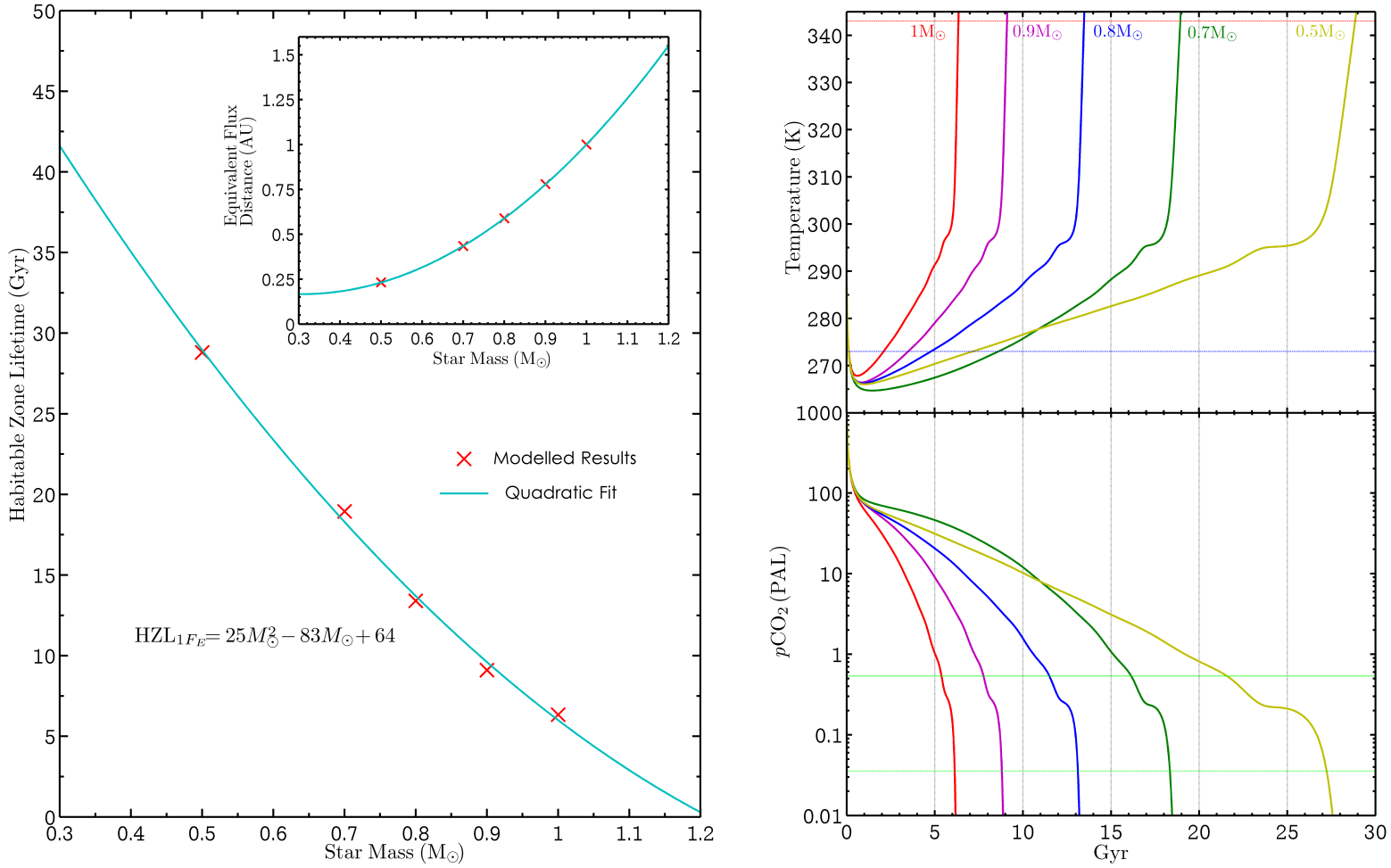

Figure 4.7: Ensemble plot representing model output as a function of star size, normalising for planet mass (1 $M_{\oplus}$) and incident flux (1 F_E). Left: Habitable zone lifetime (for temperature) as a function of stellar mass. A polynomial fit is applied to the modelled results (shown top right). The inset plot displays the relative distance around stars of varying mass at which $F_E = 1$. Top right: Planetary climate evolution as a function of time and stellar mass. Bottom right: Atmospheric CO_2 as a function of time and stellar mass

4.4.5 Eccentricity & Habitability

The eccentricity of a planet describes the shape of the planet's orbit, in particular the amount by which it deviates from a circle. The orbits of high eccentricity planets resemble parabola, where an eccentricity (e) of 1 represents an escape trajectory, whereas low eccentricity orbits are elliptical in shape. The eccentricity of the Earth's orbit is low ($e = 0.016$), which provides a nearly circular orbit (Berger & Loutre, 1991). The energy balance of the planet will be undoubtedly affected by eccentricity; the greater e, the greater the fluctuations in climate one could expect as the incident flux on the surface fluctuates between extremes of high and low as the planet approaches the star (perihelion) and reaches aphelion (the furthest distance in its orbit), respectively. The effects of these orbital eccentricities are evident in the Milankovich cycles affecting Earth; the evolution of the planet's eccentricity over a ∼100,000 year period due to gravitational perturbations by Jupiter and Saturn produces discernible effects on the Earth's climate, as presented by paleoclimate studies (Petit *et al.*, 1999). More generally, this raises the possibility of 'snowball' catastrophes on planets with high orbital eccentricities at apastron, where the entire planet becomes glaciated due to the low radiative flux and runaway ice-albedo effect, and extreme greenhouse scenarios at periastron associated with extremely high irradiation, with deleterious effects on habitability, biogeochemical cycling and atmospheric stability. The effect of eccentricity on habitability has been investigated by other workers, e.g. Barnes *et al.*, 2009; Dressing *et al.*, 2010.

In this simple formulation, a parameterisation for eccentricity is included in the incident flux term, in the form:

$$S = \left(\frac{S_j(L_\odot)}{4\pi} \right) a^2 (1 - e^2)^{1/2} \tag{4.4}$$

Where S is the normalised incident stellar flux at planet, S_j is the incident flux (in W m^{-2}) derived from a fit to results from the Dartmouth Stellar Evolution Database (see 'methods' in chapter 1 for more details), $L_\odot$ is the normalised luminosity of the star, a is the planet's semi-major axis (in AU)

and e is the planet's eccentricity. It should be noted that this simple formulation excludes the effects of other variations in orbital dynamics, such as obliquity and precession, as the mechanics of these processes are difficult to resolve in a zero-dimensional model that lacks a latitudinal dimension.

From this equation it is evident that the effect of eccentricity on average incident flux (and planetary temperature) is relatively small, following Kepler's second law of planetary motion (i.e. that the orbital velocity of the planet will be greatest nearest the star) and the non-linear nature of the Stefan Boltzmann law. This is further illustrated by figure 4.8. For example, the highest eccentricity in the Earth's orbit over the past 50 million years is purported to be ∼0.0679 (Laskar *et al.*, 2011), representing a Δe of 0.0512 from present, which, if other variables such as stellar luminosity are held constant at present day values, would result in a ΔS of ∼0.74 W m^{-2}, or a 0.002% drop in irradiation (assuming present day top-of-the-atmosphere irradiance of 341.09 W m^{-2}). With an extreme eccentricity of 0.5, ΔS would be on the order of 45 W m^{-2} (13.2%) between apastron and periastron.

For planets with smaller semi-major axes, the differences in insolation between apastron and periastron would produce marked changes in climate over the relatively shorter orbital period. A planet with a semi-major axis of 0.7 AU for example, (with a period of 211 days (around the Sun) derived from Kepler's third law), but with a high eccentricity (0.5) would experience large swings in insolation, up to 13.3% (∼93.3 W m^{-2}), between closest and furthest approach. This is a comparable relative percentage variation in S with planets with more distant orbits, but the shorter orbital period further compounds the effect of these extreme swings in insolation and temperature. Therefore, it is expected that the habitability of planets near the inner, warm edge of the habitable zone with high eccentricities would be disproportionately affected.

Figure 4.9 displays the effect of eccentricity on the boundaries of the habitable zone as a function of incident stellar flux, assuming a 1 $M_\oplus$ planet and using the radiative-convective climate model coupled to the carbon-cycle model described above. For a planet with an eccentricity of 0

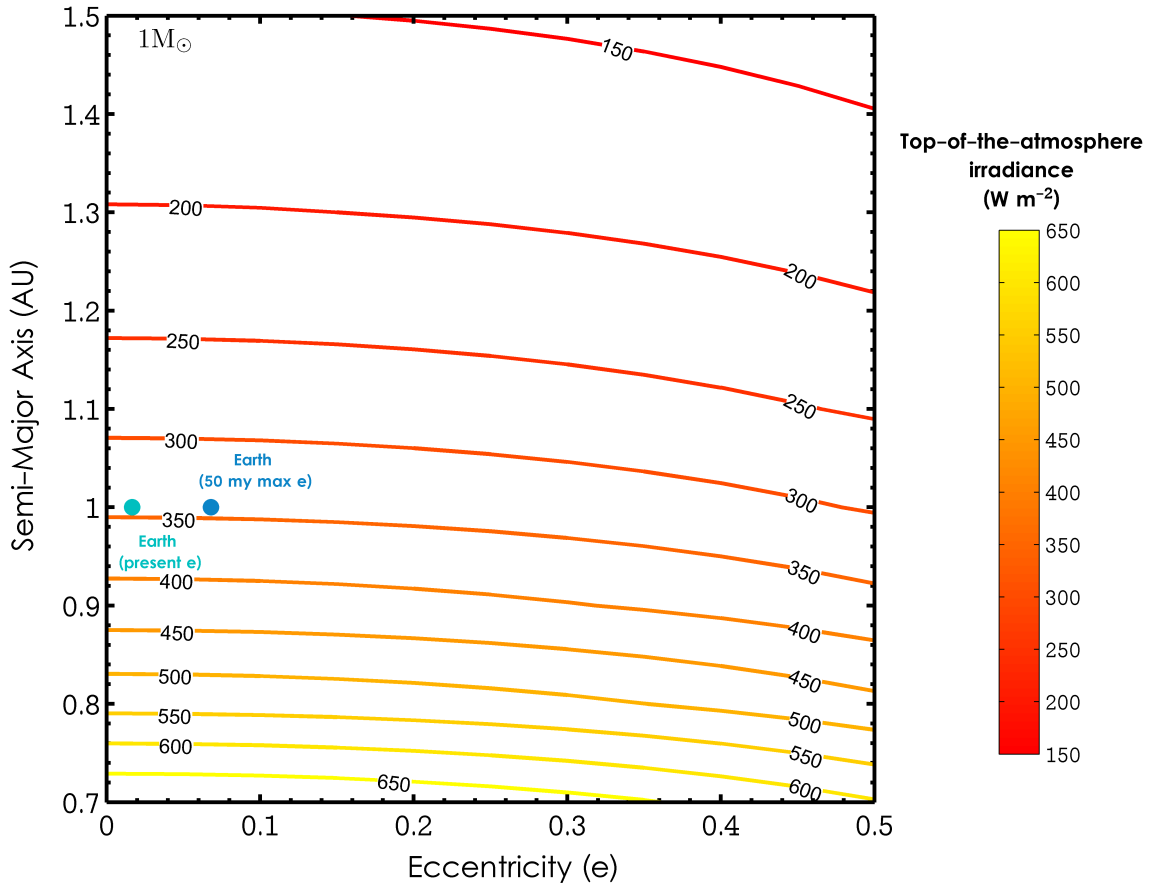

Figure 4.8: Downward top-of-the-atmosphere flux (in W m^{-2}) as a function of orbital eccentricity and distance from star (in AU). The light blue marker represents the present-day Earth, and the dark blue marker represents the maximum eccentricity of the Earth for the past 50 million years.

(default conditions), the habitable zone boundaries are the same as those described in the preceding paragraphs: habitable temperatures are initiated at $S \sim 0.78$, the C3 and C4 photosystem boundaries are at $S \sim 1.06$ and $S \sim 1.16$ respectively, and a runaway greenhouse regime can be expected at incident flux values of ~1.18 or greater. As eccentricity increases, the boundaries move outwards in S parameter space; high eccentricity planets require higher initial values of S to initiate habitable conditions (0.91 when $e = 0.5$), the photosystem boundaries are also less sensitive to higher

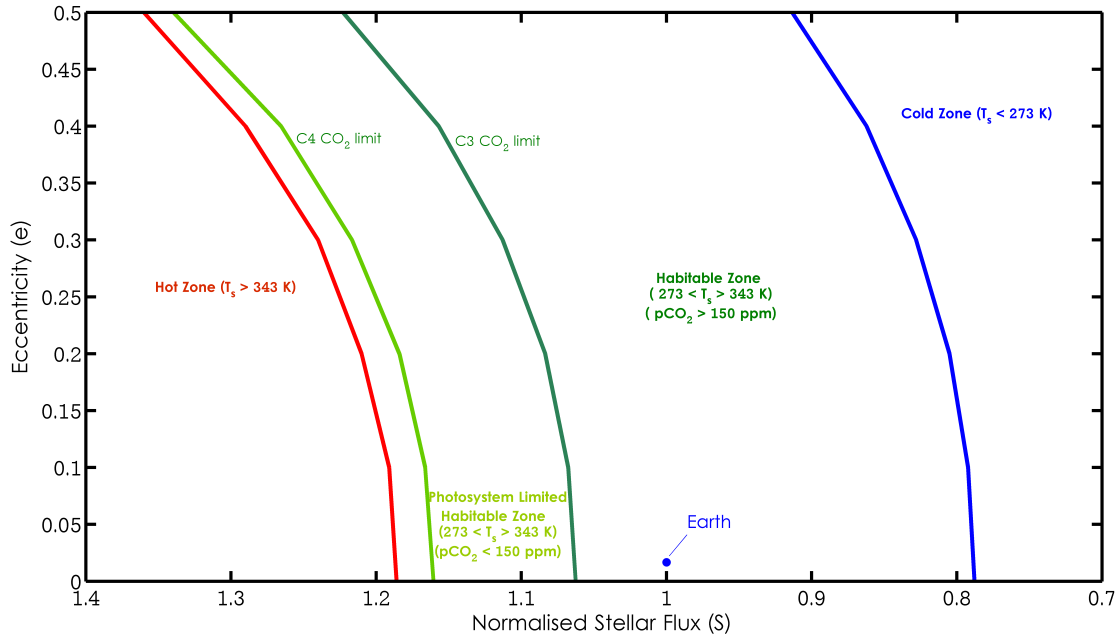

Figure 4.9: Habitable zone boundaries (temperature and photosystem) as a function of stellar flux and orbital eccentricity.

irradiation, with the C3 and C4 limits falling at $S \sim 1.22$ and 1.34 respectively, while the high temperature limit is passed at S ~ 1.36. This illustrates that the habitable parameter space is greater around more eccentric planets, with a 90%, 82% and 86% reduction in the habitable S space between the cold boundary, C3, C4 and hot boundaries respectively for $e = 0$ planets versus $e = 0.5$ planets. This is a response to a simple change in the model: a reduction in available average stellar flux at the top of the atmosphere; the higher the eccentricity the lower the average incident flux. Transient snowball or super-greenhouse events are not captured due to the low temporal resolution of the model, and the complexities of atmospheric transport, zenith angle etc. are also not included. The effect of planetary eccentricity on both long- and short-term habitability is therefore not well resolved by this model. Furthermore, whilst this model suggests a general expansion of the habitable zone in stellar flux space, the actual habitable zone is closer to the star for more eccentric planets. These results are in general disagreement with those presented by Dressing *et al.* (2010),

in which it was shown that high eccentricity planets may have habitable semi-major axes at much greater distances than low eccentricity planets due to the buffering of the climate by thermal inertia preventing snowball events at apastron. This study also incorporated orbital obliquity, zenith angle and rotation rate, suggesting that this more detailed parameterisation for eccentricity is required to accurately describe the effect of orbital variations on habitability, particularly a shorter temporal resolution with multi-dimensional atmospheric heat flow parameterisations. In light of this, eccentricity is held at 0.0167 (the current eccentricity of the Earth) throughout the rest of this work.

4.4.6 Latin Hypercube Sampling Analysis

Having investigated the effect of several parameters on the output of the model, and in particular the length of the habitable period/habitable zone lifetime, it remains essential to determine whether these effects are attributable to the effect of the input parameters, or whether they can be attributed to some other factor. For this section, the evolution of incident stellar flux follows the standard 1 $M_{\odot}$ trajectory, as predicted by the stellar evolution model described in chapter 2 of this work. Drawing on the LHS methodology introduced earlier in this chapter, descriptive statistics of the habitable periods of the sample of 1645 simulations described previously can be seen in the box plot (figure 4.10). These represent the averaged habitable periods for runs conforming to the full range of input variables, and described in table 4.2. The mean habitable period varies considerably between the photosystem and temperature-only cases, where the photosystem limit is consistently reached before the surface temperatures exceed the upper boundary. For the cases presented here, the mean photosystem habitable period(τ_{hCO_2}) is 6.18 Gyr ($\sigma = 0.285$), the mean temperature habitable period (τ_{htemp}) is 6.78 Gyr ($\sigma = 0.25$). The standard error at the 95% confidence interval for these estimates (computed by $(\sigma/\sqrt{n}) \times 1.96$ (i.e. 95% of the values fall within 1.96σ of the mean.)) is ± 0.014 and ± 0.012 Gyr respectively. While the timing of the photosystem limit is earlier, the runs exhibit a larger standard deviation suggesting the

input variables have a greater effect on this timing.

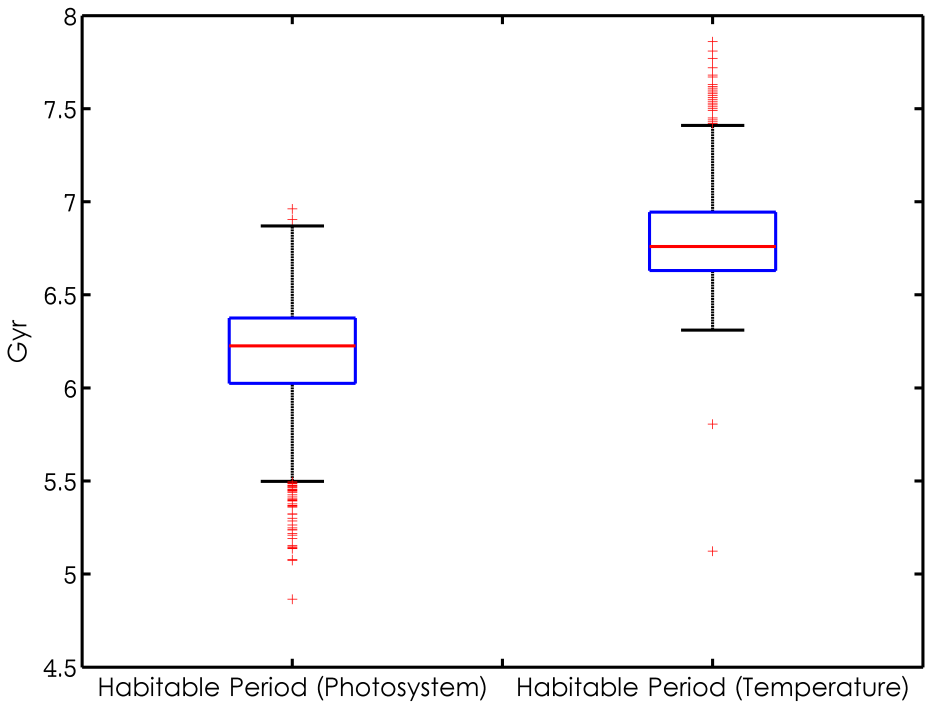

Figure 4.10: Box plot illustrating the differences in mean duration between the temperature-only and photosystem habitable periods.

The output data were then binned according to the square-root approach (i.e. the number of bins is equal to the square root of the number of elements and fits a normal density function), to produce a histogram (and normal fit) of photosystem and temperature-only habitable periods, as shown in figure 4.11 and figure 4.12 respectively, further illustrating the differences in timing between the two habitability limits. The timing of the photosystem habitability termination is skewed slightly towards the later end of the distribution, whilst the temperature case exhibits approximately the opposite effect.

Using the binned histogram data it is possible to turn the likely length of

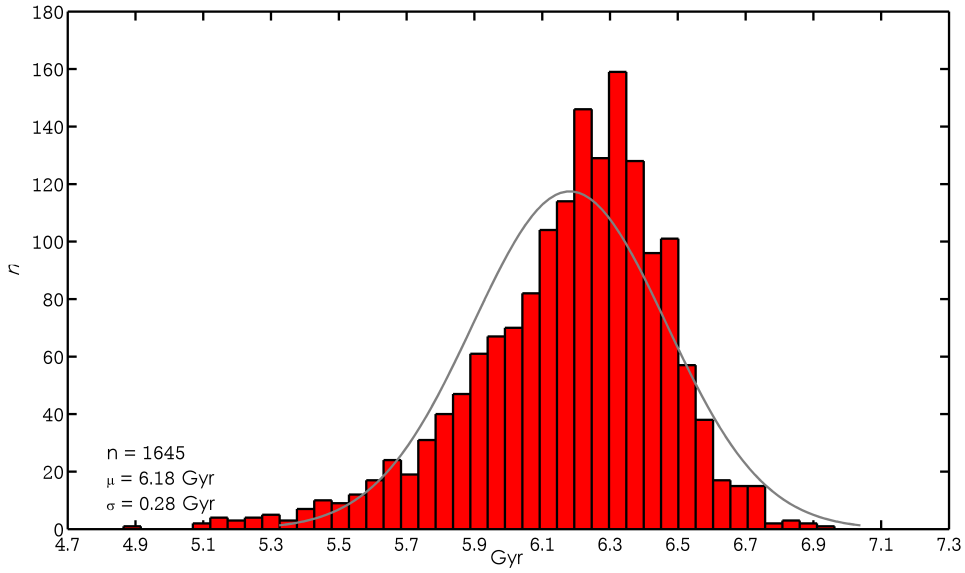

Figure 4.11: Histogram (with normal fit) of photosystem habitable periods of successful model runs.

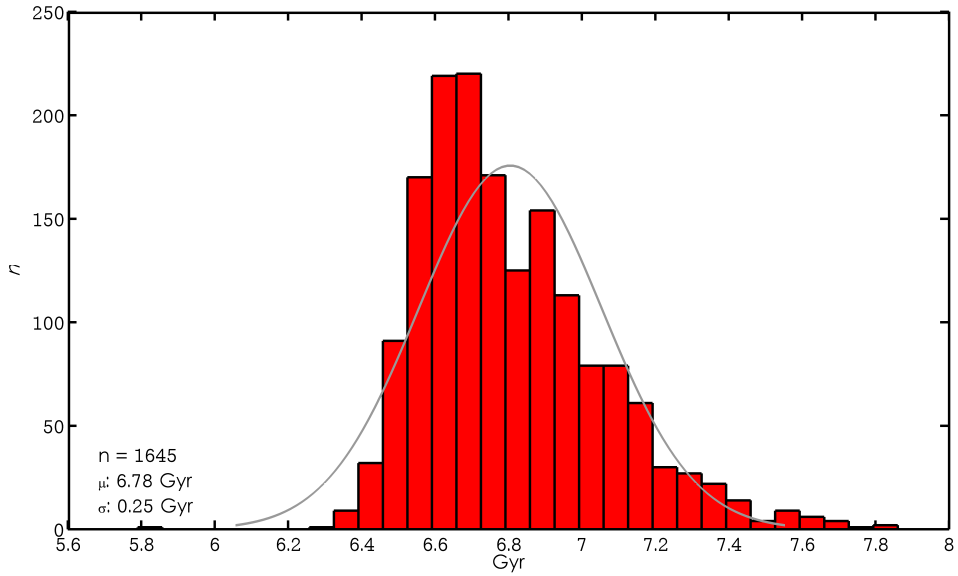

Figure 4.12: Histogram (with normal fit) of temperature-only habitable periods of successful model runs.

the photosystem and temperature habitable periods into a probability density distribution, and by integrating these functions a probability of the

length of the two habitable periods can be computed, as shown in figure 4.13. The data has been smoothed by fitting a spline interpolant. These figures suggest that the photosystem limit in ∼33% of the successful runs was passed at ∼6.28 Gyr, whilst the temperature limit was exceed in ∼36% of the runs at 6.7 Gyr. Therefore, even accounting for the variability in the input parameters of the carbon cycle model and planet size, the likely habitable period (as defined above) for photosynthetic life is considerably shorter than the temperature-only habitability limit, further illustrating the limitations of using temperature alone as a proxy for habitable conditions, and for the inclusion of a dynamic biogeochemical carbon cycle response in future calculations of the habitable zone.

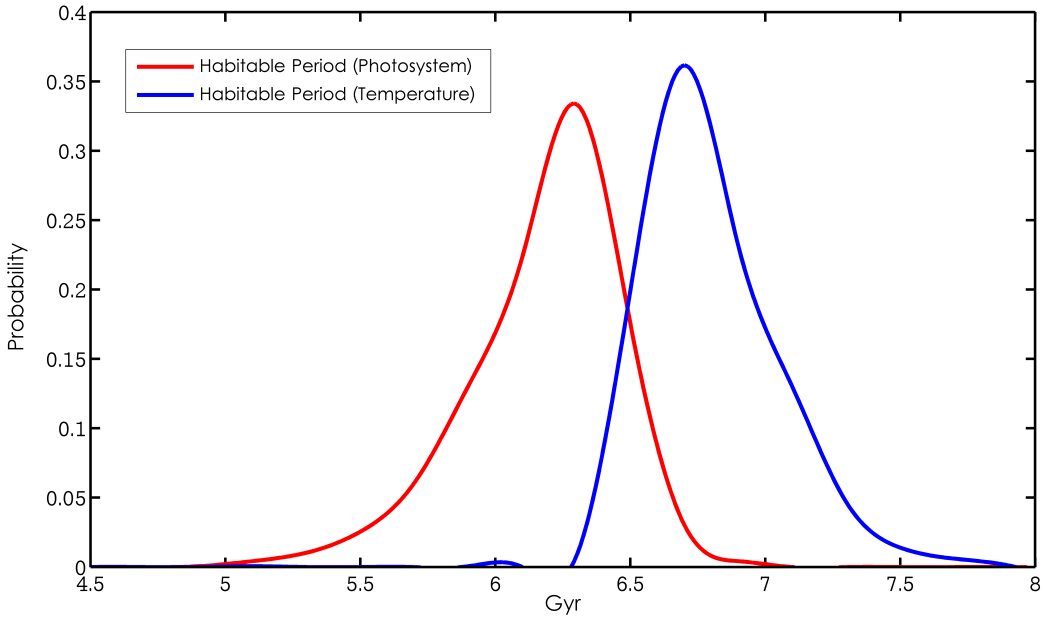

Figure 4.13: Probability distribution of habitable periods over all runs.

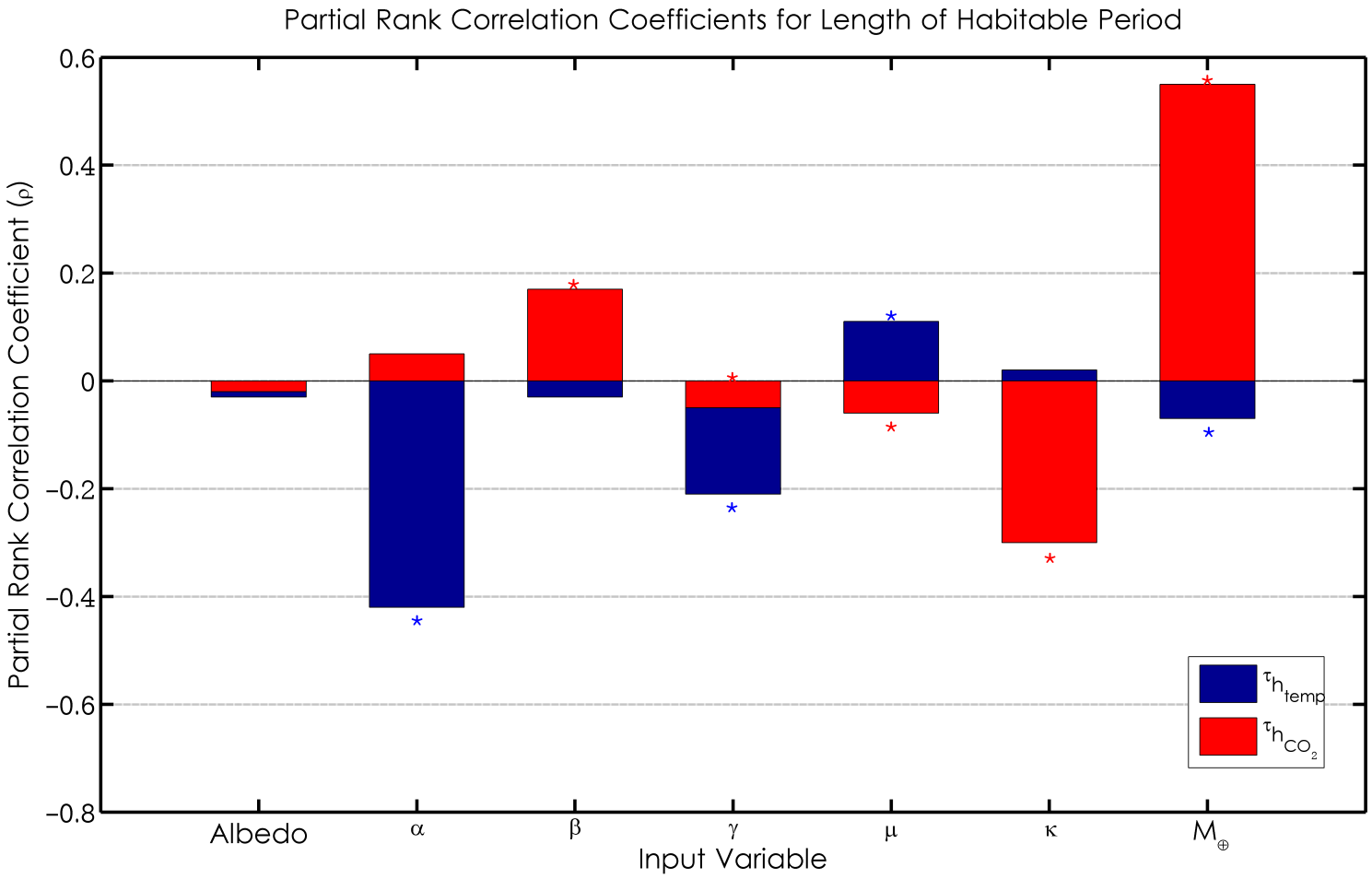

Figure 4.14: Result of partial rank correlation analysis for input variables, relative to length of photosystem (red) and temperature-only (blue) habitable periods. Asterisks indicate statistically significant relationships ($P < 0.05$).

	ρ_{photo}	$\boldsymbol{P}$
Albedo	-0.02	0.326
α	0.05	0.056
β	0.17	0.000
γ	-0.05	0.028
μ	-0.06	0.008
κ	-0.30	0.000
$M_{\oplus}$	0.55	0.000

Table 4.3: Results of partial rank correlation analysis for length of photosystem habitable period.

	ρ_{temp}	$\boldsymbol{P}$
Albedo	-0.03	0.181
α	-0.42	0.000
β	-0.03	0.291
γ	-0.21	0.000
μ	0.11	0.000
κ	0.02	0.354
$M_{\oplus}$	-0.07	0.003

Table 4.4: Results of partial rank correlation analysis for length of temperature habitable period.

The results of the partial rank correlation analysis described in the previous section are shown in figure 4.14, as well as table 4.3 (for the photosystem limit) and table 4.4 (for the temperature-only limit), where ρ is the correlation coefficient and P is the p-value. Several statistically significant ($P < 0.05$) correlations between the input variables and the diagnostic output variable are identifiable (highlighted in red). The need for some restraint in extrapolating these relationships to 'real-world' cases is recognised however, as their statistical significance only exists within the model, suggesting that within this particular model framework planet mass does result in a measurable variation in the habitable period. Perhaps the most interesting of these is the relatively strong, statistically significant correlation ($\rho = 0.55$) between planet mass and the length of the photosystem habitable period, suggesting a strong control by this parameter

on the operation of the carbon cycle, even accounting for variability in the other model inputs. Given the default model output presented earlier in this chapter, this relationship is not unexpected but the strong statistical significance lends credence to these earlier results and confirms that, within this formulation at least, planet mass is indeed a fundamentally important component of planetary habitability, as it is a powerful driver of several parameters in the carbon-cycle model, including the rate of geothermal heat flow, the size of the mantle carbon reservoir, the rate of subduction, ridge degassing and seafloor carbonatization. Therefore, it's expected that this parameter will have a powerful control on the timing of the critical CO_2 limit, and the incorporation of an accurate estimate of planet mass should form a primary component of future habitability assessments.

Other correlations of note in terms of the duration photosystem habitability is the inverse relationship (ρ = -0.30) between the biotic weathering enhancement factor (κ), as well as the weak relationship (ρ = 0.17) with silicate weathering dependence on atmospheric carbon dioxide (β). κ describes the enhancement of terrestrial weathering expected by land plants that break down rocks via the action of their roots and organic acids. The inverse relationship exhibited by this variable and the length of the photosystem habitable zone suggests that as the acceleration of weathering of the terrestrial geosphere by plants increases, the rate at which CO_2 is drawn out of the atmosphere also increases, in turn shortening the length of time over which photosynthesis could operate effectively, as would be expected. In the case of β, the increased sensitivity of silicate weathering to the amount of CO_2 in the atmosphere would also increase the rate of terrestrial weathering resulting in a decline in pCO_2 over the long term and a reduction in the possible length of the photosystem habitable zone.

When considering the PRCCs for the temperature-only habitability scenario, it should be noted that the size of the planet, in this case, has little effect on the timing of the termination of habitable conditions, as defined by the 343 K upper boundary. This is likely due to the fact this parameter has a much stronger control on the operation of the carbon cycle (and therefore the photosystem habitable period). Once carbon dioxide levels in the atmosphere reach negligible levels, their greenhouse forcing is

also significantly reduced and therefore once the photosystem limit has been passed the primary surface temperature forcing remains incident stellar flux, which is independent of planet size. However, an inverse relationship between the sensitivity of seafloor carbonatization to pCO_2 (α) and the duration of habitable conditions within the temperature limits is evident (ρ = -0.42), suggesting that as rate of weathering of the seafloor becomes more sensitive to CO_2, the window of habitability in terms of temperature is markedly reduced. This process is particularly important early in the history of the planet, before terrestrial weathering forms a significant weathering sink for carbon, and it is likely that a high sensitivity to CO_2 during this period would reduce surface temperatures via a reduced greenhouse forcing and exacerbate the 'faint young sun' problem under an analogous incident stellar flux environment to that of the early history of the Earth (S∼0.7). Therefore, it seems more likely that the reduction in habitable conditions demonstrated by this relationship is due to a delay in the initiation of habitable conditions early in the planet's history i.e. keeping the planet too cold. Hydrothermal carbonatization is a poorly constrained and understood process but these results suggest that, given the Earth was not plunged into a snowball state very early in its history, it is more likely that the sensitivity of this process likely falls towards the lower end of the range investigated here (where the range of $\alpha = 0.23$ — 1). However, a number of other factors may have affected the early climate of the Earth, including continental distribution and configuration, atmospheric composition, impactor flux as well as higher rates of volcanic outgassing and geothermal heat flow than considered here.

4.4.7 Exoplanet Case Studies

A small sample of potentially habitable exoplanets were selected to act as case studies in order for the model to attempt to reproduce their potential biogeochemical evolution. Based on the limited data that is currently available for these worlds, significant uncertainty exists in these estimates, but these case studies can serve as a useful example of the output of the model under varying planet mass, star size and incident stellar flux, as well

as an effective comparison to the history of the Earth.

Exoplanets Kepler 22b, Kepler 440b, GJ 832 c and Tau Ceti e are presented alongside the Earth in figure 4.15 as estimates for their mass, host star mass and orbital distance were available, and these exhibit relatively similar habitable periods to the Earth for effective comparison. Figure 4.16 also shows the habitable period of the Earth, and includes extremely long habitable period exoplanets for comparison, including Kepler 62 e, Kepler 283 c and GJ 667 CC. These results are summarised by table 4.7 figure 4.17. Planetary and stellar parameters used to initialise the model are taken from The Extrasolar Planets Encyclopaedia, The Habitable Planet Catalog and NASA's Exoplanet Archive, and are shown in table 4.6.

Planet	**Planet Mass ($M_\oplus$)**	**Star Mass ($M_\odot$)**	**Orbital Distance (AU)**
Earth	1	1	1
GJ 832 c	4.98	0.45	0.162
Kepler 440b	7.7	0.57	0.24
Kepler 22b	52.8	0.97	0.85
Tau Ceti e	4.3	0.78	0.55
Kepler 62 e	4.17	0.69	0.42
Kepler 283 c	7.04	0.59	0.341
GJ 667 Cc	3.8	0.31	0.125

Table 4.6: Planet and star properties for model initialisation. Taken from The Extrasolar Planets Encyclopaedia, The Habitable Planet Catalog, NASA Exoplanet Archive.

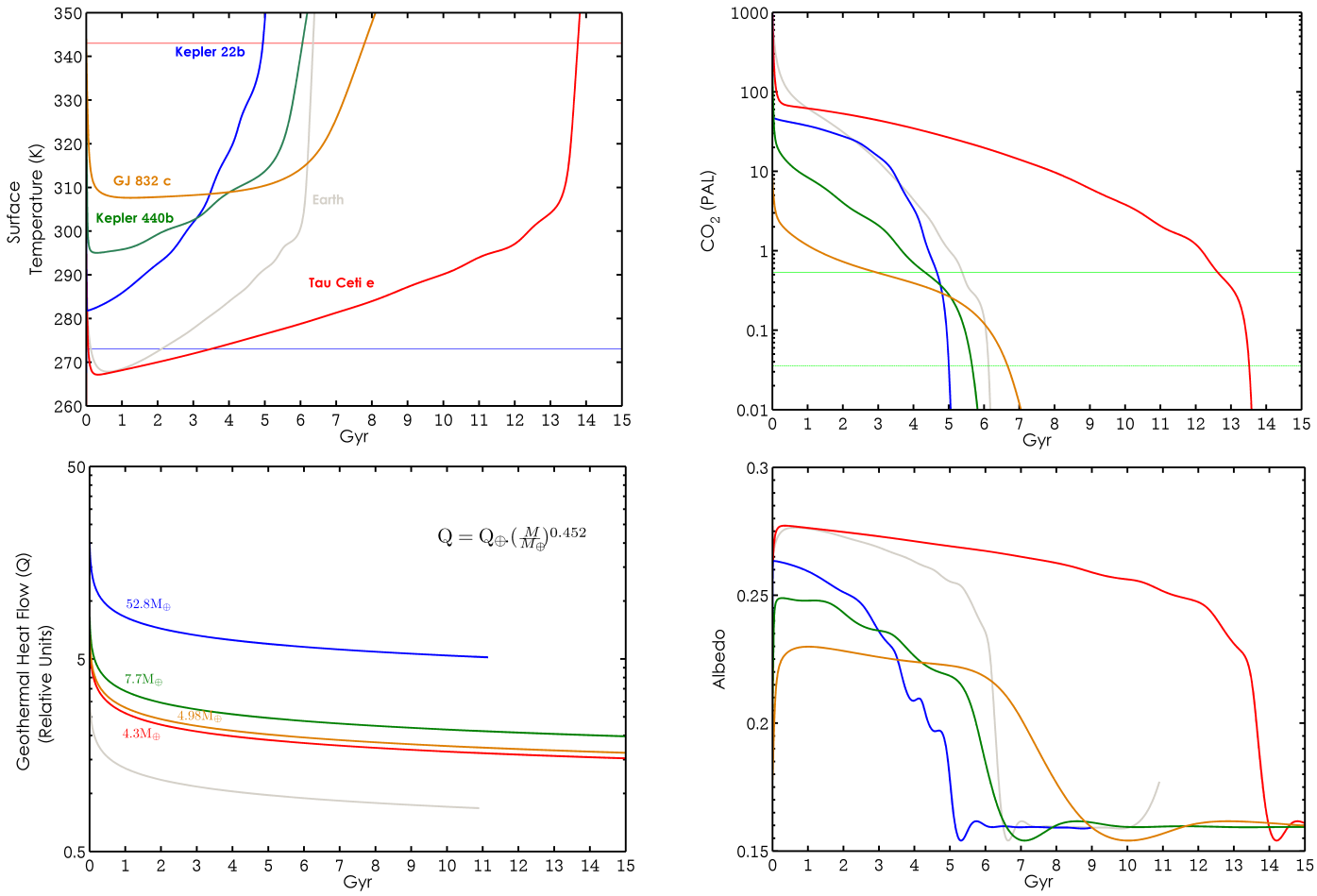

Figure 4.15: Top left: Climatological evolution of the Earth, as well as the exoplanets Kelper 22b (blue), Kepler 440b (green), GJ 832 c (brown) and Tau Ceti e (red), as a function of time in billions of years (Gyr). Top right: Changes in atmospheric carbon dioxide (pCO_2) as a function of time, identifying key photosynthetic limits for organisms using C3 and C4 photosystems. Colour scheme is the same as top right. Bottom left: Evolution of geothermal heat flux over time. Bottom right: Changes in planetary albedo as a function of time.

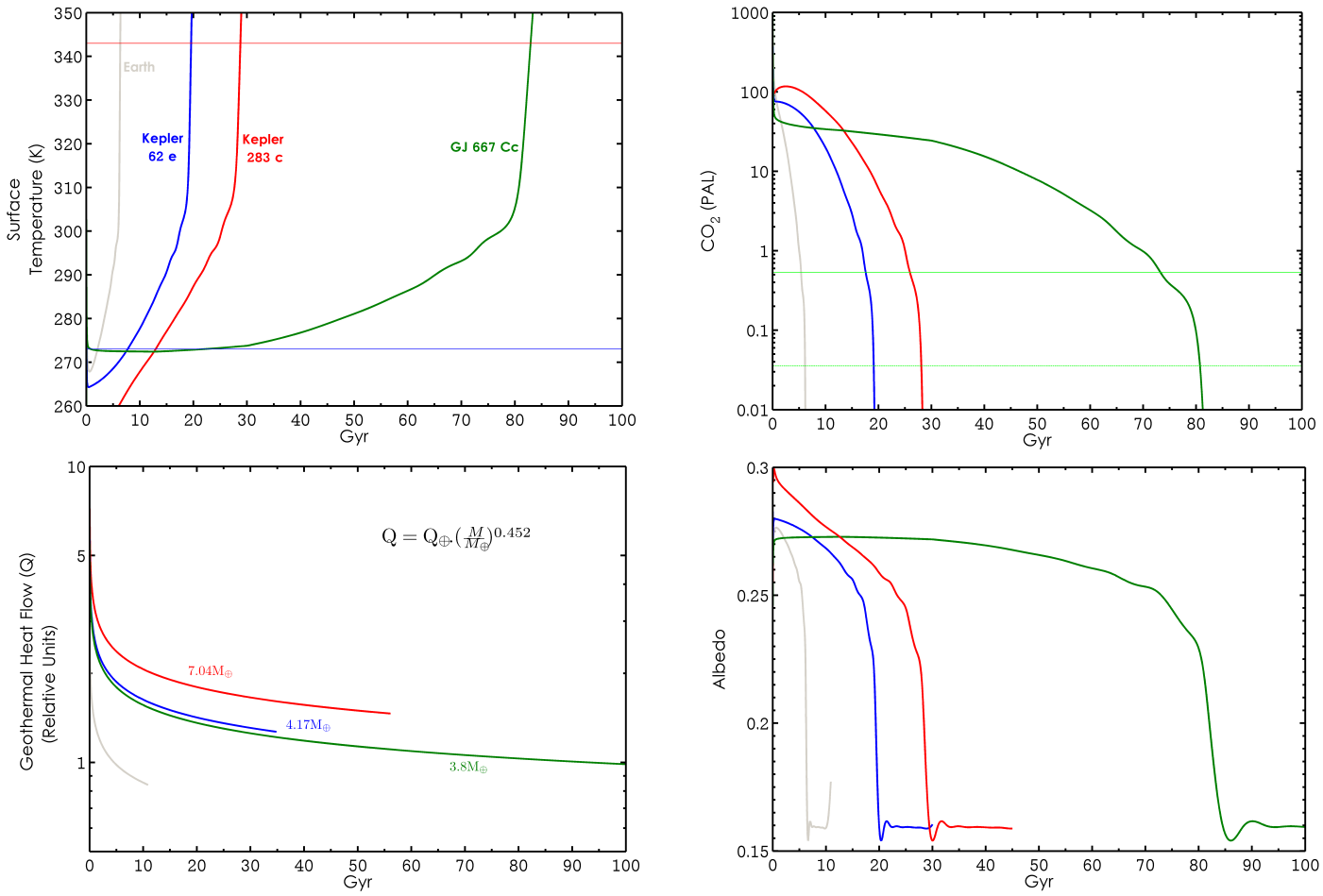

Figure 4.16: Top left: Climatological evolution of the Earth, as well as the extremely long habitable period exoplanets Kelper 62e (blue), GJ667 Cc (green) and Kepler 283 c (red), as a function of time in billions of years (Gyr). Top right: Changes in atmospheric carbon dioxide (pCO_2) as a function of time, identifying key photosynthetic limits for organisms using C3 and C4 photosystems. Colour scheme is the same as top right. Bottom left: Evolution of geothermal heat flux over time. Bottom right: Changes in planetary albedo as a function of time.

Planet	Habitable Period (CO_2)(Gyr)	Habitable Period (Temp)(Gyr)
Earth	5.38	6.34
GJ 832 c	2.94	7.8
Kepler 440b	4.28	6.06
Kepler 22b	4.65	4.94
Tau Ceti e	12.6	13.8
Kepler 62 e	17.5	19.5
Kepler 283 c	25.9	28.7
GJ 667 Cc	73.2	82.9

Table 4.7: Habitable periods computed from model output

These results indicate a relatively great diversity in the evolution of habitable conditions on these worlds, suggesting that the effect of individual planetary characteristics is significant. As shown in figure 4.16, the results have been normalised to the present day based on the age of the host star of the planet where available. The age of the stars Kepler 22 and Kepler 283 have been estimated from a stellar evolution model, and have not been confirmed in the wider literature. The age of GJ 832 remains unknown. What is clear is that planets in the orbit of small stars with longer main sequence lifetimes have considerably longer habitable periods, possibly up to 80 billion years in the case of GJ 667 Cc. However, the surface temperature for much of Gliese 667Cc's first $\sim$30 Gyr remains at the very limit of habitability, and in a region in parameter space where the behaviour of the model is less well constrained. Cloud cover, atmospheric composition, continental distribution, varying albedo surfaces and an alternative tectonic regime would affect these results, but cannot be controlled for given the limited data available. Furthermore, as discussed in Chapter 2, the age of Gliese 667C (and by implication its radiative output) is not well constrained. Of interest to astrobiologists and astronomers concerned with the detection of life on exoplanets are are worlds with long (>4 Gyr) habitable periods contemporaneous with the present day Earth. Tau Ceti e, Kepler 62 e and 283 c as well as Gliese 667Cc make for interesting candidates for future study as they satisfy this criteria.

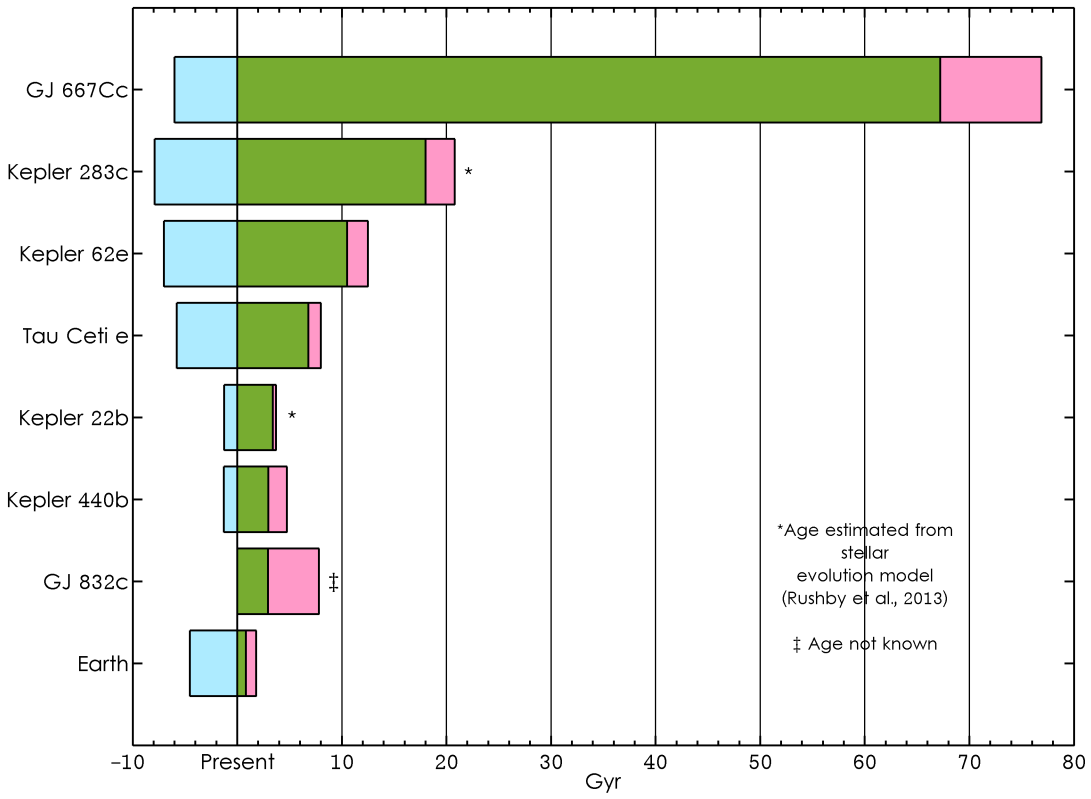

Figure 4.17: Habitable periods computed from model output for 7 exoplanets as well as the Earth. The red bars indicate the temperature habitable period, and the green the CO_2 habitable period. The results have been normalised to the present day based on the age of the host star of the planet. The age of the stars Kepler 22 and Kepler 283 have been estimated from a stellar evolution model, and have not been confirmed in the wider literature. The age of GJ 832 remains unknown.

4.5 Discussion

This work demonstrates the importance of an Earth- or planetary-system modelling approach to the topic of exoplanetary habitability. The advantages of this method have been known to researchers studying the climate, geochemistry, atmosphere and biosphere of the Earth for many years, and the study of exoplanetary habitability seems a logical extension of the paradigm. The circumstellar habitable zone concept has its benefits, primarily in its simplicity and degree of 'observability', but will continue to

obscure the complexities inherent in the study of exoplanets and their potential for hosting life. This would be detrimental for continued original research, as well as public perception of the discipline. Repeated exaltations of newly-discovered 'Earth-twins' and 'Earth 2.0s' espoused in the popular media, but based on extremely limited evidence, will only serve to dilute and desensitise the wider public to truly exciting discoveries made in this multidisciplinary field. Several statistically significant correlations have been identified in this study that support the hypothesis that a wider approach to this concept is required, and that improving estimates of planet size and a move towards biogeochemical modelling of exoplanets may be a means to address these shortcomings. Possible avenues for further research in this area are advanced in chapter 5.

Referring then to the various components of habitability outlined in Chapter 3 from Cockell *et al.*, (2015) this work draws on planet size, surface temperature and atmospheric CO_2 to first order, but these parameters can also be interpreted as proxies for other facets of the habitability regime, including the likely availability of liquid surface water and energy (in the form of fixable carbon) for metabolism. A time-dependent geothermal heat flow parameterisation also allows the model output to be interpreted relative to planet age.

4.5.1 Putting a Limit on the Lifespan of the Biosphere

This work, in its most practical of applications, provides an upper limit on the lifespan of the Earth's biosphere, whilst also attempting to illustrate the difficulties in considering this limit as a binary distinction between 'habitable' and 'uninhabitable' states. The upper temperature boundary considered here represents the endmember case for habitability, but before this limit is reached the biosphere will undergo significant and dramatic reorganisation, in terms of spatiotemporal distribution, habitat and resource availability, and metabolic stress exacerbated by falling pCO_2 levels. It is unlikely that a eukaryotic biosphere will persist long enough to face a temperature and runaway-greenhouse catastrophe, but this remains uncertain. For more detailed discussion of the transitions that the

biosphere will likely undergo, see O'Malley-James *et al.*, (2013).

As in much of science, the assumptions contained herein represent a necessary oversimplification of an incredibly complex system, but these generalisations can nevertheless provide an insight into this problem, at least to first order. This upper limit represents an important component in our understanding of the Earth system; a biogeochemical 'tipping point' beyond which the homeostatic climatic regulation mechanisms that have been operating for the past 4.5 billion years collapse and life on this planet will become impossible. Any system can defined by its limits; the limits to which that system can be perturbed by an external forcing, and the mechanisms and magnitude of the system's response, allows for a greater understanding of the controls on the feedbacks operating to stablise the system. The steady increase in stellar luminosity that will insolate the planet in the coming eons will provide that external forcing, the buffer to this input will be the carbonate-silicate cycle herein described. The diagnostic measure for the collapse of this buffer, the heroic last stand of Gaia, is the secular decline in atmospheric CO_2 below levels required for photosynthesis, as described by the 'photosystem limit' in this chapter.

Providing an estimate for the lifespan of Earth's biosphere goes beyond a diagnostic investigation of the operation of feedback processes on the planet. This limit provides a terminal limit for biological evolution and speciation on the planet, with some bearing on the 'anthropic principle' introduced in an earlier chapter. The anthropic principle (AP) describes a series of observations that laws of nature and parameters of the Universe take on a narrow range of values that are consistent with the conditions of life as we are familiar with, rather than a set of values that would be inconsistent with this life, thereby introducing a fundamental and irrevocable bias into our observations of Universe. By drawing on an interpretation of the multiverse theory, the AP suggests that a statistical population of Universes exist, some of which exhibit different universal constants or parameters that would ultimately make life impossible or unlikely under these conditions, but that by implication a subset of Universes also exist in which these parameters appear 'fine-tuned' for life (Barrow & Tipler, 1986; Bostrom, 2002; Watson, 2008). We find ourselves

in one of those Universes. Quantifying this bias mathematically in order to explore the possibility of life on other planets is problematic as it is difficult and statistically irresponsible to extrapolate from a sample of life-bearing planets that currently stands at one. Applying a model of the AP to life on Earth does however provide some insight into the likelihood of life on Earth. As mentioned in Chapter 2, Watson (2008), drawing on the earlier work of Carter (1983) and Szathmary & Maynard-Smith (1995), develops a probabilistic model that attempts to quantify the timing and likelihood of several critical (defined broadly as only occurring once in Earth history) steps in evolution en route to intelligent observers. A key parameter in these calculations is the habitable period of the planet, which exhibits a strong control over the expected timing on these critical steps, and indeed the number of steps themselves. It holds that only a planet with an extensive habitable period ($>10^9$ years) could support complex life, and intelligent life may require longer still, as these critical steps are incredibly unlikely (on the order of 10^{-9} yr^{-1}) to occur.

From the PHL sample of known, potentially habitable exoplanets discussed above, a number of candidates prove interesting from this perspective. Kepler 62e for example falls within the temperature and photosystem habitable zones (not accounting for uncertainty in its mass estimate), and its red-dwarf host star is reported to be 7±4 Gyr old (Borucki *et al.*, 2013). Kepler 62e therefore represents, in terms of temporal habitability at least, a strong Earth analogue with the potential to host a biosphere of an advanced age. In reality, localised planetary factors and stochastic, random events will play a significant role in the development of a biosphere (as they have done on Earth) should one exist. Further investigation of this planet, and an improved estimate on the age of its host star, would be beneficial in constraining the possibility of this planet hosting life. The age of the host stars of exoplanets GJ 832 c and Kepler 283 c remain unknown at this time, and few inferences regarding the age of a potential biosphere can therefore be drawn for these worlds. Future improvements in the understanding of stellar evolution will hopefully provide a refined estimate for star age, but this remains an extremely complex undertaking.

There remain many unknowns and uncertainties in the input and operation

of this model pertaining to habitability through time. However, by adopting a latin hypercube sampling approach across the expected range of input variables and by producing an ensemble of simulations from which a probability distribution can be computed, an estimate of the most likely habitable period for an Earth-like planet with analogous mechanisms for carbon cycling at similar distance from its star can be derived. These results suggest that, accounting for planet size (between 0.5 and 10 $M_{\oplus}$), the mean habitable period of this type of world is 6.2±0.01 Gyr for photosynthetic life, and 6.8±0.01 Gyr in terms of a basic temperature limit, with ∼33% of the successful runs passing the photosystem limit at ∼6.28 Gyr and ∼36% of these runs surpassing the temperature limit at 6.7 Gyr. The habitable zone lifetime estimate for Earth initially introduced in Chapter 1, based on stellar evolution and already-existing habitable zone models, was 6.29 Gyr, suggesting this estimate and approach is still fairly useful when considering cases in which relatively little is known about the planet, and has the benefit of wide and straightforward applicability in exoplanet surveys. However, the limitations of this method, primarily the assumption of Earth-like planet size, density and static atmospheric composition, should be stressed.

4.5.2 Limitations of this Work

A major limitation of this work, and of many studies in this field, remains the very limited sample of inhabited, habitable planets from which data to reduce the various uncertainties in the model input and operation can be extracted, and upon which these hypotheses can be tested. However, by continuing to develop our understanding of the Earth as a habitable environment our ability to validate these findings will improve. In particular, the process of hydrothermal alteration of the seafloor remains very poorly constrained and understood, despite its importance to the carbon cycle during the early history of the Earth. Furthermore, by populating exoplanet databases with new discoveries, and by exploring other habitable environments in our own solar system, more data will help to refine our ability to critically assess the habitability of this planet

relative to the billions of other planets that exist in this galaxy to eventually determine whether the Earth is unique or one of many planets that are able to host life as we currently understand it. Further restrictions to the applicability of this model arise when considering complex orbital dynamics (obliquity, eccentricity, precession), habitable moons, subsurface habitability, as well as very dry or oceanic worlds. A 3-D climate modelling approach would provide a solution to some of these issues, but also introduces further limitations in terms of temporal resolution whilst continuing to suffer from a lack of available data for exoplanetary candidates.

Furthermore, throughout their respective lifetimes planets can experience catastrophic events that could result in the extinction of the biosphere that are not included in this assessment, for example asteroid impacts or massive volcanic eruptions. The stochastic nature of these events make them difficult to predict and model successfully, but taking account of similar events during the history of the Earth (the K-Pg impact event for example), their effect on the biosphere cannot be understated. Some direct impacts to this model from events of this nature include neglecting the Late Heavy Bombardment event that likely occurred from 3.8 to 4.1 Gyr, which would likely have significantly affected geochemical processes and any potential biosphere that may have been present on the planet at the time, possibly introducing a massive pulse of extraterrestrial organic carbon and altering the composition of the atmosphere and Archean climate (SZ01).

In addition, Segura *et al.* (2005) suggest that planets in the orbit of M-dwarfs (in this case, GJ 832c, GJ667 Cc) can support higher levels of $p\mathrm{CH_4}$ in their atmospheres due to the effect that "M star spectral energy distribution has on the photochemical removal of $\mathrm{CH_4}$." (pp. 714). This is due to the fact that M dwarfs emit a much higher proportion of shorter-wavelength UV radiation than active G dwarfs, for example, and that at these wavelengths the photochemical production of $\mathrm{O}(^1\mathrm{D})$ and OH are much lower, as is the methane removal flux from this pathway. Therefore, the lifetime of $\mathrm{CH_4}$ in the atmosphere of a planet in the orbit of a red dwarf star might be on the order of $\sim$200 years, as opposed to 10-12 years in the current Earth atmosphere (Segura *et al.*,2005). As previously

mentioned, the methane cycle and effect of habitability in this model remains relatively unexplored. The longer lifetime and higher concentrations of CH_4 expected to be present in the atmospheres of planets in the orbit of M dwarfs will undoubtedly have a significant effect on surface temperatures, potential metabolic pathways for life and biosignature detection. Future improvements and developments to this model will aim to better resolve the methane cycle and its effect.

4.6 Conclusions

This study continues to expand the scope of the model that has been introduced over the course of the previous two chapters to include the effect of planet size on the operation of biogeochemically important cycling mechanisms that ultimately effect the long term habitability of Earth-like worlds. In drawing on the stellar, planetary and geochemical factors that influence this complex concept, a move away from habitable zone models based on star size and planet distance alone is suggested.

5 Conclusions & Future Work

> When you want to build a ship, do not begin by gathering wood, cutting boards, and distributing work, but awaken within the heart of man the desire for the vast and endless sea.
>
> **Antoine de Saint-Exupery**
> *Citadel* (1948)

5.1 Thesis Conclusions

Exoplanetary modelling is in its relative infancy as a discipline, but the field continues to grow with the number of confirmed extrasolar planets, and the importance of in-depth planetary-scale modelling for habitability assessments is becoming evident. Gaps in our knowledge that have persisted for decades, either due to a lack of available data, computing resources or available researchers, can begin to be addressed as a network of dedicated astrobiologists, planetary scientists and astronomers interested in these questions takes shape. Conclusions drawn from recent observations of terrestrial planets (both in our Solar System and beyond) have been reached through the use of 1-D chemical, and more recently, 3-D climate models (GCMs) that parametrize surface and atmospheric processes for habitability assessments (for example, Kopparapu *et al.*, 2013) and for the identification of possible spectral biosignatures to assist in defining future spectroscopic survey targets (for example Domagal-Goldman *et al.*, 2011).

The 'systems science' paradigm that dominates climate, ecological and atmospheric modelling of the Earth illustrates the fundamental interconnectivity of the various spheres of the planetary system, and stresses the importance of incorporating cross-domain biogeochemical processes when considering the evolution of any aspect of the planet. The application of biogeochemical modelling to the Earth system is an approach

that has been successfully exploited for many decades to investigate unanswered questions pertaining to the geochemical and climatological evolution of this planet (for example, Berner, 2006; Claire *et al.*, 2006; Haqq-Misra *et al.*, 2008; Walker *et al.*, 1981). The co-evolution of life and the planet is evident in many aspects of the contemporary Earth-system. Gases that comprise a significant fraction the atmosphere of this planet are of biogenic origin, namely oxygen (O_2), ozone (O_3) and methane (CH_4). Due to the propensity of CH_4 to undergo redox reactions with O_2 in the atmosphere, the pCH_4 reservoir requires constant replenishment from biological sources. It was noted that discovering gases in analogous 'thermodynamic disequilibrium' in the atmospheres of other planets may be a convincing sign of the action of life, and is therefore a priority for future biosignature surveys (Lovelock, 1975). In order to rigorously investigate the past, future and present behaviour of these gases in the atmosphere however, it is necessary to consider processes operating on the land surface, in the ocean, in the biosphere and at their respective interfaces.

Furthermore, biogeochmical cycles that operate over geological timescales serve to regulate the climate and composition of the atmosphere via a series of feedback loops. For example, the operation of the carbonate-silicate cycle serves to determine the concentration of atmospheric carbon dioxide (pCO_2) via the action of the weathering of terrestrial silicate minerals (and the associated draw down of CO_2) and the burial (and subsequent volcanic or metamorphic expulsion) of carbon (Walker *et al.*, 1982). This process is strongly temperature-dependent, with increased temperatures associated with more vigorous weathering and higher rates of CO_2 draw down. Results from this thesis suggests that the carbonate-silicate cycle exerts a strong control on the length of the habitable period of rocky planets, and that the inclusion of this feedback is crucial in future models and in habitability assessments.

The so-called 'habitable lifetime' of terrestrial planets is expected to exert a strong control on the possible evolutionary history of any potential biosphere, and also has implications for atmospheric evolution and the spectroscopic detection of biosignature gases (Caldeira & Kasting, 1992; O'Malley-James *et al.*, 2013; O'Malley-James *et al.*, 2015; Rushby *et al.*,

2013; Watson, 2008). Terrestrial planets may undergo transitions between several states of 'habitability' that are not strictly dependent on temperature alone: as carbon dioxide is drawn out of the atmosphere by the action of the carbonate-silicate cycle - which would be greatly accelerated towards the end of the planet's lifetime - photosynthetic primary producers would be placed under increasing stress. Eventually succumbing to the lack of atmospheric carbon would result in the likely collapse of the planetary biosphere at some considerable time *before* the planet becomes too warm. Placing the the habitability of the Earth in a temporal perspective reveals that this planet may not be the pinnacle of long-term habitability, its habitable lifetime eclipsed by terrestrial planets in the orbit of smaller stars with proportionally longer main-sequence lifetimes.

However, several limitations in this work can be identified. Assumptions implicit in the operation of the carbonate-silicate cycle are one such shortcoming; it is not known at this stage if analogous processes will operate on terrestial exoplanets with oceans and continental units. Furthermore, our understanding of the operation of this cycle on the Earth reveals biological amplification and mediation at several junctures, including terrestrial weathering and the fixation and burial of inorganic carbon in the ocean. Separating biotic and abiotic processes implicit in the carbonate-silicate cycle therefore remains problematic.

Additionally, this approach makes no allowance for stochastic variability over the sub-million year timescales. These processes, which include orbital variations, asteroid strikes and large volcanic CO_2 events could detrimentally affect the long-term habitability of the planet. Pulses of greenhouse gases and carbon dioxide liberated into the atmosphere could result in non-linear responses and positive feedback processes (calthrate melting, atmospheric hazes, ice-albedo effects) which are difficult to capture with this model. Bolide impacts may conversely deliver water and organic compounds to the planet, which may prove to be fundamentally important and beneficial to the habitability of the planet over geological timescales.

5.2 Future Work

As our understanding of planetary habitability continues to develop and be refined, it is becoming increasingly clear that previous definitions of the term are becoming obsolete. Recent analyses of many of the factors thought to affect the ability of a planet to support life have revealed complex and multifaceted interactions between many components of the planet and star system, and these studies have stressed inherent difficulties in quantifying the term with a single parameter; surface temperature or the availability of liquid water for example (Cockell *et al.*, 2016). More detailed biogeochemical modelling of the geochemical evolution of terrestrial planets, including cycles of oxygen and sulfur, would greatly improve the predicative capability of the these models, and incorporating improved standardized metrics (for example, the 'energy balance' approach of Hoehler (2007)) for measuring the potential for planets to support life would assist in removing 'Earth-bias' from the output and interpretation of habitability studies.

The growing catalogue of exoplanets has prompted the development of integrated 'habitability indices' that incorporate a number of factors into a single measure to determine how similar an exoplanet is to the Earth. One such measure, called the Earth Similarity Index (ESI) attempts to rank planets discovered in the habitable zone on a scale from 0 (completely dissimilar to the Earth) to 1 (identical to the Earth) across a range of factors including size, density, atmospheric properties and temperature (Schulze-Makuch *et al.*, 2011). Furthermore, Rushby *et al.*, (2013) suggested including a temporal component into habitability metrics. However, at this stage, indices of this variety have been poorly implemented and fail to incorporate new and emerging statistics (primarily from the *Kepler* team) on obliquity, eccentricity, metallicity, star-planet mass relations and tidal interactions, to name but a few. Re-examining multi-tiered habitability indices to include new *Kepler* data products should form a crucial element of the modelling studies in the future. This will serve to not only strengthen our understanding of this complex concept, but to also assist in the effective communication of contemporary habitable exoplanet research to the wider public.

5.2.1 Other areas of possible development in the future

1. To continue to develop and improve the zero-D carbon cycle model to incorporate cycles of oxygen and sulphur. While estimates of pCO_2 are predominantly computed by the response of silicate weathering rate to pCO_2 and temperature, multiple negative feedback processes, and the coupling of the carbon, oxygen, phosphorus and sulphur cycles are necessary for regulating pO_2 over geological time. Sulphur oxidation requires the presence of atmospheric oxygen, and stresses the co-evolution of these two cycles on this planet. Effectively integrating an oxygen cycle into the current model framework will involve including or reformulating biological oxygen production, carbon burial, reductant input from volcanic and hydrothermal sources, and hydrogen escape from the exobase. Claire *et al.* (2006) adopt a simple reductant/oxidant ratio in their formulation; a similar approach which could be incorporated into the model framework to provide a first-order estimate of the redox balance of the planet surface.

    (a) Developing improved methods of modelling surface/subsurface biogeochemical interactions requires coupling atmospheric and ocean chemistry to subsurface processes, which includes terrestrial and seafloor weathering, sediment transport, carbon burial, volcanism, metamorphism, and subduction, as well as benthic biogeochemical and crustal geochemical processes. The effects of these parameters could be investigated by incorporating existing biogeochemical carbon cycle models (e.g. this work) with 1-D photochemistry (e.g. Domagal-Goldman *et al.*, 2014) and 3-D climate models (e.g. GISS NExSS ROCKE3D) in order to better conceptualize atmospheric photochemistry in a more rigorous and self-consistent model framework. Crucially, recent advances in the modelling of these, at present, disparate systems means that we are now well poised to merge existing approaches by leveraging an extant and interdisciplinary network of researchers who are currently working in these areas.

2. Previous habitability indices often utilize methods taken from ecological modelling, for example an adapted version of the Bray-Curtis dissimilarity index in the case of Schulze-Makuch *et al.* (2011), in which various components of the planet system are weighted relative to their expected influence on the ability of the planet to include life, returning a single value between 0 (completely dissimilar to the Earth), to 1 (identical to the Earth). However, given the subjective nature of the weighting methodology this approach suffers from an anthropic bias. Furthermore, in light of recent findings from the *Kepler* mission, as well as developments that suggest that Earth may not be the *prima facie* best-case scenario for planetary habitability, formulating a new index, or addressing flaws in previous attempts, is key (Rushby *et al.*, 2013; Heller & Armstrong, 2014). Drawing on these recent findings, incorporating a measure of temporal habitability (as already outlined in Rushby *et al.*, 2013)), and readdressing considerations of spatial habitability across a number of similarity matrices including the Bray-Curtis, Kulczynski and Relativized Manhattan measures, would be beneficial to the field (Faith *et al.*, 1987). Failing to satisfy triangle inequality, these methods may be less robust than 'distance' approaches (e.g. relative Euclidean, correlation distance etc.). A detailed study of the comparative strength of these techniques could be carried out using parameters that are relevant to planetary habitability, and available from contemporary or near-future detection campaigns or modelling studies. These include: planet mass, orbital properties (semi-major axis/incident radiative flux, eccentricity, tidal interactions), atmospheric composition, bulk density, habitable period and potential carrying capacity.

    (a) Revisiting the concept of 'habitability' itself by drawing on innovative perspectives on the definition of the term (Cockell *et al.*, 2016). In particular, a move towards an 'energy-balance' approach, as outlined by Hoehler (2007), as opposed to a Earth-relative measure will mitigate any potential anthropic bias evident in current formulations of the theory.

6 References

Abe, Y., Abe-Ouchi, A., Sleep, N.H. & Zahnle, K. J. (2011). Habitable Zone Limits for Dry Planets. *Astrobiology* **11**(5) pp. 443 - 460

Abbot, D.S. & Switzer, E.R. (2011). The Steppenwolf: A Proposal for a Habitable Planet in Interstellar Space. *The Astrophysical Journal Letters* **735**: L27

Altermann, W. & Kazmierczak, J. (2003). Archean microfossils: a reappraisal of early life on Earth. *Research in Microbiology* **154** pp. 611 - 617

Anthony, J.W., Bideaux, R.A., Bladh, K.W. & Nichols, M.C. (2001). *Handbook of Minerology.* Volume III, 2nd ed. Chantilly: Mineralogical Society of America

Baraffe, I., Chabrier, G., Allard, F. & Hauschildt, P.H. (1998). Evolutionary models for solar metallicity low-mass stars: mass magnitude relationships and color-magnitude diagrams. *Astronomy & Astrophysics* **337** pp.403 - 412

Barnes, R., Jackson, B., Raymond, S.N., West, A. A. & Greenberg, R. (2009). The HD40307 Planetary System: Super-Earths or Mini-Neptunes? *The Astrophysical Journal.* **695** pp.1006 - 1011

Barnes, R., Mullins, K., Goldblatt, C., Meadows, V.S., Kasting, J. F. & Heller, R. (2012). Tidal Venuses: Triggering a Climate Catastrophe via Tidal Heating. *Astrobiology* in press

Barnes, R., Raymond, S.N., Jackson, B. & Greenberg, R. (2009). Tides and the evolution of planetary habitability. *Astrobiology* **8**(3) pp. 557 - 568

Barrow, J.D., & Tipler, F.J. (1986). The Anthropic Cosmological Principle. *Oxford Paperbacks*: Oxford.

Berger, A. & Loutre, M.F. (1991). Insolation values for the climate of the last 10 million years. *Quaternary Science Review* **10** pp. 297 - 317

Bergman, N.M., Lenton, T.M. & Watson, A.J. (2004). COPSE: A new Model of Biogeochemical Cycling Over Phanerozoic Time. *American Journal of Science* **304** pp.397 - 437

Berner, R.A. (1991). A model for atmospheric CO_2 over Phanerozoic time. *American Journal of Science* **291** pp. 339 - 376

Berner, R.A. (1994). GEOCARB II: A revised model for atmospheric CO_2 over Phanerozoic time. *American Journal of Science* **294** pp. 56 - 91

Berner, R.A (1997). The rise of plants and their effect on weathering atmospheric CO_2. *Science* **276** pp.544 - 546

Berner, R.A. (2004). The Phanerozoic carbon cycle: A History of Atmospheric CO_2 and its Effects on Plants, Animals and Ecosystems and O2. 1st ed. Oxford University Press: Oxford.

Berner, R.A. (2005) The Rise of Trees and How They Changed Paleozoic Atmospheric CO_2, Climate, and Geology in: Ehleringer, J.R., Cerling, T., Dearing, M.D. (eds.) (2005) *A History of Atmospheric CO_2 and its Effects on Plants, Animals and Ecosystems*. Springer: London.

Berner, R.A. (2006). GEOCARBSULF: A combined model for Phanerozoic atmospheric O_2 and CO_2. *Geochemica et Cosmochemica Acta* **70**(23) pp. 5653 - 5664

Berner, R.A. & Kothavala, Z. (2001). GEOCARB III: A Revised Model of Atmospheric CO_2 over Phanerozoic Time. *American Journal of Science* **301**(2) pp. 182 - 204

Berner, R.A., Lasaga, A.C. & Garrels, R.M. (1983). The carbonate-silicate geochemical cycle and its effect on atmospheric carbon dioxide over the past 100 million years. *American Journal of Science* **283** pp. 641 - 683

Borucki, W.J., Agol, E., Fressin, F., Kalteneggar, L., Rowe, J., Isaacson, H., Fischer, D., Batalha, N., Lissauer, J.J., Marcy, G.W., Fabrycky, D., Dsert, J-M., Bryson, S.T., Barclay, T., Bastien, F., Boss, A., Brugamyer, E., Buchhave, L.A., Burke, C., Caldwell, D.A., Carter, J., Charbonneau, D., Crepp, J.R., Christensen-Dalsgaard, J., Christiansen,

J.L., Ciardi, D., Cochran, W.D., DeVore, E., Doyle, L., Dupree, A.K., Endl, M., Everett, M.E., Ford, E.B., Fortney, J., Gautier, T.N., Geary, J.C., Gould, A., Haas, M., Henze, C., Howard, A. W., Howell, S.B., Huber, D., Jenkins, J.M., Kjeldsen, H., Kolbl, R., Kolodziejczak, J., Latham, D.W., Lee, B.L., Lopez, E., Mullally, F., Orosz, J.A., Prsa, A., Quintana, E.V., Sanchis-Ojeda, R., Sasselov, D., Seader, S., Shporer, A., Steffen, J.H., Still, M., Tenenbaum, P., Thompson, S.E., Torres, G., Twicken, J.D., Welsh, W.F. & Winn, J.N. (2013). Kepler-62: A Five-Planet System with Planets of 1.4 and 1.6 Earth Radii in the Habitable Zone. *Science* **340**(6132) pp. 587 - 590

Bostrom, N. (2002). Anthropic Bias: Observation Selection Effects in Science and Philosophy. *Routledge*: New York & London.

Brady, P.V. & Gslason, S.R. (1997). Seafloor weathering controls on atmospheric CO_2 and global climate. G*eochemica et Cosmochemica Acta* **61**(5) pp. 965 - 973

Broecker, W.S. & Peng, T.,-H. (1982). Tracers in the Sea *Lamont-Doherty Geological Observatory/Columbia University Press*: New York.

Broecker, W.S., Takahashi, T., Simpson, H.J., Peng, T.,-H. (1979). Fate of Fossil Fuel Carbon Dioxide and the Global Carbon Budget. *Science***206**(4417) pp. 409 - 418

Caldeira, K. & Kasting, J. F. (1992). The life span of the biosphere revisited. *Nature*. **360** pp.721 - 723

Carter, B. (1983). The anthropic principal and its implications for biological evolution. *Philosophical Transactions of the Royal Society of London A*. **310** pp. 347 - 363

Catling, D.C., Glein, C.R., Zahnle, K.J. & McKay, C.P. (2005). Why O2 is required by complex life on habitable planets and the concept of planetary oxygenation time. *Astrobiology* **5** pp.415 - 438

Charlson, R.J., Lovelock, J.E., Andreae, M.O. & Warren, S.G. (1987). Oceanic phytoplankton, atmospheric sulphur, cloud albedo and climate. *Nature* **326** pp. 655 - 661

Claire, M.W., Catling, D.C. & K. J. Zahnle (2006). Biogeochemical modeling of the rise in atmospheric oxygen. *Geobiology* **4** 239 - 269

Claire, M. W., Sheets, J., Cohen, M., Ribas, I., Meadows, V.S & Catling, D. C. (2012) The evolution of solar flux from 0.1 nanometers to 160 microns: quantitative estimates for planetary studies. *The Astrophysical Journal* **757** 95

Cleland, C.E., & Chyba, C.F. (2002) Defining 'life'. *Origins of Life and Evolution of Biospheres* **32** pp. 387-393.

Cockell, C.S. (2011). Vacant habitats in the Universe. *Trends in Ecology & Evolution* **26** pp. 73 - 80.

Cockell, C.S., Balme, M., Bridges, J.C., Davila, A. & Schwenzer, S.P. (2012). Uninhabited habitats on Mars. *Icarus* **217**(1) pp. 184 - 193

Cockell, C.S., Bush, T., Bryce, C., Direito, S., Fox-Powell, M., Harrison, J.P., Lammer, H., Landenmark, H., Martin-Torres, J., Nicholson, N., Noack, L., O'Malley-James, J., Payler, S., **Rushby, A.J.**, Samuels, T., Schwendner, P., Wadsworth, J., & Zorzano, M.P. (2016) http://online.liebertpub.com/doi/pdfplus/10.1089/ast.2015.1295Habitability: A Review *Astrobiology* (**16**)(1) pp. 89 — 117

Colaprete, A. & Toon, O. B. (2003). Carbon dioxide clouds in an early dense Martian atmosphere. *Journal of Geophysical Research* **108** (E4)

Collins, W.J., N. Bellouin, M. Doutriaux-Boucher, N. Gedney, T. Hinton, C. D. Jones, S. Liddicoat, G. Martin, F. O'Connor, J. Rae, C. Senior, I. Totterdell, S. Woodward, T. Reichler, J. Kim (2008). Evaluation of the HadGEM2 model. *Met Office Hadley Centre Technical Note* HCTN 74.

Coogan, L.A. & Gillis, K.M. (2013). Evidence that low-temperature oceanic hydrothermal systems play an important role in the silicate-carbonate weathering cycle and long-term climate regulation. *Geochemistry, Geophysics and Geosystems* **14**(6) pp. 1771 - 1786

Cowan, D.A. (2004) The upper temperature limit of life: how far can we go? *Trends in Microbiology* **12** pp.58 - 60.

Davies, J.H. & Davies, D.R. (2010). Earth's surface heat flux. *Solid Earth* **1** pp. 5 - 24

de Pater, I. and Lissauer, J.J. (2007) *Planetary Sciences* (5th ed.) Cambridge: Cambridge University Press

Des Marais, D. J., Nuth III, J.A., Allamandola, L. J., Boss, A. P., Farmer, J. D., Hoehler, T.M., Jakosky, B.M., Meadows, V.S., Pohorille, A., Runnegar, B. & Spormann, A. M. (2008). The NASA Astrobiology Roadmap. *Astrobiology.* **8** (4) pp. 715 - 730

Domagal-Goldman, S. D., Seguar, A., Claire, M.W., Robinson, T.D. & Meadows, V.S. (2014). Abiotic Ozone and Oxygen In Atmospheres Similar to Prebiotic Earth. *The Astrophysical Journal* **792** (2)

Doodge, J.C.I. (2001) Integrated Management of Water Resources In: Ehlers, E. And Krafft, T. (2001) (eds.). *Understanding the Earth System: compartments, processes and interactions.* Berling: Springer-Verlag

Dotter, A., Chaboyer, B., Jevremovi, D., Kostov, V., Baron, E., & Ferguson, J. W. (2008). The Dartmouth Stellar Evolution Database. *The Astrophysical Journal.* **178** pp. 89 - 101

Dressing, C.D., Spiegel, D.S., Scharf, C.A., Menou, K. & Raymond, S.N. (2010). Habitable climates: the influence of eccentricity. *The Astrophysical Journal* **721**(2) pp. 1295 - 1307

Dunne, J.P., John, J.G., Shevliakova, E., Stouffer, R.J., Krasting, J.P., Malyshev, S.L., Milly, P.C.D., Sentman, L.T., Adcroft, A.J., Cooke, W., Dunne, K.A., Griffies, S.M., Hallberg, R.W., Harrison, M.J., Levy, H., Wittenberg, A.T., Phillips, P.J. & Zadeh, N. (2013). GFDL's ESM2 Global Coupled ClimateCarbon Earth System Models. Part II: Carbon System Formulation and Baseline Simulation Characteristics. *Journal of Climate* **26** pp. 2247 - 2267

Ernst, W.G. (2006). Speculations on evolution of the terrestrial lithosphere-asthenosphere system Plumes and plates. *Gondwana Research.* 11 pp. 38 - 49

ESO (2009). Lightest exoplanet yet discovered [Online]. Available at: http://www.eso.org/public/news/eso0915/ (Last accessed on 15th May 2010)

Faith, D.P., Minchin, P.R. & Belbin, L. (1987). Compositional dissimilarity as a robust measure of ecological distance. *Vegetatio* **69** pp. 57 - 68

Forveille, T., Bonfils, X., Delfosse, X., Alonso, R., Udry, S., Bouchy, F., Gillon, M., Lovis, C., Neves, V., Mayor, M., Pepe, F., Queloz, D., Santos, N.C., Sgransan, D., Akmenara, J.-M., Deeg, H.J. & Rabus, M. (2011) The HARPS search for southern extra-solar planets XXXII. Only 4 planets in the Gl581 system. *Astronomy & Astrophysics* submitted (arXiv:1109.2505)

Franios, L. M., & Walker, J.C.G (1992). Modelling the Phanerozoic Carbon Cycle and Climate: Constraints from the 87Sr/86Sr Isotopic Ratio of Seawater. American Journal of Science 202 pp.81 - 135

Franck, S., Block, A., Von Bloh, W., Bounama, C., Schellnhuber, H. J. & Svirezhev, Y. (2000). Reduction of biosphere life span as a consequence of geodynamics. *Tellus* **52**(B) pp. 94 - 107.

Franck, S. & Bounama, C. (1999). Continental growth and volatile exchange during Earth's evolution. *Physics of the Earth and Planetary Interiors* **100** pp. 189 - 196

Franck, S., Kossacki, K. & Bounama, C. (1999). Modelling the global carbon cycle for the past and future evolution of the earth system. *Chemical Geology* **159** pp.305 - 317

Frank, E.A., Meyer, B.S. & Mojzsis (2014). A radiogenic heating evolution model for cosmochemically Earth-like exoplanets. *Icarus* in press

Fuelner, G. (2012). The Faint Young Sun Problem. *Rev. Geophys.* **50** RG2006. doi:10.1029/2011RG000375

Garrels. R.M., & Mackenzie, F.T. (1969). Sedimentary rock types: relative proportions as a function of geological time. *Science* **163** pp. 570 - 571

Giridhar, S. (2010). Spectral Classification; Old and Contemporary In:

Goswami, A. and Reddy, B.E. (eds.) (2010) *Principals and Perspectives in Cosmochemistry*. Berlin: Springer Berlin Heidelberg

Goldblatt, C., Robinson, T.D., Zahnle, K.J., & Crisp, D. (2013). Low simulated radiation limit for runaway greenhouse climates. *Nature Geoscience* **6** pp.661 - 667

Goldblatt, C. & Watson, A.J. (2012) The Runaway Greenhouse: implications for future climate change, geoengineering and planetary atmospheres. *Phil. Trans. Roy. Soc.* **370** pp. 4170 - 4216

Goldblatt, C. & Zahnle, K. J. (2011) Clouds and the Faint Young Sun Paradox. *Climate of the Past* **7** pp. 203 - 220

Gomes, R., Levison, H.F., Tsiganis, K., and Morbidelli, A. (2005). Origin of the cataclysmic Late Heavy Bombardment period of the terrestrial planets. *Nature*. **435** pp. 466 - 469

Gray, R.O. and Corbally, C.J. (2009). *Stellar Spectral Classification*. Woodstock: Princeton University Press

Grasset, O., Schneider, J., & Sotin, C. (2009). A study of the accuracy of mass-radius relationships for silicate-rich and ice-rich planets up to 100 Earth masses. *Astrophysical Journal* **693** pp.722 - 733

Gregory, P. C. (2011). Bayesian re-analysis of the Gliese 581 exoplanet system. *Monthly Notices of the Royal Astronomical Society*. **415** pp. 2523 - 2545

Grotzinger, J.P., Sumner, D.Y., Kah, L.C., Stack, K., Gupta, S., Edgar, L., Rubin, D., Lewis, K., Schieber, J., Mangold, N., Milliken, R., Conrad, P.G., Des Marais, D., Farmer, J., Siebach, K., Calef, F., Hurowitz, J., McLennan, S.M., Ming, D., Vaniman, D., Crisp, J., Vasavada, A., Edgett, K.S., Malin, M., Blake, D., Geliert, R., Mahaffy, P., Wiens, R.C., Maurice, S., Grant, J.A., Wilson, S., Anderson, R.C., Beegle, L., Arvidson, R., Hallet, B., Sletten, R.S., Rice, M., Bell, J., Griffes, J., Ehlmann, B., Anderson, R.B., Bristow, T.F., Dietrich, W.E., Dromart, G., Eigenbrode, J., Fraeman, A., Hardgrove, C., Herkenhoff, K., Jandura, L., Kocurek, G., Lee, S., Leshin, L.A., Leveille, R., Limonadi,

D., Maki, J., McCloskey, S., Meyer, M., Minitti, M., Newsom, H., Oehler, D., Okon, A., Palucis, M., Parker, T., Rowland, S., Schmidt, M., Squyres, S., Steele, A., Stolper, E., Summons, R., Treiman, A., Williams, R., Yingst, A., & the MSL Science Team. (2014) A habitable fluvio-lacustrine environment at Yellowknife Bay, Gale Crater, Mars. *Science* **343**: doi:10.1126/science.1242777.

Guangyu, S. & Xiaobiao, F. (1992). Past, Present and Future Climatic Forcing due to Greenhouse Gases. *Advances in Atmospheric Sciences* **9**(3) pp. 279 - 286

Guo, J., Zhang, F., Chen, X. and Han, Z (2009) Probability distribution of terrestrial planets in habitable zones around host stars. *Astrophysics and Space Science* **323** pp. 367 - 373

Haberle, R. M., Tyler, D., McKay, C.P. & Davis, W.L. (1994). A Model for the Evolution of CO_2 on Mars. *Icarus* **109** pp. 102 - 120

Hagermann, A. (2005). Planetary heat flow measurements. Philosophical Transactions of the Royal Society A 363 pp. 2777 2791 Hansen, J., Fung, A., Lacis, D., Rind, S., Lebedeff, S., Ruedy, R., Russell, G. & Stone, P. (1988). Global Climate Changes as Forecast by Goddard Institute for Space Studies Three-Dimensional Model. *Journal of Geophysical Research* **93**(D8) pp. 9341 - 9364

Haqq-Misra, J. D., Domagal-Goldman, S. D., Kasting, P. J., & Kasting, J. F. (2008). A Revised, Hazy Methane Greenhouse for the Archean Earth. *Astrobiology* **8**(6) pp.1127 - 1137

Hart, M.H. (1979). Habitable Zones about Main Sequence Stars. *Icarus* **37** pp. 351 - 357

Hayashi, C. (1981). Structure of the Solar Nebula, Growth and Decay of Magnetic Fields and Effects of Magnetic and Turbulent Viscosities on the Nebula. *Progress of Theoretical Physics Supp* **70** pp. 35 - 53

Hayes, J.M. & Waldbauer, J.R. (2006). The carbon cycle and associated redox processes through time. *Philosophical Transactions of the Royal Society B* **361** pp.931 - 950

Heath, M.J., Doyle, L.R., Joshi, M.M. and Haberle, R.M. (1999). Habitability of Planets around Red Dwarf Stars. *Origins of Life and the Evolution of the Biosphere*. **29** pp. 405 - 424

Heller, R. & Armstrong, J. (2014). Superhabitable worlds. *Astrobiology* **14**(1) pp. 50 - 66

Heller, R. & Barnes, R. (2012). Exomoon habitability constrained by illumination and tidal heating. *Astrobiology* (Forthcoming).

Heller, R., Leconte, J. & Barnes, R. (2011) Tidal obliquity evolution of potentially habitable planets. *Astronomy & Astrophysics* **528** (A27)

Hoehler T.M. (2007) An energy balance concept for habitability. *Astrobiology* **7** pp.824 - 838.

Holland, H.H. (2006). The oxygenation of the atmosphere and oceans. *Philosophical Transactions of the Royal Society B* **381** pp. 903 - 915

Hu, Y. & Ding, F. (2010) Radiative constraints on the habitability of exoplanets Gliese 581c and Gliese 581d. *Astronomy & Astrophysics* **526** A135

Ida, S. & Lin, D.N.C. (2005) Toward a deterministic model of planetary formation. III. Mass Distribution of short-period planets around stars of various masses. *The Astrophysical Journal*. **626** pp. 1045 - 1060

Iwamori, H. (1998). Transportation of H2O and melting in subduction zones. *Earth and Planetary Science Letters* **160** pp. 65 - 80

Jenkins, J.M., Caldwell, D.A. & Borucki, W.J. (2002). Some tests to establish confidence in planets discovered by transit photometry. *The Astrophysical Journal* **564** pp. 495 - 507

Jones, E.G. & Lineweaver, C.H. (2010). To What Extent Does Terrestrial Life 'Follow The Water'? *Astrobiology* **10**(3) pp. 349 - 361

Jones, B.W., Sleep, P.N. & Underwood, D.R. (2006). Habitability of known exoplanets based on measured stellar properties. *The Astrophysical Journal*. **649** pp. 1010 - 1019

Joshi, M.M. (2003). Climate model studies of synchronously rotating planets. *Astrobiology* **3**(2) pp. 415 - 42 7

Joshi, M. M. & Haberle, R.M. (2012). Suppression of the water ice and snow albedo feedback on planets orbiting red dwarf stars and the subsequent widening of the habitable zone. *Astrobiology* **12**(1)

Joshi, M.M., Haberle, R.M. & Reynolds, R.T. (1997). Simulations of the Atmospheres of Synchronously Rotating Terrestrial Planets Orbiting M Dwarfs: Conditions for Atmospheric Collapse and the Implications of Habitability. *Icarus* **129**(2) pp. 450 - 465

Junge, K., Eicken, H., & Deming, J.W. (2004) Bacterial activity at -2 to -20 C in Arctic wintertime sea ice. *Applied Environmental Microbiology* **70** pp. 550 - 557.

Kaler, J.B. (1997) *Stars and their Spectra: An Introduction to the Spectral Sequence*. (2nd ed.) Cambridge: Cambridge University Press

Kasting, J. F. (1988). Runaway and Moist Greenhouse Atmospheres and the Evolution of Earth and Venus. *Icarus* **74** pp. 472 - 494

Kasting, J. F. & Catling, D. (2003). Evolution of a Habitable Planet. *Annual Reviews in Astronomy and Astrophysic*s. **41** pp. 429 - 463

Kasting, J. F., Whitmire, D.P., Reynolds, R.T. (1993). Habitable Zones around Main Sequence Stars. *Icarus* **101** pp. 108 - 128

Keeley, J. E. & Rundel, P.W. (2003). Evolution of CAM and C4 carbon concentration mechanisms. *International Journal of Plant Sciences* **164** (No. Suppl. 3) pp. S55 - S77

Keltenegger, L., Henning, W.G. and Sasselov, D.D. (2010). Detecting volcanism on extrasolar planets. *The Astronomical Journal* **140** pp. 1370 - 1380

Keltenegger, L., Udry, S. & Pepe, F. (2011). A Habitable Planet around HD85512? *Astronomy and Astrophysics* in review arXiv: 1108.3561

Kite, E.S., Manga, M. And Gaidos, E. (2009). Geodynamics and rate of

volcanism on massive Earth-like planets. *The Astrophysical Journal* **700** pp. 1732 - 1749

Kitzmann, D., Alibert, Y., Godolt, M., Grenfell, J.L., Heng, K., Patzer, A.B.C., Rauer, H., Stracke, B. & von Paris, P. (2015). The unstable CO_2 feedback cycle on ocean plants. *Monthly Notices of the Royal Astronomical Society* **452**(4) pp. 3752 - 3758

Kitzmann, D., Patzer, A.B.C, von Paris, P., Godolt, M., Stracke, B., Gebauer, S., Grenfell, J.L. & Rauer, H. (2010). Clouds in the atmospheres of extrasolar planets I: Climatic effects of multi-layered clouds for Earth-like planets and implications of habitable zones. *Astronomy & Astrophysics*. **511** A66.

Kleine, T., Mnker, C., Mezger, K. and Palme, H. (2002). Rapid accretion and early core formation on asteroids and the terrestrial planets from Hf-W chronometry. *Nature*. **418** pp. 952 - 955

Knoll, A.H. & Barghoorn, E.S. (1977). Archean Mircofossils Showing Cell Disvision from the Swaziland System of South African. *Science* **198**(4315) pp. 396 - 398

Koch, D.G., Borucki, W.J., Basri, G., Batalha, N.M., Brown, T.M., Caldwell, D., Christensen-Dalsgaard, J., Cochran, W.D., DeVore, E., Dunham, E.W., Gautier, T.N., Geary, J.C., Gilliland, R.L., Gould, A., Jenkins, J., Kondo, Y., Latham, D. W., Lissauer, J.J., Marcy, G., Monet, D., Sasselow, D., Boss, A., Brownlee, D., Cladwell, J., Dupree, A.K., Howell, S.T., Dotson, J.L., Gazis, P., Hass, M. R., Kolodziejczak, J., Rowe, J.F., Van Cleve, J.E., Allen, C., Chandrasekaran, H., Clarke, B.D., Li, J., Quintana, E.V., Tenenbaum, P., Twicken, J.D. & Wu, H. (2010). Kepler mission design, realized photometric performance, and early science. *The Astrophysical Journal Letters* **713** L79 - L86

Kokubo, E. and Ida, S (2002) Formation of protoplanet systems and diversity of planetary systems. *The Astrophysical Journal* **581** pp. 666 - 680

Kopparapu, R., Ramirez, R., Kasting, J. F., Eymet, V., Robinson, T. D.,

Mahadevan, S., Terrien, R.C., Domagal-Goldman, S., Meadows, V. & Deshpande, R. (2013). Habitable Zones Around Main-Sequence Stars: New Estimates. *The Astrophysical Journal* **765** 131

Kopparapu, R.K., Ramirez, R., SchottelKotte, J., Kasting, J. F., Domagal-Goldman, S.D. & Eymet, V. (2013a). Habitable Zones Around Main-Sequence Stars: Dependence on Planetary Mass. *The Astrophysical Journal* **787** (131) doi:10.1088/0004-637X/765/2/131

Korenaga, J. (2012). Plate tectonics and planetary habitability: current status and future challenges. *Annuals of the New York Academy of Sciences* 2012 pp. 1 - 8

Kump, L. R. & Arthur, M.A (1999). Interpreting carbon isotope excursions: carbonates and organic matter. *Chemical Geology* **161** pp. 181 - 198

Lammer, H. (2007). Preface: M Star Planet Habitability. *Astrobiology* **7**(1) pp.27 - 29

Lammer, H., Bredehft, J.H., Coustenis, A., Khodachenko, M.L., Kaltenegger, L., Grasset, O., Prieur, D., Raulin, F., Ehrenfruend, P., Yamauchi, M., Wahlund, J.-E., Griebmeier, J. M., Stangl, G., Cockell, C.S., Kulikov, Yu.N., Grenfell, J.L. and Rauer, H. (2009) What makes a planet habitable? *Astronomy and Astrophysics* **17** pp. 181 - 249

Laskar, J., Correia, A.C.M., Gastineau, M., Joutel, F., Levard, B. & Robutel, P. (2004). Long term evolution and chaotic diffusion of the insolation quantities of Mars. *Icarus* **170**(2) pp. 343 - 364

Laskar, J., Fienga, A., Gastineau, M. & Manche, H. (2011). La2010: a new orbital solution of the long-term motion of the Earth. *Astronomy & Astrophysics* **532** (A89)

Laughlin, G. (1997). The end of the Main Sequence. *The Astrophysical Journal* **48**2 pp. 420 - 432

Ledrew, G (2001). The Real Starry Sky. *Journal of the Royal Astronomical Society of Canada*. **95** pp. 32 - 33

Lenton, T. M. (1998). Gaia and natural selection. *Nature* **394** pp.439 - 447

Levison, H.F., Morbidelli, A., Tsiganis, K., Nesvorny, D. & Gomes, R. (2011). Late orbital instabilities in the outer planets induced by interaction with a self-gravitating planetesimal disk. *The Astronomical Journal* **142**(152) doi:10.1088/0004-6256/142/5/152

Lineweaver, C.H. (2001). An Estimate of the Age Distribution of Terrestrial Planets in the Universe: Quantifying Metallicity as a Selection Effect. *Icarus* **151** (2) pp. 307 - 313

Lineweaver, C.H. & Davis, T.M. (2002). Does the rapid appearance of life on Earth suggest that life is common in the Universe? *Astrobiology* **2**(2) pp. 293 - 304

Lineweaver, C. H., Fenner, Y. & Gibson, B. K. (2004). The Galactic Habitable Zone and the Age Distribution of Complex Life in the Milky Way. *Science* **303** (5654) pp. 59 - 62

Lissauer, J.J., Dawson, R.I. & Tremaine, S. (2014). Advances in exoplanet science from Kepler. *Nature* **513** pp. 336 - 344

Lissauer, J.J. and Stevenson, D.J. (2006) Formation of Giant Planets. In: Reipurth, B., Jewitt, D. and Keil, K. (eds.) *Protostars and Planets V.* Tucson: University of Arizona Press

Lovelock, J. & Watson, A.J. (1983) Biological homeostatsis of the global environment: the parable of Daisyworld. *Tellus* **35**(B) pp. 284 - 289

Lovelock, J. E. & Whitfield, M. (1982). The lifespan of the biosphere. *Nature* **296** pp. 561 - 563

Lowell, R.P. & Keller, S. M. (2003). High-temperature seafloor hydrothermal circulation over geologic time and Archean banded iron formations. *Geophysical Research Letters* **30**(7) doi:10.1029/2002GL016536

Martin, R.G. & Livio, M. (2012). On the evolution of the snow line in protoplanetary discs. *MNRAS Letters* **425**(1) pp. L6 - L9

Massey, P., Levesque, E.M. and Plez, B. (2006) Bringing VY Canis Majoris Down to Size: An Improved Determination of its Effective Temperature.

The Astrophysical Journal. **646** pp. 1203 - 1208

Mayor, M., Pepe, F., Queloz, D., Bouchy, F., Rupprecht, G., Lo Curto, G., Avila, G., Benz, W., Bertaux, J.-L., Bonfils, X., Dall, Th., Dekker, H., Delabre, B., Eckert, W., Fleury, M., Gilliotte, A., Gojak, D., Guzman, J.C., Kohler, D., Lizon, J.-L., Longinotti, A., Lovis, C., Megevand, D., Pasquini, L., Reyes, J., Sivan, J.-P., Sosnowska, D., Soto, R., Udry, S., Van Kesteren, A., Weber, L. & Weilenmann, U. (2003). Setting new standards with HARPS. *The Messenger* **114** pp. 20 - 24

McDougall, I., Brown, F. & Fleagle, J. G. (2005). Stratigraphic placement and age of modern humans from Kibish, Ethiopia. *Nature* **433** pp. 733 - 736

McKay, C.P., Pollack, J.B. & Courtin, R. (1991). The greenhouse and antigreenhouse effects on Titan. *Science* **253**(5024) pp. 1118 - 1121

McKay, M.D., Beckman, R.J. & Conover, W.J. (1979). A comparison of three methods for selecting values of input variables in the analysis of output from a computer code. *Technometrics* **21**(2) pp. 239 - 245

Mills, B., Lenton, T.M. & Watson, A.J. (2014). Proterozoic oxygen rise linked to shifting balance between seafloor and terrestrial weathering. *Proceedings of the National Academy of Sciences of the United States of America* **111**(25) pp. 9073 - 9078

Mills, B., Watson, A.J., Goldblatt, C., Boyle, R. & Lenton, T.M. (2011). Timing of Neoproterozoic glaciations linked to transport-limited global weathering. *Nature Geoscience* **4** pp.861 - 864

Mojzsis, S.J., Harrison, T.M., Pidgeon, R.T. (2001). Oxygen-isotope evidence from ancient zircons for liquid water at the Earths surface 4,300 Myr ago. *Nature*. **409** pp. 178 - 181

Montmerle, T., Augereau, J.-C., Chaussidon, M., Gounelle, M., Marty, B. And Morbidelli, A. (2006). 3.Solar System Formation and Early Evolution: The First 100 Million Years. *Earth, Moon and Planets*. **98** pp. 39 - 95

Morbidelli, A., Levison, H.F., Tsiganis, K. and Gomes, R. (2005). Chaotic capture of Jupiters Trojan asteroids in the early Solar System. *Nature* **436** pp. 462 - 465

Myhre, G., Highwood, E.J., Shine, K.P & Stordal, F. (1998). New estimates of radiative forcing due to well mixed greenhouse gases. *Geophysical Research Letters* **25**(14) pp.2715 - 2718

Myhre, G., D. Shindell, F.-M. Bron, W. Collins, J. Fuglestvedt, J. Huang, D. Koch, J.-F. Lamarque, D. Lee, B. Mendoza, T. Nakajima, A. Robock, G. Stephens, T. Takemura & H. Zhang (2013). Anthropogenic and Natural Radiative Forcing Supplementary Material. In: *Climate Change 2013: The Physical Science Basis*. Contribution of Working Group I to the Fifth Assessment Report of the Intergovernmental Panel on Climate Change [Stocker, T.F., D. Qin, G.-K. Plattner, M. Tignor, S.K. Allen, J. Boschung, A. Nauels, Y. Xia, V. Bex & P.M. Midgley (eds.)]. Available from: www.climatechange2013.org and www.ipcc.ch.

NASA (2014). Kepler Discovery Table. [Online] Available at: http://kepler.nasa.gov/Mission/discoveries/ (Last accessed on: 17th September 2014)

Nebojsa, D. (2004). *Advanced Astrophysics*. Cambridge: Cambridge University Press.

Newman, W.L. (2007). Age of the Earth: USGS Publications Services. [Online] Available at: http://pubs.usgs.gov/gip/geotime/age.html (Last accessed on 18th September 2014)

Nutman, A.P. (2006). Antiquity of the Oceans and Continents. *Elements*. **2** pp. 223 - 227

Ohmoto, Y. Kakegawa, T., Ishida, A., Nagase, T. & Rosing, M.T. (2014). Evidence for biogenic graphite in early Archean Isua metasedimentary rocks. *Nature Geoscience* **7** pp. 25 - 28

OMalley-James, J.T., Greaves, J.S., Raven, J.A. & Cockell, C.S. (2013). Swansong biospheres: refuges for life and novel microbial biospheres on terrestrial planets near the end of their habitable lifetimes.

International Journal of Astrobiology doi: 10.1017/S147355041200047X Published online by Cambridge University Press 27 November 2012

OMalley-James, J.T., Greaves, J.S., Raven, J.A. & Cockell, C.S. (2014). Swansong biospheres II: the final signs of life on terrestrial planets near the end of the habitable lifetimes. *International Journal of Astrobiology* **13**(3) pp. 229 - 243

Omta, A.W., Dutkiewicz, S. & Follows, M.J. (2011). Dependence of the ocean-atmosphere partitioning of carbon on temperature and alkalinity. *Global Biogeochemical Cycles* **25** GB1003

ONeill, C.O. and Lenardic, A. (2007). Geological consequences of super sized Earths. *Geophysical Research Letters*. **34** L19204

Osborne, C.P. & Beerling, D.J. (2006). Nature's green revolution: the remarkable evolutionary rise of C4 plants. *Philosophical Transactions of the Royal Society B* **361** pp. 173 - 194

Pace, N.R. (2001). The universal nature of biochemistry. *Proceedings of the National Academy of Science*. **98** (3) pp. 805 - 808

Pappalardo, R. T. (2010). Seeking Europa's Ocean. Galileos Medicean Moons: their impact on 400 years of discovery. *Proceedings of IAU Symposium* **269** pp. 101 - 114

Pepe, F., Lovis, C., Sgransan, D., Benz, W., Bouchy, F., Dumusque, X., Mayor, M., Queloz, D., Santos, N.C. & Udry, S. (2011). The HARPS search for Earth-like planets in the habitable zone: I. Very low-mass planets around HD20794, HD85512, and HD192310. *Astronomy & Astrophysics* **534**(A58) doi: 10.1051/0004-6361/201117055

Petit, J.R., Jouzel, J., Raynaud, D., Barkov, N.I., Barnola, J. M., Basile, I., Bender, M., Chappellaz, J., Davis, M., Delaygue, G., Delmotte, M., Kotlyakov, V.M., Legrand, M., Lipenkov, V.Y., Lorius, C., Ppin, L., Ritz, C., Saltzmann, E. & Stievenard, M. (1999). Climate and atmospheric history of the past 420,000 years from the Vostok ice core, Antarctica. *Nature* **399** pp. 429 - 436

Pierrehumbert, R. (2010). *Principals of Planetary Climate*. 1st ed. Cambridge: Cambridge University Press.

Pierrehumbert, R. & Gaidos, E. (2011). Hydrogen Greenhouse Planets Beyond the Habitable Zone. *The Astrophysical Journal Letters* **734**: L13

Planetary Habitability Laboratory (2012). The Habitable Exoplanets Catalog. [online] Available at: http://phl.upr.edu/projects/habitable-exoplanets-catalog (Last Accessed: 01/02/13)

Podolak, M., & Zucker, S. (2010). A note on the snow line in protostellar accretion disks *Meteoritics & Planetary Science* **39**(11) pp. 1859 - 1868

Pupac, A. M. and Davies, G.F. (2007). The internal activity and thermal evolution of Earth-like planets. *Icarus* **195** pp. 447 - 458

Ramirez, R. M., Kopparapu, R. K., Chester, H., Zugger, M. & Kasting, J.F. (2014a). Warming Early Mars with CO_2 and H_2. *Nature Geoscience* **7** pp. 59 - 63

Ramirez, R. M., Kopparapu, R. K., Linder, V., & Kasting, J.F. (2014). Can Increased Atmospheric CO_2 Levels Trigger a Runaway Greenhouse? *Astrobiology* **14**(8) pp. 714 - 731

Raymond, S.N., Scalo. J. And Meadows, V.S. (2007). A Decreased Probability of Habitable Planet Formation Around Low-Mass Stars. *The Astrophysical Journal*. **669** pp. 606 - 614

Robinson, T.D., Meadows, V.S., Crisp, D., Deming, D., AHearn, M.F., Charbonneau, D., Livengood, T.A., Seager, S., Barry, R.K., Hearty,T., Hewagama, T., Lisse, C.M., McFadden, L.A. & Wellnitz, D.D. (2011). Earth as an Extrasolar Planet: Earth Model Validation Using EPOXI Earth Observations. *Astrobiology* **11**(5) pp. 393 - 408

Rosing, M.T., Bird, D.K., Sleep, N.H. & Bjerrum, C.J. (2010). No climate paradox under the faint early Sun. *Nature* **464** pp. 744 - 747

Rothschild, L.J. (2007). Extremophiles: defining the envelope for the search

for life in the universe. In: Pudritz, R., Higgs, P. and Stone, J. (2007). *Planetary Systems and the Origins of Life*. Cambridge: Cambridge University Press

Rushby, A.J., Claire, M.W., Osborn, H. & Watson, A.J (2013). Habitable Zone Lifetimes of Exoplanets around Main Sequence Stars. *Astrobiology* **13** (9) pp. 833 - 849

Santos, N.C., Isrealian, G., and Mayor, M. (2003). Confirming the Metal-Rich Nature of Stars with Giant Planets. *The Future of Cool-Star Astrophysics. 12th Cambridge Workshop on Cool Stars, Stellar Systems and the Sun (2001 July 30th to August 3rd).*: Boulder: University of Colorado

Scalo, J., Kaltenegger, L., Seura, A., Fridlund, M., Bibas, I., Kulikov, Yu.N., Grenfell, J.L., Rauer, H., Odert, P., Leitzinger, M., Selsis, F., Khodachenko, M.L., Eiroa, C., Kasting, J. and Lammer, H. (2007) M-stars as Targets for Terrestrial Exoplanet Searches and Biosignature Detection. *Astrobiology*. **7**(1) pp. 85 - 166

Scharf, C. (2014). *The Copernicus Complex: Our Cosmic Significance in a Universe of Planets and Probabilities*. 1st ed. New York: Scientific American/Farrar, Straus and Giroux.

Schneider, J., Dedieu, C., Le Sidaner, P. & Zolothkhin, I. (2011). Defining and cataloguing exoplanets: The exoplanet.eu database. *Astronomy & Astrophysics* **532** A79

Schoene, B. (2014). U-Th-Pb Geochronology in: Holland, H.D., & Turekian, K.K. (2014). *Treatise on Geochemistry* 2nd ed (4). Oxford: Elsevier

Schulze-Makuch, D., & Irwin, L. (2004) Energy Sources and Life In: *Life in the Universe. Advances in Astrobiology and Biogeophysics*, (Springer Berlin / Heidelberg) **3** pp. 67 - 104.

Schulze-Makuch, D., Mndez, A., Fairn, A.G., von Paris, P., Turse, C., Boyer, G., Davila, A. F., Resendes de Sousa Antnio, Catling, D. & Irwin, L. N. (2011). A Two-Tiered Approach to Assessing the

Habitability of Exoplanets. *Astrobiology.* **11**(10) pp. 1041 - 1052

Schwartzmann, D.W. & Volk, T. (1989). Biotic enhancement of weathering and the habitability of Earth. Nature 340 pp. 457 460 Schmidt, G.A., Ruedy, R., Hansen, J.E., Aleinov, I., Bell, N., Bauer, M., Bauer, S., Cairns, B., Canuto, V., Cheng, Y., Del Genio, A., Faluvegi, G., Friend, A.D., Hall, T.M., Hu, Y., Kelley, M., Kiang, N.Y., Koch, D., Lacis, A.A., Lerner, J., Lo, K.K., Miller, R.L., Nazarenko, L., Oinas, V., Perlwitz, J.P., Perlwitz, Ju., Rind, D., Romanou, A., Russel, G.L., Sato, Mki., Shindell, D.T., Stone, P.H., Sun, S., Tausnev, N., Thresher, D., & Yao, M.-S. (2006). Present day atmospheric similations using GISS ModelE: Comparison to in-situ satellite and reanalysis data. *Journal of Climate* **19** pp. 153 - 192

Seager, S. (2013). Exoplanet Habitability. *Science* **340** pp. 577 - 581

Seager, S., Kuchner, M., Her-Majumder, C.A., Militzer, B. (2007). Mass-Radius Relationships for Solid Exoplanets. *The Astrophysical Journal.* **669** pp. 1279 - 1297

Seager, S. and Lissauer, P. (2010) in Seager, S.(eds) (2010) *Exoplanets.* Tucson: University of Arizona Press.

Segura, A., Kasting, J.F., Meadows, V., Cohen, M., Scalo, J., Crisp, D., Butler, R.A.H. & Tinetti, G. (2005). Biosignatures from Earth-Like Planets Around M Dwarfs. *Astrobiology* **5**(6) pp.706 - 725

Selsis, F., Kasting, J.F., Levard, B., Paillet, J., Ribas, I & Delfosse, X. (2007). Habitable planets around the star Gliese 581? *Astronomy & Astrophysics* **476** pp. 1373 - 1387

Shaw, G.H. (2008). Earths atmosphere - Hadean to early Proterozoic. Chemie der Erde Geochemistry. 68 pp. 235 - 264

Smith, R.C. (1995) *Observational Astrophysics.* Cambridge: Cambridge University Press Syndicate

Shields, A. L., Meadows, V. S., Bitz, C.M., Pierrehumbert, R.T., Joshi, M.M. & Robinson, T.D. (2013). The Effect of Host Star Spectral

Energy Distribution and Ice-Albedo Feedback on the Climate of Extrasolar Planets. *Astrobiology* **13**(8) pp. 715 - 739

Showman, A.P., Cho, J.Y.-K. & Menou, K. (2010). Atmospheric Circulation of Exoplanets in: Seager, S. (eds.) (2010) *Exoplanets* 1st edition: Tucson: Arizona University Press

Sleep, N. H. & Zahnle, K. (2001). Carbon dioxide cycling and implications for climate on ancient Earth. *Journal of Geophysical Research* **106** (E1) pp.1373 - 1399

Sotin, C., Grasset, O. & Mocquet, A. (2007). Mass radius curve for extrasolar Earth-like planets and ocean planets. *Icarus* **191** pp. 337 - 351

Sotin, C., Jackson, J.M. & Seager, S. (2010). Terrestrial Planet Interiors in: Seager, S. (eds.) (2010) *Exoplanets* 1st edition. Tucson: Arizona University Press.

Southam, G., Rothschild, L.J. and Westall, F. (2007) The Geology and Habitability of Terrestrial Planets: Fundamental Requirements for Life. In: Fishbaugh, K.E., Logonn, P., Raulin, F., Des Marais, D.J. and Korablev, O. (2007) Geology and Habitability of Terrestrial Planets. London: Springer Tarter, J.C., Backus, P.R., Mancinelli, R.L., Aurnou, J.M., Backman, D.E., Basri, G.S., Boss, A.P., Clarke, A., Deming, D., Doyle, L.R., Feigelson, E.D., Freund, F., Grinspoon, D.H., Haberle, R.M., Hauck, S.A., Heath, M.J., Henry, T.J., Hollingsworth, J.L., Joshi, M.M., Kilston, S., Liu, M.C., Meikle, E., Reid, I.N., Rothschild, L.J., Scalo, J., Segura, A., Tang, C.M., Tiedje, J.M., Turnbull, M.C., Walkowicz, L.M., Weber, A.L. and Young, R.E. (2007). A reappraisal of the Habitability of Planets Around M Dwarf Stars. *Astrobiology* **7**(1) pp. 30 - 65

Spiegel, D.S. & Turner, E.L. (2012). Bayesian Analysis of the astrobiological implications of life's early emergence of Earth. *PNAS* **109**(2) pp. 395 - 400

Stamenkovi, V., Noack, L., Breuer, D. & Spohn, T. (2012). The Influence

of Pressure-Dependent Viscosity on the Thermal Evolution of Super-Earths. *The Astrophysical Journal* **748**(1) doi:10.1088/0004-637X/748/1/41.

Stephens, G.L., O'Brien, D., Webster, P.J., Pilewski, P., Kato, S. & Li, J.-L. (2015). The albedo of Earth. *Reviews of Geophysics* **53** doi: 10.1002/2014RG000449

Swain, M. R., Vasisht, G. & Tinetti, G. (2008). The presence of methane in the atmosphere of an extrasolar planet. *Nature* **452** pp. 329 - 331

Szathmry, E. & Maynard-Smith, J. (1995) The Major Evolutionary Transitions. *Nature*. **374** pp. 227 - 232

Takai, K., Nakamura, K., Toki, T, Tsunogai, U., Miyazaki, M., Miyazaki, J.-I., Hirayama, H., Makagawa, S., Nunoura, T., & Horikoshi, K. (2008) Cell proliferation at 122 C and isotopically heavy CH_4 production by a hyperthermophilic methanogen under high-pressure cultivation. *Proceedings of the National Academy of Science* **105** pp. 10,949 - 10,954.

Tarter, J.C., Backus, P.R., Mancinelli, R.L., Aurnou, J.M., Backman, D.E., Basri, G.S., Boss, A.P., Clarke, A., Deming, D., Doyle, L.R., Feigelson, E.D., Freund, F., Grinspoon, D.H., Haberle, R.M., Hauck, S.A., Heath, M.J., Henry, T.J., Hollingsworth, J.L., Joshi, M.M., Kilston, S., Liu, M.C., Meikle, E., Reid, I.N., Rothschild, L.J., Scalo, J., Segura, A., Tang, C.M., Tiedje, J.M., Turnbull, M.C., Walkowicz, L.M., Weber, A.L. & Young, R.E. (2007). A reappraisal of the Habitability of Planets Around M Dwarf Stars. *Astrobiology* **7**(1) pp. 30 - 65

Trail, D., Watson, E.B and Taiby, N. D. (2011). The oxidation state of the Hadean magams and implications for early Earths atmosphere. *Nature*. **480** pp. 79 - 83

Tsiganis, K., Gomes, R., Morbidelli, A. & Levison, H.F. (2005). Origin of the orbital architecture of the giant planets of the Solar System. *Nature* **435** pp. 459 - 461

Tuomi, M. (2011). Bayesian re-analysis of the radial velocities of Gliese 581. *Astronomy & Astrophysics* **528** L5

Tuomi, M., Anglada-Escud, G., Gerlach, E., Jones, H.R.A., Reiners, A., Rivera, E.J., Vogt, S.S., & Butler, R.P. (2013). Habitable-zone super-Earth candidate in a six-planet system around the K2.5V star HD 40307. *Astronomy & Astrophysics* **549**(A48) doi: 10.1051/0004-6361/201220268

Urban, M.A., Nelson, D.M., Jimenez,-Moreno, G., Chateauneuf, J-J., Pearson, A. & Hu, F.S. (2010). Isotopic evidence of C4 grasses in southwestern Europe during the Early Oligocene-Middle Miocene. *Geology* **38** (12) pp. 1091 - 1094

Valencia, D., OConnell, R.J. & Sasselov, D.D. (2007). Inevitability of Plate Tectonics on Super-Earths. *The Astrophysical Journal* **670** pp. 45 - 48

Valencia, D., OConnell, R.J. & Sasselov D. D. (2006). Internal structure of massive terrestrial planets. *Icarus* **181** pp. 545 - 555

Vogt, S. S., Butler, R. P. & Haghighipour, N. (2012). GJ 581 update: additional evidence for a Super-Earth in the habitable zone. *Astronomische Nachrichten* **333** pp. 1 - 15

Von Bloh, W., Bounama, C., Cuntz, M. And Franck, S. (2007) The Habitability of super-Earths in Gliese 581. *Astronomy & Astrophysics.* **476** pp. 1365 - 1371

Von Paris, P., Selsis, F., Kitzmann, D. & Rauer, H. (2013). The Dependence of the Ice-Albedo Feedback on Atmospheric Properties. *Astrobiology* **13**(10) pp. 899 - 909

Wadhwa, M., Srinivasan, G. and Carlson, R.W. (2006). *Timescales of Planetesimal Differentiation in the Early Solar System.* In: Lauretta, D.S. and McSween Jr., H.Y. (eds.) *Meteorites and the Early Solar System II.* Tucson: University of Arizona Press

Walker, J.C.G., Hays, P.B., & Kasting, J.F. (1981). A negative feedback mechanism for the long-term stabilization of Earth's surface temperature. *Journal of Geophysical Research* **86** (10) pp. 9776 - 9782

Waltham, D. (2011). Anthropic selection and the habitability of planets

orbiting M and K dwarfs. *Icarus* **215** pp.518 - 521

Watson, A.J. (2008). Implications of an Anthropic Model of Evolution for Emergence of Complex Life and Intelligence. *Astrobiology.* **8**(1) pp. 1 - 12

Wells, L.E. & Deming, J.W. (2006) Characterization of a cold-active bacteriophage on two psychrophilic marine hosts. *Aquatic Microbial Ecology* **45** pp.15 - 29.

West, A.J., Galy, A., & Bickle, M. (2005). Tectonic and climatic controls on silicate weathering. *Earth and Planetary Science Letters* **235** pp.211 - 228

Wilde, S.A., Valley, J.W., Peck, W.H and Graham, C.M. (2001). Evidence from detrital zircons for the existence of continental crust and oceans on the Earth 4.4 Gyr ago. *Nature.* **409** pp.175 - 178

Williams, D.R. (2014). Earth Fact Sheet [Online]. Available at: http://nssdc.gsfc.nasa.gov/planetary/factsheet/earthfact.html (Last accessed on 15th September 2014)

Wordsworth, R. D., Forget, F., Selsis, F., Madeleine, J.-B, Millour, E., & Eymet, V. (2010). Is Gliese 581d habitable? Some constraints from radiative-convective climate modeling. *Astronomy and Astrophysics* **522** A52.

Wood, B.J., Walter, M.J. and Wade, J. (2006). Accretion of the Earth and segregation of its core. *Nature.* **441** pp. 825 - 833

Yin, Q., Jacobson, S.B., Yamashita, K., Blichert-Toft, J., Telouk, P. & Albarede, F. (2002). A short timescale for terrestrial planet formation from Hf-W chronometry of meteorites. *Nature* **418** pp. 949 - 952

Zahnle, K., Arndt, N., Cockell, C., Halliday, A., Nisbet, E., Selsis, F. & Sleep, N.H. (2007). Emergence of a Habitable Planet. *Space Science Reviews* **129** pp. 35 - 78

Zeilik, M.A., & Gregory, S.A., (1998). *Introductory Astronomy & Astrophysics.* (4th ed.) Philadelphia: Saunders College Publishing

Zerkle, A.L., Claire, M.W., Domagal-Goldman, S.D., Farquhar, J. & Poulton, S.W. (2012). A bistable organic-rich atmosphere on the Neoarchean Earth. *Nature Geoscience* **5**(5) pp. 359

Zsom, A., Keltenegger, L. & Goldblatt, C. (2012). A 1D microphysical cloud model for Earth, and Earth-like exoplanets: Liquid water and water ice clouds in the convective troposphere. *Icarus* **221**(2) pp.603 - 616